

**Development of aptamer-functionalized biodegradable  
polymeric nanoparticles for targeted prostate cancer  
therapy: *in vitro* and *in vivo* study**



**Thesis submitted by  
ASHIQUE AL HOQUE**

**DOCTOR OF PHILOSOPHY (SCIENCE)**

**Department of Chemistry  
Faculty Council of Science  
Jadavpur University  
Kolkata-700032, India**

**2024**

**JADAVPUR UNIVERSITY**  
**KOLKATA-700032, INDIA**

**INDEX NO. 2/17/Chem./25**

**1. Title of the thesis:** Development of aptamer-functionalized biodegradable polymeric nanoparticles for targeted prostate cancer therapy: *in vitro* and *in vivo* study

**2. Name, Designation and institution of supervisor:**

Professor (Dr.) Biswajit Mukherjee

Professor,

Department of Pharmaceutical Technology,

Jadavpur University,

Kolkata-700032, India.

**3. List of publications (related to thesis)**

- (i) **Ashique Al Hoque**, Debasmita Dutta, Brahamacharry Paul, Leena Kumari, Iman Ehsan, Moumita Dhara, Biswajit Mukherjee, Mohiuddin Quadir, Benny Abraham Kaiparettu, Soumik Laha, Shantanu Ganguly.  $\Delta$ PSap4# 5 surface-functionalized abiraterone-loaded nanoparticle successfully inhibits carcinogen-induced prostate cancer in mice: a mechanistic investigation. *Cancer Nanotechnology*. 2023; 14(1):73. **(Impact Factor: 6.9)**

**Other Publications**

- (ii) Moumita Dhara, **Ashique Al Hoque**, Ramkrishna Sen, Debasmita Dutta, Biswajit Mukherjee, Brahamacharry Paul & Soumik Laha. Phosphorothioated amino-AS1411 aptamer functionalized stealth nanoliposome accelerates bio-therapeutic threshold of apigenin in neoplastic rat liver: a mechanistic approach. *Journal of Nanobiotechnology* 21, no. 1 (2023): 1-23. **(Impact Factor: 11.5)**
- (iii) Adhikary, Sourav, **Ashique Al Hoque**, Manisheet Ray, Swastik Paul, Akbar Hossain, Subrata Goswami, and Rajib Dey. Investigation of Paracetamol Entrapped Nanoporous Silica Nanoparticles in Transdermal Drug Delivery System. *Applied Biochemistry and Biotechnology* (2023): 1-16. **(Impact Factor: 3.0)**

- (iv) Leena Kumari, Iman Ehsan, Arunima Mondal, **Ashique Al Hoque**, Biswajit Mukherjee, Pritha Choudhury, Arunima Sengupta, Ramkrishna Sen, Prasanta Ghosh. Cetuximab-conjugated PLGA nanoparticles as a prospective targeting therapeutics for non-small cell lung cancer, *Journal of Drug Targeting* 31 (2023) 521-536. <https://doi.org/10.1080/1061186X.2023.2199350> (**Impact Factor: 5.016**)
  
- (v) Ke Wang, Raj Shankar Hazra, Qian Ma, Md Rakib Hasan Khan, **Ashique Al Hoque**, Long Jiang, Mohiuddin Quadir, Yuanming Zhang, Shudong Wang, Guangting Han. Robust biocompatible bacterial cellulose/silk nonwoven fabric/silk sericin sandwich membrane with strong UV-blocking and antioxidant properties. *Cellulose* (2023): 1-21. (**Impact Factor: 5.7**)
  
- (vi) Iman Ehsan, **Leena Kumari**, Ramkrishna Sen, Ashique Al Hoque, Biswajit Mukherjee, Alankar Mukherjee, Prasanta Ghosh, Sanchari Bhattacharya. J591 functionalized Paclitaxel loaded PLGA nanoparticles successfully inhibited PSMA overexpressing LNCaP cells, *Journal of Drug Delivery Science and Technology*, 75 (2022) 103689. <https://doi.org/10.1016/j.jddst.2022.103689> (**Impact Factor: 5.062**)
  
- (vii) Nayim Sepay, Nadir Sepay, **Ashique Al Hoque**, Rina Mondal, Umesh Chandra Halder & Mohd. Muddassir. In silico fight against novel coronavirus by finding chromone derivatives as an inhibitor of coronavirus main proteases enzyme. *Structural Chemistry* (2020). <https://doi.org/10.1007/s11224-020-01537-5> (**Impact Factor: 1.7**)

## **Book Chapters**

- (i) Biswajit Mukherjee, **Ashique Al Hoque**, Brahamacharry Paul, Laboni Das, Samrat Chakraborty, Apala Chakraborty Apoptosis-Associated Markers: Potential Targets to Develop Cancer Therapy. In book: *Novel Molecular Oncotargets and Nano-oncotherapeutics*. 2023 June 16, ISBN: 1-5275-0713-0, (pp. 240-284), Cambridge Scholars Publishing.

- (ii) Biswajit Mukherjee, Brahamacharry Paul, **Ashique Al Hoque**, Samrat Chakraborty, Laboni Mondal, Apala Chakraborty, Alankar Mukherjee. Targeted Nanotherapeutics: Promising Therapeutic Arsenal Against Hepatocellular Carcinoma. In book: Novel Molecular Oncotargets and Nano-oncotherapeutics. 2023 June 16, ISBN: 1-5275-0713-0, (pp. 495-554), Cambridge Scholars Publishing.
- (iii) Md Rakib Hasan Khan, **Ashique Al Hoque**, Mohiuddin Quadir. Polymersomes as Novel Strategies for Delivery of Nanotherapeutics for Cancer Control. In book: Novel Molecular Oncotargets and Nano-oncotherapeutics. 2023 June 16, ISBN: 1-5275-0713-0, (pp. 620-647), Cambridge Scholars Publishing.
- (iv) Biswajit Mukherjee, Brahamacharry Paul, **Ashique Al Hoque**, Ramkrishna Sen, Samrat Chakraborty, Apala Chakraborty. Polymeric nanoparticles as tumor-targeting theranostic platform. In Design and Applications of Theranostic Nanomedicines 2023 Jan 1 (pp. 217-259). Woodhead Publishing.
- (v) Biswajit Mukherjee, **Ashique Al Hoque**, Apala Chakraborty, Samrat Chakraborty, Lopamudra Dutta, Debasmita Dutta, Soumyabrata Banerjee, Moumita Dhara, R Manasa Deepa. Recent developments in cancer vaccines: where are we?. Nanotherapeutics in Cancer Vaccination and Challenges. 2022 Jan 1:29-75.
- (vi) Biswajit Mukherjee, Leena Kumari, Iman Ehsan, Prasanta Ghosh, Soumyabrata Banerjee, Samrat Chakraborty, Manisheet Ray, **Ashique Al Hoque**, Ratan Sahoo, Guar gum-based nanomaterials in drug delivery and biomedical applications, In: H. Bera, C. M. Hossain, S. Saha (Eds.), Biopolymer-Based Nanomaterials in Drug Delivery and Biomedical Applications, Academic Press, 2021, pp. 143-164. <https://doi.org/10.1016/B978-0-12-820874-8.00016-6>
- (vii) Biswajit Mukherjee, **Ashique Al Hoque**, Debasmita Dutta, Brahamacharry Paul, Alankar Mukherjee, Sahajit Mallick. Nanoformulated drug delivery of potential betulinic acid derivatives: A promising approach toward cancer therapy. Nanomedicine for Bioactives: Healthcare applications. 2020:127-53.



- (viii) Biswajit Mukherjee, Soma Sengupta , Soumyabrata Banerjee, Moumita Dhara, **Ashique Al Hoque**, Leena Kumari, Ray, Manisheeta Ray, Iman Ehsan, Alankar Mukherjee, Transdermal Nanomedicines for Reduction of Dose and Site-Specific Drug Delivery, 2020. In: M. K. Das, Y. V. Pathak (Eds.), Nano Medicine and Nano Safety, Springer, Singapore, 2020, pp. 175-211. [https://doi.org/10.1007/978-981-15-6255-6\\_8](https://doi.org/10.1007/978-981-15-6255-6_8)
- (ix) Biswajit Mukherjee, **Ashique Al Hoque**, Shreyasi Chakraborty, Leena Kumari, Roy S, Paul P. Nanomedicine: Could It Be a Boon for Pulmonary Fungal Infections?. In: Nanomedicine for the Treatment of Disease 2019 Sep 25 (pp. 141-164). Apple Academic Press.

#### **4. List of patents: Nil**

#### **5. List of Presentations in National/ International/ Conferences/Workshops:**

##### **National:**

National Seminar on Advancing Healthcare through Pharmaceutical and Biomedical Applications held on 19<sup>th</sup> January 2024 at Jadavpur University, Kolkata.

National Conference on Advanced Therapeutics for Life-Threatening and Chronic Diseases held on 19-20 September 2023 at JIS University, Kolkata.

National Seminar on Pharmacy & Healthcare: Traditional Knowledge to Modern Techniques held on 14<sup>th</sup> September, 2018 at Jadavpur University, Kolkata.

National Seminar on ‘Quality Control and Standardization of Ethnopharmaceuticals in the Present Era’ held on 4-5 March 2018, at Centurion University of Technology and Management, Bhubaneswar, Odisha, India.

National seminar on ‘Current Developments in Chemical Sciences’ held on March 7, 2018 at Department of Chemistry, Jadavpur University, Kolkata, India.

**International:**

International Seminar on 'Emerging Fields of Research in Biotechnology and Biomedicine' held on 16<sup>th</sup> November 2022 at Jadavpur University, Kolkata, India.

3<sup>rd</sup> Pharm. Tech. IAPST International Conference on 'Molecular mechanism of diseases and novel therapeutic approaches' held on 19<sup>th</sup>-20<sup>th</sup> January, 2019 at School of Pharmacy and Life Sciences, Centurion University of Technology and Management, Bhubaneswar, India.

6<sup>th</sup> International Postgraduate Conference on Pharmaceutical Sciences 2018 held on 15<sup>th</sup> - 16<sup>th</sup> August, 2018 at International Medical University, Kuala Lumpur, Malaysia.

24<sup>th</sup> International Conference on Cancer Research and Pharmacology held on 5<sup>th</sup> - 6<sup>th</sup> August, 2019 in Singapore.

## “Statement of Originality”

I, **Ashique Al Hoque**, registered myself on **31.01.2017**, do hereby declare that this thesis entitled “**Development of aptamer-functionalized biodegradable polymeric nanoparticles for targeted prostate cancer therapy: *in vitro* and *in vivo* study**” contains a literature survey and original research work done by the undersigned candidate as part of Doctoral studies. All information in this thesis has been obtained and presented in accordance with existing academic rules and ethical conduct. As required by these rules and conduct, I declare that I have fully cited and referred all materials and results that are not original to this work.

I also declare that I have checked this thesis as per the “Policy on Anti Plagiarism, Jadavpur University, 2019”, and the level of similarity as checked by iThenticate software is **9%**.

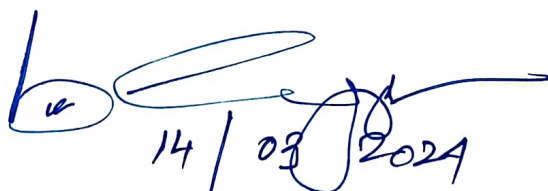


**Signatures of Candidate:**

**Date:** 14.03.2024

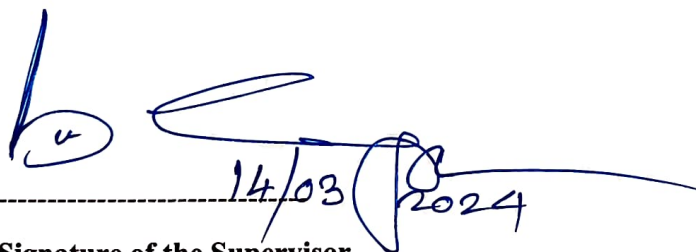
**Certified by Supervisor:**

**(Signature with date, seal)**

  
14 / 03 / 2024  
Professor (Dr.) Biswajit Mukherjee  
Department of Pharmaceutical Technology  
Jadavpur University  
Kolkata-700032, India

## CERTIFICATE FROM THE SUPERVISOR

This is to certify that the thesis entitled “**Development of aptamer-functionalized biodegradable polymeric nanoparticles for targeted prostate cancer therapy: *in vitro* and *in vivo* study**”, submitted by **Mr. Ashique Al Hoque** who got his name registered on **31.01.2017** in the Department of Chemistry under the Faculty council of Science for the award of Ph.D. (Science) degree of Jadavpur University is absolutely based upon his own work and neither the thesis nor any part of the thesis has been submitted for any degree/diploma or any other academic award anywhere before.



14/03/2024

**Signature of the Supervisor**

*Professor (Dr.) Biswajit Mukherjee*  
Department of Pharmaceutical Technology  
Jadavpur University  
Kolkata-700032, India

## ACKNOWLEDGEMENTS

*As I take a moment to reflect on my journey so far, I am filled with an overwhelming sense of gratitude for the blessings and opportunities that have led me to this point. It has been an incredible experience, and I remain hopeful that my hard work and dedication will pave the way for greater success in the future.*

*When I look back, I feel a deep sense of fulfillment and indebtedness to the many individuals who have supported and encouraged me along the way. However, there is one person in particular who has played an especially significant role in my journey: **Prof. (Dr.) Biswajit Mukherjee**.*

***Prof. (Dr.) Biswajit Mukherjee** has been an unwavering source of guidance and mentorship throughout my PhD journey. His support, advice, and attention to detail have been absolutely invaluable to me. He has always been there to answer my questions, provide me with feedback, and encourage me to push the boundaries of my research. His erudite suggestions and unwavering support have allowed me to grow and develop as a researcher in ways that I never thought possible. Working under Prof. Mukherjee's guidance has been a true honor. His untiring support and encouragement have been a constant source of inspiration for me, and I am incredibly grateful for the opportunity to learn from him. I am confident that the knowledge and skills that I have gained under his tutelage will serve me well in my future endeavors.*

*I would like to express my heartfelt appreciation to the esteemed **Department of Science and Technology (DST Inspire)**, Government of India, for graciously providing me with financial assistance from 2017 to 2022. This support was granted through DST/INSPIRE Fellowship/ (IF160466), dated 29th March 2017. It is with great honor that I acknowledge the invaluable contribution of DST Inspire towards my academic pursuits.*

*I would like to express my profound gratitude to my esteemed lab mates and seniors, **Iman Ehsan, Leena Kumari, Brahamacharry Paul, Moumita Dhara, Prasanta Ghosh, Ramkrishna Sen, Soumyabrata Banerjee, Bhabani Sankar Satapathy, Samrat Chakraborty, Manisheeta Ray, Alankar Mukherjee, Sahajit Mallick, Sandipan Mallick, Mrinmoy Barman, Ratna Roy, and Rima Chandra**, for their invaluable friendship, motivation, and knowledge-sharing throughout my academic journey. I am particularly*

indebted to **Debasmita Dutta** and **Koushik Das** for their unwavering technical assistance and moral support during the course of my research study.

I am grateful to **Dr. Md. Maidul Islam**, Assistant Professor, Allah University, Kolkata, for his valuable scientific advice and enormous encouragement.

I extend my special thanks to **Mrs. Dipa Mukherjee (Madam)** for all her moral support, love, and blessings. I also want to thank **Hasan Parvej, Nayim Sepay, Barun Mandal, Avinaba Mukherjee** and **Sourav Adhikary** for their constant support and encouragement.

Words are not enough to extend my special thanks to my beloved wife, **Shahnaz Begum**, for her endless support, technical help, and motivational words throughout the journey.

With profound gratitude, I acknowledge my late father, **Aijul Hoque**, whose solid support and belief in my abilities fueled my academic pursuits. His wisdom, encouragement, and sacrifices remain etched in every page of this thesis. Though he is no longer with us, his legacy of resilience and dedication endures, shaping the very essence of this work. I am forever indebted to his profound influence and unconditional love. This thesis stands as a tribute to his memory, a symbol of how his support and guidance have helped me achieve my goals and reach new heights.

I express my profound gratitude to my mother, **Ismatara Begom**, and younger brother, **Ijaj Al Hoque**, for their love, support, and encouragement throughout my academic journey. Their selfless sacrifices, unflinching belief in my abilities, and ceaseless encouragement have been a constant source of strength and inspiration. Their guidance, sagacity, and affection have enabled me to surmount the challenges of doctoral research and have helped shape the person I am today. Additionally, I want to thank the rest of my family members for their love and blessings. With the deepest love and gratitude, I dedicate this work to them also.


Date: 14.03.2024

Place: Kolkata



Ashique Al Hoque





*I dedicate this thesis to  
My Parents and family  
For their constant support and  
encouragement*

## PREFACE

The research related to the thesis for the Doctor of Philosophy (Science) degree has been carried out under the supervision of Prof. (Dr.) Biswajit Mukherjee, Department of Pharmaceutical Technology, Jadavpur University, Kolkata, India.

Prostate cancer is a highly prevalent form of cancer, ranking as the second leading cause of cancer-related mortality among American males, following lung cancer. The long-term efficacy of conventional medicines, including radiation, chemotherapy, and hormone therapy, is limited due to the occurrence of off-target side effects on healthy organs and the emergence of drug-resistance traits following many doses of treatment.

Abiraterone, a metabolite derived from abiraterone acetate, exhibits strong specific inhibitory effects on 17 $\alpha$ -Hydroxylase/C17,20-lyase (CYP17), an essential enzyme involved in testosterone synthesis. By inhibiting CYP17, abiraterone effectively suppresses androgen production in testicular, adrenal, and prostatic tumor tissues. The drug is currently being considered as a potential therapeutic option for prostate cancer is a BCS (Biopharmaceutics Classification System) class IV medication. Nevertheless, certain unavoidable limitations, such as inadequate solubility, permeability, and poor biodistribution, pose challenges for the drug's effective clinical application. In order to mitigate the negative side effects and reduce the impact of the disease, tailored nanocarrier-mediated therapy can effectively transport the medicine to the specific organ of interest, thereby enhancing the management of prostate cancer.

The utilization of nanoparticles (NPs) in the field of anticancer medication delivery has garnered considerable interest. Nanoparticles have the potential to facilitate the delivery of a diverse array of anticancer medicines that exhibit suboptimal pharmacokinetic characteristics. The site-specific delivery of drug molecules via ligand attachment to the nanoparticles can maintain drug levels at an appropriate therapeutic rate in a sustained way in the target organ. Poly(lactic-co-glycolic acid) (PLGA) is one of the most extensively used United States Food and Drug Administration (US-FDA)-approved biodegradable polymers, for systemic application upon its hydrolysis it releases two monomers, lactic acid and glycolic acid. These two monomers are endogenous and swiftly degraded by the body through the Krebs cycle; no systemic toxicity is involved in employing PLGA to deliver medication or biomaterial applications.



Targeting antigens overexpressed on the surface of cancer cells is one of the most promising therapeutic techniques for targeting cancer cells. Aptamers are a type of targeting ligands that are synthetic single-stranded RNA or DNA oligonucleotides (usually consisting of 25-90 nucleotide bases). They have the ability to fold into complex three-dimensional structures through intramolecular interactions. Aptamers are advantageous and exclusive over antibodies and other targeting molecules due to their target specificity, low immunogenicity, and high tissue penetration ability. Aptamers have been recognized as prospective candidates for the building of a number of smart systems, including drug administration, treatment, diagnostics, and bioimaging. Aptamers exhibit superior stability across a wide pH range, temperatures, and organic solvents when compared to antibodies. Additionally, they possess cost-effectiveness, easy manufacturing procedures, high sensitivity, and a strong affinity for binding pockets of diverse target antigens.

Preclinical data in a carcinogen-induced prostate cancer animal model are quite scarce. Few such data are known in the immune-compromised prostate cancer animal xenograft paradigm. However, there is no data so far available for aptamer-mediated medication targeting the prostate-specific surface antigen (PSMA) overexpressed in chemically produced prostate cancer in mice.

The current investigation aimed to examine the effectiveness of  $\Delta$ PSap4#5 aptamer-conjugated abiraterone (ABR)-loaded PLGA nanoparticles (Apt-ABR-NP) delivered intraperitoneally for site-specific drug delivery to prostate cancer, as well as the formulation's ability to prevent prostate cancer in mice induced by a chemical carcinogen. An attempt was made to determine the formulation-mediated prostate cancer inhibitory mechanism based on the data that were analyzed. The capacity of the aptamer to bind to the prostate cancer antigen was examined using molecular docking.

## LIST OF ABBREVIATIONS

°C	Celsius
Abs	Absorbance
ABR	Abiraterone acetate
ABR-NP	Abiraterone acetate-loaded nanoparticles
AEC	Animal Ethics Committee
ADT	Androgen deprivation therapy
AR	Androgen receptor
AST	Aspartate transaminase
ALT	Alanine transaminase
ALP	Alkaline phosphatase
ANOVA	Analysis of variance
AUC	Area under the curve
AUMC	Area under the moment curve
bp	Base pair
BSA	Bovine serum albumin
BUN	Blood urea nitrogen
CBC	Complete blood count
cDNA	Complementary DNA
CK	Carbon counts
C <sub>L</sub>	Clearance
CPPA	3-(4-cyclohexylpiperazine-1-yl) propyl amine
CRP	C-Reactive Protein
CRPC	Castration-resistant prostate cancer
DAPI	4',6-diamidino-2-phenylindole
DCM	Dichloromethane
DDS	Drug delivery system
DMEM	Dulbecco's Modified Eagle Medium
DMSO	Dimethyl Sulfoxide
DNA	Deoxyribonucleic Acid

DRE	Digital rectal examination
DTA	Data Transfer Assistance
DTX	Docetaxel
EDC	1-(3-dimethylaminopropyl)-3-ethylcarbodiimide hydrochloride
EDCs	Endocrine disrupting chemicals
EDTA	Ethylenediamine tetraacetic acid
EDX	Energy dispersive X-Ray
ELISA	Enzyme-linked immunosorbent assay
EMA	European Medicines Agency
EPR	Enhanced permeability and retention
FACS	Fluorescence Activated Cell Sorter
FBS	Fetal bovine serum
FDG	Fluorodeoxyglucose
FESEM	Field emission scanning electron microscopy
FITC	Fluorescein Isothiocyanate
FTIR	Fourier Transform Infrared Spectroscopy
g	gram
GAPDH	Glyceraldehyde-3-phosphate dehydrogenase
GTP	Guanosine triphosphate
HRP	Horseradish peroxidase
I.D	Injected dose
I.V.	Intravenous
IC <sub>50</sub>	Inhibitory Concentration
ICH	International Council for Harmonization
ISO/TR	International Organization for Standardization/Technical Report
KBr	Potassium bromide
K <sub>D</sub>	Dissociation constant
kDa	Kilo Dalton
LC-MS/MS	Liquid Chromatography and Mass Spectroscopy
L <sub>D</sub>	Lethal dose

LPO	Lipid peroxidation
mAbs	Monoclonal antibodies
MBq	Megabecquerel
mCRPC	Metastatic Castration-Resistant Prostate Cancer
MDR	Multidrug resistance
mg	milligram
ml	milliliter
Mm	Millimetre
MNU	N-nitroso-N-methyl urea
mRNA	Messenger ribonucleic acid
MRI	Magnetic Resonance Imaging
MRT	Mean residence time
MST	Mean survival time
MTD	Maximum tolerated dose
MTT	3-(4,5-dimethylthiazol-2-yl)-2,5-diphenyltetrazolium bromide
mV	Millivolt
ng	Nanogram
NHS	N-hydroxysuccinimide
NIN	National Institution of Nutrition
NK	Nitrogen counts
nM	Nanomolar
nm	Nanometer
NPs	Nanoparticles
NSCLC	Non small cell lung cancer
OD	Optical density
OK	Oxygen counts
PAHs	Polycyclic aromatic hydrocarbons
PBS	Phosphate buffer saline
PCa	Prostate cancer
PCL	Polycaprolactone
PDI	Polydispersity index

PDLA	Poly D-lactic acid
PET-CT	Positron Emission Tomography
PGA	Polyglycolic acid
PHI	Prostate health index
PI	Propidium iodide
PIN	Prostatic intraepithelial neoplasia
PLGA	Poly Lactic Co-Glycolic Acid
PLLA	Poly L-lactic acid
PSA	Prostate-Specific Antigen
PSMA	Prostate-Specific Membrane Antigen
PVA	Polyvinyl alcohol
R <sup>2</sup>	Coefficient of determination
RES	Reticuloendothelial system
RH	Relative humidity
RIPA buffer	Radioimmunoprecipitation assay buffer
RLT	Radioligand therapy
ROS	Reactive oxygen species
RPM	Rotation per minute
RPMI	Roswell Park Memorial Institute Medium
RT-PCR	Real-time reverse transcriptase-polymerase chain reaction
SCLC	Small cell lung cancer
SD	Standard deviation
SELEX	Systematic evolution of ligands by exponential enrichment
SGPT	Serum Glutamic Pyruvic Transaminase
SK	Sulphur counts
SNPs	Single-nucleotide-polymorphisms
STDs	Sexually transmitted diseases
t <sub>1/2</sub>	Half-life
TBARS	Thiobarbituric acid reactive substance
TEM	Transmission Electron Microscopy
TGF- $\alpha$	Transforming growth factor-alpha

TKIs	Tyrosine kinase inhibitors
TMB	Tetramethylbenzidine
TRUS	Transrectal ultrasound scan
USFDA	United States Food and Drug Administration
UV/vis	Ultraviolet-visible spectroscopy
v/v	Volume/volume
VEGF	Vascular endothelial growth factor
V <sub>ss</sub>	Steady State Volume Distribution
w/v	Weight/volume
WHO	World Health Organization
XPS	X-ray photoelectron spectroscopy
$\lambda_{\text{max}}$	Wavelength of maximum absorbance
$\mu\text{g}$	Microgram
$\mu\text{l}$	Microliter
$\mu\text{M}$	Micromolar

# CONTENTS

Chapter		Page No.
Chapter 1	<b>Introduction</b>	<b>1-30</b>
	1.1. Prostate cancer	1
	1.2. Epidemiology of prostate cancer risk	2-3
	1.3. Endogenous risk factors	3-5
	1.3.1. Family history	4
	1.3.2. Hormones	4
	1.3.3. Race	4
	1.3.4. Aging and oxidative stress	4-5
	1.4. Exogenous risk factors	5-6
	1.4.1. Diet	5
	1.4.2. Environmental agents	5-6
	1.4.3. Occupation and other factors	6
	1.5. Symptoms of prostate cancer	6-8
	1.5.1. Urinary symptoms	7
	1.5.2. Blood in semen or urine	7
	1.5.3. Pain and discomfort	7
	1.5.4. Erectile dysfunction	7
	1.5.5. Fatigue and weight loss	7-8
	1.6. Advanced prostate cancer symptoms	8
	1.7. Diagnosis of prostate cancer	8-11
	1.7.1. Digital rectal examination (DRE)	8-9
	1.7.2. Prostate-specific antigen (PSA) test	9
	1.7.3. Free PSA test	9
	1.7.4. Biomarker tests	9
	1.7.5. Transrectal ultrasonography (TRUS) and biopsies	10
	1.7.6. MRI fusion biopsy	10
	1.7.7. Positron emission tomography (PET) or PET-CT scan	10-11

	1.8. Grading and stages of prostate cancer	11-12
	1.8.1. Gleason score for grading prostate cancer	11-12
	1.9. Stage groups for prostate cancer	12-13
	1.10. Various treatment options	13-16
	1.10.1. Chemotherapy	13-14
	1.10.2. Compounds targeting androgen signalling	14
	1.10.3. Signaling pathway inhibitors	14-15
	1.10.4. DNA damage repair pathway	15-16
	1.10.5. Targeted alpha therapy approach	16
	1.11. Androgen receptor and signalling	16-17
	1.12. Cytochrome P17 enzyme	18
	1.13. Abiraterone acetate and its mechanism of action	18
	1.14. Aptamer and its importance in prostate cancer therapy	19-20
	1.15. PSMA as a target in prostate cancer	20-22
	1.16. Aptamer-conjugated PLGA nanoparticles for prostate cancer therapy.	22-24
	1.17. References	25-30
<b>Chapter 2</b>	<b>Literature Review</b>	<b>31-50</b>
	2. Prostate cancer	31
	2.1. Characteristics features of prostate cancer	31-34
	2.1.1. Correlation with aging	31-35
	2.1.2. Environmental factors	32
	2.1.3. Familial inheritance	32
	2.1.4. Role of steroid hormones	32
	2.1.5. Diet	32
	2.1.6. Obesity	33
	2.1.7. Sexual behaviour and sexually transmitted diseases (STDs)	33
	2.1.8. Occupation	33
	2.1.9. Smoking	33-34



	2.2. Different treatments for prostate cancer	34-37
	2.2.1. Active Surveillance	34
	2.2.2. Radical prostatectomy	34
	2.2.3. Cryotherapy	34
	2.2.4. Radiation	35
	2.2.5. Hormonal therapy	35
	2.2.6. Abiraterone	35-36
	2.2.7. Chemotherapy	36
	2.2.8. Docetaxel	36
	2.2.9. Cabazitaxel	36
	2.2.10. Enzalutamide	36-37
	2.3. Nanoparticle-based drug delivery for the treatment of cancer	37-38
	2.4. PLGA nanoparticles for prostate cancer therapy	38-40
	2.5. Prostate cancer-targeted therapies using surface-modified nanoparticles	40-42
	2.6. Aptamer-conjugated PLGA nanoparticles and prostate cancer	43
	2.7. References	44-50
<b>Chapter 3</b>	<b>Objectives and Plan of Study</b>	<b>51-53</b>
	3.1. Objectives	51
	3.2. Plan of study	52-53
<b>Chapter 4</b>	<b>Materials and Equipment</b>	<b>55-60</b>
	4.1. Chemicals used in the study	55-57
	4.2. Animals and different cells used in the study	58
	4.3. Instruments	58-60
<b>Chapter 5</b>	<b>Methodology</b>	<b>61-80</b>
	5.1. Preparation of PLGA nanoparticles containing abiraterone acetate	61
	5.2. Selection of aptamer	61-62
	5.3. Conjugation of aptamer on the surface of nanoparticles	62-63
	5.4. Drug excipient interaction study using Fourier Transform Infrared Spectroscopy (FTIR)	63

5.5. Determination of particle size and zeta potential	63-64
5.6. Determination of surface morphology by Field emission scanning electron microscopy (FESEM), Atomic force microscopy (AFM), and High-resolution transmission electron microscopy (HR-TEM)	64
5.7. X-ray photoelectron spectroscopy (XPS)	64-65
5.8. Analysis of aptamer-PSMA interactions by molecular docking	65
5.9. Percentage of drug loading and encapsulation efficiency	65-66
5.10. Stability of the nanoparticles	66
5.11. Hydrolytic stability study	66-67
5.12. <i>In vitro</i> drug release study	67
5.13. <i>In vitro</i> cellular uptake analysis by flow cytometry (FACS) and confocal microscopy	67-68
5.14. <i>In vitro</i> cell cytotoxicity assay	68-69
5.15. Apoptosis assay	69-70
5.16. Mitochondrial membrane depolarization analysis using JC-1	70
5.17. Clonogenic assay for the prostate cancer cell line	70-71
5.18. <i>In vivo</i> animal studies	71
5.19. Pharmacokinetic study	71-72
5.20. Hemolysis study	72
5.21. Biodistribution study and gamma scintigraphy imaging	72-73
5.22. Development of prostate cancer in mice, treatment undergone, and histopathological assessment	73-75
5.23. Efficacy of aptamer-conjugated nanoparticles on LNCaP tumor spheroids	75
5.24. Hematological Evaluations	75-76
5.25. Estimation of serum-specific toxicity markers	76
5.26. Statistical analysis	76
5.27. References	77-80

<b>Chapter 6</b>	<b>Results and Discussion</b>	<b>81-126</b>
	6.1. The UV absorption spectrum of Abiraterone acetate (ABR)	81-82
	6.2. The calibration curves of ABR	82-83
	6.3. Drug-excipient interaction by FTIR analysis	83-85
	6.4. X-ray photoelectron spectroscopy (XPS)	85-86
	6.5. Aptamer conjugation on the surface of nanoparticles through agarose gel electrophoresis	86
	6.6. Aptamer-PSMA interactions study by molecular docking	87-88
	6.7. Determination of particle size and zeta potential	88-89
	6.8. <i>In-vitro</i> drug release study	89-97
	6.9. Surface morphology by Field emission scanning electron microscopy (FESEM), High-resolution transmission electron microscopy (HRTEM), and Atomic force microscopy (AFM)	97-98
	6.10. Drug loading and entrapment efficiency	98-99
	6.11. Stability study of the nanoparticles	99-100
	6.12. Hydrolytic stability study	100-101
	6.13. <i>In vitro</i> cellular uptake analysis by flow cytometry and confocal microscopy	101-104
	6.14. <i>In vitro</i> cytotoxicity assay	104-105
	6.15. Apoptosis assay	105-107
	6.16. Mitochondrial membrane depolarization analysis using JC-1	107
	6.17. <i>In vitro</i> colony formation assay	107-108
	6.18. Hemolysis study	108-109
	6.19. Pharmacokinetics study	109-111
	6.20. Biodistribution study and gamma scintigraphy imaging	111-113
	6.21. Antitumor activity study	114-116
	6.22. Efficacy of Apt-ABR-NP on tumor spheroid model	117-118
	6.23. Hematological evaluations	118-119
	6.24. Estimation of serum-specific toxicity markers	120-122
	6.25. References	123-126

<b>Chapter 7</b>	<b>Conclusion</b>	<b>127</b>
<b>Chapter 8</b>	<b>Summary</b>	<b>129-132</b>
	<b>Annexure</b>	
	<b>Publications</b>	
	<b>Presentation in National/International Conferences</b>	

## LIST OF FIGURES

Figure No.	Legend	Page No
<b>Figure 1</b>	Anatomy of the prostate gland and prostate cancer	<b>2</b>
<b>Figure 2</b>	Figure shows the evaluation criteria and characteristics of a low or intermediate-favorable risk prostate cancer versus intermediate-unfavorable or high-risk prostate cancer.	<b>3</b>
<b>Figure 3</b>	Symptoms of prostate cancer	<b>8</b>
<b>Figure 4</b>	Different stages of prostate cancer	<b>13</b>
<b>Figure 5</b>	Chemical structure of abiraterone acetate	<b>18</b>
<b>Figure 5.1</b>	Schematic representation of aptamer conjugation process to the surface of the polymeric nanoparticles containing ABR	<b>63</b>
<b>Figure 6</b>	This diagram shows a general pictorial representation of transmembrane glycoprotein prostate-specific membrane antigen, PSMA	<b>21</b>
<b>Figure 7</b>	Schematic diagram of the aptamer-PSMA binding through conformational recognition	<b>23</b>
<b>Figure 6.1</b>	The UV absorption maxima of ABR in acetonitrile: dichloromethane (3:1) showing $\lambda_{\max}$ at 253.0 nm.	<b>81</b>
<b>Figure 6.2</b>	The UV absorption maxima of ABR in ethanol: PBS (pH 7.4) mixture (1:3) showing $\lambda_{\max}$ at 253.0 nm.	<b>82</b>
<b>Figure 6.3</b>	Calibration curve of ABR in ethanol: PBS (pH 7.4)	<b>83</b>
<b>Figure 6.4</b>	FTIR spectra of different excipients, drug, and formulations. FTIR spectra of PLGA, Abiraterone acetate (ABR), physical Mixture of excipients (PM), blank nanoparticles (BL-NP), PLGA nanoparticles containing Abiraterone acetate (ABR-NP), and aptamer-conjugated PLGA nanoparticles (Apt-ABR-NP)	<b>84</b>

<b>Figure 6.5</b>	Aptamer conjugation assessed by X-ray photoelectron spectroscopy study, and agarose gel electrophoresis. (A) XPS graph for combined ABR-NP and Apt-ABR-NP, (B) XPS graph for enlarged N1s peak of Apt-ABR-NP, (C) XPS graph for enlarged N1s peak of ABR-NP, (D) Aptamer conjugation to ABR-NP using agarose gel electrophoresis.	<b>86</b>
<b>Figure 6.6</b>	Aptamer-PSMA binding by molecular docking. (A) Aptamer-PSMA (Protein data bank, PDB: 1Z8L) interactions by hydrogen bonding through molecular docking; (B) Aptamer-PSMA (PDB: 1Z8L) hydrophobic interactions through molecular docking	<b>88</b>
<b>Figure 6.7</b>	Determination of particle size and zeta potential of the experimental nanoparticles. (A) represents particle size distribution of ABR-NP and Apt-ABR-NP (B) represents zeta potential values of ABR-NP and Apt-ABR-NP.	<b>89</b>
<b>Figure 6.8</b>	<i>In vitro</i> drug release study of the experimental nanoparticles in phosphate buffer saline (PBS pH-7.4), PBS containing 1% $\beta$ -hydroxy-cyclodextrin, acetate buffer (pH 5), bicarbonate buffer (pH 10) and citrate buffer (pH 3)	<b>91</b>
<b>Figure 6.9</b>	<i>In vitro</i> drug release kinetics in Phosphate-buffered saline (PBS, pH 7.4) using various kinetic models. (A) Zero order kinetics, (B) 1 <sup>st</sup> order kinetics, (C) Higuchi model of kinetics, (D) Korsemeyer-peppas model of kinetics, and (E) Hixson Crowell model of kinetics.	<b>93</b>
<b>Figure 6.10</b>	<i>In vitro</i> drug release kinetics in Phosphate-buffered saline (PBS, pH 7.4) with $\beta$ -cyclodextrin using various kinetic models. (A) Zero order kinetics, (B) 1 <sup>st</sup> order kinetics, (C) Higuchi model of kinetics, (D) Korsemeyer-peppas model of kinetics, and (E) Hixson Crowell model of kinetics.	<b>94</b>

<b>Figure 6.11</b>	<i>In vitro</i> drug release kinetics in acetate buffer (pH 5) using various kinetic models. (A) Zero order kinetics, (B) 1 <sup>st</sup> order kinetics, (C) Higuchi model of kinetics, (D) Korsemeyer-peppas model of kinetics, and (E) Hixson Crowell model of kinetics.	<b>95</b>
<b>Figure 6.12</b>	<i>In vitro</i> drug release kinetics in citrate buffer (pH 3) using various kinetic models. (A) Zero order kinetics, (B) 1 <sup>st</sup> order kinetics, (C) Higuchi model of kinetics, (D) Korsemeyer-peppas model of kinetics, and (E) Hixson Crowell model of kinetics.	<b>96</b>
<b>Figure 6.13</b>	<i>In vitro</i> drug release kinetics in bicarbonate buffer (pH 10) using various kinetic models. (A) Zero order kinetics, (B) 1 <sup>st</sup> order kinetics, (C) Higuchi model of kinetics, (D) Korsemeyer-peppas model of kinetics, and (E) Hixson Crowell model of kinetics.	<b>97</b>
<b>Figure 6.14</b>	Electron microscopic imaging and atomic force microscopic evaluation of the experimental nanoparticles. (A & B) represents the FESEM images of ABR-NP and Apt-ABR-NP respectively, (C) HR-TEM image of Apt-ABR-NP and (D & E) depicts AFM images of Apt-ABR-NP.	<b>98</b>
<b>Figure 6.15</b>	Surface morphology, drug content, particle size and hydrolytic degradation of the nanoparticles for the stability study. (A) The formulations stored at 30 °C, 75% R.H for 45 days and 90 days and (B) at 40 °C, 75% R.H for 45 days and 90 days, respectively. (C) Drug content of the stored formulations, (D) Mean particle size (E) Hydrolytic stability study of Apt-ABR-NP in various buffers. The bar diagram and graph data are the average of the three individual experiments demonstrated as mean ± SD. The statistical level of significance is considered as p<0.05, analyzed by Student's t-test.	<b>100</b>

<b>Figure 6.16</b>	Cellular uptake study (A) FACS histogram PC3 cells after the treatment with ABR-NP and Apt-ABR-NP at 6 h and 12 h. (B) FACS histogram LNCaP cells after the treatment with ABR-NP and Apt-ABR-NP at 6 h and 12 h. (C) Confocal laser microscopy images of PC3 cells at 12 h after the treatment with ABR-NP and Apt-ABR-NP. (D) Confocal laser microscopic images of LNCaP cells at 12 h after the treatment with ABR-NP and Apt-ABR-NP.	<b>103</b>
<b>Figure 6.17</b>	Cell cytotoxicity, apoptosis, and mitochondrial membrane depolarization assay of ABR, ABR-NP, and Apt-ABR-NP evaluated in vitro. (A) IC <sub>50</sub> values of ABR, ABR-NP, and Apt-ABR-NP on LNCaP and (B) PC3 cells after 48 h of treatment (Data show mean $\pm$ SD, n=3). (C) Induction of apoptosis in LNCaP cells after treatment with ABR, ABR-NP, and Apt-ABR-NP for 48 h. (D) Mitochondrial membrane depolarization after 48 hours of treatment, with ABR, ABR-NP, and Apt-ABR-NP for 48 h.	<b>105</b>
<b>Figure 6.18</b>	<i>In vitro</i> evaluation of cellular uptake, cytotoxicity, and apoptosis in 22Rv1 Cells (A) FACS histogram for cellular uptake measurement after the treatment with ABR-NP and Apt-ABR-NP at 6 h and 12 h. (B) IC <sub>50</sub> values of ABR, ABR-NP, and Apt-ABR-NP on 22Rv1 cells and (C) Induction of apoptosis in 22Rv1 cells after treatment with ABR, ABR-NP, and Apt-ABR-NP for 48 h.	<b>106</b>



<b>Figure 6.19</b>	<p>Clonogenic assay with LNCaP cells using ABR, ABR-NP, and Apt-ABR-NP for 14 days after treatment, changing the media and treatments in every three days. (A) More growth in untreated (control) was followed by ABR, ABR-NP, or Apt-ABR-NP treated LNCaP cells. (B) Absorbance values of untreated (control) and ABR, ABR-NP, or Apt-ABR-NP treated LNCaP cells, after crystal violet staining, represent the colonies' density. Values represent mean <math>\pm</math>SD (n=3), Where <math>p &lt; 0.05</math> is the statistical level of significance, compared against the control value as assessed by Student's t-test.</p>	<b>108</b>
<b>Figure 6.20</b>	<p>Hemolytic activity of developed nanoparticles. Hemolytic activity of ABR, ABR-NP, and Apt-ABR-NP was measured by incubating each sample for 1 hour at 37°C with red blood cells and measuring the amount of hemoglobin released. The percentage of hemolysis was plotted against the concentration of the samples. Data show mean <math>\pm</math>SD (n=3) where <math>p &lt; 0.05</math> is the statistical level of significance as assessed by Dunnett's test (compared against control group)</p>	<b>109</b>
<b>Figure 6.21</b>	<p>Pharmacokinetic profile of ABR, ABR-NP, and Apt-ABR-NP was assessed in mice by measuring the concentration of ABR from each sample in the bloodstream over time. The data were plotted as the mean concentration of each sample at each time point. Error bars indicate standard deviation (n=3). * marks represent significant values (<math>p &lt; 0.05</math>) when ABR-NP and Apt-ABR-NP were compared with ABR through the Two-Way ANOVA test, and the statistical significance of data was analyzed through Bonferroni's post-test</p>	<b>110</b>

<b>Figure 6.22</b>	Biodistribution study of radiolabelled nanoparticles in various organs using gamma scintigraphic imaging. Radiolabelled nanoparticles (99mTc-ABR-NP and 99mTcApt-ABR-NP) were injected into mice via tail vein, and gamma scintigraphic images were acquired at different time points (1, 2, and 5 hours post-injection) using a gamma camera. Arrows indicate the prostate region in the mice.	<b>113</b>
<b>Figure 6.23</b>	Anti-tumor efficacy of ABR, ABR-NP, and Apt-ABR-NP in prostate cancer (PCa) tissues. Histological examination of prostate cancer tissues and normal prostate tissues was performed using hematoxylin and eosin (HE) staining. Representative images of prostate cancer tissues and normal prostate tissues are shown. The expression of Ki67, a marker of cell proliferation, in prostate cancer tissues and in the normal prostate tissue sections was analyzed by immunohistochemistry. The staining/immunohistochemistry and magnification of the photographs done are mentioned above each column.	<b>116</b>
<b>Figure 6.24</b>	LNCaP tumor spheroid with or without the treatment of Apt-ABR-NP. Scale bars 100 $\mu$ m.	<b>117</b>
<b>Figure 6.25</b>	Estimation of serum-specific hepatic and nephrotic toxicity markers. (A) Aspartate transaminase (AST) enzyme levels of the various groups (B) Alanine transaminase (ALT) enzyme levels of the various groups (C) Alkaline phosphatase (ALP) enzyme levels of the various groups (D) Creatinine blood levels of the various groups, and (E) Blood Urea Nitrogen (BUN) levels of the various groups	<b>122</b>

LIST OF TABLES

Table No.	Legend	Page No.
Table 1	Aptamer-PSMA binding using molecular docking analysis	87
Table 2	Regression coefficient ( $R^2$ ) values of the data of <i>in vitro</i> drug release tested on various kinetic models	92
Table 3	Composition of experimental nanoparticles and their drug encapsulation efficiencies	99
Table 4	Pharmacokinetic parameters of ABR, ABR-NP, and Apt-ABR-NP in Swiss Albino mice following intraperitoneal administration (400µg/kg).	111
Table 4.1	List of materials/chemicals used in the study	55-57
Table 4.2	The source of animals and different cells used in the study	58
Table 4.3	List of instruments and equipment used in the study	58-60
Table 5	Biodistribution of $^{99m}\text{Tc}$ -ABR-NP and $^{99m}\text{Tc}$ -Apt-ABR-NP in testosterone/MNU-induced prostate cancer-bearing mice.	112
Table 6	CBC profile of experimental animals before and after treating with carcinogen/ nanoparticle formulations.	119
Table 7	Estimation of serum-specific markers of the experimental animals	120



## **1. Introduction**

### **1.1. Prostate cancer**

The prostate, approximately the size of a walnut, is a gland situated behind the penis, in front of the rectum, and below the bladder. It encloses the urethra, which is responsible for transporting urine and sperm through the penis. The primary role of the prostate is to produce seminal fluid, which protects, supports, and carries sperm. Prostate cancer is a medical condition that arises when healthy cells in the prostate gland start to mutate and multiply uncontrollably, leading to the formation of a lump known as a tumor (Gandhi et al., 2018; Chatterjee 2003). This tumor can be benign, meaning it won't spread, or will not be malignant. Some prostate tumors grow slowly and can remain asymptomatic for several years. Metastasis is a process where prostate cancer cells spread to other parts of the body through the circulation or lymphatic system. Though prostate cancer can spread to any area of the body, it usually spreads to the regional lymph nodes first, which are tiny, bean-shaped organs that help fight infection surrounding the prostate. Prostate cancer can also spread to other parts of the body, such as the lungs, liver, and bones (Jacobs et al., 1983; Arya et al., 2006). Nevertheless, it is distinct from other forms of cancer because many prostate tumors do not spread beyond the prostate. Even if they do, metastatic prostate cancer is commonly treatable, allowing patients to lead a good quality of life for many years following diagnosis.

As the landscape of prostate cancer research continues to evolve, ongoing efforts persist in improving early detection methods, refining treatment algorithms, and unraveling the molecular mechanisms underlying disease progression and resistance. Emerging technologies, such as liquid biopsy and advanced imaging techniques, hold promise in enhancing diagnostic accuracy and prognostication. At the same time, novel therapeutic strategies, including targeted therapies and immunomodulation, offer new avenues for personalized and precision medicine approaches. Collaborative initiatives aimed at enhancing public awareness, promoting screening uptake, and advocating for equitable access to healthcare services strive to reduce the burden of prostate cancer on individuals, families, and communities worldwide. Therefore, the advancement of understanding and application of these novel and emerging technologies, along with the development of collaborative strategies, will significantly impact the future of prostate cancer research, diagnosis, treatment, and prevention.

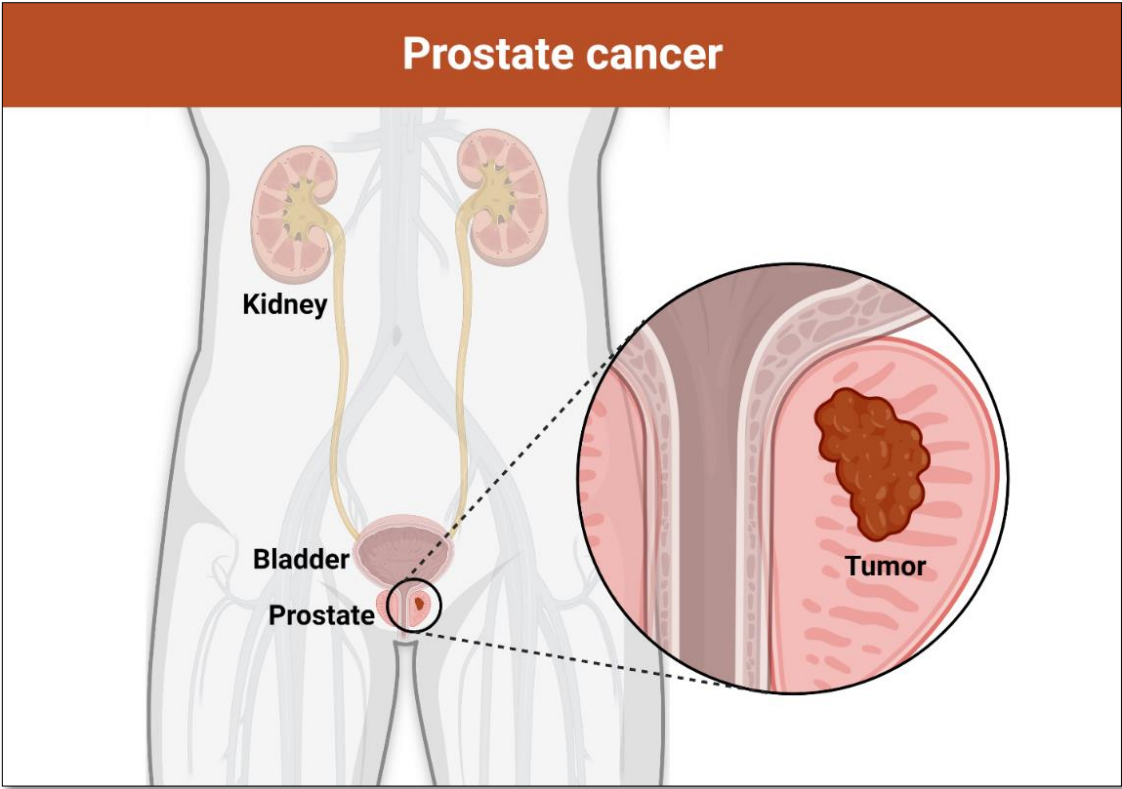


**Figure 1:** Anatomy of the prostate gland and prostate cancer

**1.2. Epidemiology of prostate cancer risk**

Studies using epidemiologic methods have yielded the most information to date about prostate cancer risk. Nevertheless, epidemiology is a very unrefined method for investigating what can turn out to be an exceptionally intricate etiology. The majority of these studies had complex issues with disease definition and exposure.

Over the past half-century, there has been a rise in the incidence of prostate cancer. The recent sharp increases in prostate cancer cases are probably the result of early detection techniques, such as measuring serum PSA, rather than natural variations in underlying risk. The incidence of clinically detectable prostate cancer varies widely between countries, although lead-time, case identification, detection, and reporting biases skew comparisons. In contrast to clinical incidence, the age-specific prevalence of prostate cancer discovered after autopsy is comparatively consistent across nations and ethnicities. Recent research reports that the rate of prostate cancer incidence can reach 80% by the age of 80 (Bostwick et al., 2004; Gann et al., 2002).

Benign prostatic hyperplasia (BPH) and prostatic intraepithelial neoplasia (PIN), a possible precursor to cancer, have some common characteristics with prostate cancer. All respond to

androgen-deprivation therapy, all become more common as hosts' age, and all depend on androgens for growth and development. Progressive disruption of the basal cell layer, abnormalities in secretory differentiation markers, increasing nuclear and nucleolar alterations, increasing cell proliferation, variation in DNA content, and increasing genetic instability are the hallmarks of the continuum that ends in high-grade PIN and early invasive cancer. As benign prostatic epithelium progresses to high-grade PIN and cancer, some biomarkers are up-regulated or gain-regulated, while others are down-regulated or lose-regulated. Compared to normal prostatic tissue, PIN, and carcinoma exhibit a markedly higher microvessel density (Bostwick, 1995; Sakr et al., 2001).

Some risk variables, such as race, aging, and oxidative stress, are not purely endogenous or exogenous; they can be categorized as such. However, some factors might exhibit both exogenous and endogenous influences, and those cases are addressed.

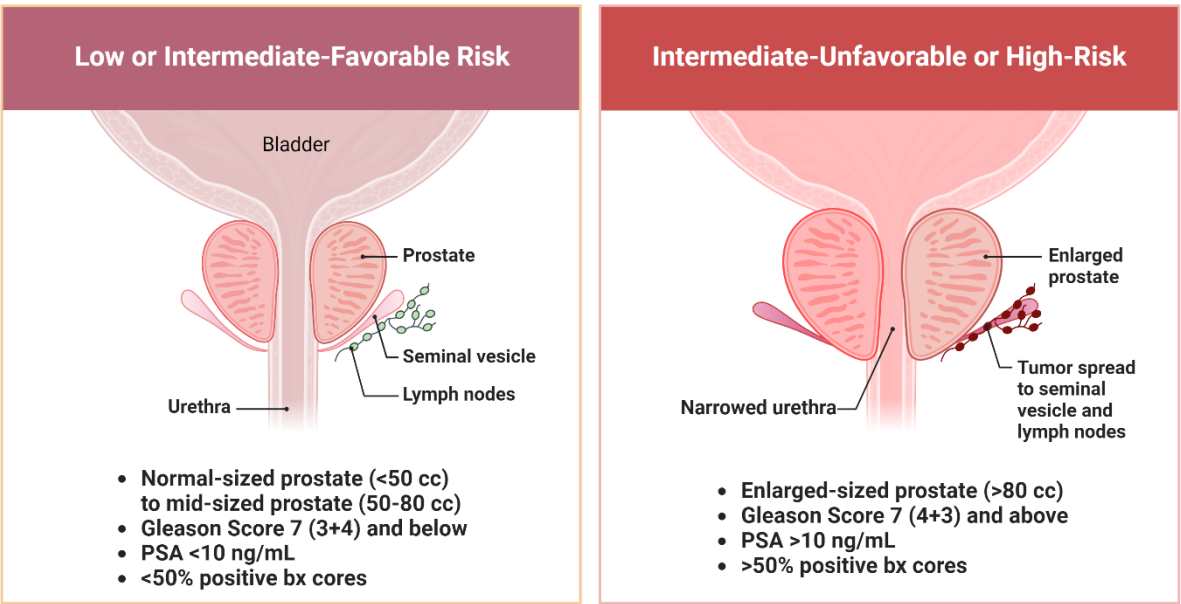


**Figure 2:** Figure shows the evaluation criteria and characteristics of a low or intermediate-favorable risk prostate cancer versus intermediate-unfavorable or high-risk prostate cancer.

**1.3. Endogenous risk factors**

Endogenous risk factors for prostate cancer relate to factors that originate within the body and lead to an increased possibility of acquiring prostate cancer (Farmer et al., 2008). These elements are generally tied to genetics, hormones, and an individual's biological traits. Here are several significant endogenous risk factors for prostate cancer:

### **1.3.1. Family history**

Epidemiological investigations have established a strong correlation between family history and the incidence of prostate cancer. However, this association may be susceptible to detection bias. Familial cancer shares many clinical and pathologic characteristics with nonfamilial cancer. Men who have a family history of prostate cancer, particularly fathers, brothers, grandfathers, or uncles, are at a higher risk of developing the condition. Moreover, recent research has identified a defective gene in some men whose mothers or sisters have had breast cancer, which may also elevate the risk. Notably, inherited genetic abnormalities are estimated to be causative in only a minor subset, approximately 5-10%, or less than 1 in 10, in the case of prostate cancer (Brook et al., 2023; Steinberg et al., 1990).

### **1.3.2. Hormones**

Androgens are known to exert a significant influence on prostate cancer growth rates. The progression of prostate cancer from preclinical to clinically relevant forms may, in part, be attributed to the altered metabolism of androgens. Prolonged exposure to elevated quantities of testosterone and its metabolite, dihydrotestosterone, has been associated with an increased risk of prostate cancer, although findings of the studies on this subject have been inconsistent. It is important to note that hormone levels may be influenced by both endogenous and exogenous factors, such as genetics and exposure to environmental substances that affect hormone action respectively (Bostwick et al., 2004).

### **1.3.3. Race**

Race-based variations in the risk of prostate cancer can be attributed to three things: exposure variations, such as food variations (exogenous variables); detection variations, which also reflect exogenous factors; and genetic variations (endogenous factors). African-American males have the highest incidence rates of prostate cancer worldwide, and their risk is higher than that of white men. Racial disparities, however, could also be caused by variations in exogenous factors such as access to care, decision-making regarding seeking medical attention and follow-up, polymorphic variation, or allelic frequencies of microsatellites at the androgen receptor (AR) locus (Bostwick et al., 2004).

### **1.3.4. Aging and oxidative stress**

Although there is little evidence to support the theory, an increase in oxidative stress may lead to prostate cancer. According to clinical research, consuming antioxidants, including lycopene



(a carotenoid), vitamin E ( $\alpha$ -tocopherol), and selenium, can protect against prostate cancer. The relationship between aging and the peroxidation-antioxidation homeostasis of the human prostate is still essentially unknown (Bostwick et al., 2004; Farmer et al., 2008).

## **1.4. Exogenous risk factors**

### **1.4.1. Diet**

Numerous dietary factors have been linked to the development of prostate cancer, as evidenced by historical studies, geographic differences, and descriptive epidemiologic studies of migrants (Bostwick et al., 2004; Gann et al., 2002). Consuming fat, particularly polyunsaturated fat, is strongly correlated with the incidence and mortality of prostate cancer. This association may be due to the changes in hormone profiles brought on by fat, the impact of fat metabolites as protein or DNA-reactive intermediates, or the increase in oxidative stress brought on by fat. Retinoids, such as vitamin A, favorably correlate with the risk of prostate cancer and aid in controlling the differentiation and proliferation of epithelial cells. Although vitamin C scavenges free radicals and reactive oxygen species (ROS), there is no reliable correlation between vitamin C intake and the incidence of prostate cancer. Prostate cancer may be predisposed to vitamin D insufficiency; 1-25-dihydroxyvitamin D (the hormone form) exerts antiproliferative and antidifferentiative actions on prostate cancer and decreases invasiveness. In a significant, controlled clinical trial from Finland, daily intake of vitamin E ( $\alpha$ -tocopherol), an antioxidant that suppresses the growth of prostate cancer cells by apoptosis, decreased the incidence of prostate cancer by 32% (Lim et al., 2023). The prostate has a higher zinc concentration (Zn) than any other organ in the body. Prostate cancer patients have a 90% reduction in zinc content, although there is unclear evidence linking dietary zinc intake to an increased risk of prostate cancer. Although there is little evidence to support a chemopreventive role for selenium in humans, it is an essential trace element that suppresses cancers caused by animal chemicals and viruses. Prostate cancer risk is not significantly correlated with alcohol consumption. There is no proof that cruciferous vegetable consumption protects against prostate cancer, but it is linked to a lower risk of many other malignancies. Lycopene, the most effective carotenoid antioxidant and a common ingredient in tomato-based products, offers a substantial protective impact (Shirai et al., 2002; Kooiman et al., 2000).

### **1.4.2. Environmental agents**

Endocrine-disrupting chemicals (EDCs) have emerged as a prominent environmental agent that can impact the endocrine system of living organisms. EDCs are known to affect hormone action

positively or negatively, thereby leading to varied impacts on reproductive and developmental processes, as well as carcinogenesis, particularly in reproductive organs. EDCs have been found to affect the activity of estrogen, androgen, and thyroid hormones, with a majority of well-studied EDCs acting as estrogen agonists that bind to the estrogen receptor (ER). However, some EDCs can also affect other hormone functions. For instance, the active metabolite of the pesticide vinclozolin has been shown to act as an androgen antagonist that binds to the AR and reduces the expression of androgen-regulated genes. Similarly, an androgen agonist has been detected in water downstream of pulp mills. Common sources of EDCs include pesticide residues on food, chemicals used in plastic production, and phytoestrogens found in food products such as soy. EDC exposure can occur through food or water consumption or inhalation. Although high-level estrogen agonist exposure is rare, males may be regularly exposed to various EDCs. Groups or individuals with relatively high endogenous estrogen or androgen concentrations may be particularly vulnerable to EDC exposure, as it may supplement endogenous action. Some epidemiological studies have linked cadmium, a major environmental pollutant, to prostate cancer, although the findings are not conclusive. It is noteworthy that zinc may alter cadmium's carcinogenic potential. (Kooiman et al., 2000; Bostwick et al., 2004).

### **1.4.3. Occupation and other factors**

The risk of prostate cancer has been linked to several industrial and occupational exposures, although the results have been mixed. The two most important concerns are farming and, to a lesser extent, working in the rubber sector. Many other factors, such as energy intake, sexual activity, marital status, vasectomy, social factors (lifestyle, socioeconomic factors, and education), physical activity, and anthropometry, have also shown conflicting results, negative associations, or minimal data with prostate cancer risk (Elghany et al., 1990).

### **1.5. Symptoms of prostate cancer**

Although it is one of the most common tumors in men, prostate cancer in its early stages sometimes exhibits no symptoms. When symptoms arise, they might differ significantly from one another and sometimes indicate illnesses other than cancer. It is noteworthy that the manifestation of these symptoms does not inevitably indicate prostate cancer; however, they need to trigger a visit to a medical professional for additional assessment.

The following is a thorough explanation of the symptoms and indicators of prostate cancer:

**1.5.1. Urinary symptoms:**

Urinary difficulty: Prostate cancer can enlarge the prostate gland, which makes it difficult to urinate and to stop urinating (Eskra et al., 2019).

Increased frequency of urination, particularly at night: Prostate cancer may be indicated by increased frequency of urination, particularly during the night (nocturia).

**1.5.2. Blood in semen or urine:**

Hematuria: While there are other possible causes, blood in the urine can indicate prostate cancer.

Though less frequent, blood in semen might be a sign.

**1.5.3. Pain and discomfort:**

Pelvic pain is one type of pain and discomfort that some men with prostate cancer may feel.

Bone pain: Prostate cancer that has progressed to an advanced stage may radiate to the bones, mainly affecting the hips, spine, and pelvis.

**1.5.4. Erectile dysfunction:**

Difficulty getting or keeping an erection: Blood vessels and nerves involved in the erectile process might be impacted by prostate cancer.

**1.5.5. Fatigue and weight loss:**

Fatigue: One sign could be a chronic weariness that does not go away with rest.

Unintentional weight loss: Prostate cancer in its advanced stages may cause unintentional weight reduction.

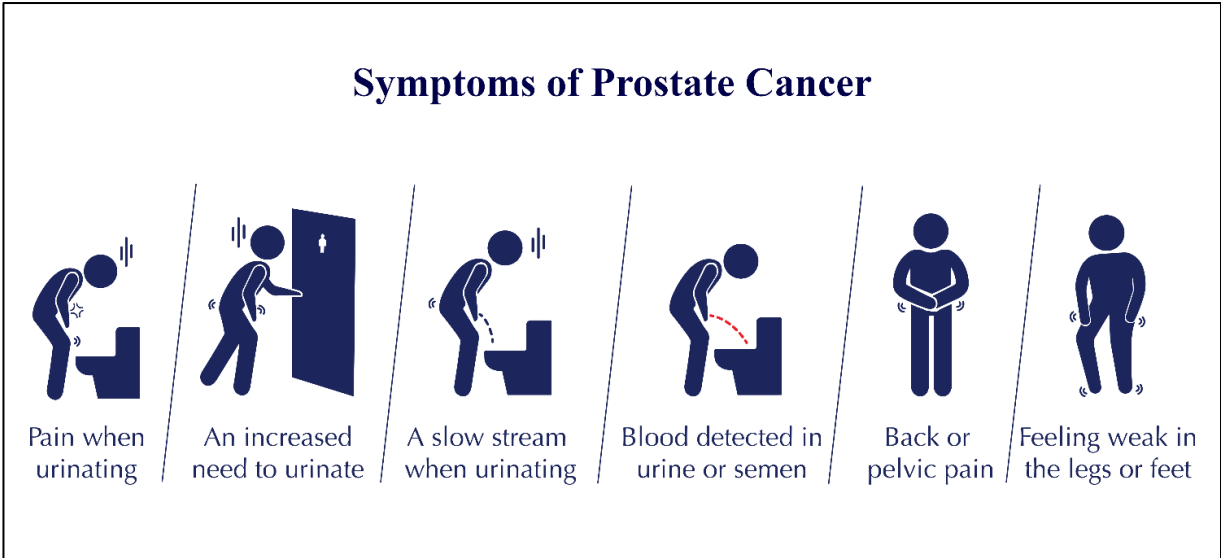


**Figure 3:** Symptoms of prostate cancer (<https://www.katellarisurology.com.au/prostate-cancer/>)

**1.6. Advanced prostate cancer symptoms:**

Leg weakness or swelling: Cancer may result in weakness or swelling in the legs if it has progressed to the lymph nodes or other body parts.

Breathing difficulties: Prostate cancer that has progressed to an advanced stage may have spread to the lungs.

It is important to note that prostate cancer in its early stages may not show any symptoms. To identify prostate cancer in its early, more curable stages, routine screening is crucial. This includes digital rectal examination (DRE) and blood testing for the prostate-specific antigen (PSA). Men should talk with their healthcare professionals about their unique risk factors and screening alternatives to choose the best course of action for their circumstances. A patient must consult a doctor right away if you have any of the symptoms mentioned above in order to ensure a correct diagnosis and course of treatment.

**1.7. Diagnosis of prostate cancer**

**1.7.1. Digital rectal examination (DRE)**

One easy way for doctors to check the lower rectum and other internal organs is with a digital rectal examination (DRE). Several factors warrant the execution of a DRE. It is a simple and fast method for determining whether a man's prostate gland is healthy (Okotie et al., 2007; Schröder et al., 1998). Both benign prostatic hyperplasia (an enlarged prostate) and prostate cancer can be detected with this method. During a DRE, the doctor inserts a gloved, lubricated

finger into the rectum to inspect the neighbouring prostate. The patient may require additional tests if the doctor discovers any irregularities in the gland's texture, shape, or size.

### **1.7.2. Prostate-specific antigen (PSA) test**

The measurement of the level of PSA in a blood sample through a blood test is referred to as a prostate-specific antigen (PSA) test, which is a widely used tool to evaluate the presence of prostate abnormalities. PSA, a protein produced by the prostate tissue, is present in the blood, and its levels can rise due to aberrant activity in the prostate, such as prostate cancer, benign prostatic hypertrophy (BPH), or prostate inflammation. The PSA value characteristics, including absolute level, change over time (commonly known as "PSA velocity"), and level in proportion to prostate size, can be used by physicians to determine whether a biopsy is necessary, thereby aiding in the screening, diagnosis, and management of prostate diseases (Catalona et al., 1991; Lilja et al., 2008 ).

### **1.7.3. Free PSA test**

The measurement of prostate-specific antigen (PSA) in men is a conventional tool used for the detection of prostate cancer. The PSA test can measure both free PSA and total PSA. Free PSA is the unbound form of PSA that circulates in the bloodstream, while total PSA is the total amount of PSA that is bound to proteins and unbound. The free PSA test calculates the ratio of free PSA to total PSA, which provides an indication of the probability of a high PSA level being related to prostate cancer. This information can be used by clinicians to decide whether further diagnostic tests are necessary. Hence, the free PSA test is a valuable tool in the early detection of prostate cancer and can help in the management of prostate cancer in men (Woodrum et al., 1998; Partin et al., 1996).

### **1.7.4. Biomarker tests**

A biomarker is a chemical discovered in a cancer patient's blood, urine, or body tissues. The tumor or the body produces it as a reaction to malignancy. A biomarker is also known as a tumor marker. The 4K score predicts the likelihood that someone has high-risk prostate cancer (Sultan et al., 2023), and the Prostate Health Index (PHI) predicts the probability that someone has prostate cancer (Zhu et al., 2015).

**1.7.5. Transrectal ultrasonography (TRUS) and biopsies**

TRUS is presently the most widely used diagnostic method for prostate cancer. A 2.5 cm diameter, 7.5 mHz biplane intra-rectal probe is used in TRUS to image the seminal vesicles and prostate. Historically, hypo-echoic lesions that might indicate TRUS diagnosed malignancy. However, 50% of non-palpable tumors were missed, and less than 20% of hypo-echoic lesions turned out to be malignancies following the biopsy. For this reason, it is not advised to use TRUS for the early identification of prostate cancer. On the other hand, it can picture the prostate's contour, detect calcifications, cysts, and abscesses inside the prostate, and estimate the prostate's volume (Borley et al., 2009; Kamoj et al., 2008).

**1.7.6. MRI fusion biopsy**

Magnetic resonance imaging and TRUS are combined in an MRI fusion biopsy. Prostate MRI evaluation has become standard clinical practice. To find prostate regions that need more investigation, the patient initially has an MRI scan. After that, the patient has a prostate ultrasound. These pictures are combined by computer software to create a three-dimensional image that aids in pinpointing the exact location of the biopsy. An MRI fusion biopsy can reveal areas more likely to be malignant than conventional procedures, although it may not altogether remove the need for repeat biopsies. Only a skilled individual with experience performing MRI fusion biopsies should carry them out (Das et al., 2019; Borley et al., 2009).

**1.7.7. Positron emission tomography (PET) or PET-CT scan**

A PET-CT scan is often a combination of a PET and a CT scan. On the other hand, a physician can call this process a PET scan. A PET scan can produce images of the body's tissues and organs. The patient receives a little injection of a radioactive material. The cells that consume the most energy or are most physiologically active absorb this chemical. Cancer absorbs more of the radioactive material since it tends to be physiologically active and uses energy. Nonetheless, the material has too little radiation to be dangerous. After that, a scanner finds this material to create photos of the interior of the body (Walker et al., 2020; Borley et al., 2009).

Fluorodeoxyglucose (FDG) is a radiopharmaceutical agent commonly used in PET-CT scans for the diagnosis and staging of various malignancies. However, it has been observed that FDG is not an optimal tracer for primary imaging of prostate cancer. Consequently, the use of gallium-68 or fluorine-18 PET scans is recommended when metastasis or recurrence is

suspected. These radiotracers bind to prostate-specific membrane antigen (PSMA), which is highly expressed in prostate cancer cells, and enable accurate visualization of tumor progression (Basuli et al., 2022).

Moreover, extensive research is being conducted to explore the potential of various radiopharmaceutical agents, in combination with PET imaging, for precise detection of prostate cancer. Sodium fluoride, for instance, is being explored as an effective tracer for detecting bone metastasis of prostate cancer, given its high affinity for bone. In addition, studies are underway on the efficacy of fluciclovine and choline acetate as radiotracers for improved detection of prostate cancer.

## **1.8. Grading and stages of prostate cancer**

### **1.8.1. Gleason score for grading prostate cancer**

Gleason score is a grading system used to classify prostate cancer (Epstein et al., 2016; Berney et al., 2016). The degree to which the malignancy resembles healthy tissue when examined under a microscope determines this score. Generally speaking, less aggressive tumors resemble healthy tissue more. Aggressive tumors have a higher propensity to develop and spread to other body areas. They appear to be less wholesome tissue.

Gleason score system is the most widely used grading scheme for prostate cancer. Based on two distinct locations and an examination of the cancer cell arrangement in the prostate, the pathologist rates the cancer using a 5-point rating system. A low score is given to cancer cells that resemble healthy cells. A higher grade is given to cancer cells that appear less like healthy cells or more aggressive. Before allocating the numbers, the pathologist looks for another area of growth after identifying the primary pattern of cell development or the location where the cancer is most visible. From 3 to 5, the doctor then assigns a score to each location. The total score ranges from 6 to 10 and is obtained by adding the individual scores.

Gleason scores of five or less are generally not used. A low-grade cancer with a Gleason score of 6 is the lowest. A Gleason score of seven indicates a medium-grade cancer; eight, nine, or ten indicates a high-grade malignancy. Compared to a high-grade cancer, a lower-grade cancer grows more slowly and is less likely to spread.

In addition to this stage, doctors consider the Gleason score while formulating a treatment plan. For example, if a patient has a tiny tumor, a low PSA level, and a Gleason score of 6, active

monitoring can be a choice. Individuals with a higher Gleason score might benefit from more aggressive treatment, especially in the case when the cancer is little or yet to spread.

Gleason X: There is no way to calculate the Gleason score.

Gleason 6 or lower: The cells are well differentiated, resembling healthy cells.

Gleason 7: The cells are moderately differentiated, meaning they somewhat resemble healthy cells.

Gleason 8, 9, or 10: The cells are poorly differentiated or undifferentiated because they differ significantly in appearance from healthy cells.

### **1.9. Stage groups for prostate cancer**

Stage 1: Cancer usually develops slowly in this stage. The tumor is not palpable and occupies one-half of one side of the prostate, if not less. PSA levels are pretty low. Cancer cells resemble healthy cells.

Stage 2: According to the medical report, the neoplasm has been detected solely in the prostate gland, depicting a stage II lesion with moderate to low levels of prostate-specific antigen. Despite its diminutive size, this type of cancer poses a high potential for metastasis.

Stage 2A: The lesion in question is impalpable and confined to a limited area of one side of the prostate gland. The prostate-specific antigen (PSA) levels are moderately elevated, and the cancer cells exhibit a high degree of differentiation. It should be noted that larger tumors, if confined solely to the prostate, may also be included within this stage, provided that the neoplastic cells remain markedly differentiated.

Stage 2B: The tumor is only identified within the prostate and is large enough to be felt during a DRE. The PSA level is moderate. Cancer cells have a modest level of differentiation.

Stage 2C: The tumor is only identified within the prostate and is large enough to be felt during a DRE. The PSA level is moderate. Cancer cells might be either moderately or poorly differentiated.

Stage 3: Elevated levels of Prostate-Specific Antigen (PSA) have been found to be indicative of advanced malignancy, which poses a greater risk of metastasis. Therefore, it can be inferred that the presence of high PSA levels may suggest the possibility of a locally advanced tumor, which may potentially spread to other parts of the body.



Stage 3A: The cancer has progressed beyond the prostate's outer layer into surrounding tissues. It could have also spread to the seminal vesicles. The PSA level is elevated.

Stage 3B: The tumor has spread beyond the prostate gland and may have infiltrated neighbouring structures such as the bladder or rectum.

Stage 3C: Cancer cells throughout the tumor are poorly differentiated, making them appear quite different from healthy cells.

Stage 4: Indicates that the cancer has gone beyond the prostate.

Stage 4A: The cancer has spread to the lymph nodes in the region.

Stage 4B: The cancer has progressed to distant lymph nodes, other bodily parts, or the bones.

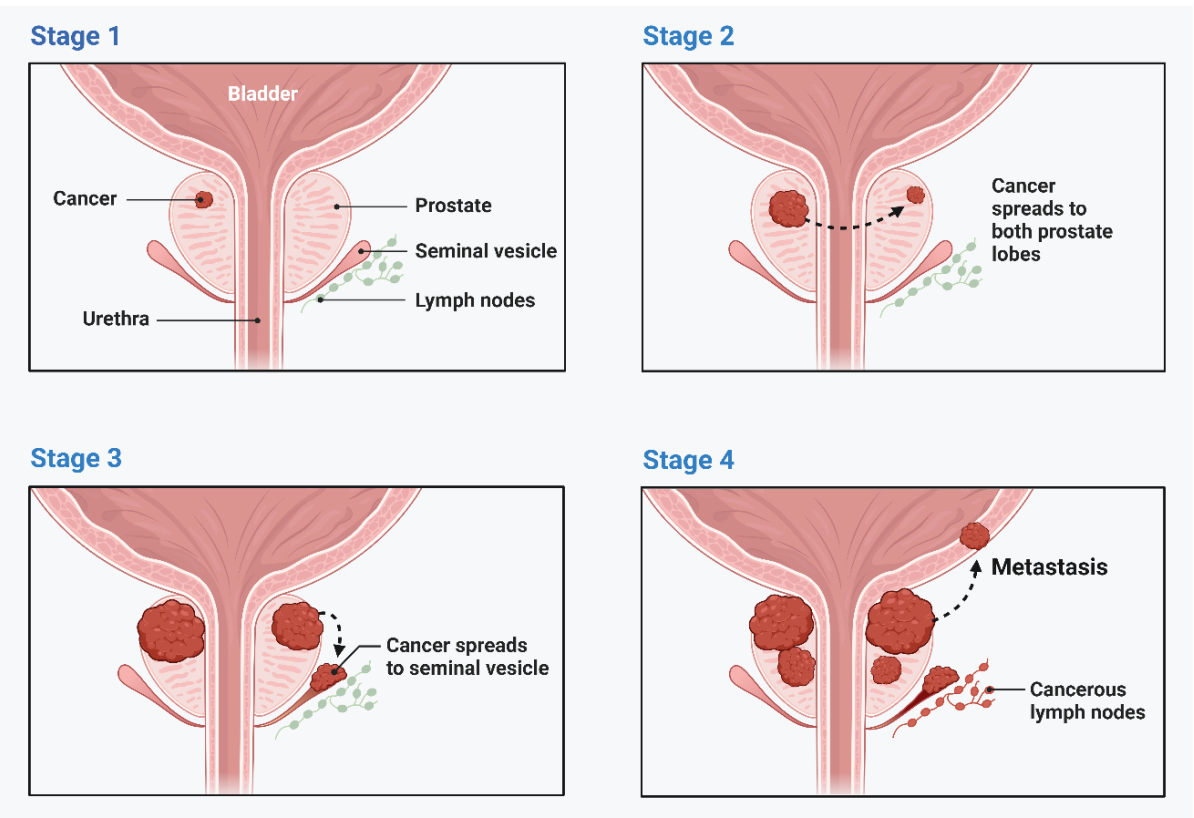


**Figure 4:** Different stages of prostate cancer

## 1.10. Various treatment options

### 1.10.1. Chemotherapy

For the treatment of prostate cancer, various chemotherapeutic medications have been authorized (Gilligan et al., 2002). To stop tubulin depolymerization and cell death by mitotic

cell division, docetaxel and cabazitaxel are administered intravenously every three weeks. Moreover, it has been shown that AR inhibitory characteristics are associated with a reduction in microtubule-dependent nuclear transport. The FDA approved docetaxel in 2004 and cabazitaxel in 2010 for mCRPC, respectively (Corn et al., 2019). Two separate clinical trials indicated positive outcomes when docetaxel was tested in mHSPC in conjunction with ADT. Neutropenia and other forms of hematological toxicity are common side effects. While mitoxantrone, a topoisomerase inhibitor, does alleviate some symptoms, it does not improve survival rates for prostate cancer patients when compared to docetaxel. Durable responses in chemo-naïve mCRPC patients are achieved when cabazitaxel is combined with other treatments. Nevertheless, the use of mitoxantrone is constrained because of severe side effects.

### **1.10.2. Compounds targeting androgen signaling**

As prostate cancer patients develop resistance to ADT, their PSA levels rise, suggesting that AR signaling is still a crucial target for pharmaceutical management at this point. Steroid synthesis inhibitors and second-generation AR antagonists are used to treat this vulnerability.

Abiraterone acetate is an irreversible inhibitor of CYP17A1, a cytochrome P450 family 17–20 lyase and 17– $\alpha$  hydroxylase that transforms pregnanes into steroid hormones, including androgen precursors. Therefore, it can inhibit androgen production in the testicles, adrenal glands, and prostate cancers, thus stopping prostate cancer progression (Hoque et al., 2023). Enzalutamide is an FDA-approved second-generation competitive oral AR antagonist that significantly increases the metastasis-free survival (MFS) of patients with high-risk non-metastatic CRPC (nmCRPC). Based on a 24-month extended maximum fixed dose, the oral AR antagonist apalutamide, which is structurally linked to enzalutamide, was recently approved for nmCRPC. Darolutamide is the second generation's innovative, chemically structured, competitive oral AR antagonist. It has been observed that a robust binding to the AR LBD translates into substantial anti-tumor efficacy in preclinical models and a distinct antagonistic action against AR mutations found in patients with treatment-resistant prostate cancer. Darolutamide has a lower blood-brain barrier penetration than other AR antagonists, which could lead to a more favorable side-effect profile.

### **1.10.3. Signaling pathway inhibitors**

The pathogenesis and progression of prostate cancer are significantly influenced by the PI3K/AKT/mTOR pathway, with hyperactive PI3K signaling being a major outcome of PTEN loss. The stages of the disease have been studied using a genetically modified mouse model in

which the *PTEN* gene has been deleted specifically in the prostate. The primary participant in PI3K is the p110 $\beta$  subunit, but when this subunit is blocked, the p110 $\alpha$  subunit is upregulated. There has been evidence of a reciprocal feedback mechanism and crosstalk between AR signaling and the PI3K/AKT/mTOR pathway (Hashemi et al., 2023; Roudsari et al., 2021). In several preclinical models, treatment with PI3K/AKT/mTOR pathway inhibitors demonstrates *in vivo* anti-tumor efficacy. Concurrent application of AR antagonists provides an even greater benefit.

Limited efficacy has been observed in the first clinical investigations involving medicines that interfere with the PI3K/AKT/mTOR pathway. Ipatasertib, the most advanced medication, is presently in clinical phase 3 for patients with metastatic colorectal cancer. Further clinical trials are being conducted, including combinations with enzalutamide or abiraterone acetate. Better outcome might result from patient classification based on PTEN loss or PI3K/AKT/mTOR pathway mutations.

In prostate cancer, FGF signaling is also involved, particularly in the advanced stages of the illness. A peptide mimic of WNT-5A is undergoing preliminary clinical trials after demonstrating encouraging outcomes in an orthotopic prostate cancer animal model. Because of abnormal downstream mTOR signaling, prostate tumor growth is further enhanced by the deregulation of both the WNT and PI3K pathways.

#### **1.10.4. DNA damage repair pathway**

Patients with advanced prostate cancer are more likely to have DNA damage response (DDR) deficiencies, which are primarily caused by mutations in the homologous recombination and DNA mismatch repair pathways (Karanika et al., 2015; Zhang et al., 2020). To mitigate this risk, the poly ADP ribose polymerase (PARP) family, which is essential for identifying damaged DNA and promoting its repair, was first blocked in the clinic. The most common side effects of the oral PARP inhibitor olaparib, tested in mCRPC patients, were fatigue and anemia. Positive phase 2 findings were also reported. Crucially, patients with mutations in ataxia telangiectasia serine/threonine kinase (ATM), BRCA 1 or 2, or both, which are critical components of DNA repair pathways, typically exhibit a better prognosis. A recent research indicates that the sensitivity to PARP inhibitors is heightened when the chromatin remodeler chromodomain-helicase-DNA-binding protein 1 (CHD1) is lost (Shenoy et al., 2017), which is frequently the case in metastatic prostate cancer. The FDA designated olaparib as a breakthrough due to the positive clinical phase 2 results. A phase 3 pivotal trial is presently

being conducted. In contrast, no statistically significant improvement was observed in the clinical outcomes of mCRPC patients receiving veliparib, a PARP inhibitor, in addition to abiraterone acetate. To inhibit ataxia telangiectasia and Rad3-related kinase (ATR), which detects single-strand DNA breaks, is an additional strategy. In a CRPC bone metastasis xenograft model, the ATR inhibitor BAY 1895344, in conjunction with radium-223 dichloride, demonstrated strong anti-tumor activity (Wengner et al., 2017). Recent research indicates that AZD7762, an inhibitor of Chk1, is additive or synergistic with enzalutamide in prostate cancer xenografts. Nevertheless, clinical investigations with this chemical have been terminated. Chk1 is a cell-cycle regulator of DNA damage response downstream of ATR.

#### **1.10.5. Targeted alpha therapy approach**

An intravenous targeted alpha treatment is radium-223 dichloride. It binds to hydroxyapatite, a key component of bone, and is specifically taken up in osteoblastic bone metastases. It functions similarly to calcium. Radium-223 dichloride has cytotoxic effects on neighbouring tumor cells, osteoclasts, and disease-promoting osteoblasts once it is deposited in the newly formed intra-tumoral bone matrix (Vincentis et al., 2019; Morris et al., 2019). This is achieved by inducing difficult-to-repair DNA double-strand breaks, which disrupt positive feedback loops between tumor microenvironment cells and osteoblasts. These *in vivo* experiments were conducted using prostate cancer xenograft models. There has been preclinical evidence of synergistic effects with the ATR inhibitor BAY 1895344. Given to patients with CRPC, radium-223 dichloride has a good safety profile, reduces pain associated with bone metastases, and increases overall survival regardless of previous use of docetaxel. For patients with CRPC who had bone metastases but no known visceral metastatic illness, the FDA first approved it in 2013. Other combination trials with enzalutamide, olaparib, and niraparib are continuing. A clinical research combining radium-223 dichloride with abiraterone acetate and prednisone was unblinded early due to increased death and fracture risk. Furthermore, radium-223 dichloride has been shown in recent studies to promote T cell-mediated lysis in a variety of tumor forms, including prostate cancer. For this reason, pairing this medication with immunotherapies may have further clinical benefits.

#### **1.11. Androgen receptor and signaling**

The androgen receptor, a ligand-dependent transcription factor found on the X chromosome, mediates androgen signaling. The receptor is made up of a hinge region, a carboxy-terminal ligand binding domain, an amino-terminal activation domain, and a DNA binding domain. The

dormant version of the androgen receptor is found in the cytoplasm, where it is still attached to heat shock proteins, which stop the activation of the androgen receptor. The dissociation of heat shock proteins and receptor phosphorylation caused by androgen binding to the receptor result in nuclear translocation, which opens the door for the transcription of androgen-dependent genes (Rehman et al., 2012).

Castration resistance in prostate cancer appears to be caused by several distinct pathways. One of them, an androgen receptor mutation, is sometimes observed in patients with advanced illness. Certain mutations in the androgen receptor in CRPC cause the androgen receptor to become less selective for androgens and more receptive to progesterone, estrogens, and even antiandrogens. Despite castrate testosterone levels, this can result in the growth of prostate cancer. Prostate cancer that is resistant to flutamide may occasionally respond to other antiandrogens, such as bicalutamide, indicating that selective pressure directly leads to changes in the androgen receptor. Amplification of the androgen receptor gene can potentially lead to androgen receptor hyperresponsiveness. Despite low androgen levels, prostate cancer can continue to grow due to copy number gains of the androgen receptor. While they have not been detected in early tumor samples without exposure to androgen ablation, androgen receptor gene amplifications are reported in 28% of patients with recurrent therapy-resistant prostate cancer who have undergone androgen ablation. This raises the prospect of clonal selection of cancer cells that are able to proliferate in the presence of extremely low amounts of androgens in the blood. In spite of low levels of circulating androgens or the presence of less strong androgens, androgen receptor-mediated gene transcription is also made possible by the upregulation of nuclear transcription coactivators. Furthermore, it has been demonstrated that prostate cancer cells upregulate intratumoral steroidogenesis in order to sustain intratumor androgen at levels necessary for tumor growth. Regardless of the body's castrate level of androgens, this pathway promotes tumor growth. Moreover, it has been observed that prostate cancer frequently involves the fusion of androgen-activated TMPRSS2 with the ETS family of oncogenes, ERG, or ETV1 (Clark et al., 2009). While androgen-regulated ERG transcription is reactivated in the context of androgen receptor reactivation in castration resistance, the exact significance of TMPRSS2/ETS translocations in castration resistance remains unknown at this time and may potentially accelerate the development of CRPC (Rehman et al., 2012).

### 1.12. Cytochrome P17 enzyme

The CYP17 enzyme belongs to the cytochrome P450 (CYP) family. CYP17 is found in the endoplasmic reticulum of the testis, ovaries, adrenals, and placenta and is responsible for the manufacture of glucocorticoids and sex hormones. The enzyme possesses  $17\alpha$ -hydroxylase and C17, 20 lyase activity, essential for cortisol and androgen synthesis. CYP17, 20 lyase activity is regulated by cytochrome b5. A high b5/CYP 17, 20 lyase ratio in the testes results in androgen production, whereas a low b5/c lyase ratio in the adrenal glands results in cortisol production (Rehman et al., 2012; Salem et al., 2011).

### 1.13. Abiraterone acetate and its mechanism of action

Abiraterone acetate (ABR) is a new antiandrogen medication that works by inhibiting the synthesis of adrenal metabolites that act as precursors for the synthesis of testosterone and DHT.

Abiraterone acetate is a powerful cytochrome P450 C17 (CYPC17) inhibitor. It is currently being used to treat castration-resistant prostate cancer (Thakur et al., 2018). The United States Food and Drug Administration (US-FDA) approved it for usage in April 2011, and the European Medicines Agency (EMA) approved it a few months later. By irreversibly blocking CYP17, which is involved in the creation of testosterone, abiraterone preferentially suppresses androgen biosynthesis in the adrenal glands, prostate tissue, and prostatic malignancies.

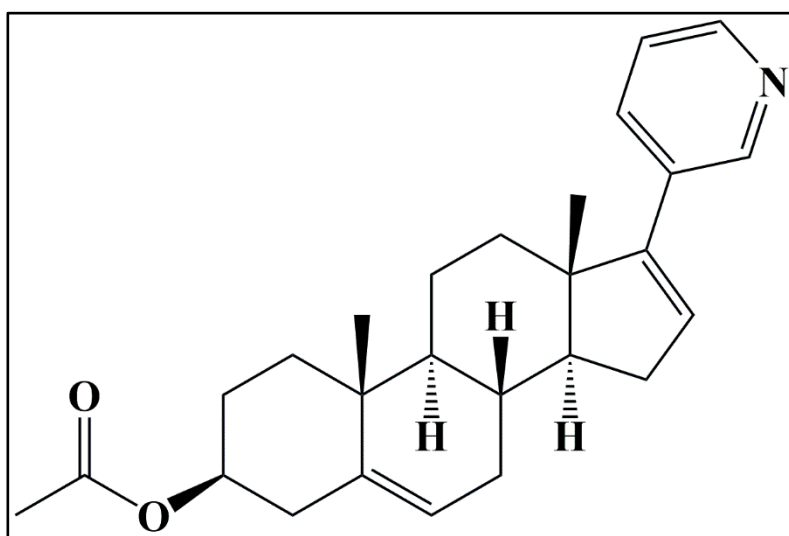


**Figure 5:** Chemical structure of abiraterone acetate

### 1.14. Aptamer and its importance in prostate cancer therapy

Aptamers are single-stranded RNA or DNA oligonucleotides that fold into particular three-dimensional shapes and have a strong affinity for their target molecules. This nucleotide sequence determines the specific structure of aptamers, which are often 20–100 nucleotides long (Cruz-Hernández et al., 2022). As aptamers bind targets with extreme specificity, the word "aptamer" comes from the Latin root "aptus," which means "to fit." Aptamers are desirable instruments for use in a variety of targeted cancer therapy applications due to a number of their distinct features. Similar to monoclonal antibodies, aptamers attach to targets with great affinity and often exhibit dissociation constants in the pico- to nano-molar range. In contrast to antibodies, aptamers maintain their structural stability over a broad range of temperatures and storage circumstances. The process of phosphorothioate modification of DNA aptamers entails the substitution of one of the non-bridging oxygen atoms in the phosphate backbone of DNA with a sulfur atom. This chemical modification confers greater stability upon aptamers, rendering them more resistant to nuclease degradation and thus potentially prolonging their biological activity in biological systems. By conferring resistance to enzymatic cleavage, this modification can enhance the aptamers' suitability for various biological applications (Dhara et al., 2023). RNA aptamers are usually endowed with nuclease resistance by utilizing 2'-modified nucleotides, primarily 2'-fluoro or 2'-O-methyl pyrimidines (Dunn et al., 2017). The nonimmunogenic nature of aptamers, especially those derived from synthetic nucleotides, may contribute to their long-term therapeutic efficacy and safety. Compared to the biological systems used to make monoclonal antibodies, aptamers may be less expensive and have less interbatch variability since they are produced chemically *in vitro*. Their chemical manufacture also makes it easier to modify them in different ways. For example, it is easier to conjugate 5' to polyethylene glycol (PEG), increasing the circulation half-life.

Methods such as systematic evolution of ligands by exponential enrichment (SELEX) can be used to produce aptamers (Sefah et al., 2010; Fang et al., 2010). After being exposed to a target of interest, SELEX allows a pool of  $10^{13}$ - $10^{15}$  oligonucleotides to bind. The oligonucleotides that bind are first extracted and amplified using polymerase chain reaction (PCR) technology, while the ones that do not bind are separated and discarded. Iteratively, the target is re-bound with the newly-enriched pool of oligonucleotides. Using a series of rounds, the SELEX method finds oligonucleotides that bind to the target very strongly.

Aptamers have numerous extra benefits in biological and production aspects, yet they are typically compared to antibodies. Their size and composition make them non-immunogenic and offer them a leg up when it comes to penetrating tissues, for example. In addition, aptamers do not require a living organism for their manufacture; they can be created *in vitro* and changed with functional groups or probes to give them more stability. Both the most recent and user-friendly chemical synthesis methods and the novel mutant enzymes enable the manufacturing of modified aptamers using polymerase chain reaction (PCR). Their mass production is both straightforward and inexpensive. The desired applications dictate the selection process for aptamers, which typically involves multiple rounds of selection (about 6-12 cycles) from an extensive library of single-stranded oligonucleotides (greater than  $1 \times 10^{16}$  molecules). Subsequently, these aptamers can be optimized by making modifications. Thus, aptamers have the potential to revolutionize medicine by facilitating drug delivery, diagnostics, imaging, and the identification of novel biomarkers, among other therapeutic uses. They may even replace conventional antibody therapy.

### **1.15. PSMA as a target in prostate cancer**

In the context of prostate cancer, prostate-specific membrane antigen (PSMA) has become a viable target that is transforming the fields of imaging, diagnosis, and therapy. Prostate cancer continues to be a primary worldwide health concern. Developing precision medicine techniques now depend on identifying particular molecular targets. Prostate cancer cells overexpress the transmembrane glycoprotein PSMA, which makes it a prime candidate for several treatment approaches (Ghosh et al., 2003; Wang et al., 2021). In addition to serving as a marker for prostate cancer, PSMA is essential to detect the aggressiveness of the disease and the course of the illness. It is a valuable biomarker for identifying and staging prostate cancer because of its higher expression in cancerous prostate cells as compared to healthy prostate tissue.



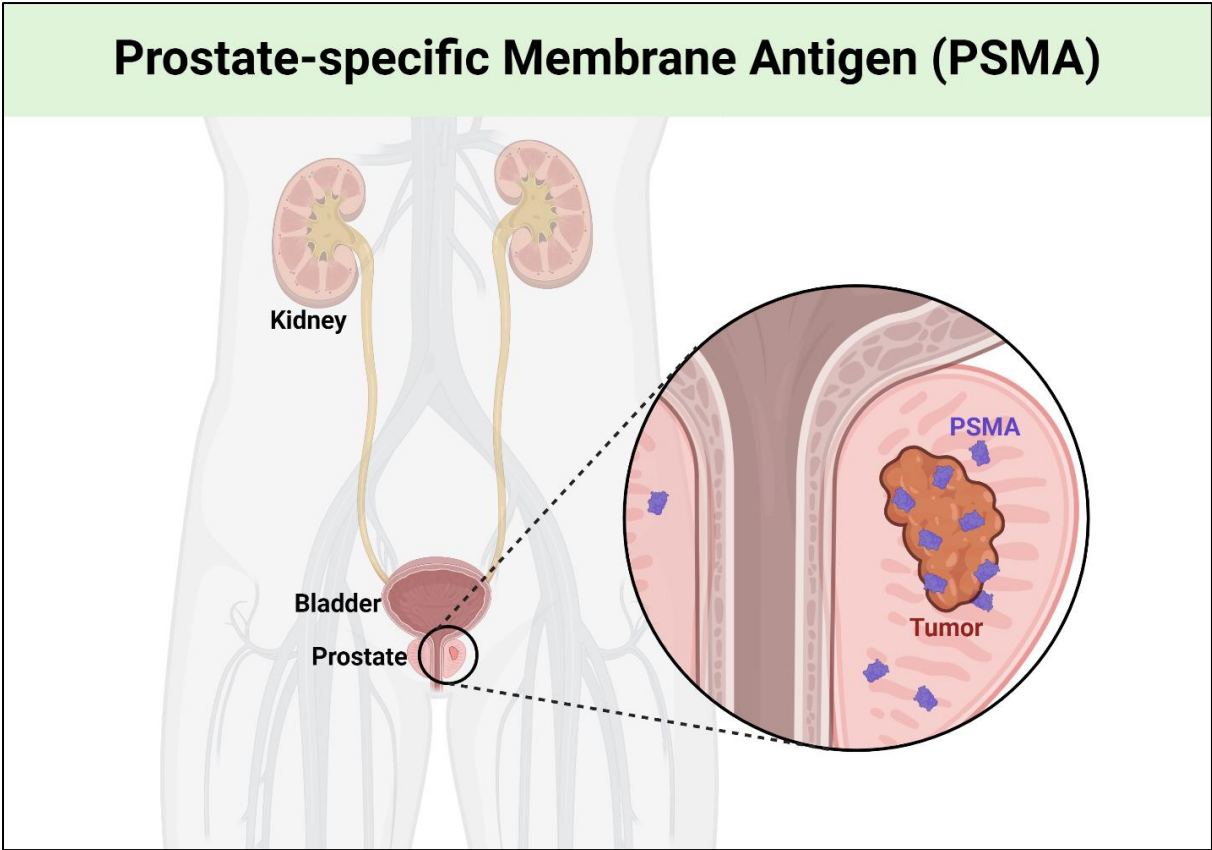


**Figure 6:** This diagram shows a general pictorial representation of transmembrane glycoprotein prostate-specific membrane antigen, PSMA

More sensitive and accurate detection is possible when PSMA is used as a diagnostic tool, which promotes early intervention and better patient outcomes. The use of PSMA in imaging techniques is one of its noteworthy applications in prostate cancer diagnosis. PSMA-based positron emission tomography (PET) scans offer accurate and comprehensive pictures of lesions related to prostate cancer. Due to its high sensitivity, this imaging modality has the ability to detect metastatic and tiny lesions that traditional imaging techniques might miss. Clinicians can make better-informed judgments using PSMA-targeted imaging's increased visibility, making staging and therapy response monitoring more accurate. In addition to being useful for diagnosis, PSMA is a desirable target for treatment approaches. A number of strategies have been investigated to use PSMA overexpression in prostate cancer cells for targeted therapy. Among the methods being looked into include antibody-drug conjugates, small molecule inhibitors, and radioimmunotherapy to target cancer cells that produce PSMA specifically. By minimizing collateral damage to healthy tissues, these tailored medicines may lower side effects and increase the effectiveness of treatment. Radioligand therapy (RLT) is a novel advancement in the field of PSMA-targeted therapy (Capasso et al., 2023). A

radiolabeled ligand that binds exclusively to PSMA on prostate cancer cells is administered as part of PSMA-targeted radioligand therapy (RLT) to provide a therapeutic dosage of radiation to the malignant tissue. Clinical trials using this method have produced encouraging outcomes, especially in more advanced cases where the efficacy of conventional treatments may be compromised. For patients with metastatic prostate cancer, PSMA-targeted radioligand therapy (RTL) has the potential to be a tailored and efficient therapeutic option.

### **1.16. Aptamer-conjugated PLGA nanoparticles for prostate cancer therapy.**

Nanoparticles made of poly (lactic-co-glycolic acid) (PLGA) have recently attracted a lot of interest because of their many potential uses as effective and flexible drug delivery vehicles. The PLGA nanoparticles, composed of biodegradable and biocompatible polymers, provide an excellent vehicle for the controlled and prolonged release of drugs (Sarkar et al., 2021; Ehsan et al., 2022). Lactic acid and glycolic acid monomers copolymerize to obtain PLGA, which has customizable physicochemical properties such as drug-loading capacity, degradation rate, and particle size. Numerous medicinal substances, such as small-molecule pharmaceuticals, proteins, peptides, and nucleic acids, can be encapsulated within the nanoparticles. Prolonged therapeutic effects with little systemic toxicity are achieved through the sustained administration of drugs by PLGA nanoparticles, which have regulated release kinetics. It is also possible to improve the targeting specificity of PLGA nanoparticles by surface engineering or ligand conjugation. Potentially revolutionizing personalized medicine and the treatment of a wide range of diseases, including cancer and infectious diseases, PLGA nanoparticles are at the vanguard of drug delivery systems due to their capacity to preserve encapsulated drugs from degradation, enhance bioavailability, and enable targeted delivery.

Aptamer technology and nanotechnology combined have opened the door to precision medicine in cancer treatment. One of the most promising therapeutic approaches for targeting cancer cells is targeting antigens overexpressed on their surface. The transmembrane glycoprotein PSMA that overexpresses on the surface of prostate cancer cells is particularly bound by anti-PSMA aptamers, which provide three-dimensional architecture with small, single-stranded nucleic acid molecules usually chosen by SELEX (Kasten et al., 2013; Kelly et al., 2021). Because of their great specificity, anti-PSMA aptamers are excellent choices for targeted therapeutic delivery. Conformational recognition is a phenomenon in which aptamers exhibit the ability to assume specific three-dimensional conformations, thereby enabling them to bind tightly and selectively to their target molecules. In the context of PSMA, aptamers can

recognize and bind to specific epitopes on the PSMA protein through conformational recognition. This entails a conformational change in the aptamer molecule that facilitates an optimal interaction with the target.

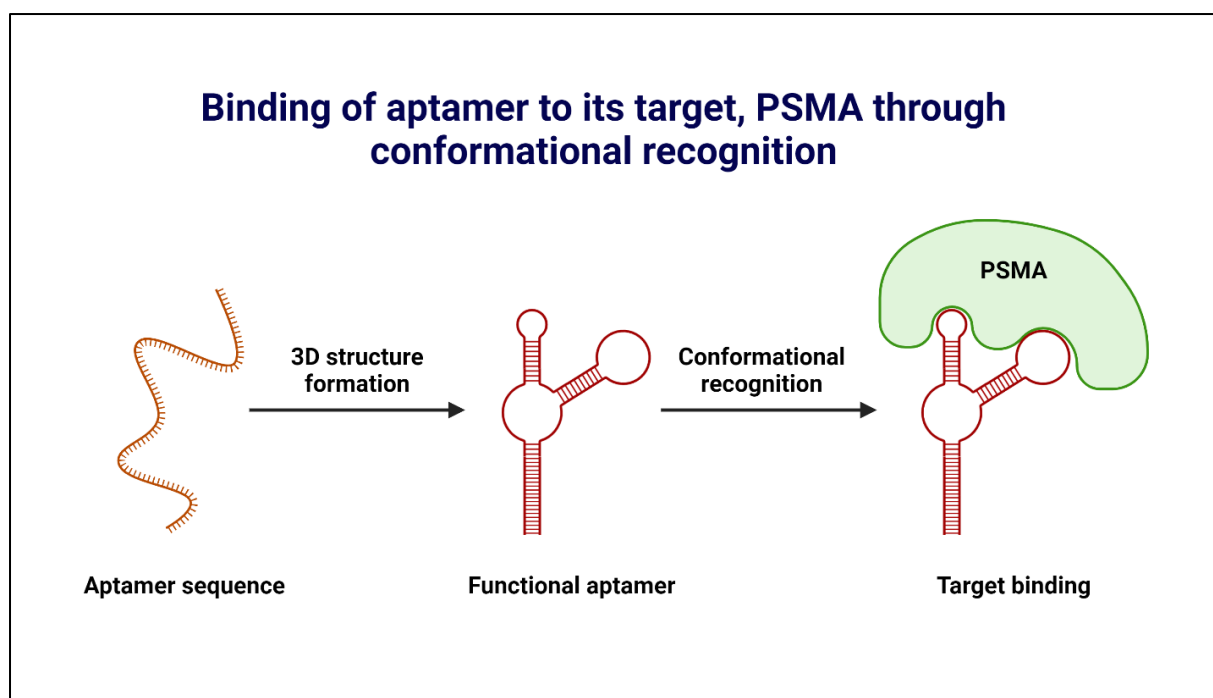


**Figure 7:** Schematic diagram of the aptamer-PSMA binding through conformational recognition

Researchers want to improve the accuracy of therapeutic interventions by conjugating these aptamers to PLGA nanoparticles, which will ensure specific recognition and binding to prostate cancer cells. Combining PLGA nanoparticles with anti-PSMA aptamers produces a hybrid nanosystem with improved targeting properties. By selectively attaching to prostate cancer cells that express PSMA, the anti-PSMA aptamers on the nanoparticle surface help direct the particles to the tumor's precise location. This tailored strategy raises the therapeutic index of the encapsulated drug cargo by reducing off-target effects. When it comes to treating prostate cancer, the anti-PSMA aptamer-conjugated PLGA nanoparticles have two benefits. The aptamer first directs the nanoparticles to prostate cancer cells to enable targeted medication administration. Secondly, the therapeutic payload is efficiently delivered intracellularly by the PLGA nanoparticles, facilitating cellular uptake through endocytosis. The combination of greater cellular uptake and selective administration boosts the treatment-related overall effectiveness.

In our study, we developed  $\Delta$ PSap4#5 aptamer surface-functionalized abiraterone-loaded biodegradable nanoparticle (Apt-ABR-NP) to investigate its targeting ability to prostate-specific membrane antigen (PSMA) in carcinogen-induced PCa mice and the therapeutic efficacy of the formulation.

### 1.17. References

- Abd Elghany N, Schumacher MC, Slattery ML, West DW, Lee JS. Occupation, cadmium exposure, and prostate cancer. *Epidemiology*. 1990 Mar 1;1(2):107-15.
- Al Hoque A, Dutta D, Paul B, Kumari L, Ehsan I, Dhara M, Mukherjee B, Quadir M, Kaiparettu BA, Laha S, Ganguly S.  $\Delta$ PSap4# 5 surface-functionalized abiraterone-loaded nanoparticle successfully inhibits carcinogen-induced prostate cancer in mice: a mechanistic investigation. *Cancer Nanotechnology*. 2023 Dec;14(1):73.
- Arya M, Bott SR, Shergill IS, Ahmed HU, Williamson M, Patel HR. The metastatic cascade in prostate cancer. *Surgical oncology*. 2006 Nov 1;15(3):117-28.
- Basuli F, Phelps TE, Zhang X, Woodroffe CC, Roy J, Choyke PL, Swenson RE, Jagoda EM. Fluorine-18 labeled urea-based ligands targeting Prostate-Specific Membrane Antigen (PSMA) with increased tumor and decreased renal uptake. *Pharmaceuticals*. 2022 May 13;15(5):597.
- Berney DM, Beltran L, Fisher G, North BV, Greenberg D, Møller H, Soosay G, Scardino P, Cuzick J. Validation of a contemporary prostate cancer grading system using prostate cancer death as outcome. *British journal of cancer*. 2016 May;114(10):1078-83.
- Borley N, Feneley MR. Prostate cancer: diagnosis and staging. *Asian journal of andrology*. 2009 Jan;11(1):74.
- Bostwick DG, Burke HB, Djakiew D, Euling S, Ho SM, Landolph J, Morrison H, Sonawane B, Shifflett T, Waters DJ, Timms B. Human prostate cancer risk factors. *Cancer: Interdisciplinary International Journal of the American Cancer Society*. 2004 Nov 15;101(S10):2371-490.
- Bostwick DG. High grade prostatic intraepithelial neoplasia. The most likely precursor of prostate cancer. *Cancer*. 1995 Apr 1;75(S7):1823-36.
- Brook MN, Raghallaigh HN, Govindasami K, Dadaev T, Rageevakumar R, Keating D, Hussain N, Osborne A, Lophatananon A, Muir KR, Kote-Jarai Z. Family history of prostate cancer and survival outcomes in the UK Genetic Prostate Cancer Study. *European Urology*. 2023 Mar 1;83(3):257-66.

- Capasso G, Stefanucci A, Tolomeo A. A systematic review on the current status of PSMA-targeted imaging and radioligand therapy. *European Journal of Medicinal Chemistry*. 2023 Nov 17;115966.
- Catalona WJ, Smith DS, Ratliff TL, Dodds KM, Coplen DE, Yuan JJ, Petros JA, Andriole GL. Measurement of prostate-specific antigen in serum as a screening test for prostate cancer. *New England journal of medicine*. 1991 Apr 25;324(17):1156-61.
- Chatterjee B. The role of the androgen receptor in the development of prostatic hyperplasia and prostate cancer. *Molecular and cellular biochemistry*. 2003 Nov;253:89-101.
- Clark JP, Cooper CS. ETS gene fusions in prostate cancer. *Nature Reviews Urology*. 2009 Aug;6(8):429-39.
- Corn PG, Agarwal N, Araujo JC, Sonpavde G. Taxane-based combination therapies for metastatic prostate cancer. *European urology focus*. 2019 May 1;5(3):369-80.
- Cruz-Hernández CD, Rodríguez-Martínez G, Cortés-Ramírez SA, Morales-Pacheco M, Cruz-Burgos M, Losada-García A, Reyes-Grajeda JP, González-Ramírez I, González-Covarrubias V, Camacho-Arroyo I, Cerbón M. Aptamers as theragnostic tools in prostate cancer. *Biomolecules*. 2022 Jul 29;12(8):1056.
- Das CJ, Razik A, Sharma S, Verma S. Prostate biopsy: when and how to perform. *Clinical radiology*. 2019 Nov 1;74(11):853-64.
- De Vincentis G, Gerritsen W, Gschwend JE, Hacker M, Lewington V, O'Sullivan JM, Oya M, Pacilio M, Parker C, Shore N, Sartor O. Advances in targeted alpha therapy for prostate cancer. *Annals of Oncology*. 2019 Nov 1;30(11):1728-39.
- Dunn MR, Jimenez RM, Chaput JC. Analysis of aptamer discovery and technology. *Nature Reviews Chemistry*. 2017 Oct 4;1(10):0076.
- Ehsan I, Kumari L, Sen R, Al Hoque A, Mukherjee B, Mukherjee A, Ghosh P, Bhattacharya S. J591 functionalized paclitaxel-loaded PLGA nanoparticles successfully inhibited PSMA overexpressing LNCaP cells. *Journal of Drug Delivery Science and Technology*. 2022 Sep 1;75:103689.
- Epstein JI, Zelefsky MJ, Sjoberg DD, Nelson JB, Egevad L, Magi-Galluzzi C, Vickers AJ, Parwani AV, Reuter VE, Fine SW, Eastham JA. A contemporary prostate cancer

- grading system: a validated alternative to the Gleason score. *European urology*. 2016 Mar 1;69(3):428-35.
- Eskra JN, Rabizadeh D, Pavlovich CP, Catalona WJ, Luo J. Approaches to urinary detection of prostate cancer. *Prostate cancer and prostatic diseases*. 2019 Sep;22(3):362-81.
- Fang X, Tan W. Aptamers generated from cell-SELEX for molecular medicine: a chemical biology approach. *Accounts of chemical research*. 2010 Jan 19;43(1):48-57.
- Farmer R. Prostate cancer: epidemiology and risk factors. *Trends in Urology, Gynaecology & Sexual Health*. 2008 May;13(3):32-4.
- Gandhi J, Afridi A, Vatsia S, Joshi G, Joshi G, Kaplan SA, Smith NL, Khan SA. The molecular biology of prostate cancer: current understanding and clinical implications. *Prostate cancer and prostatic diseases*. 2018 Apr;21(1):22-36.
- Gann PH. Risk factors for prostate cancer. *Reviews in urology*. 2002;4(Suppl 5):S3.
- Ghosh A, Heston WD. Tumor target prostate specific membrane antigen (PSMA) and its regulation in prostate cancer. *Journal of cellular biochemistry*. 2004 Feb 15;91(3):528-39.
- Gilligan T, Kantoff PW. Chemotherapy for prostate cancer. *Urology*. 2002 Sep 1;60(3):94-100.
- Hashemi M, Taheriazam A, Daneii P, Hassanpour A, Kakavand A, Rezaei S, Hejazi ES, Aboutalebi M, Gholamrezaie H, Saebfar H, Salimimoghadam S. Targeting PI3K/Akt signaling in prostate cancer therapy. *Journal of Cell Communication and Signaling*. 2023 Sep;17(3):423-43.
- Jacobs SC. Spread of prostatic cancer to bone. *Urology*. 1983 Apr 1;21(4):337-44.
- Kamoi K, Okihara K, Ochiai A, Ukimura O, Mizutani Y, Kawauchi A, Miki T. The utility of transrectal real-time elastography in the diagnosis of prostate cancer. *Ultrasound in medicine & biology*. 2008 Jul 1;34(7):1025-32.
- Karanika S, Karantanos T, Li L, Corn PG, Thompson TC. DNA damage response and prostate cancer: defects, regulation and therapeutic implications. *Oncogene*. 2015 May;34(22):2815-22.

- Kasten BB, Liu T, Nedrow-Byers JR, Benny PD, Berkman CE. Targeting prostate cancer cells with PSMA inhibitor-guided gold nanoparticles. *Bioorganic & medicinal chemistry letters*. 2013 Jan 15;23(2):565-8.
- Kelly L, Maier KE, Yan A, Levy M. A comparative analysis of cell surface targeting aptamers. *Nature Communications*. 2021 Nov 1;12(1):6275.
- Kooiman GG, Martin FL, Williams JA, Grover PL, Phillips DH, Muir GH. The influence of dietary and environmental factors on prostate cancer risk. *Prostate cancer and prostatic diseases*. 2000 Dec;3(4):256-8.
- Lilja H, Ulmert D, Vickers AJ. Prostate-specific antigen and prostate cancer: prediction, detection and monitoring. *Nature Reviews Cancer*. 2008 Apr;8(4):268-78.
- Lim J, Hong HG, Weinstein SJ, Playdon MC, Cross AJ, Stolzenberg-Solomon R, Freedman ND, Huang J, Albanes D. Metabolomic Analysis of Vitamin E Supplement Use in the Prostate, Lung, Colorectal, and Ovarian Cancer Screening Trial. *Nutrients*. 2023 Jun 22;15(13):2836.
- Morris MJ, Corey E, Guise TA, Gulley JL, Kevin Kelly W, Quinn DI, Scholz A, Sgouros G. Radium-223 mechanism of action: implications for use in treatment combinations. *Nature Reviews Urology*. 2019 Dec;16(12):745-56.
- Okotie OT, Roehl KA, Han M, Loeb S, Gashti SN, Catalona WJ. Characteristics of prostate cancer detected by digital rectal examination only. *Urology*. 2007 Dec 1;70(6):1117-20.
- Partin AW, Catalona WJ, Southwick PC, Subong EN, Gasior GH, Chan DW. Analysis of percent free prostate-specific antigen (PSA) for prostate cancer detection: influence of total PSA, prostate volume, and age. *Urology*. 1996 Dec 1;48(6):55-61.
- Rehman Y, Rosenberg JE. Abiraterone acetate: oral androgen biosynthesis inhibitor for treatment of castration-resistant prostate cancer. *Drug design, development and therapy*. 2012 Jan 16:13-8.
- Roudsari NM, Lashgari NA, Momtaz S, Ahaft S, Jamali F, Safaiepour P, Narimisa K, Jackson G, Bishayee A, Rezaei N, Abdolghaffari AH. Inhibitors of the PI3K/Akt/mTOR pathway in prostate cancer chemoprevention and intervention. *Pharmaceutics*. 2021 Aug 3;13(8):1195.



- Sakr WA, Partin AW. Histological markers of risk and the role of high-grade prostatic intraepithelial neoplasia. *Urology*. 2001 Apr 1;57(4):115-20.
- Salem M, Garcia JA. Abiraterone acetate, a novel adrenal inhibitor in metastatic castration-resistant prostate cancer. *Current oncology reports*. 2011 Apr;13:92-6.
- Sarkar C, Kommineni N, Butreddy A, Kumar R, Bunekar N, Gugulothu K. PLGA nanoparticles in drug delivery. *Nanoengineering of Biomaterials*. 2022 Feb 14:217-60.
- Schröder FH, Kruger AB, Rietbergen J, Kranse R, Maas PV, Beemsterboer P, Hoedemaeker R. Evaluation of the digital rectal examination as a screening test for prostate cancer. *Journal of the National Cancer Institute*. 1998 Dec 2;90(23):1817-23.
- Sefah K, Shangguan D, Xiong X, O'donoghue MB, Tan W. Development of DNA aptamers using Cell-SELEX. *Nature protocols*. 2010 Jun;5(6):1169-85.
- Shenoy TR, Boysen G, Wang MY, Xu QZ, Guo W, Koh FM, Wang C, Zhang LZ, Wang Y, Gil V, Aziz S. CHD1 loss sensitizes prostate cancer to DNA damaging therapy by promoting error-prone double-strand break repair. *Annals of Oncology*. 2017 Jul 1;28(7):1495-507.
- Shirai T, Asamoto M, Takahashi S, Imaida K. Diet and prostate cancer. *Toxicology*. 2002 Dec 27;181:89-94.
- Steinberg GD, Carter BS, Beaty TH, Childs B, Walsh PC. Family history and the risk of prostate cancer. *The prostate*. 1990;17(4):337-47.
- Sultan MI, Huynh LM, Kamil S, Abdelaziz A, Hammad MA, Gin GE, Lee DI, Youssef RF. Utility of noninvasive biomarker testing and MRI to predict a prostate cancer diagnosis. *International Urology and Nephrology*. 2023 Sep 24:1-8.
- Thakur A, Roy A, Ghosh A, Chhabra M, Banerjee S. Abiraterone acetate in the treatment of prostate cancer. *Biomedicine & Pharmacotherapy*. 2018 May 1;101:211-8.
- Walker SM, Lim I, Lindenberg L, Mena E, Choyke PL, Turkbey B. Positron emission tomography (PET) radiotracers for prostate cancer imaging. *Abdominal Radiology*. 2020 Jul;45:2165-75.
- Wang F, Li Z, Feng X, Yang D, Lin M. Advances in PSMA-targeted therapy for prostate cancer. *Prostate Cancer and Prostatic Diseases*. 2022 Mar;25(1):11-26.

- Wengner AM, Siemeister G, Luecking U, Lefranc J, Lienau P, Deeg G, Lagkadinou E, Liu L, Golfier S, Schatz C, Scholz A. ATR inhibitor BAY 1895344 shows potent anti-tumor efficacy in monotherapy and strong combination potential with the targeted alpha therapy radium-223 dichloride in preclinical tumor models. *Cancer Research*. 2017 Jul 1;77(13\_Supplement):836-.
- Woodrum DL, Brawer MK, Partin AW, Catalona WJ, Southwick PC. Interpretation of free prostate specific antigen clinical research studies for the detection of prostate cancer. *The Journal of urology*. 1998 Jan 1;159(1):5-12.
- Zhang W, Van Gent DC, Incrocci L, Van Weerden WM, Nonnekens J. Role of the DNA damage response in prostate cancer formation, progression and treatment. *Prostate cancer and prostatic diseases*. 2020 Mar 1;23(1):24-37.
- Zhu Y, Han CT, Zhang GM, Liu F, Ding Q, Xu JF, Vidal AC, Freedland SJ, Ng CF, Ye DW. Development and external validation of a prostate health index-based nomogram for predicting prostate cancer. *Scientific reports*. 2015 Oct 16;5(1):15341.

## **2. Literature review**

### **2. Prostate cancer**

The second most frequent disease and the fifth most significant cause of cancer-related mortality in males is prostate cancer (PCa). Prostate cancer was predicted to account for 375,000 deaths and 1.4 million new cases globally in 2020. Prostate cancer has a complex etiology. However, some risk factors for its onset include advanced age, a favorable family history, and African heritage. The incidence of PCa varies geographically and among ethnic groups. Worldwide, the incidence and mortality rates are higher among individuals of Black African heritage. There is variation in the United States among the various ethnic groups, with Black men of African heritage having the highest prevalence and death (Rawla, 2019). Different ethnic groups have different prevalence of several genetic risk loci for prostate cancer, which may explain the differences in incidence and death. According to recent epidemiological research, there is a clear causative link between genetic variables and the development of prostate cancer, and PCa is a highly heritable illness. According to twin research, 57% of men with prostate cancer had a family history of the disease. According to recent research, over 100 widely known single-nucleotide-polymorphisms (SNPs) have been linked to prostate cancer and are a significant risk factor for the disease development (Vieira et al., 2022).

#### **2.1. Characteristics features of prostate cancer**

Most prostate tumors are adenocarcinomas, sharing multiple traits in common with other prominent epithelial cancers, such as breast and colon cancer. The various essential elements of prostate cancer that are relevant for the study of the disease process are mentioned below.

##### **2.1.1. Correlation with aging**

Prostate cancer stands out due to its close relationship with aging; in fact, aging is the single most significant risk factor for prostate cancer. Clinically identifiable prostate cancer often does not emerge until the age of 60 or 70. However, preneoplastic lesions known as prostatic intraepithelial neoplasia (PIN) can be identified in men as early as their twenties and are very frequent in men by their fifties. Moreover, the incidence of carcinoma (about 1 in 9 males) is much lower than the prevalence of precancerous lesions (approximately 1 in 3 men). As a result, whereas the morphological alterations linked to initiation are somewhat common and

happen early in life, the development of invasive carcinoma is a far less common event that results from aging and occurs in a smaller population (Verma et al., 2011).

### **2.1.2. Environmental factors**

While the incidence of histological pre-neoplastic lesions has been observed to be similar globally, the incidence of prostate cancer in the United States is much greater than in most other nations, predominantly Asian countries. Therefore, it has been assumed that dietary and environmental variables, like those in other prevalent epithelial malignancies, play a significant role in the development of prostate carcinogenesis. However, new research raises doubts about whether Asian and American males genuinely have different relative incidences of preneoplastic lesions (Loeb et al., 2015; Sartor and Savarese, 2020).

### **2.1.3. Familial inheritance**

Only around 10% of prostate cancers are caused by hereditary factors, which are typically linked to early onset of the disease. Although the corresponding candidate genes have not yet been discovered, two family susceptibility loci have been localized to the X chromosome and a region of chromosome 1q. Furthermore, many investigations have found a statistical correlation between prostate and breast cancer; nevertheless, the underlying molecular mechanism of this interaction remains unclear (Vietri et al., 2021).

### **2.1.4. Role of steroid hormones**

Throughout the whole course of prostate carcinogenesis, signaling from steroid hormone receptors is essential. Specifically, males experience a typical age-related decline in the androgen-to-estrogen ratio, which may play a role in the development of prostate cancer. Furthermore, many studies have focused on the transition to androgen independence that characterizes advanced prostate cancer (Auchus and Sharifi, 2020).

### **2.1.5. Diet**

The Western lifestyle may cause an increased risk of prostate cancer, specifically the increased consumption of fat, red meat, and dairy products. Prostate cancer risk was positively correlated with total fat intake in African Americans, Asian Americans, and White Americans in a multiethnic investigation of dietary variables. Numerous studies found a strong correlation between the risk of prostate cancer and higher consumption of fat-containing foods, particularly dairy and red meat (Liss et al., 2019).

### **2.1.6. Obesity**

The body mass index (BMI) is used to quantify obesity. It is computed as follows: weight in kilograms divided by height in meters squared ( $\text{kg/m}^2$ ). If a person's BMI is equal to or higher than 25, they are deemed obese. While research on obesity has yielded conflicting results, some recent investigations indicate a continuous link between obesity and aggressive prostate cancer. Men who were obese had an almost two-fold increased risk of prostate cancer. The risk of prostate cancer was about six times higher in obese men than in non-obese men (Wilson et al., 2022).

### **2.1.7. Sexual behaviour and sexually transmitted diseases (STDs)**

Several case-control studies have shown a positive correlation between a history of STDs and the risk of prostate cancer. A positive correlation between history and the risk of prostate cancer has been discovered. However, many prospective investigations have failed to find a meaningful correlation between a history of syphilis or gonorrhea and prostate cancer. Prostate cancer development and the frequency of sexual activity have been proven to be directly correlated in many researches (Caini et al., 2014).

### **2.1.8. Occupation**

Numerous studies have demonstrated a strong association between the risk of prostate cancer and occupation. One such study investigated the relationship between prostate cancer and exposure to a range of agricultural chemicals, including pesticides, acetic acid, arsenic compounds, polycyclic aromatic hydrocarbons, petrol and diesel engine emissions, mono nuclear aromatic hydrocarbons, lubricating oils and greases. The study found that farmers who were exposed to these chemicals had double the likelihood of developing prostate cancer as compared to non-exposed farmers. These findings underscore the importance of implementing adequate safety measures to minimize exposure to potentially hazardous chemicals in the agricultural industry (Krstev and Knutsson, 2019; Pardo et al., 2020).

### **2.1.9. Smoking**

There is conflicting evidence regarding how smoking affects the epidemiology of prostate cancer. Prostate cancer risk factors have not traditionally included smoking. A meta-analysis study found that heavy smokers had a significantly higher risk of prostate cancer. Prostate cancer risk was increased in smokers, both current and former, although the relationship was statistically significant only in smokers who had smoked in the past. Moreover, there is a

favorable correlation between smoking and prostate cancer mortality. Through a number of reasons, including impacts on sex steroid hormone levels and ongoing exposure to carcinogens such as polycyclic aromatic hydrocarbons found in cigarette smoke, smoking may promote the development of more aggressive, hormone-sensitive malignancies (Al-Fayez and El-Metwally, 2023).

## **2.2. Different treatments for prostate cancer**

### **2.2.1. Active Surveillance**

Monitoring and anticipated action are the primary approaches used in the systematic "active surveillance" program to control prostate cancer. Active surveillance is considered to be the best option for patients with low-risk malignancies or those with little time to live. The following variables are typically taken into consideration as recommending criteria for active surveillance: illness features, health conditions, life expectancy, side effects, and patient desire. Prostate cancer trigger points include PSA level, clinical progression, and histology progression (Kinsella et al., 2018).

### **2.2.2. Radical prostatectomy**

A radical prostatectomy is the surgical excision of the prostate gland, performed either openly or through laparoscopy. To accomplish the procedure, small incisions must be made on the abdomen or via the perineum. A salvage radical prostatectomy is usually recommended for individuals with a local recurrence without metastases following cryotherapy, brachytherapy, or external beam radiation therapy. However, this may also lead to increased morbidity. For individuals under 70 years old with organ-confined prostate cancer, a life expectancy longer than 10 years, and few to no comorbidities, a radical prostatectomy is a recommended course of action. There are a few problems with its use, though. Incontinence and erectile dysfunction are possible outcomes of surgical damage to the urinary sphincter and erectile nerves (Costello, 2020).

### **2.2.3. Cryotherapy**

Using ultrasound guidance, cryoprobes are surgically inserted into the prostate as part of this technique. The prostate gland is frozen for approximately ten minutes at temperatures between -100 to -200 °C. Nevertheless, there have been reports of side effects from using this technique, such as fistula, rectal pain, erectile dysfunction, and urine incontinence and retention (Kotamarti and Polascik, 2023).

#### **2.2.4. Radiation**

One of the best treatments for killing prostate cancer cells with high radiation levels is radiation therapy. Several methods, including external beam therapy, which projects radiation through the skin to the malignant spots, and brachytherapy, which uses seeds inserted into the body, are used to deliver radiation to the diseased cells. The goal of radiation therapy is to target the prostate with high-energy radiation or particle doses while sparing surrounding tissues. The degree of prostate cancer determines these dosages. Patients who are not candidates for surgery are thought to benefit from this course of treatment (Kamran and D'Amico, 2020).

#### **2.2.5. Hormonal therapy**

Hormonal therapy is frequently referred to as androgen deprivation therapy (ADT). Prostate cancer that has progressed or spread is treated with this approach. The blocking of testosterone production and other male hormones, which stops them from feeding prostate cancer cells, is the basis of its therapeutic process (Desai et al., 2021). Thus, the suppression of androgen's effect on the androgen receptor is caused by markedly reduced male hormone levels. This is frequently accomplished by medical castration with the use of luteinizing hormone-releasing hormone (LHRH) analogs or antagonists or bilateral orchiectomy. By activating hypophysis receptors, the LHRH analog predominantly increases luteinizing hormone (LH) and follicle-stimulating hormone (FSH). This allows the drug to downregulate hypophysis receptors, which in turn lowers LH and FSH levels and suppresses the generation of testosterone. The standard LHRH agonists include histrelin, goserelin, triptorelin, and leuprolide. The antagonists block the hypophysis receptors, which results in the instantaneous suppression of testosterone production. However, both short-term and long-term adverse effects, including anemia, osteoporosis, insulin resistance, cardiovascular disease, hot flashes, lethargy, and sexual dysfunction, have been linked to ADT (Choi et al., 2022).

#### **2.2.6. Abiraterone**

A treatment of second-generation abiraterone targets the production of androgens in tumors and the adrenal glands. It is used to treat prostate cancer that has spread to other parts of the body and is linked to the irreversible inhibition of the hydroxylase and lyase activities of CYP17A, AR pathways, and 3-hydroxysteroid dehydrogenase activity. It has also been demonstrated that abiraterone effectively inhibits CYP1A2 and CYP2D6, two more microsomal drug-metabolizing enzymes (Stein et al., 2014; Thakur et al., 2018). Although abiraterone's clinical data have shown impressive outcomes, there have also been reports of

inconsistent responses and concurrently rising PSA levels. Abiraterone is associated with elevated levels of upstream mineralocorticoids CYP17A, which can lead to edema, hypertension, tiredness, and hypokalemia, among other side effects (Mostaghel, 2014; Auchus et al., 2014).

### **2.2.7. Chemotherapy**

Anticancer drugs are used in chemotherapy to destroy or stop malignant cell growth. Prostate cancer treatment has advanced in the decades since genetics, diagnostics, and treatment were first studied and understood. For prostate cancer, docetaxel is the most often prescribed chemotherapeutic drug.

### **2.2.8. Docetaxel**

When it comes to treating castration-resistant prostate cancer cells, docetaxel is considered the gold standard. Attaching itself to  $\beta$ -tubulin, this antimicrotubule drug prevents microtubule depolymerization, stopping mitotic cell division and triggering death. One important prerequisite for docetaxel activation is CYP3A. Relapse and the development of docetaxel resistance have been linked. The upregulation of the P-glycoprotein-encoding multidrug resistance (MDR) 1 gene has been linked to docetaxel resistance (Puente et al., 2017; Sekino and Teishima, 2020).

### **2.2.9. Cabazitaxel**

A novel antineoplastic semi-synthetic called cabazitaxel is produced from different kinds of yew tree needles (Taxus). One second-generation treatment for prostate cancer targeted at lowering docetaxel resistance is cabazitaxel (Barve et al., 2020). It has a low affinity for it because it contains more methyl groups than P-glycoprotein. In the hepatic tissues, CYP3A4/5 and CYP2C8 (10–20%) metabolize it. Among the frequent adverse effects linked to its use include alopecia, neurotoxicity, bronchospasm, renal failure, hypotension, tiredness, and erythema/rash. Additionally, deaths from diarrhea linked to cabazitaxel that resulted in electrolyte imbalances and dehydration have been reported (Baciarrello et al., 2022).

### **2.2.10. Enzalutamide**

Ezelutamide, a second-generation AR inhibitor, is one of the chemotherapy drugs for prostate cancer. Targeting the androgen pathway, the drug has three main actions: (1) competitively blocking androgen's ability to bind to the androgen receptor, (2) blocking nuclear translocation



and cofactor recruitment, and (3) blocking the association of the activated androgen receptor. Enzalutamide works against androgens such as dihydrotestosterone and testosterone (Chen et al., 2023).

### **2.3. Nanoparticle-based drug delivery for the treatment of cancer**

For many years, scientists have been particularly interested in the early identification and efficient cancer treatment. A body cell is the source of cancer. To preserve the body's homeostasis and steady state, healthy cells divide and create new ones to replace the old ones. However, if a cell's genetic material is altered, the cells may develop abnormally and eventually form a tumor. Cancer cells spread to many parts of the body through the blood and lymphatic vessels, accumulating into tumorigenic masses of cells. With almost 9 million fatalities from the disease in 2018, cancer is the second most significant cause of mortality globally. The highest likelihood of using suitable therapeutic intervention tactics is when cancer is diagnosed early. Several techniques have been used to detect cancer efficiently in its early stages. These include the use of tumor markers, imaging methods like computed tomography (CT), magnetic resonance imaging (MRI), positron emission tomography (PET), ultrasound scanning, endoscopy, and screening for cytogenetic and cell genetic abnormalities (Raj et al., 2021).

The drug delivery system (DDS) has been utilized in clinical and pre-clinical studies to provide therapeutic compounds to treat various diseases. Oral ingestion or injection is the two most common methods used to administer conventional DDS. Many of the drawbacks of traditional drug delivery systems can be solved by controlled drug delivery systems. For example, chemotherapeutic drugs that are used to treat cancer are typically administered non-specifically, which damages both cancerous and healthy cells, leading to low efficacy and high toxicities. Chemotherapeutic chemicals would be well-carried by controlled DDSs, which would direct the drugs to the tumor site, boosting their concentration in cancer cells and preventing harm in healthy cells. Furthermore, controlled DDSs assist in delivering proteins and novel therapeutic agents, such as RNA interference and gene therapy, by shielding the medicines from degradation and clearance. They can aid in avoiding enzymatic degradation and reticuloendothelial or other tissue uptake of DNA and siRNA (Senapati et al., 2018; Yu et al., 2023).

Because of the development of nanotechnology, nanoparticles are now a viable option for controlled drug delivery systems. Particles with a diameter of between 10 and 1000 nm are commonly referred to as nanoparticles. As a drug delivery system (DDS), nanoparticles can

increase the drug's half-life, make some hydrophobic drugs more soluble, and release the drug gradually or under controlled conditions. Additionally, stimuli-responsive nanoparticles can assist in reducing toxicity and regulating the drug biodistribution. In the 1960s, liposomes—the first nanocarrier to be discovered—were employed as protein and drug carriers. Ever since many materials have been synthesized into nanoparticles and utilized as DDSs (Dang and Guan, 2020).

The discovery of a breakthrough in nanotechnology research has made it comparatively more accessible for scientists and medical professionals worldwide to identify cancer early and treat it successfully. The fields of nanotechnology and nanomedicine have blessed scientists with a blessing that makes accurate and timely diagnosis and treatment possible. Due to their high sensitivity and specificity, nanodevices, such as nano-enabled sensors, are being explored to detect biomarkers, such as ctDNA, tumor biomarkers (prostate-specific antigen), cancer-related proteins (either cell surface glycoproteins or secreted proteins), etc. According to mounting data, nanotechnology is becoming useful for cancer treatment and early diagnosis. Many nanomedicines, including lipid nanocarriers, polymer nanocarriers, viral vectors, and drug conjugates, have been used in cancer treatment (Chehelgerdi et al., 2023).

#### **2.4. PLGA nanoparticles for prostate cancer therapy**

The United States Food and Drug Administration (US-FDA) has approved polymeric nanoparticles and their copolymers made from poly lactic acid-co-glycolic acid (PLGA) containing different ratios of poly(lactic acid) (PLA) and poly(glycolic acid) (PGA). They have been used as delivery systems for a range of drugs. The goal of developing nanoparticles that are more stable and long-lasting in systemic circulation—particularly for drugs with limited solubility—while also having higher solubility, larger drug loading capacity, and a more homogenous particle size distribution is still being researched (Pandey and Jain, 2015). A polymer's physicochemical features can vary based on the type, quantity, and ratio of monomers it contains in its PLGA structure. As a result, depending on the PLA/PGA ratio and the technique used to produce the nanoparticles, PLGA polymer-based nanoparticles are shown to have varying physical and pharmacological properties and may respond differently to therapy. Furthermore, several features have been added to the NP, including molecular weight (Mw), viscosity, glass transition temperature, and polymer terminal. The treatment's efficacy is largely determined by how these variables are determined in relation to the drug to be used,

the disease being treated, and how the NP is designed to achieve optimal efficiency (Tsachouridis et al., 2022).

In a study by Simitcioglu et al. (2022), Docetaxel-loaded polylactic-co-glycolic acid nanoparticles with varying molecular weights (Resomer 502 and 504) and terminal groups (Resomer 502H and 504H) were prepared, and the impact of these resomers on the characteristics of the nanoparticles, prostate cancer, and healthy cells was examined. PLGA nanoparticles loaded with docetaxel were developed using a single emulsion solvent evaporation technique. Electron microscopy and zeta sizer were used to characterize the surface. Cytotoxic activity, *in vitro* drug release patterns, and encapsulation efficiency were measured. The polymer's molecular weight primarily influenced the surface shape of the nanoparticles. Higher encapsulation efficiency was found in the groups having acid terminal functions. *In vitro* drug release was seen in all formulations after 240 h at pH 5.6 and 334 h at pH 7.4. Moreover, the high molecular weight groups displayed selective cytotoxicity. Prostate cancer treatment may benefit from the use of these receptors, particularly RG 504 and RG 504H, as a low-dose and very effective extended-release drug delivery method.

Nassir et al. (2018) also conducted a study whereby they developed polymeric nanoparticles containing resveratrol (RLPLGA) and assessed its cytotoxicity and mechanism of apoptotic cell death against the prostate cancer cell line (LNCaP). When RLPLGA was used against LNCaP cells, its 50% and 90% inhibitory concentrations ( $IC_{50}$  and  $IC_{90}$ ) were  $15.6 \pm 1.49$  and  $41.1 \pm 2.19$   $\mu$ M, respectively, indicating a considerable decrease in cell viability. The cell cycle arrest at the G1-S transition phase, phosphatidylserine externalization, DNA nicking, loss of mitochondrial membrane potential, and production of reactive oxygen species in LNCaP cells all indicated that apoptosis was the mechanism causing this impact. Additionally, at all tested dosages, nanoparticles showed much higher cytotoxicity to LNCaP cells than free resveratrol (RL). Even at 200  $\mu$ M, RLPLGA nanoparticles did not exhibit any harmful cytotoxic effects on mouse macrophages.

In another study, the therapeutic activity of eupatorin in human prostate cancer cell lines DU-145 and LNCaP was assessed in relation to the usage of mPEG-b-poly (lactic-co-glycolic) acid (PLGA) coated iron oxide nanoparticles as a carrier. The MTT experiment showed that the  $IC_{50}$  doses of eupatorin-loaded  $Fe_3O_4@mPEG-b-PLGA$  nanoparticles were 75 mM and 100 mM, respectively, and that they significantly reduced the growth rate of DU-145 and LNCaP cells. Subsequently, nuclear condensation, an increase in the sub-G1 phase cell population, and

an elevated NO level were used to confirm apoptosis. Fe<sub>3</sub>O<sub>4</sub>@mPEG-b-PLGA nanoparticles loaded with eupatorin were shown by Annexin/PI analysis to boost apoptosis and decrease necrosis frequency. Lastly, Western blotting analysis validated these findings and demonstrated that the designed nanoparticles up-regulated the cleaved caspase-3 level and the Bax/Bcl-2 ratio. When eupatorin was encapsulated in Fe<sub>3</sub>O<sub>4</sub>@mPEG-b-PLGA nanoparticles instead of being free, it enhanced its anticancer activities in prostate cancer cell lines (Tousi et al., 2021).

The purpose of the study conducted by Essa et al. (2023) was to prepare and optimize quercetin-loaded PLGA nanoparticles and investigate the potential effects of coating with chitosan on cellular uptake. Additionally, the study aimed to determine whether folic acid, as a ligand, could provide selective toxicity and improved uptake in model LNCaP prostate cancer cells, which express high levels of the receptor prostate-specific membrane antigen (PSMA), in contrast to PC-3 cells that have relatively low PSMA expression. The results indicate that quercetin (and other comparable chemotherapeutics) can be targetedly delivered and released from the nano-system as an effective nanocarrier against prostate cancer cells.

Panda and colleagues (2023) developed new PEGylated PLGA nanoparticles (CPDNPs) loaded with doxorubicin and coupled with peptides for efficient and extended delivery to prostate cancer (PCa) cells. Compared to PC-3 cell lines, CPDNPs showed decreased hemolysis and increased cellular uptake and death. The pharmacokinetic analysis verified that CPDNPs outperformed DOX, DNPs, and PDNPs in terms of AUC (μg h/mL) and T (h).

Co-encapsulation of docetaxel (DTX) and abiraterone acetate (AbrA) in polymeric nanoparticles was designed in another work by Sokol et al. (2019) as novel prototypes for prostate cancer treatment combining hormonal and chemotherapy. Confocal microscopy observations demonstrated the efficient accumulation of NP-AbrA/Dtx in the cell cytoplasm. Research demonstrated that NPs loaded with both AbrA and Dtx had a synergistic mechanism of action, in contrast to the combination of chemicals, and exhibited a high cytotoxic activity on the LNCaP cell line. The results validate the possible application of generated NPs in additional *in vivo* investigations.

## **2.5. Prostate cancer-targeted therapies using surface-modified nanoparticles**

Surface modification of the nanoparticles with ligands that can bind to receptors overexpressed on the surface of those cancer cells is a viable strategy to increase the selectivity of nanostructures toward PCa cells (Ashrafizadeh et al., 2022). Emerging synthetic nucleic acid-

based agents with potential for diagnosis and treatment are aptamers. The excellent selectivity and affinity of these small single-stranded RNA or DNA molecules to different ligands make them attractive for use in medicinal applications (Cruz-Hernández et al., 2022). Aptamers are easily synthesized and do not cause immunogenotoxicity. Aptamers have been thoroughly studied for the therapy of PCa in experiments. In order to inhibit the growth of PCa, self-assembled polymeric nanoparticles made of PLGA and PEG have been functionalized with Wy5a aptamer. For the goal of magnetic resonance imaging, docetaxel (DTX) and superparamagnetic iron oxide nanoparticles (SPIONs) were enclosed into polymeric nanostructures to facilitate simultaneous sustained drug delivery. Conjugating the Wy5a aptamer to these nanoparticles enhanced their selectivity toward PC-3 cells while posing the least systemic toxicity (Fang et al., 2020). Targeted nanostructures outperformed ordinary nanoparticles in their ability to inhibit PCa. A medicinal plant-derived naphthoquinone called plumbagin (5-hydroxy-2-methyl-1,4-naphthoquinone) has the ability to stop PCa cells from spreading. In order to encapsulate plumbagin, PLGA-PEG nanoparticles with a terminal carboxylic acid group (PLGA-PEGCOOH) have been produced. PSMA aptamer was used to modify these nanoarchitectures in order to increase their ability to target PCa cells. Up to 90% of the nanostructures are internalized in PCa cells due to their surface modification with PSMA aptamer, greatly enhancing plumbagin's anti-tumor effect (Pan et al., 2017).

The ability of SPIONs to deliver image-guided PCa treatment is one of its benefits. PSMA-aptamer-conjugated SPIONs that specifically targeted androgen-sensitive human prostate cancer LNCaP cells *in vitro* and *in vivo* were produced using a hybridization technique. By means of intercalation using a cytosine-guanine (CG)-rich duplex comprising the PSMA aptamer and electrostatic contact with the polymer covering of the nanostructures, doxorubicin was loaded onto these nanostructures. These nanoparticles exhibited growth retardation in a xenograft experiment and markedly enhanced cellular uptake of doxorubicin to eradicate PCa cells (Yu et al., 2011). According to the previously described research, modifying nanoparticle surfaces with aptamer seems to enhance their internalization into PCa cells (Chen et al., 2020; Dhar et al., 2008).

Hyaluronic acid is another agent that is commonly utilized to modify the surface of nanostructures. N-acetyl-D-glucosamine and D-glucuronic acid residues are present in this linear glycosaminoglycan (Fallacara et al., 2018). It has been documented that hyaluronic acid contributes to physiological processes such as cell division, migration, and proliferation, as well as embryonic development (Toole, 2004; Abatangelo et al., 2020). Hyaluronic acid has

been shown to bind to CD44 surface receptors on cells through van der Waals forces and hydrogen bonds (Paidikondala et al., 2019; Tiwari and Bahadur, 2019). PCa treatment has made use of hyaluronic acid-modified nanoparticles to administer epigallocatechin-3-gallate. By binding to the CD44 receptor, these PEG nanostructures treated with hyaluronic acid increased the intracellular accumulation of epigallocatechin-3-gallate in PCa cells. Following cell cycle arrest at the G2/M phase, the proliferation rate of PCa cells sharply declined (Huang et al., 2016).

Numerous malignancies, such as lung, PCa, and breast cancer, have overexpressed sigma receptors (Zeng et al., 2012). In PCa therapy, anisamide, a ligand for the sigma receptor, can facilitate the targeted transport of doxorubicin via liposomes (Banerjee et al., 2004). However, one of their disadvantages is the inability of sigma receptor ligands such as anisamide or haloperidol to discriminate between sigma receptors 1 and 2. Targeting sigma receptor 2 has garnered attention recently. This is due to the fact that this receptor is positively correlated with the pace of cancer growth and is expressed at a higher level on tumor cells than sigma receptor 1 (Chen et al., 2021). With the purpose of treating prostate cancer, 3-(4-cyclohexylpiperazine-1-yl) propyl amine (CPPA) has been loaded into lipid nanocarriers containing telmisartan, an angiotensin II receptor blocker. The benefits of CPPA-modified telmisartan-loaded nanoparticles included their small size, high encapsulation efficacy, and negative zeta potential. The application of CPPA to the nanoparticle surface caused the internalization of the particles by receptor-mediated endocytosis. The stimulation of apoptosis led to a considerable decrease in the viability of tumor cells. Comparing the CAPP-modified nanoparticles to non-targeted nanoparticles, the  $IC_{50}$  value of the former was noticeably lower (Puri et al., 2016). It seems that altering a nanostructure's surface enhanced its selectivity and decreased its  $IC_{50}$  value in PCa treatment (Sanjee et al., 2021). A key factor in improving the biocompatibility of nanoparticles is surface modification. For example, chitosan is a naturally occurring substance separated from algae. Because it enhances drug delivery and nanoparticle stability, chitosan has drawn much interest in anti-cancer therapy (Ahmad et al., 2022; Yee Kuen and Masarudin, 2022). Chitosan-modified nanoparticles are stable and exhibit good biocompatibility. They have a high encapsulation efficiency, which is crucial for making anti-cancer drugs more harmful to PCa cells (Zhang et al., 2021).

## 2.6. Aptamer-conjugated PLGA nanoparticles and prostate cancer

The clinical prognosis for patients with castration-resistant prostate cancer (CRPC) is still dismal despite recent advancements in prostate cancer therapy, including enhanced surgical techniques and novel medications in androgen deprivation therapy (Gravis, 2019). As a targeting ligand, aptamer (Apt) has garnered significant interest. Aptamers are single-stranded oligonucleotides that fold into distinctive tertiary structures in order to bind to their targets. Similar to antibodies, aptamers have great affinity and specificity. Aptamers, on the other hand, offer a number of unique benefits, including low molecular weight, high stability, quick tissue penetration, absence of immunogenicity, and ease of chemical synthesis and modification. Prostate-specific membrane antigen (PSMA) is bound by A10 2'-fluoropyrimidine RNA aptamer, commonly used as the targeting ligand for targeted nanoparticles in prostate cancer (Thoma, 2018). Nonetheless, PSMA expression in CRPC cancer cells is relatively modest. Through the use of living whole cells and SELEX technology (Systematic Evolution of Ligands by Exponential Enrichment), a new aptamer called Wy5a has been produced that specifically binds to the cancer cells of CRPC (PC-3) (Wang et al., 2014).

In another investigation, the "core-shell" targeted nanoparticles (NPs) were synthesized through the self-assembly of a prefunctionalized amphiphilic triblock copolymer made of poly(lactic-co-glycolic acid) (PLGA), polyethylene glycol (PEG), and the Wy5a aptamer (Apt). This copolymer was screened using the cell-SELEX technique to determine its ability to target the CRPC cell line PC-3. The targeted nanoparticles were co-encapsulated with a cluster of hydrophobic superparamagnetic iron oxide (SPIO) nanoparticles and docetaxel (Dtx). The targeted NPs demonstrated enhanced contrast-enhanced MRI performance and regulated drug release. The transport of Wy5a to PC-3 cells *in vitro* and *in vivo* was cancer-targeted due to its presence on the nanoparticle surface. The enhanced cytotoxicity and ultrasensitive MRI of these targeted NPs were shown by *in vitro* cytotoxicity and magnetic resonance imaging investigations. The targeted NPs showed a more potent anticancer capacity without appreciable systemic toxicity, according to *in vivo* investigations. Based on the available data, using targeted NPs as a drug delivery system could be a viable approach to treat CRPC effectively (Fang et al., 2020).

## 2.7. References

- Abatangelo G, Vindigni V, Avruscio G, Pandis L, Brun P. Hyaluronic acid: redefining its role. *Cells*. 2020 Jul 21;9(7):1743.
- Ahmad MZ, Rizwanullah M, Ahmad J, Alasmay MY, Akhter MH, Abdel-Wahab BA, Warsi MH, Haque A. Progress in nanomedicine-based drug delivery in designing of chitosan nanoparticles for cancer therapy. *International Journal of Polymeric Materials and Polymeric Biomaterials*. 2022 May 24;71(8):602-23.
- Al-Fayez S, El-Metwally A. Cigarette smoking and prostate cancer: A systematic review and meta-analysis of prospective cohort studies. *Tobacco Induced Diseases*. 2023;21.
- Ashrafizadeh M, Aghamiri S, Tan SC, Zarrabi A, Sharifi E, Rabiee N, Kadumudi FB, Pirouz AD, Delfi M, Byrappa K, Thakur VK. Nanotechnological approaches in prostate cancer therapy: integration of engineering and biology. *Nano Today*. 2022 Aug 1;45:101532.
- Auchus RJ, Sharifi N. Sex hormones and prostate cancer. *Annual review of medicine*. 2020 Jan 27;71:33-45.
- Auchus RJ, Yu MK, Nguyen S, Mundle SD. Use of prednisone with abiraterone acetate in metastatic castration-resistant prostate cancer. *The oncologist*. 2014 Dec 1;19(12):1231-40.
- Baciarello G, Delva R, Gravis G, Tazi Y, Beuzeboc P, Gross-Goupil M, Bompas E, Joly F, Greilsamer C, Hon TN, Barthelemy P. Patient preference between cabazitaxel and docetaxel for first-line chemotherapy in metastatic castration-resistant prostate cancer: the CABADOC trial. *European Urology*. 2022 Mar 1;81(3):234-40.
- Banerjee R, Tyagi P, Li S, Huang L. Anisamide- targeted stealth liposomes: a potent carrier for targeting doxorubicin to human prostate cancer cells. *International journal of cancer*. 2004 Nov 20;112(4):693-700.
- Barve A, Jain A, Liu H, Zhao Z, Cheng K. Enzyme-responsive polymeric micelles of cabazitaxel for prostate cancer targeted therapy. *Acta biomaterialia*. 2020 Sep 1;113:501-11.
- Caini S, Gandini S, Dudas M, Bremer V, Severi E, Gherasim A. Sexually transmitted infections and prostate cancer risk: a systematic review and meta-analysis. *Cancer epidemiology*. 2014 Aug 1;38(4):329-38.



- Chehelgerdi M, Chehelgerdi M, Allela OQ, Pecho RD, Jayasankar N, Rao DP, Thamaraikani T, Vasanthan M, Viktor P, Lakshmaiya N, Saadh MJ. Progressing nanotechnology to improve targeted cancer treatment: overcoming hurdles in its clinical implementation. *Molecular cancer*. 2023 Oct 9;22(1):169.
- Chen AF, Ma WH, Xie XY, Huang YS. Sigma-2 receptor as a potential drug target. *Current Medicinal Chemistry*. 2021 Jun 1;28(21):4172-89.
- Chen X, Wang Q, Pan Y, Wang S, Li Y, Zhang H, Xu M, Zhou H, Liu X. Comparative efficacy of second-generation androgen receptor inhibitors for treating prostate cancer: A systematic review and network meta-analysis. *Frontiers in Endocrinology*. 2023 Mar 9;14:1134719.
- Chen Y, Deng Y, Zhu C, Xiang C. Anti prostate cancer therapy: aptamer-functionalized, curcumin and cabazitaxel co-delivered, tumor targeted lipid-polymer hybrid nanoparticles. *Biomedicine & Pharmacotherapy*. 2020 Jul 1;127:110181.
- Choi E, Buie J, Camacho J, Sharma P, de Riese WT. Evolution of androgen deprivation therapy (ADT) and its new emerging modalities in prostate cancer: an update for practicing urologists, clinicians and medical providers. *Research and Reports in Urology*. 2022 Mar 30:87-108.
- Costello AJ. Considering the role of radical prostatectomy in 21st century prostate cancer care. *Nature Reviews Urology*. 2020 Mar;17(3):177-88.
- Cruz-Hernández CD, Rodríguez-Martínez G, Cortés-Ramírez SA, Morales-Pacheco M, Cruz-Burgos M, Losada-García A, Reyes-Grajeda JP, González-Ramírez I, González-Covarrubias V, Camacho-Arroyo I, Cerbón M. Aptamers as theragnostic tools in prostate cancer. *Biomolecules*. 2022 Jul 29;12(8):1056.
- Desai K, McManus JM, Sharifi N. Hormonal therapy for prostate cancer. *Endocrine reviews*. 2021 Jun 1;42(3):354-73.
- Dhar S, Gu FX, Langer R, Farokhzad OC, Lippard SJ. Targeted delivery of cisplatin to prostate cancer cells by aptamer functionalized Pt (IV) prodrug-PLGA-PEG nanoparticles. *Proceedings of the National Academy of Sciences*. 2008 Nov 11;105(45):17356-61.

- Essa D, Kondiah PP, Kumar P, Choonara YE. Design of Chitosan-Coated, Quercetin-Loaded PLGA Nanoparticles for Enhanced PSMA-Specific Activity on LnCap Prostate Cancer Cells. *Biomedicines*. 2023 Apr 18;11(4):1201.
- Fallacara A, Baldini E, Manfredini S, Vertuani S. Hyaluronic acid in the third millennium. *Polymers*. 2018 Jun 25;10(7):701.
- Fang Y, Lin S, Yang F, Situ J, Lin S, Luo Y. Aptamer-conjugated multifunctional polymeric nanoparticles as cancer-targeted, MRI-ultrasensitive drug delivery systems for treatment of castration-resistant prostate cancer. *BioMed Research International*. 2020 Apr 27;2020.
- Gravis G. Systemic treatment for metastatic prostate cancer. *Asian journal of urology*. 2019 Apr 1;6(2):162-8.
- Huang WY, Lin JN, Hsieh JT, Chou SC, Lai CH, Yun EJ, Lo UG, Pong RC, Lin JH, Lin YH. Nanoparticle targeting CD44-positive cancer cells for site-specific drug delivery in prostate cancer therapy. *ACS applied materials & interfaces*. 2016 Nov 16;8(45):30722-34.
- Kamran SC, D'Amico AV. Radiation therapy for prostate cancer. *Hematology/Oncology Clinics*. 2020 Feb 1;34(1):45-69.
- Kinsella N, Helleman J, Bruinsma S, Carlsson S, Cahill D, Brown C, Van Hemelrijck M. Active surveillance for prostate cancer: a systematic review of contemporary worldwide practices. *Translational andrology and urology*. 2018 Feb;7(1):83.
- Kotamarti S, Polascik TJ. Focal cryotherapy for prostate cancer: a contemporary literature review. *Annals of Translational Medicine*. 2023 Jan 1;11(1).
- Krstev S, Knutsson A. Occupational risk factors for prostate cancer: a meta-analysis. *Journal of Cancer Prevention*. 2019 Jun;24(2):91.
- Liss MA, Al-Bayati O, Gelfond J, Goros M, Ullevig S, DiGiovanni J, Hamilton-Reeves J, O'Keefe D, Bacich D, Weaver B, Leach R. Higher baseline dietary fat and fatty acid intake is associated with increased risk of incident prostate cancer in the SABOR study. *Prostate cancer and prostatic diseases*. 2019 May;22(2):244-51.

- Loeb S, Peskoe SB, Joshu CE, Huang WY, Hayes RB, Carter HB, Isaacs WB, Platz EA. Do environmental factors modify the genetic risk of prostate cancer?. *Cancer Epidemiology, Biomarkers & Prevention*. 2015 Jan 1;24(1):213-20.
- Mostaghel EA. Abiraterone in the treatment of metastatic castration-resistant prostate cancer. *Cancer management and research*. 2014 Jan 28:39-51.
- Nassir AM, Shahzad N, Ibrahim IA, Ahmad I, Md S, Ain MR. Resveratrol-loaded PLGA nanoparticles mediated programmed cell death in prostate cancer cells. *Saudi Pharmaceutical Journal*. 2018 Sep 1;26(6):876-85.
- Paidikondala M, Rangasami VK, Nawale GN, Casalini T, Perale G, Kadekar S, Mohanty G, Salminen T, Oommen OP, Varghese OP. An Unexpected Role of Hyaluronic Acid in Trafficking siRNA Across the Cellular Barrier: The First Biomimetic, Anionic, Non-Viral Transfection Method. *Angewandte Chemie International Edition*. 2019 Feb 25;58(9):2815-9.
- Pan M, Li W, Yang J, Li Z, Zhao J, Xiao Y, Xing Y, Zhang X, Ju W. Plumbagin-loaded aptamer-targeted poly D, L-lactic-co-glycolic acid-b-polyethylene glycol nanoparticles for prostate cancer therapy. *Medicine*. 2017 Jul;96(30).
- Panda PK, Jain SK. Doxorubicin bearing peptide anchored PEGylated PLGA nanoparticles for the effective delivery to prostate cancer cells. *Journal of Drug Delivery Science and Technology*. 2023 Jun 10:104667.
- Pandey A, Jain DS. Poly Lactic- Co- Glycolic Acid (PLGA) copolymer and its pharmaceutical application. *Handbook of polymers for pharmaceutical technologies: processing and applications*. 2015 Aug 10;2:151-72.
- Pardo LA, Beane Freeman LE, Lerro CC, Andreotti G, Hofmann JN, Parks CG, Sandler DP, Lubin JH, Blair A, Koutros S. Pesticide exposure and risk of aggressive prostate cancer among private pesticide applicators. *Environmental Health*. 2020 Dec;19(1):1-2.
- Puente J, Grande E, Medina A, Maroto P, Lainez N, Arranz JA. Docetaxel in prostate cancer: a familiar face as the new standard in a hormone-sensitive setting. *Therapeutic advances in medical oncology*. 2017 May;9(5):307-18.
- Puri R, Kaur Bhatia R, Shankar Pandey R, Kumar Jain U, Katare OP, Madan J. Sigma-2 receptor ligand anchored telmisartan loaded nanostructured lipid particles augmented

drug delivery, cytotoxicity, apoptosis and cellular uptake in prostate cancer cells. Drug development and industrial pharmacy. 2016 Dec 1;42(12):2020-30.

Raj S, Khurana S, Choudhari R, Kesari KK, Kamal MA, Garg N, Ruokolainen J, Das BC, Kumar D. Specific targeting cancer cells with nanoparticles and drug delivery in cancer therapy. In Seminars in cancer biology 2021 Feb 1 (Vol. 69, pp. 166-177). Academic Press.

Rawla P. Epidemiology of prostate cancer. World journal of oncology. 2019 Apr;10(2):63.

Saniee F, Shabani Ravari N, Goodarzi N, Amini M, Atyabi F, Saeedian Moghadam E, Dinarvand R. Glutamate-urea-based PSMA-targeted PLGA nanoparticles for prostate cancer delivery of docetaxel. Pharmaceutical Development and Technology. 2021 Apr 21;26(4):381-9.

Sartor AO, Savarese M. Risk factors for prostate cancer. Waltham, MA: UpToDate. 2020.

Sekino Y, Teishima J. Molecular mechanisms of docetaxel resistance in prostate cancer. Cancer Drug Resistance. 2020;3(4):676.

Senapati S, Mahanta AK, Kumar S, Maiti P. Controlled drug delivery vehicles for cancer treatment and their performance. Signal transduction and targeted therapy. 2018 Mar 16;3(1):7.

Simitcioglu B, Karagoz ID, Ilbasimis-Tamer S, Tamer U. Effect of different molecular weight and terminal group PLGA on docetaxel nanoparticles: characterization and cytotoxic activity of castration-resistant prostate cancer cells. Pharmaceutical Development and Technology. 2022 Aug 9;27(7):794-804.

Sokol MB, Nikolskaya ED, Yabbarov NG, Zenin VA, Faustova MR, Belov AV, Zhunina OA, Mollaev MD, Zabolotsky AI, Tereshchenko OG, Severin ES. Development of novel PLGA nanoparticles with co-encapsulation of docetaxel and abiraterone acetate for a highly efficient delivery into tumor cells. Journal of Biomedical Materials Research Part B: Applied Biomaterials. 2019 May;107(4):1150-8.

Stein MN, Patel N, Bershadskiy A, Sokoloff A, Singer EA. Androgen synthesis inhibitors in the treatment of castration-resistant prostate cancer. Asian journal of andrology. 2014 May;16(3):387.

- Thakur A, Roy A, Ghosh A, Chhabra M, Banerjee S. Abiraterone acetate in the treatment of prostate cancer. *Biomedicine & Pharmacotherapy*. 2018 May 1;101:211-8.
- Thoma C. Aptamer effective in vivo. *Nature Reviews Urology*. 2018 Jul;15(7):396-7.
- Tiwari S, Bahadur P. Modified hyaluronic acid based materials for biomedical applications. *International journal of biological macromolecules*. 2019 Jan 1;121:556-71.
- Toole BP. Hyaluronan: from extracellular glue to pericellular cue. *Nature Reviews Cancer*. 2004 Jul 1;4(7):528-39.
- Tousi MS, Sepehri H, Khoee S, Farimani MM, Delphi L, Mansourizadeh F. Evaluation of apoptotic effects of mPEG-b-PLGA coated iron oxide nanoparticles as a eupatorin carrier on DU-145 and LNCaP human prostate cancer cell lines. *Journal of Pharmaceutical Analysis*. 2021 Feb 1;11(1):108-21.
- Tsachouridis K, Christodoulou E, Zamboulis A, Michopoulou A, Barmpalexis P, Bikiaris DN. Evaluation of poly (lactic acid)/and poly (lactic-co-glycolic acid)/poly (ethylene adipate) copolymers for the preparation of paclitaxel loaded drug nanoparticles. *Journal of Drug Delivery Science and Technology*. 2022 Nov 1;77:103918.
- Verma M, Patel P, Verma M. Biomarkers in prostate cancer epidemiology. *Cancers*. 2011 Sep 30;3(4):3773-98.
- Vieira GM, Gellen LP, da Veiga Borges Leal DF, Pastana LF, Vinagre LW, Aquino VT, Fernandes MR, de Assumpção PP, Burbano RM, Dos Santos SE, Dos Santos NP. Correlation between genomic variants and worldwide epidemiology of prostate cancer. *Genes*. 2022 Jun 10;13(6):1039.
- Vietri MT, D'Elia G, Caliendo G, Resse M, Casamassimi A, Passariello L, Albanese L, Cioffi M, Molinari AM. Hereditary prostate cancer: genes related, target therapy and prevention. *International journal of molecular sciences*. 2021 Apr 4;22(7):3753.
- Wang Y, Luo Y, Bing T, Chen Z, Lu M, Zhang N, Shangguan D, Gao X. DNA aptamer evolved by cell-SELEX for recognition of prostate cancer. *PLoS One*. 2014 Jun 23;9(6):e100243.
- Wilson RL, Taaffe DR, Newton RU, Hart NH, Lyons-Wall P, Galvão DA. Obesity and prostate cancer: A narrative review. *Critical Reviews in Oncology/Hematology*. 2022 Jan 1;169:103543.

- Yee Kuen C, Masarudin MJ. Chitosan nanoparticle-based system: A new insight into the promising controlled release system for lung cancer treatment. *Molecules*. 2022 Jan 12;27(2):473.
- Yu L, Liu S, Jia S, Xu F. Emerging frontiers in drug delivery with special focus on novel techniques for targeted therapies. *Biomedicine & Pharmacotherapy*. 2023 Sep 1;165:115049.
- Yu MK, Kim D, Lee IH, So JS, Jeong YY, Jon S. Image- guided prostate cancer therapy using aptamer- functionalized thermally cross- linked superparamagnetic iron oxide nanoparticles. *Small*. 2011 Aug 8;7(15):2241-9.
- Zeng C, Rothfuss J, Zhang J, Chu W, Vangveravong S, Tu Z, Pan F, Chang KC, Hotchkiss R, Mach RH. Sigma-2 ligands induce tumour cell death by multiple signalling pathways. *British journal of cancer*. 2012 Feb;106(4):693-701.
- Zhang J, Zhou J, Yuan Q, Zhan C, Shang Z, Gu Q, Zhang J, Fu G, Hu W. Characterization of ginsenoside compound K loaded ionically cross-linked carboxymethyl chitosan–calcium nanoparticles and its cytotoxic potential against prostate cancer cells. *Journal of Ginseng Research*. 2021 Mar 1;45(2):228-35.

### 3. Objectives and plan of study

#### 3.1. Objectives

The objectives of this research are to develop and optimize Abiraterone acetate (the drug) loaded Poly-lactic-co-glycolic acid (PLGA) nanoparticles and further conjugate the nanoparticles with  $\Delta$ PSap4#5 DNA aptamer and investigate them as a targeted therapy against prostate cancer cells, *in vitro* and *in vivo*.

This study is divided into the following sections:

- Abiraterone acetate-loaded nanoparticles (ABR-NP) will be prepared and conjugated with an  $\Delta$ PSap4#5 DNA aptamer for site-specific delivery. The physicochemical properties of the prepared formulation will be studied.
- Further, the *in vitro* efficacy will be determined using the prepared nanoparticles (ABR-NP and Apt-ABR-NP) toward the prostate cancer cells that overexpress Prostate-specific membrane antigen (PSMA), LNCaP and 22Rv1 cells and the prostate cancer cells that do not overexpress Prostate-specific membrane antigen (PSMA), PC3 with Aptamer-conjugated nanoparticles containing Abiraterone acetate (Apt-ABR-NP). *In vitro* cellular studies include cellular uptake analysis, cytotoxicity assay, apoptosis assay, mitochondrial membrane depolarization analysis, and colony formation assay.
- Determination of *in vivo* efficacy of the prepared nanoparticles in carcinogen-induced prostate cancer-bearing mice by carrying out the hemolysis study, pharmacokinetics study, biodistribution study and gamma-scintigraphy imaging, antitumor activity study, LNCaP tumor spheroid model, hematological evaluation, and estimation of serum-specific toxicity markers studies.

#### 3.2. Plan of study

The study is planned as outlined below-

##### ➤ Preformulation studies

- Development of standard calibration curve of Abiraterone acetate by UV-Vis Spectroscopy.
- Detection of interactions between drug and excipients by Fourier-transform infrared spectroscopy (FTIR)

- Preparation and optimization of PLGA nanoparticles encapsulating Abiraterone acetate
  - Preparation of Abiraterone acetate-loaded polymeric nanoparticles (ABR-NP) by multiple emulsion solvent evaporation technique.
  - Conjugation of the prepared nanoparticle with  $\Delta$ PSap4#5 aptamer to ensure site-specific delivery to the prostate cancer cells (Apt-ABR-NP).
  - Confirmation of the successful aptamer conjugation by FTIR, agarose gel electrophoresis and X-ray photoelectron spectroscopy (XPS).
  - Evaluation of morphological characterizations of the prepared experimental nanoparticles will be done by using field emission scanning electron microscopy (FESEM), high-resolution transmission electron microscopy (HR-TEM), and atomic force microscopy (AFM). Particle size distribution and zeta potential will be measured using the dynamic light scattering (DLS) method.
  - Assessment of stability of prepared optimized nanoparticles by accelerated stability study and hydrolytic stability study.
- ***In vitro* drug release studies**
  - *In vitro* ABR release from the optimized nanoparticles will be carried out in five different media, i.e., phosphate buffer saline (PBS) (pH 7.4), PBS with 1%  $\beta$ -hydroxy cyclodextrin (pH 7.4), citrate buffer (pH 3), acetate buffer (pH 5), and bicarbonate buffer (pH 10).
  - Assessment of various drug release kinetics and regression coefficients ( $R^2$ ) of the prepared formulation in different buffers.
- ***In vitro* cellular experiments in LNCaP, 22Rv1 and PC3 cells**
  - *In vitro* cytotoxicity study by MTT assay.
  - *In vitro* cellular uptake study (both qualitative and quantitative study) by confocal laser microscopy and flow cytometry.
  - Apoptosis assay by Annexin V-FITC/PI dual staining.
  - Mitochondrial membrane depolarization analysis using JC-1.
  - *In vitro* colony formation assay



➤ ***In-vivo* experiments**

- Hemolysis study with the experimental nanoparticles.
- Pharmacokinetic studies of free drug, ABR-NP and Apt-ABR-NP will be performed in Swiss albino mice and evaluation of pharmacokinetic parameters will be done.
- Biodistribution study and gamma-scintigraphy imaging with  $^{99m}\text{Tc}$ -radiolabeled nanoparticles.
- Antitumor activity study will be done using hematoxylin and eosin (HE) stained tissue images and expression of Ki67 stained images.
- The efficacy of Apt-ABR-NP will be evaluated using the LNCaP tumor spheroid model.
- Hematological evaluation study will be carried out using the experimental nanoparticles.
- Estimation of serum-specific toxicity markers.

➤ **Statistical Analysis**

- Statistical analysis of data will be used using Student's t-test, Dunnett's test, and one-way ANOVA, followed by Tukey's post hoc test, two-way ANOVA analysis, and tested by Bonferroni's post-test. The images, graphical, and bar diagrammatic representations will be accomplished using various software such as Origin, Graph Pad Prism software, Gimp, ImageJ, AutoDock, and BIOVIA Discovery Studio Visualizer.



## 4. Materials and Equipment

### 4.1. Chemicals used in the study

**Table 4.1:** List of materials/chemicals used in the study

Serial No	Name	Source
1.	$\Delta$ PSap4#5 aptamer	Eurofins Genomics India Pvt. Ltd., Bangalore, India
2.	Acetonitrile	Merck Life Science Pvt. Ltd, Bengaluru, India
3.	Abiraterone acetate	MSN laboratories Pvt. Ltd, Hyderabad, Telangana, India
4.	Testosterone propionate	Sisco Research Laboratories Pvt. Ltd. Mumbai, India
5.	4',6' Diamidino-2-phenylindole (DAPI)	Thermo Fisher Scientific, Mumbai, India
6.	Dichloromethane (DCM)	Merck Life Science Pvt. Ltd, Bengaluru, India
7.	Disodium hydrogen phosphate	Merck Life Science Pvt. Ltd, Bengaluru, India
8.	Dimethylsulfoxide (DMSO)	Merck Life Science Pvt. Ltd, Bengaluru, India
9.	Dulbecco's Modified Eagle Medium (DMEM)	Thermo Fisher Scientific, Waltham, USA
10.	Ethylene diamene tetra acetic acid (EDTA)	Merck Life Science Pvt. Ltd, Bengaluru, India
11.	1-(3-dimethylaminopropyl)-3-ethylcarbodiimide hydrochloride (EDC)	Himedia Laboratories Pvt. Ltd., Maharashtra, Mumbai, India.
12.	Ethyl Acetate	Merck Life Science Pvt. Ltd, Bengaluru, India India
13.	Fetal bovine serum (FBS)	HiMedia Laboratories, Mumbai, India
14.	Fluorescein isothiocyanate (FITC)	Sigma-Aldrich Co., St Louis, MO, USA

Serial No	Name	Source
15.	FITC annexin V/dead cell apoptosis kit	Thermo Fisher Scientific, Waltham, MA, USA
16.	Glacial acetic acid	Merck Life Science Pvt. Ltd, Bengaluru, India
17.	Methanol	Merck Life Science Pvt. Ltd, Bengaluru, India
18.	3-(4,5-dimethylthiazol-2-yl)-2,5-diphenyltetrazolium bromide (MTT)	Sigma-Aldrich Co., St Louis, MO, USA
19.	N-hydroxysuccinimide (NHS)	HiMedia Laboratories Pvt. Ltd., Maharashtra, Mumbai, India.
20.	Penicillin-Streptomycin	HiMedia Laboratories, Mumbai, India
21.	Acid-terminated Poly lactic-co-glycolic acid (ratio, 75:25; molecular weight, 4,000–15,000 Da)	Sigma-Aldrich Co, St Louis, MO, USA.
22.	Potassium dihydrogen phosphate	Merck Life Science Pvt. Ltd, Bengaluru, India
23.	Polyvinyl alcohol (M.W. 85,000- 1,24,000) (M.W. 150,000)	SD Fine-Chemicals limited, Mumbai, India
24.	Roswell Park Memorial Institute Medium (RPMI 1640)	HiMedia Laboratories, Mumbai, India
25.	Sodium acetate	Merck Life Science Pvt. Ltd, Bengaluru, India
26.	Sodium bicarbonate	Merck Life Science Pvt. Ltd, Bengaluru, India
27.	Sodium carbonate	Merck Life Science Pvt. Ltd, Bengaluru, India
28.	Sodium citrate	Merck Life Science Pvt. Ltd, Bengaluru, India

Serial No	Name	Source
29.	Sodium hydroxide	Merck Life Science Pvt. Ltd, Bengaluru, India
30.	Trypsin	HiMedia Laboratories, Mumbai, India
31.	Tween 80	SD Fine Chemicals limited, Mumbai, India
32.	Water for HPLC Corp. Billerica, MA, USA 41. Millex-GP Syringe Filter Unit, 0.22 µm, polyethersulfone, 33 mm, gamma sterilized Millipore Corp. Billerica, MA, USA	Merck Life Sc. Pvt. Ltd., Mumbai, Maharashtra, India
33.	Milli-Q water Millipore	Corp. Billerica, MA, USA
34.	C-reactive protein (CRP) bioassay kits	Weldon Biotech India Pvt. Ltd., New Delhi, India
35.	AutoZyme Creatinine kit	Accurex, Mumbai, India
36.	AutoZyme BUN kit	Accurex, Mumbai, India
37.	Cell lysis buffer	Abcam
38.	Acetone	Merck Life Science Pvt. Ltd, Bengaluru, India
39.	Chloroform	Merck Life Science Pvt. Ltd, Bengaluru, India
40.	Citric acid	Merck Life Science Pvt. Ltd, Bengaluru, India
41.	5,5',6,6'-Tetrachloro- 1,1',3,3'-tetraethyl benzimidazolylcarbocyanine iodide (JC-1)	Invitrogen, Carlsbad, CA, USA
42.	Cyanine5 (Cy5) dye	Thermo Fisher Scientific, Waltham, MA, USA
43.	N-Nitroso-N-methylurea	Sigma-Aldrich Co, St Louis, MO, USA.

4.2. Animals and different cells used in the study

Table 4.2: The source of animals and different cells used in the study

Animals	Source
Swiss albino male mice	National Institute of Nutrition (NIN), Hyderabad, Telangana, India.154/GO/RBiBt- S/RL/99/CPCSEA
Human Cells	Source
LNCaP and PC3 cells	National Centre for Cell Sciences, Pune, India
22Rv1 cells	American Type Culture Collection (ATCC, Rockville, MD, USA).

4.3. Instruments

Table 4.3: List of instruments and equipment used in the study

Serial No	Name	Source
1.	Bath sonicator	Trans-O-Sonic, Mumbai, India
2.	Flow Cytometer	BD Accuri C6, BD Bioscience, San Diego, CA and BD LSR Fortessa, B.D. Biosciences
3.	CO <sub>2</sub> incubator	Thermo Fisher Scientific, Waltham, MA USA
4.	Cold centrifuge	HERMLE Labortechnik GmbH, Wehingen, Germany
5.	Confocal laser microscope	ZEISS LSM 900, Carl Zeiss, Oberkochen, Germany)
6.	Digital pH meter (EUTECH)	Thermo Fisher Scientific India Pvt. Ltd., Hiranandani Business Park, Mumbai, India
7.	Digital weigh balance	Sartorius Corporate Administration, Otto-Brenner-Straße 20, Goettingen, Germany

Serial No	Name	Source
8.	Disposable syringe (Dispo Van)	Hindustan Syringes and Medical Devices Limited, Ballabgarh, Faridabad, Haryana, India
9.	FTIR instrument	Bruker FTIR, Tensor-II, Bruker Optic GmbH, Karlsruhe, Germany
10.	Normal Freezer	LG double door, Yeouido-dong, Seoul, South Korea
11.	-80° C Freezer (Model no U410-86)	New Brunswick Scientific, Eppendorf House, Arlington Business Park, Stevenage, UK
12.	High-speed homogenizer	IKA Laboratory Equipment, Model T10B Ultras-Turrax, Staufen, Germany
13.	Incubator shaker	BOD-INC-1S, Incon, India
14.	Laminar airflow bio- safety hood	Thermo Fisher Scientific, Waltham, MA USA
15.	Tandem liquid chromatography and mass spectrophotometry (LC-MS/MS)	LC: Shimadzu Model 20AC, MS: AB-SCIEX, Model: API4000, Software: Analyst 1.6
16.	Laboratory Freeze Dryer (lyophilizer)	Instrumentation India, Kolkata, India
17.	Magnetic stirrer	Remi Sales & Engineering Ltd, Ganesh Chandra Avenue, Bando House, Dharmatala, Kolkata, India
18.	0.22 $\mu$ membrane filter	Merck Life Science Pvt. Ltd, Mumbai, India

Serial No	Name	Source
19.	Microplate reader	Spectromax, Japan
20.	Particle size and zeta sizer	Zetasizer nano ZS 90, Malvern Zetasizer Limited, Malvern, UK
21.	Field Emission Scanning Electron microscope	FESEM Joel JSM-7600 F, Tokyo, Japan
22.	Transmission electron microscope	TEM, JEOL JEM-2010, JEOL, USA
23.	UV-VIS spectrophotometer	LI-295 UV VIS Single Beam, Lasany International, India
24.	Vortex mixture	Remi Sales & Engineering Ltd, Ganesh Chandra Avenue, Bando House, Dharmatala, Kolkata, India
25.	Zeiss Light microscope.	Carl Zeiss: Axiostar plus, Jena, Germany
26.	Gamma-scintillation counter	ECIL, Hyderabad, India
27.	Gamma-scintigraphy camera (GE Infinia $\gamma$ Camera)	Xeleris Work Station, Milwaukee, WI, USA
28.	LC-MS instrument	Agilent 6545 Q-TOF LC/MS system
29.	Kratos Axis X-ray photoelectron spectrometer	Shimadzu, Japan



## 5. Methodology

### 5.1. Preparation of PLGA nanoparticles containing abiraterone acetate

In this experimental study, the synthesis of nanoparticles was carried out using a double emulsion solvent evaporation technique. Specifically, 50mg of PLGA (75:25) and 5mg of abiraterone acetate were dissolved in a 2.5ml organic phase consisting of dichloromethane and acetone in a 1:1 ratio (v/v). The organic phase containing the drug and polymer was subjected to homogenization at 20000 rpm using an IKA Laboratory Equipment, Model T10B Ultra-Turrax in Staufen, Germany, followed by vigorous emulsification with a 3% aqueous PVA solution to form a w/o emulsion.

The resulting primary emulsion was added dropwise to a 75ml 1.5% aqueous PVA solution and homogenized at 20000 rpm for 5 minutes to form a double emulsion (w/o/w). The double emulsion was sonicated while keeping ice-cold water in the bath for 30 minutes to reduce the particle size. Subsequently, the solution was allowed to stir on a magnetic stirrer overnight at room temperature to remove the organic solvents, resulting in the formation of nanoparticles during the evaporation of the solvents and solidification of the polymers.

The larger particles were separated by centrifugation of the nanoparticle aqueous suspension at 5000 rpm for 10 minutes, followed by centrifugation of the nanoparticles at 16000 rpm for 45 minutes, and the supernatant was collected using a cooling centrifuge. To remove excess PVA associated with the nanoparticles, the pellets obtained after centrifugation were washed three times with Milli-Q water and precipitated by centrifugation at 16000 rpm. The pellet was dispersed in 2-3ml of double-distilled water and subsequently frozen in a deep freezer (So-Low, Environmental Equipment, Ohio, USA) and lyophilized in a freeze dryer (Laboratory Freeze Dryer, Instrumentation India, Kolkata, India) to obtain the dry powdered nanoparticles (Dutta et al., 2018; Ehsan et al., 2022; Kumari et al., 2023).

### 5.2. Selection of aptamer

For the selection of an aptamer for use in conjugation to nanoparticles for cancer therapy, several crucial criteria must be considered to ensure optimal targeting, delivery, and therapeutic efficacy. Target specificity, binding affinity, stability, biocompatibility, etc., are some key factors to consider (Cai et al., 2018).

The dissociation constant ( $K_d$ ) is a measure of the strength of binding between a ligand (such as an aptamer) and its target molecule (such as a protein or cell surface receptor) (Thevendran

et al., 2020). In the context of aptamer binding, the dissociation constant quantitatively describes the equilibrium between the bound complex (aptamer-target) and the unbound molecules (free aptamer and free target) at equilibrium. A low dissociation constant ( $K_d$ ) indicates a strong binding affinity between the aptamer and its target molecule. In contrast, a high dissociation constant ( $K_d$ ) suggests a weaker binding affinity between the two.  $\Delta$ PSap4#5, A10-3.2, A9g, and E3 are some of the widely studied aptamers used as a PSMA targeting moiety (Savory et al. 2010; Dassie et al. 2009; Rockey et al. 2011; Gray et al. 2018)

The  $\Delta$ PSap4#5 aptamer, with a sequence of 5'-TTT TTA ATT AAA GCT CGC CAT CAA ATA GCT TT-3', has a lower  $K_d$  value (2.6 nM), which means it has a stronger affinity for its target molecule, PSMA. This aptamer is highly sensitive to PSMA (detection level in the picogram range) and is easier to synthesize due to its shorter chain length. The success of PSMA- $\Delta$ PSap4#5 aptamer *in vitro* has been reported, making it an excellent choice for targeting PSMA with the assistance of a  $\Delta$ PSap4#5 aptamer-conjugated nanosize drug delivery system.

### **5.3. Conjugation of aptamer on the surface of nanoparticles**

Initially, we dispersed 5 mg/mL of ABR-NP in deionized water, followed by agitation for 30 minutes at 25°C with 200 mM of EDC and 100 mM of NHS. Subsequently, the activated ABR-NP was washed with DNase-RNase-free water to eliminate excess EDC/NHS from the –COOH-activated ABR-NP. The aptamer suspension, with a concentration of 0.5 mg/mL, was denatured and then renatured by heating it to 85°C for 10 minutes, followed by cooling it in an ice bath for 10 minutes. The activated ABR-NP dispersion was then combined with the denatured-renatured aptamer, and the reaction was allowed to proceed for at least 6 hours with slow rotation (Chakraborty et al. 2020a; Aravind et al., 2012). Finally, the covalently coupled Apt-ABR-NP was washed with deionized water.

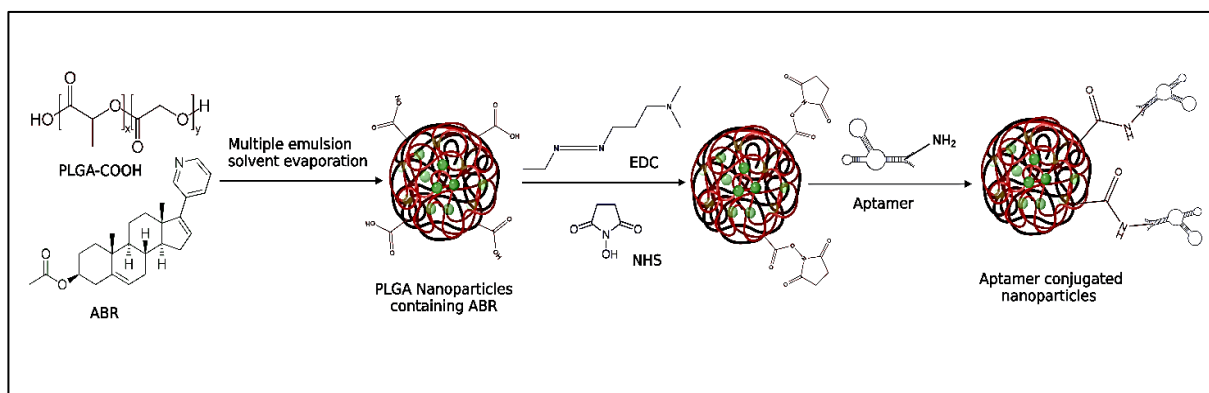


**Figure 5.1:** Schematic representation of aptamer conjugation process to the surface of the polymeric nanoparticles containing ABR

#### 5.4. Drug excipient interaction study using Fourier Transform Infrared Spectroscopy (FTIR)

Fourier Transform Infrared Spectroscopy (FTIR) is a highly valuable analytical technique commonly employed to investigate drug-excipient interactions in pharmaceutical formulations (Ewing et al., 2015). The present study utilized Fourier-transform infrared (FTIR) spectroscopy to analyze the interaction between the drug and the selected excipients. The analysis was performed on blank nanoparticles (i.e., nanoparticles without any drug), drug (ABR), PLGA, ABR-loaded-PLGA nanoparticles, and a physical mixture of drug and excipients. The sample was mixed with high-quality KBr at a 1:100 ratio in each case and then pressed into pellets. Subsequently, they were analyzed for their spectral response over a range of 4000-600  $\text{cm}^{-1}$  using a Bruker FTIR instrument (Bruker FTIR, Tensor-II, Bruker Optic GmbH, Karlsruhe, Germany).

#### 5.5. Determination of particle size and zeta potential

In a Dynamic Light Scattering (DLS) study, the size distribution of particles in a solution is determined by measuring the intensity autocorrelation function of scattered light. Electrophoretic mobility measurements can also be conducted to calculate the zeta potential. The hydrodynamic diameter and zeta potential of developed nanoparticles were measured using the DLS method. For this purpose, approximately 2 mg of ABR-NP and Apt-ABR-NP were weighed and dispersed in Milli-Q water (Millipore Corp., MA, USA) using a bath sonicator (Trans-o-sonic, Mumbai, India) for 30 minutes. Finally, the particle size and zeta potential were analyzed using the Malvern Zetasizer Nano-ZS 90 (Malvern Instruments, Malvern, U.K.). This analytical technique allows for the accurate determination of the size and

charge of nanoparticles, making it an essential tool in the field of nanotechnology (Garms et al., 2021; Gaspar et al., 2018).

### **5.6. Determination of surface morphology by Field emission scanning electron microscopy (FESEM), Atomic force microscopy (AFM), and High-resolution transmission electron microscopy (HR-TEM)**

In the realm of nanotechnology, the determination of nanoparticle surface morphology is crucial to understanding their properties and potential applications. To achieve this, advanced microscopy techniques such as Field Emission Scanning Electron Microscopy (FESEM), Atomic Force Microscopy (AFM), and High-Resolution Transmission Electron Microscopy (HR-TEM) are employed. In this study, lyophilized nanoparticles were subjected to field emission scanning electron microscopy (FESEM) after being coated with a thin layer of gold. The particle morphology of hydrated nanoparticles was analyzed using AFM in Milli-Q water. To remove any pre-existing large aggregates, the nanoparticles were passed through 0.22-micron filters. The filtered dispersion was then applied to a cleaved mica sheet and air-dried. The high-resolution transmission electron microscope (HR-TEM) was used to investigate the internal morphology of the nanoparticles and drug distribution. For this purpose, a nanoparticle suspension in Milli-Q water was allowed to air dry on a standard carbon-coated copper grid (mesh) for 5-6 hours. Subsequently, image analysis was performed using a high-resolution Transmission Electron Microscope (JEOL HR, Tokyo, Japan). The findings of this study contribute to the understanding of nanoparticle surface morphology and pave the way for further research in this area.

### **5.7. X-ray photoelectron spectroscopy (XPS)**

X-ray photoelectron spectroscopy (XPS), also referred to as electron spectroscopy for chemical analysis (ESCA), is a surface-sensitive analytical technique that provides valuable information about the chemical composition and electronic state of a material's surface (Gajendiran et al., 2014; Spek et al., 2015). In the present study, XPS was employed to investigate the elemental composition of ABR-NP and Apt-ABR-NP nanoparticle samples. Prior to examination, the samples were suspended in double distilled water, transferred to a clean Silicon substrate, and subjected to vacuum-drying. The KratosAxis X-ray photoelectron spectrometer (Shimadzu, Japan) equipped with a monochromatic Al K Alpha source was utilized to obtain the spectral data, with a passage of energy of 200 eV. The elemental composition was calculated, and curve fitting was carried out using the Spectral Data Processor v4.3 software. The results of this study

provide novel insights into the chemical composition of the nanoparticle samples and could have significant implications for future research in this field.

### **5.8. Analysis of aptamer-PSMA interactions by molecular docking**

Molecular docking is a widely used computational modeling technique in structural bioinformatics and drug discovery to understand the molecular basis of protein-ligand interactions. In the present study, we aimed to analyze the interaction between an aptamer molecule and the prostate-specific membrane antigen (PSMA) protein using molecular docking.

To perform the molecular docking analysis, we selected the PSMA protein as the receptor to which the aptamer molecule specifically binds *in silico*. The crystal structure of PSMA (1Z8L) was obtained from the RCSB protein data bank, and the DNA aptamer structure was prepared by adding the 32 bp DNA sequence in Discovery Studio Visualizer 2021 and converting it to PDB format. Prior to the docking analysis, we prepared the receptor by removing water molecules and adding polar hydrogen atoms and charges. We also prepared the ligand molecule using Discovery Studio Visualizer 2021. HDock blind docking server was used to further examine the interactions between the aptamer and PSMA (Yan et al. 2020). The quality of a predicted protein-nucleotide binding mode was measured by its docking score. The docking analysis was carried out using the Discovery Studio 2021 client program, and the interactions were visualized through Biovia Discovery Studio 2021. The present study provides insights into the molecular interactions between the aptamer and PSMA protein, which could pave the way for the development of new therapeutic agents targeting PSMA.

### **5.9. Percentage of drug loading and encapsulation efficiency**

The percentage of drug loading and encapsulation efficiency are fundamental parameters in drug delivery systems. They are crucial in determining the effectiveness of the encapsulation process and the quantity of drug that has been successfully loaded into the nanoparticles (Kumari et al., 2023). To determine drug loading, ABR-NP (2 mg) and blank nanoparticles (2 mg) were weighed into a centrifuge tube. Then, 2 mL of acetonitrile:dichloromethane (2:1) solvent combination was added to each tube. The nanoparticles-containing tubes were incubated in an incubator shaker for 4 hours at 37°C. After that, the mixture was sonicated for 30 minutes, and the continuous phase was separated by centrifugation at a speed of 16000 rpm using a cold centrifuge (Hermle refrigerated centrifuge, Siemensstr, Wehingen, Germany). Finally, UV spectrophotometric analysis was performed at 254 nm to determine the drug

release after collecting the supernatants from the ABR-NP/blank nanoparticle solutions. The UV absorbance of the supernatant from blank nanoparticles was subtracted from the ABR-NP nanoparticles to obtain the absorbance for ABR only. Equations 1, 2 and 3 were utilized to compute the percentage of drug loading and entrapment efficiency.

$$\text{Theoretical drug loading (\%)} = \frac{\text{Amount of drug}}{\text{Amount of drug+Excipients}} \times 100 \dots\dots\dots(1)$$

$$\text{Drug loading (actual)\%} = \frac{\text{Amount of drug in nanoparticles}}{\text{Amount of nanoparticles obtained}} \times 100 \dots\dots\dots(2)$$

$$\text{Entrapment efficiency (\%)} = \frac{\text{Drug loading (actual) (\%)}}{\text{Amount of drug loading (theoretical) (\%)}} \times 100 \dots\dots\dots(3)$$

### 5.10. Stability of the nanoparticles

The stability of nanoparticles was thoroughly examined in accordance with the ICH guidelines to ensure their safety and efficacy. The International Conference on Harmonization (ICH, 2003) requirements were followed, wherein fixed amounts of ABR-NP and Apt-ABR-NP were weighed and stored under specific conditions. These conditions included storage in a refrigerator at a temperature range of 4-8°C, zone III at a temperature of 30°C and 75% relative humidity, and at 40°C and 75% relative humidity for 45 and 90 days, respectively, in a stability chamber. This was done to evaluate the nanoparticles' stability under different storage conditions. After 45 and 90 days, samples were taken for FESEM imaging and drug assay to assess whether any changes occurred in the formulations during the storage period. The FESEM imaging was done to observe any morphological changes in the nanoparticles, while the drug assay was done to quantify the amount of drug present in the formulations. This detailed examination was conducted to ensure the safety, efficacy, and stability of the nanoparticles (Kumari et al., 2023).

### 5.11. Hydrolytic stability study

A study was conducted to assess the hydrolytic stability of nanoparticles in aqueous environments. The focus was on their susceptibility to hydrolysis, which occurs when compounds react with water molecules and break down. This research is essential for understanding the long-term behavior and potential applications of nanoparticles in fields like medicine, environmental science, and materials science.

To evaluate the hydrolytic degradation of Apt-ABR-NP, 10 mg of nanoparticles were taken separately in 2 ml of buffer with varying pH levels (3.0, 5.0, 7.4, and 10.0). The study used

citrate buffer with a pH of 3, acetate buffer with a pH of 5, phosphate buffer saline with a pH of 7.4, and bicarbonate buffer with a pH of 10. The solutions were stored at a constant temperature of  $37\pm2^{\circ}\text{C}$  in an incubator with gentle shaking. After 7, 14, 21, and 28 days, the samples were removed from the incubator and centrifuged. The precipitate was rinsed twice with double distilled water, dried, and weighed to measure the mass of the nanoparticles (Ehsan et al., 2022). The initial weight of the nanoparticles was then compared with that of the obtained nanoparticles after drying. The weight change was calculated according to the following formula-

$$\text{Weight change (\%)} = \frac{W_0 - W_t}{W_0} \times 100$$

$W_0$  and  $W_t$  represent the initial and weight at time  $t$ , respectively.

### 5.12. *In vitro* drug release study

An *in vitro* drug release study is a crucial step in understanding how drugs are released from nanoparticles in simulated physiological conditions in a lab setting. This assessment is essential for optimizing drug delivery systems by determining the controlled release behavior of drug-loaded nanoparticles.

In the experiment, the pre-weighed freeze-dried ABR-NP (1 mg/ml, 2 ml) was resuspended in different buffers at  $37^{\circ}\text{C}$  with slow agitation (60 shaking/minute) in an incubator shaker. The buffers used were phosphate-buffered saline (PBS) (pH 7.4), 1%  $\beta$ -hydroxy cyclodextrin containing PBS (pH 7.4), citrate buffer (pH 3), acetate buffer (pH 5), and bicarbonate buffer (pH 10). After centrifugation (at 16,000 rpm for 10 minutes in a cold centrifuge), the supernatant was collected, and the pellet was resuspended with fresh buffer. At different intervals, ranging from 30 minutes to 28 days, the supernatants were collected, and the volume removed was replaced with 2 mL of fresh buffer each time. The bottom pellets were resuspended using a vortexing technique, and the samples were placed back in the incubator shaker until the next sampling. To determine the drug concentration in the collected samples, a UV-VIS spectrophotometric analysis was conducted at 254 nm (Kumari et al., 2023).

### 5.13. *In vitro* cellular uptake analysis by flow cytometry (FACS) and confocal microscopy

Cellular uptake analysis is a widely used method to evaluate the internalization of molecules or particles by cells. Flow cytometry (FACS) and confocal microscopy are two commonly employed techniques for this purpose (Lee et al., 2015; Kennedy et al., 2018). FACS is a quantitative technique that provides information about the overall uptake levels in a cell

population, while confocal microscopy is a qualitative technique that offers detailed spatial information about the distribution of the substance within individual cells. Both techniques are valuable tools for studying cellular uptake processes and are often used in combination to obtain complementary information.

To quantitatively analyze the uptake of nanoparticles (ABR-NP and Apt-ABR-NP) using FACS, they were loaded with tetramethylindo(di)-carbocyanine (Cy5) in ABR-NP (Cy5-ABR-NP). The comparative cellular uptake of these nanoparticles in LNCaP, 22Rv1, and PC3 cells was measured. Specifically, LNCaP and PC3 cells were seeded in 60 mm cell culture dishes at a density of  $1.5 \times 10^6$  per plate and incubated overnight in a humidified incubator at 37°C under a 5% CO<sub>2</sub> environment (Wang et al. 2013). The following day, the cells were treated with Cy5-containing formulations (ABR-NP/Apt-ABR-NP) for different time periods (6 h and 12 h), except for the control group, where the cells received no treatment. After treatment, the cells were washed with PBS (pH 7.4) and dispersed in PBS (pH 7.4) in light-protected tubes. Flow cytometry was performed using the Cy5 filter (Excitation/Emission 651 nm/670 nm) on a BD LSR Fortessa (B.D. Biosciences).

Confocal laser microscopy was employed to interpret Cy5-loaded Apt-ABR-NP uptake in LNCaP and PC3 cells (Fan et al. 2015). However, this study was not performed for 22Rv1 cells. PC3 and LNCaP cells were seeded separately on different coverslips at a density of  $1.0 \times 10^4$  cells per coverslip and placed inside a 35 mm cell culture dish with adequate media (1 mL). The cells were incubated overnight at 37°C and then treated with Cy5-loaded Apt-ABR-NP for 6 h and 12 h. After treatment, the cells were washed with PBS, fixed using 70% ethanol, counter-stained with DAPI, and mounted on a slide using Prolong Diamond anti-fade-mount. The slides were then scanned under a confocal laser microscope (ZEISS LSM 900, Carl Zeiss, Oberkochen, Germany) simultaneously using dual filters, Cy5 (Excitation/Emission 651 nm/670 nm) and DAPI (Excitation/Emission 359 nm/461 nm). Images were collected from individual channels and merged using Image J or ZEN 2012 SP2 software (ZEISS, Germany).

#### **5.14. *In vitro* cell cytotoxicity assay**

The MTT assay is a commonly used colorimetric test for determining cell viability and cytotoxicity. This test measures the metabolic activity of cells and is often employed to evaluate the potential toxic effects of nanoparticles on cells.

To conduct this assay,  $1.5 \times 10^4$  cells were seeded onto each well of a 96-well plate and allowed to incubate overnight at 37°C and 5% CO<sub>2</sub>. The cells were then treated with varying



concentrations of ABR, ABR-NP, and Apt-ABR-NP formulations, all containing the same amount of drug, for 48 hours. A parallel control series was maintained without any drug treatment. Once the treatment period was complete, the treatment solutions were removed, and MTT solution (1 mg/ml) was added to the cells in the dark for 2 hours. Afterwards, the MTT solution was removed, and tissue culture grade DMSO was added to dissolve the formazan crystals formed during the MTT reaction. The 96-well plate was gently swirled to ensure uniform dissolution of the crystals, and the optical density was measured at 540 nm using an ELISA reader (Bio-Rad, CA, USA). Cell viability (%) was calculated by comparing the absorbance values of treated cells with untreated cells. IC<sub>50</sub> values were determined by preparing a % cell viability vs concentration plot using Graph Pad Prism software (version 5.0, Graph Pad Prism Inc., USA) and applying the graphical method (Afshari et al., 2013; Azandeh et al., 2017).

### 5.15. Apoptosis assay

Apoptosis is a crucial biological mechanism that helps to maintain tissue balance and control cell populations in multicellular organisms. This process plays important role in various physiological processes, including embryonic development, tissue remodeling, and immune response.

To evaluate the induction of apoptosis, a study was conducted using ABR, ABR-NP, and Apt-ABR-NP on 22Rv1 and LNCaP cells with the Annexin V-FITC and propidium iodide (P.I.) dual staining method (Dutta et al. 2018a; Hazra et al. 2021). First,  $1.5 \times 10^6$  LNCaP cells were placed in 60mm dishes and incubated overnight with RPMI 1640 media. The following day, the cells were treated with ABR, ABR-NP, and Apt-ABR-NP at their respective IC<sub>50</sub> concentrations in an incomplete medium (without serum) for 24 and 48 hours. Two control sets were maintained in parallel for each time point with media alone to provide the unstained and control group (P.I. alone). After the treatment, the cells were collected through trypsinization, counted to  $10^5$  in 100  $\mu$ l binding buffer, and incubated with annexin V-FITC (5  $\mu$ l) for 15 min in the dark. Finally, the cells were diluted to 500  $\mu$ l, and 5  $\mu$ l of propidium iodide was added to each tube except for the unstained group. The cells were analyzed using a FACS instrument (BD Accuri C6, BD Bioscience, San Diego, CA) with the channels of FITC (B530-A) and propidium iodide (YG586-A). The data were plotted in a four-quadrant plot to differentiate live, early apoptotic, late apoptotic, and necrotic cells. The Apt-ABR-NP showed the most cytotoxicity, maximum cellular uptake, and maximum apoptosis induction in LNCaP cells

among the experimental nanoparticles. Therefore, further studies were conducted using this formulation in LNCaP cells only.

#### **5.16. Mitochondrial membrane depolarization analysis using JC-1**

The technique of measuring changes in mitochondrial membrane potential via mitochondrial membrane depolarization analysis is a widely used method to assess cellular health and function. Apoptosis, a programmed form of cell death, is characterized by a decrease in mitochondrial membrane potential. The initial stage of apoptosis is marked by a depolarized mitochondrial membrane, which is detected by a change in the trans-mitochondrial membrane potential difference. This change can be measured by using JC-1, a cationic dye that accumulates in normal mitochondria to form J-aggregates, emitting red fluorescence (~590 nm). However, in depolarized mitochondria, JC-1 accumulates less and predominantly remains in the cytosol in a monomeric form, emitting green fluorescence (~529 nm). Consequently, mitochondrial membrane depolarization can be monitored by measuring an increase in green fluorescence or the green/red fluorescence intensity ratio.

To evaluate fluorescence emission after JC-1 staining, a standard protocol was followed (Dutta et al., 2018; Melo et al., 2009). Specifically, LNCaP cells were seeded in 60 mm dishes at a density of  $1 \times 10^6$  cells/dish and incubated overnight in a humidified incubator. Subsequently, the cells were treated with ABR, ABR-NP, and Apt-ABR-NP for 24 h and 48 h. Following treatment, the cells were removed from the dishes and incubated with 10  $\mu$ L of 200  $\mu$ M JC-1 in 1 ml complete media for 10 min at 37 °C under dark conditions. The media was removed by centrifugation, and the cells were resuspended in PBS, pH 7.4, and analyzed in a FACS instrument.

#### **5.17. Clonogenic assay for the prostate cancer cell line**

The *in vitro* cell colony formation assay was performed to assess the clonogenic potential of a single cell after exposure to free drug and experimental formulations in comparison to an untreated control group. LNCaP cells were seeded in 12-well plates (750 cells/well) and allowed to grow overnight. The following day, fresh complete media was introduced, and the cells were treated with ABR, ABR-NP, or Apt-ABR-NP while the control group remained untreated. The media and treatments were changed every three days, and the experiment was terminated after a period of 12-14 days, depending on the colony numbers in the control well. When the colony confluency in the control well reached the optimal level, the media and treatment suspensions were removed, and the cells were washed with PBS. Next, 1 ml of 10%

acetic acid (in methanol) was added to fix the colonies, which were stained with a crystal violet solution (0.5% crystal violet in 25% methanol-water) and shaken for 15 minutes. The crystal violet solution was removed, and the cells were washed with PBS thrice. The plates were air-dried overnight, and optical microscope images were captured. After imaging, the plates were shaken with 10% acetic acid solution for 15 minutes to dissolve all the colonies, and the absorbance was measured at 510 nm using a plate reader with the supernatant (Papachristou et al. 2021).

### 5.18. *In vivo* animal studies

The Swiss albino mice used in this study were procured from the esteemed National Institution of Nutrition (NIN) in Hyderabad, India. It is pertinent to note that all *in vivo* experimental procedures involving the animals were subjected to rigorous ethical scrutiny and were approved by the Jadavpur University Animal Ethics Committee (JU-AEC) under protocol approval number AEC/PHARM/1704/04/2020, in accordance with the norms prescribed by the Committee for the Purpose of Control and Supervision of Experiments on Animals (CPCSEA), Govt. of India. (Jadavpur University Registration Number in CPCSEA: 1805/G.O./Re/S/15/CPCSEA). The guidelines of CPCSEA were meticulously followed in all animal experiments to ensure the highest standards of animal welfare and ethical conduct.

### 5.19. Pharmacokinetic study

A pharmacokinetic study is a vital component of drug development that elucidates the processes by which a substance is absorbed, distributed, metabolized, and excreted within a biological system. These investigations are crucial in establishing optimal dosage regimens, evaluating potential drug interactions, and assessing the overall safety and efficacy profile of a medication.

In the present study, the pharmacokinetics of ABR and its nanoformulations were evaluated in Swiss albino mice weighing an average of 25 g (Dutta et al. 2019). Thirty-six mice were allocated to each group, with the first group receiving ABR at a dose of 400 µg/kg body weight, the second group receiving ABR-NP, and the third group receiving Apt-ABR-NP. In the case of the formulations, an equivalent dose to the free ABR dose was administered through the formulations. Group I mice were administered the free drug (ABR) suspension in water for injection via intraperitoneal injection, while the formulations were directly dispersed in water for injection and injected intraperitoneally in animals of Groups II and III, respectively. Blood samples were collected from three animals at each time point (2, 10, 15, 20, 30, 60, 90, 120,

240, 360, 480, 720 min) in heparin-coated tubes. The samples were centrifuged (10,000 x g for 10 min at 4°C) to separate the plasma (200 µl each). A volume of 500 µl of ethanol was added to each plasma sample and mixed well with a vortex mixer to dissolve the drug content. The samples were then subjected to further centrifugation, and the clear supernatant was analyzed using an LC-MS instrument (Agilent 6545 Q-TOF LC/MS system). The data was analyzed through MassLynx 4.1 software and quantified by comparing it with a calibration curve of ABR prepared. Thereafter, the plasma concentration vs time plot was generated using GraphPad Prism 5.0, and the pharmacokinetic parameters (AUC,  $C_{\max}$ ,  $T_{\max}$ ,  $t_{1/2}$ , MRT,  $V_d$ , CL) were calculated.

### **5.20. Hemolysis study**

A hemolysis study is a fundamental process that involves investigating the rupture or destruction of red blood cells and the release of their contents into the surrounding fluid. Hemolysis can occur due to various reasons, including physical trauma, chemical exposure, or underlying medical conditions. In biomedical applications where nanoparticles might come into contact with blood, investigating the potential for nanoparticles to induce hemolysis is of paramount importance.

In this study, blood samples were collected from male Swiss albino mice and placed in heparinized tubes. The tubes were then centrifuged at 4°C for 5 minutes at 1000 g, and the supernatant was removed. The erythrocytes were washed three times in PBS (pH 7.4) before being used to create a 2% suspension employed in the hemolysis study. To determine the hemolytic activity of nanoparticles, 190 µl of the suspension was placed in each well of a 96-well plate. A volume of 10 µl of ABR/ABR-NP/Apt-ABR-NP was added to each well, with an increasing concentration of ABR ranging from 10 to 100 µM. The negative control was normal saline (0% lysis), while the positive control was distilled water (100% lysis). Following incubation at 37°C for 1 hour with gentle stirring, the unlysed erythrocytes were separated by centrifugation at 10,000 g for 5 minutes. The supernatant's optical density (O.D.) was determined at 570 nm. The percent lysis was measured by comparing the O.D. value to that of the supernatant (positive control) where full lysis occurred. The tests were repeated three times, and the results were averaged to ensure accuracy (Ehsan et al., 2022; Thasneem et al., 2011).

### **5.21. Biodistribution study and gamma scintigraphy imaging**

Biodistribution studies and gamma scintigraphy imaging have emerged as promising techniques for improving the diagnosis and treatment of prostate cancer using radiolabeled

nanoparticles. In a Swiss albino prostate-cancer mice model, *in vivo* biodistribution of ABR-NP and Apt-ABR-NP was studied utilizing technetium-99m (Dutta et al. 2019) radiolabeled nanoparticles. The nanoparticles were labeled with  $^{99m}\text{Tc}$  by using an acidic solution of stannous chloride ( $\text{SnCl}_2$ ) as a reducing agent to synthesize  $^{99m}\text{Tc}$ -labeled nanoparticles ( $^{99m}\text{Tc}$ -ABR-NP and  $^{99m}\text{Tc}$ -Apt-ABR-NP).

The mice were hydrated intraperitoneally with normal saline and anesthetized with diethyl ether. Subsequently, radiolabeled nanoparticles containing 3.7 MBq radioactivity were administered intravenously. Biodistribution and gamma scintigraphy imaging was performed using  $^{99m}\text{Tc}$  labeled nanoparticles. Due to the short half-life of  $^{99m}\text{Tc}$  (6 h) (Ramdhani et al. 2023), the study was conducted using the intravenous route to avoid erroneous data due to the loss of radioactivity of  $^{99m}\text{Tc}$ , in order to obtain the most optimal level of biodistribution and the localization of radio labeled Apt-ABR-NP. In the case of the pharmacokinetic and anticancer efficacy study, since no  $^{99m}\text{Tc}$  material was involved, it was administered to animals by the intended intraperitoneal route.

For the biodistribution study, the animals were sacrificed after 1 h, 2 h, and 5 h of post-injection through cervical dislocation. Different organs (liver, kidney, stomach, intestine, heart, lungs, and prostate) and body fluids (blood and urine) were collected in scintillation counting tubes, and radioactivities present in them were measured in a gamma-scintillation counter (ECIL, Hyderabad, India). The results were expressed as a percentage of injected dose (% I.D.) accumulated in the organs and as % I.D. per gram (wet weight) in the case of blood.

In another experiment, scintigraphy imaging was performed in live anesthetized animals at 1 h, 2 h, and 5 h post-injection of radiolabeled nanoparticles under a gamma-scintigraphy camera (GE Infinia) in a head-supine anterior position under static conditions. The images were analyzed using GE Infinia  $\gamma$  Camera facilitated along with Xeleris Work Station, Milwaukee, WI, USA (Dhara et al. 2023).

## **5.22. Development of prostate cancer in mice, treatment undergone, and histopathological assessment**

In this study, adult male Swiss albino mice were utilized to establish prostate cancer-bearing mice, as previously reported (Nahata and Dixit 2012). Healthy male mice weighing 25-30 g were procured from the National Institute of Nutrition (Hyderabad, India). The mice were housed in polypropylene cages under controlled conditions, with a temperature of  $25^\circ\text{C} \pm 1^\circ\text{C}$ , a relative humidity of  $55\% \pm 5\%$ , and a 12-hour day/night photoperiod. The animals were

allowed to acclimate to their surroundings for two weeks before any experiments were conducted.

The mice were subjected to subcutaneous injections of testosterone propionate (40 mg/kg) twice a week for 12 weeks. Furthermore, N-nitroso-N-methyl urea (4 mg/kg) was administered once a week via intraperitoneal injection as a cancer promoter for the first four weeks of testosterone treatment (Schleicher et al. 1996). The development of prostate cancer was confirmed after 12 weeks of testosterone propionate treatment through histopathological examination of the prostate tissue. Throughout the study period, a normal control group was maintained that received normal saline treatment only (the 'Normal' group, Group A).

The animals diagnosed with prostate cancer were separated into four distinct groups. The first group, known as the 'Cancer' control group (Group B), received only normal saline. The second group, known as the 'ABR' group (Group C), was given a free abiraterone acetate suspension. The third group, known as the 'ABR-NP' group (Group D), received ABR-NP. Finally, the fourth group, known as the 'Apt-ABR-NP' group (Group E), was given Apt-ABR-NP. Each group consisted of a minimum of five animals. For the 'ABR,' 'ABR-NP,' and 'Apt-ABR-NP' groups, 100 mg/kg of ABR or equivalent was maintained through intraperitoneal injection three times per week for eight weeks. An additional group of normal mice received the same Apt-ABR-NP treatment as the carcinogen-treated Apt-ABR-NP group of animals (Group F) to evaluate the formulation's impact on normal animals. The 'Normal' and 'Cancer control' groups received only saline throughout the eight-week treatment period. After eight weeks of treatment with ABR, ABR-NP, or Apt-ABR-NP, all animals were sacrificed, and their prostates were isolated, fixed with 4% formalin, embedded in paraffin blocks, sectioned into thin slices (5  $\mu$ m thickness), and stained with hematoxylin and eosin (H&E) for microscopic observation (Chen et al., 2020).

The study employed Ki67-immunostaining on the 'Normal control', 'Cancer control', 'ABR-NP', and 'Apt-ABR-NP' groups using a similar approach. Notably, histopathological changes were observed in the prostates of the 'Cancer', 'ABR-NP', and 'Apt-ABR-NP' groups compared to the 'Normal' group under an optical microscope at 10 $\times$  and 40 $\times$  magnifications. H&E stained sections were utilized for the estimation of Gleason score, lymphovascular invasion, and perineural invasion (Tătaru et al. 2021). Further, the Gleason grading system was applied to establish distinct patterns of tumor tissues, with scores assigned to represent their stages (Pierorazio et al. 2013). ImageJ software (version 1.53k) was utilized to analyze Ki67-stained

sections and measure Ki67-positive cells. Based on the observed results, areas with 3% or fewer Ki67+ cells were considered negative, while 3-25% Ki67+ cells were considered grade 1 (1+ or low grade), 26-50% Ki67+ cells were considered grade 2 (2+ or intermediate grade), 51-75% Ki67+ cells were considered grade 3 (3+ high grade), and areas with 76-100% Ki67+ cells were considered grade 4 (4+ or very high/ worse grade) (Madani et al. 2011). For statistical analysis, a minimum of 10-12 images were captured for each slide.

### **5.23. Efficacy of aptamer-conjugated nanoparticles on LNCaP tumor spheroids**

LNCaP tumor spheroids are three-dimensional cell culture models that comprise LNCaP cells, a widely used human prostate cancer cell line. These spheroids are created by allowing the cells to grow and aggregate in a controlled environment, typically within a gel-like matrix such as Matrigel or agarose. These models are extensively utilized in cancer research to investigate tumor biology, drug screening, and mechanisms of drug resistance. They provide valuable insights into tumor growth dynamics, invasion, metastasis, and response to various treatments, which ultimately aid in the development of more effective cancer therapies.

To generate the spheroids, a single cell suspension of LNCaP cells was seeded in ultra-low attachment plates in serum-free media (DMEM/F12) with additional supplements such as 20% methylcellulose (Sigma), B27 (1:50, Invitrogen), 10 ng/ml bFGF (Invitrogen), 4 µg/ml insulin (Sigma), and 20 ng/ml epidermal growth factor (EGF) (Peprotech). The spheroids were formed by allowing seven days for cell seeding. After the formation of the spheroids, one group was the untreated control group, and the other group was treated with Cy5-loaded Apt-ABR-NP for three consecutive days at its IC<sub>50</sub> value. For each dose, the media was replaced with fresh media. Upon completion of the treatment period, the spheroids were washed with ice-cold PBS (pH 7.4), and photographs were captured using a confocal laser microscope (Sen et al., 2023; Wolff et al., 2022).

### **5.24. Hematological Evaluations**

Hematological evaluations are vital for the diagnosis of various blood-related diseases and conditions. These evaluations involve the analysis of different blood components and properties and are typically performed in a clinical laboratory setting.

In this study, a complete blood count (CBC) profile was obtained for mice in different experimental groups. Blood samples were collected through cardiac puncture and cardiocentesis, and the standard method (Weatherby et al. 2004) was used to analyze the total

count of red blood cells (RBC), hemoglobin, hematocrit, total count of white blood cells (WBC), lymphocytes, monocytes, neutrophils, eosinophils, platelets, and PSMA. C-reactive protein (CRP) was evaluated using commercially available bioassay kits (Weldon Biotech India Pvt. Ltd., New Delhi, India).

It is worth noting that hematological evaluations are crucial for the accurate diagnosis of various diseases and conditions related to the blood, and the findings of this study will contribute to the body of knowledge in this field.

### **5.25. Estimation of serum-specific toxicity markers**

The determination of serum-specific toxicity markers is a critical aspect of assessing toxicity or damage to specific organs or systems in the body. Serum biomarkers can help evaluate the extent of injury or dysfunction and guide medical management.

In the context of nanotechnology research, the presence of systemic toxicity in mice treated with nanoparticles was evaluated through serum biomarkers for hepatic and renal toxicity. The blood of each sacrificed animal was collected, and serum was extracted by centrifugation. To assess hepatic toxicity, serum levels of AST (aspartate aminotransferase), ALT (alanine transaminase), and alkaline phosphatase (ALP) were determined using commercially available bioassay kits (Coral Clinical Systems, Goa, India), following manufacturer protocols. For nephrotoxicity, creatinine and blood urea nitrogen (BUN) were estimated using AutoZyme Creatinine kit (Accurex, Mumbai, India) and AutoZyme BUN kit (Accurex, Mumbai, India), respectively, in a UV–Visible spectrophotometer (Intech-295, Advanced Microprocessor UV–Vis Single Beam) as per the manufacturer's instructions (Mudavath et al., 2014; Pandian et al., 2014).

### **5.26. Statistical analysis**

All experiments were performed in triplicate, and the resulting data was represented as the mean value accompanied by its standard deviation. Various statistical tests were employed to analyze the data, including Student's t-test, Dunnett's test, one-way ANOVA with Tukey's post hoc test, and two-way ANOVA with Bonferroni's post-test. The images, graphical, and bar diagrammatic representations were produced using sophisticated software such as Origin 2021, GraphPad Prism software (version 5, GraphPad Prism software Inc, San Diego, CA, USA), Gimp 2.10.30, ImageJ, AutoDock 4.2, and BIOVIA Discovery Studio Visualizer. The probability value is indicated as  $p$ , where  $p < 0.05$  was considered statistically significant.



## 5.27. References

- Afshari M, Derakhshandeh K, Hosseinzadeh L. Characterisation, cytotoxicity and apoptosis studies of methotrexate-loaded PLGA and PLGA-PEG nanoparticles. *Journal of microencapsulation*. 2014 May 1;31(3):239-45.
- Aravind A, Varghese SH, Veerananarayanan S, Mathew A, Nagaoka Y, Iwai S, Fukuda T, Hasumura T, Yoshida Y, Maekawa T, Kumar DS. Aptamer-labeled PLGA nanoparticles for targeting cancer cells. *Cancer nanotechnology*. 2012 Dec;3(1):1-2.
- Azandeh SS, Abbaspour M, Khodadadi A, Khorsandi L, Orazizadeh M, Heidari-Moghadam A. Anticancer activity of curcumin-loaded PLGA nanoparticles on PC3 prostate cancer cells. *Iranian journal of pharmaceutical research: IJPR*. 2017;16(3):868.
- Cai S, Yan J, Xiong H, Liu Y, Peng D, Liu Z. Investigations on the interface of nucleic acid aptamers and binding targets. *Analyst*. 2018;143(22):5317-38.
- Chakraborty S, Dlie ZY, Mukherjee B, Besra SE, Sengupta S, Sen R, et al (2020) A Comparative Investigation of the Ability of Various Aptamer-Functionalized Drug Nanocarriers to Induce Selective Apoptosis in Neoplastic Hepatocytes: In Vitro and In Vivo Outcome *AAPS PharmSciTech*. 21(3):1–13
- Chen ML, Lai CJ, Lin YN, Huang CM, Lin YH (2020) Multifunctional nanoparticles for targeting the tumor microenvironment to improve synergistic drug combinations and cancer treatment effects. *J. Mater. Chem. B*. 8(45):10416–27
- Dassie JP, Liu XY, Thomas GS, Whitaker RM, Thiel KW, Stockdale KR, et al (2009) Systemic administration of optimized aptamer-siRNA chimeras promotes regression of PSMA-expressing tumors *Nat Biotechnol* 27(9):839–46
- Dhara M, Al Hoque A, Sen R, Dutta D, Mukherjee B, Paul B, et al (2023) Phosphorothioated amino-AS1411 aptamer functionalized stealth nanoliposome accelerates bio-therapeutic threshold of apigenin in neoplastic rat liver: a mechanistic approach *J. Nanobiotechnology*. 21(1)
- Dutta D, Chakraborty A, Mukherjee B, Gupta S (2018) Aptamer-Conjugated Apigenin Nanoparticles To Target Colorectal Carcinoma: A Promising Safe Alternative of Colorectal Cancer Chemotherapy *ACS Appl Bio Mater* 1(5):1538–56
- Dutta D, Chakraborty A, Mukherjee B, Gupta S (2018) Aptamer-Conjugated Apigenin Nanoparticles To Target Colorectal Carcinoma: A Promising Safe Alternative of Colorectal Cancer Chemotherapy *ACS Appl Bio Mater* 1(5):1538–56

- Dutta D, Paul B, Mukherjee B, Mondal L, Sen S, Chowdhury C, et al (2019) Nanoencapsulated betulinic acid analogue distinctively improves colorectal carcinoma in vitro and in vivo Sci Rep 9(1)
- Ehsan I, Kumari L, Sen R, Al Hoque A, Mukherjee B, Mukherjee A, et al (2022) J591 functionalized paclitaxel-loaded PLGA nanoparticles successfully inhibited PSMA overexpressing LNCaP cells J. Drug Deliv. Sci. Technol. 75:103689
- Ewing AV, Biggart GD, Hale CR, Clarke GS, Kazarian SG. Comparison of pharmaceutical formulations: ATR-FTIR spectroscopic imaging to study drug-carrier interactions. International journal of pharmaceutics. 2015 Nov 10;495(1):112-21.
- Fan L, Campagnoli S, Wu H, Grandi A, Parri M, De Camilli E, et al (2015) Negatively charged AuNP modified with monoclonal antibody against novel tumor antigen FAT1 for tumor targeting J Exp Clin Cancer Res 34(1)
- Gajendiran M, Yousuf SM, Elangovan V, Balasubramanian S. Gold nanoparticle conjugated PLGA–PEG–SA–PEG–PLGA multiblock copolymer nanoparticles: synthesis, characterization, in vivo release of rifampicin. Journal of Materials Chemistry B. 2014;2(4):418-27.
- Garms BC, Poli H, Baggley D, Han FY, Whittaker AK, Anitha A, Grøndahl L. Evaluating the effect of synthesis, isolation, and characterisation variables on reported particle size and dispersity of drug loaded PLGA nanoparticles. Materials Advances. 2021;2(17):5657-71.
- Gaspar LM, Dórea AC, Droppa-Almeida D, de Mélo Silva IS, Montoro FE, Alves LL, Macedo ML, Padilha FF. Development and characterization of PLGA nanoparticles containing antibiotics. Journal of Nanoparticle Research. 2018 Nov;20:1-9.
- Gray BP, Kelly L, Ahrens DP, Barry AP, Kratschmer C, Levy M, et al (2018) Tunable cytotoxic aptamer–drug conjugates for the treatment of prostate cancer Proc. Natl. Acad. Sci. U. S. A. 115(18):4761–6
- Hazra RS, Dutta D, Mamnoon B, Nair G, Knight A, Mallik S, et al (2021) Polymeric Composite Matrix with High Biobased Content as Pharmaceutically Relevant Molecular Encapsulation and Release Platform ACS Appl Mater Interfaces 13(34):40229–48
- Kennedy PJ, Sousa F, Ferreira D, Pereira C, Nestor M, Oliveira C, Granja PL, Sarmiento B. Fab-conjugated PLGA nanoparticles effectively target cancer cells expressing human CD44v6. Acta biomaterialia. 2018 Nov 1;81:208-18.

- Kumari L, Ehsan I, Mondal A, Al Hoque A, Mukherjee B, Choudhury P, et al (2023) Cetuximab-conjugated PLGA nanoparticles as a prospective targeting therapeutics for non-small cell lung cancer *Journal of Drug Targeting* 31(5):521-536
- Lee SS, Lee YB, Oh IJ. Cellular uptake of poly (dl-lactide-co-glycolide) nanoparticles: effects of drugs and surface characteristics of nanoparticles. *Journal of Pharmaceutical Investigation*. 2015 Dec;45:659-67.
- Madani SH, Ameli S, Khazaei S, Kanani M, Izadi B (2011) Frequency of Ki-67 (MIB-1) and P53 expressions among patients with prostate cancer *Indian J Pathol Microbiol* 54(4):688–91
- Melo PS, De Azevedo MM, Frungillo L, Anazetti MC, Marcato PD, Durán N. Nanocytotoxicity: violacein and violacein-loaded poly (D, L-lactide-co-glycolide) nanoparticles acting on human leukemic cells. *Journal of Biomedical Nanotechnology*. 2009 Apr 1;5(2):192-201.
- Mudavath SL, Talat M, Rai M, Srivastava ON, Sundar S. Characterization and evaluation of amine-modified graphene amphotericin B for the treatment of visceral leishmaniasis: in vivo and in vitro studies. *Drug design, development and therapy*. 2014 Sep 4:1235-47.
- Nahata A, Dixit VK (2012) *Ganoderma lucidum* is an inhibitor of testosterone-induced prostatic hyperplasia in rats *Andrologia* 44:160–74
- Pandian V, Aravindan N, Subramanian S, Somasundaran ST. Lipid-lowering effect of molluscan (*Katelysia opima*) glycosaminoglycan (GAG) in hypercholesterolemic induced rats. *Biological Chemistry*. 2014 Mar 1;395(3):355-64.
- Papachristou F, Anninou N, Koukoulis G, Paraskakis S, Sertaridou E, Tsalikidis C, et al (2021) Differential effects of cisplatin combined with the flavonoid apigenin on HepG2, Hep3B, and Huh7 liver cancer cell lines *Mutat Res Genet Toxicol Environ Mutagen* 866: 503352
- Pierorazio PM, Walsh PC, Partin AW, Epstein JI (2013) Prognostic Gleason grade grouping: data based on the modified Gleason scoring system *BJU international*, 111(5):753-760
- Ramdhani D, Listiani N, Sriyani ME, Maria W E, Watabe H, Mustarichie R, et al (2023) Estrogen receptor targeting with genistein radiolabeled Technetium-99m as radiotracer of breast cancer: Its optimization, characterization, and predicting stability constants by DFT calculation. *Heliyon* 9(2):e13169

- Rockey WM, Hernandez FJ, Huang SY, Cao S, Howell CA, Thomas GS, et al (2011) Rational truncation of an RNA aptamer to prostate-specific membrane antigen using computational structural modeling *Nucleic Acid Ther* 21(5):299–314
- Savory N, Abe K, Sode K, Ikebukuro K (2010) Selection of DNA aptamer against prostate specific antigen using a genetic algorithm and application to sensing *Biosens.* 26(4):1386–91
- Sen R, Mukherjee B, Ganguly S, Sinha S (2023) Surface-functionalized luteolin-loaded nanocarriers successfully delayed lung cancer progress in rats. *J Mater Sci* 58(18):7731–57
- Spek S, Haeuser M, Schaefer MM, Langer K. Characterisation of PEGylated PLGA nanoparticles comparing the nanoparticle bulk to the particle surface using UV/vis spectroscopy, SEC, <sup>1</sup>H NMR spectroscopy, and X-ray photoelectron spectroscopy. *Applied Surface Science*. 2015 Aug 30;347:378-85.
- Tătaru OS, Martha O, Crocetto F, Barone B, Voidazan S, Borda A, et al (2021) Fascin-1 and its role as a serological marker in prostate cancer: a prospective case–control study *Future Science OA* 7(9):FSO745
- Thasneem YM, Sajeesh S, Sharma CP (2011) Effect of thiol functionalization on the hemocompatibility of PLGA nanoparticles *J Biomed Mater Res A* 99(4):607–17
- Thevendran R, Navien TN, Meng X, Wen K, Lin Q, Sarah S, Tang TH, Citartan M. Mathematical approaches in estimating aptamer-target binding affinity. *Analytical biochemistry*. 2020 Jul 1;600:113742.
- Wang Y, Li P, Kong L (2013) Chitosan-modified PLGA nanoparticles with versatile surface for improved drug delivery *AAPS PharmSciTech* 14(2):585–92
- Weatherby D. Signs and symptoms analysis from a functional perspective. Weatherby & Associates, LLC; 2004.
- Wolff A, Frank M, Staehlke S, Peters K (2022) A Comparative Study on the Adipogenic Differentiation of Mesenchymal Stem/Stromal Cells in 2D and 3D Culture. *Cells* 11(8):1313
- Yan Y, Tao H, He J, Huang SY (2020) The HDock server for integrated protein–protein docking *Nat. Protoc.* 15(5):1829–52

## 6. Results and discussion

### 6.1. The UV absorption spectrum of Abiraterone acetate (ABR)

The maximum wavelength ( $\lambda_{\max}$ ) of Abiraterone acetate (ABR) was determined by using two different solvent systems. In the first case, the drug absorbance maxima in acetonitrile-dichloromethane (3:1) mixture (3:1 v/v) was found to be 253 nm utilizing UV-Vis spectrophotometer with UV Professional V1.39.0 Software (Figure 6.1). In the other solvent system, i.e. ethanol-PBS (pH 7.4) mixture (1:3), the absorbance spectrum showed the maximum absorbance peak of ABR at 253 nm (Figure 6.2).

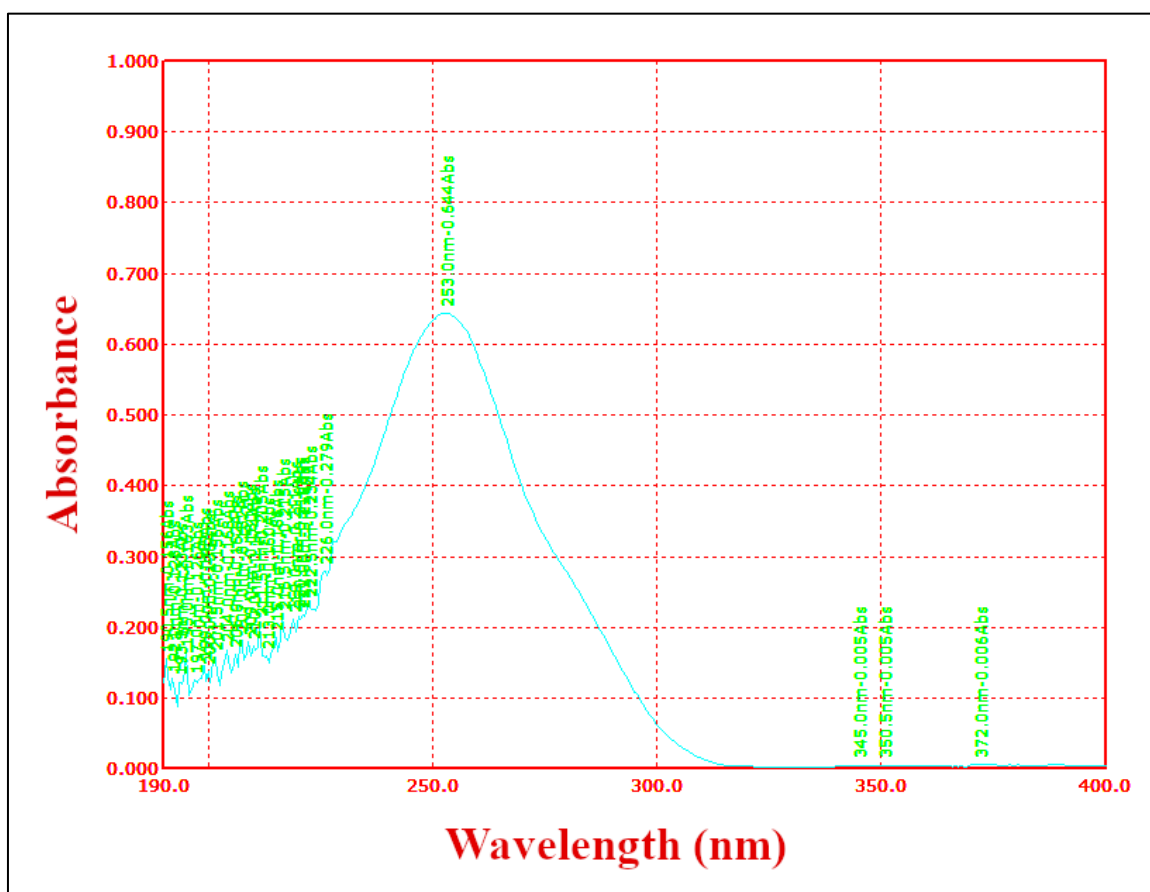


**Figure 6.1:** The UV absorption maxima of ABR in acetonitrile: dichloromethane (3:1) showing  $\lambda_{\max}$  at 253.0 nm.

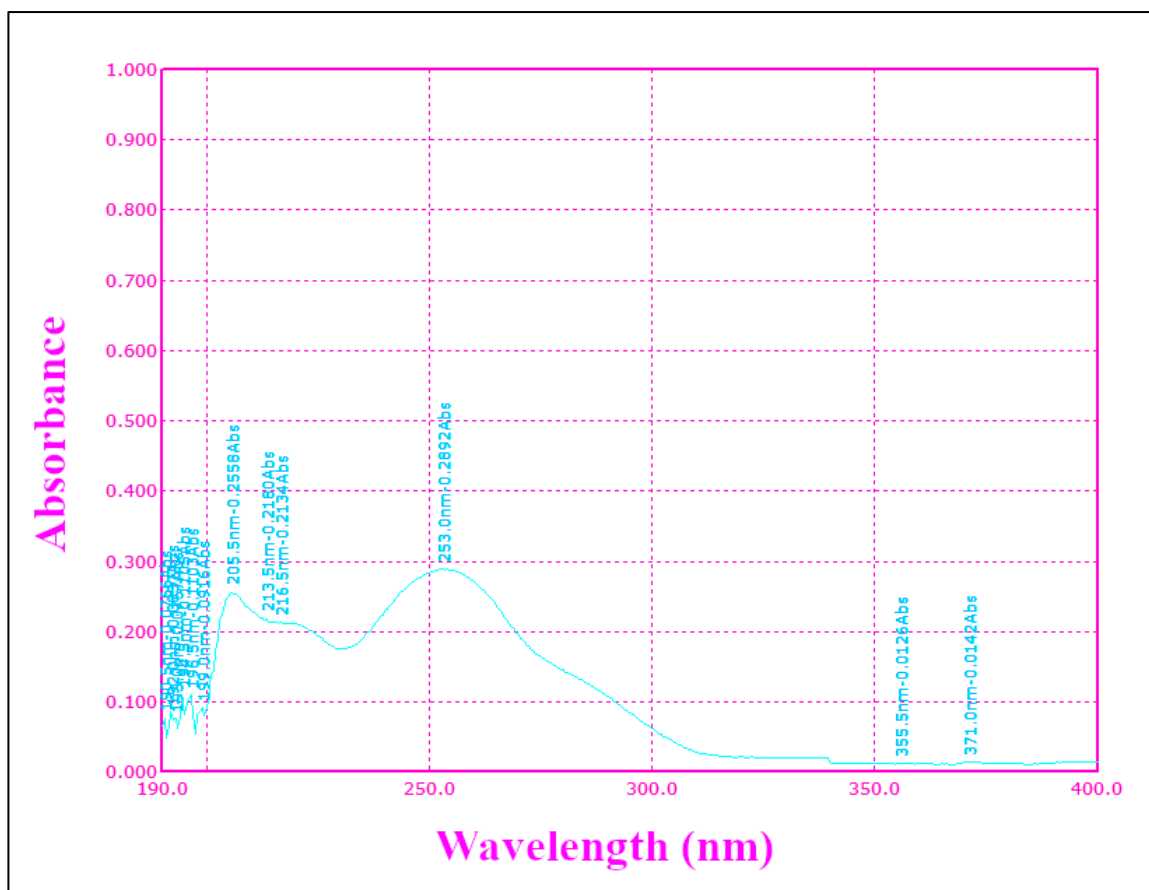


**Figure 6.2:** The UV absorption maxima of ABR in ethanol: PBS (pH 7.4) mixture (1:3) showing  $\lambda_{\text{max}}$  at 253.0 nm.

## 6.2. The calibration curves of ABR

The calibration curve of ABR was prepared using ethanol: PBS (pH 7.4) mixture (1:3) to study the *in vitro* drug release and drug loading determination of the developed nanoparticles. The absorbance values at 5  $\mu\text{g/ml}$ , 10  $\mu\text{g/ml}$ , 15  $\mu\text{g/ml}$ , 20  $\mu\text{g/ml}$ , 25  $\mu\text{g/ml}$  and 30  $\mu\text{g/ml}$  drug concentrations were recorded at 253 nm. A high regression coefficient ( $R^2=0.999$ ) was achieved, which suggests that the absorbance and concentrations of the drug were linearly related to each other, and it followed Beer–Lambert law. The calibration curve of ABR is depicted in Figure 6.3.

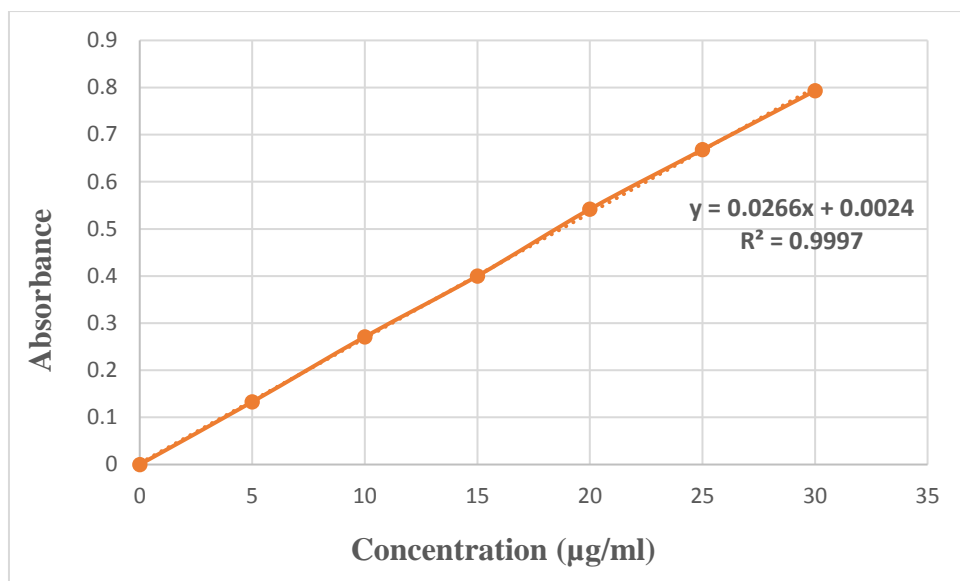


**Figure 6.3:** Calibration curve of ABR in ethanol: PBS (pH 7.4)

### 6.3. Drug-excipient interaction by FTIR analysis

Fourier Transform Infrared (FTIR) spectroscopy is a widely used technique to investigate the chemical interactions between the drug molecule and the excipients (Song et al., 2020; Chadha et al., 2014). In this study, FTIR analysis was performed to detect any chemical interactions between the drug molecule and the excipients. The results demonstrate that PLGA exhibited peaks at  $3650\text{ cm}^{-1}$ ,  $2935\text{ cm}^{-1}$ , and  $1735\text{ cm}^{-1}$  for the O-H stretching, asymmetric stretching of  $-\text{CH}_2$ , and C=O stretching band of the carboxylic acid group, respectively. Similarly, ABR showed characteristic peaks at  $3440\text{ cm}^{-1}$ ,  $2940\text{ cm}^{-1}$ ,  $1735\text{ cm}^{-1}$ ,  $1440\text{ cm}^{-1}$ ,  $1370\text{ cm}^{-1}$ , and  $1245\text{ cm}^{-1}$  for intermolecular bonded O-H stretching vibrations, C-H stretching, C=O stretching,  $\text{CH}_3$  bending vibration of the acetate group,  $\text{CH}_3$  bending vibration of the methyl groups, and C-O-C stretching vibration of the acetate group, respectively.

Additionally, FTIR spectra of PVA showed peaks at  $3420\text{ cm}^{-1}$  for intermolecular bonded O-H stretching vibrations,  $2925\text{ cm}^{-1}$  for asymmetric stretching of  $-\text{CH}_2$ , and  $1740\text{ cm}^{-1}$  due to water absorption. Furthermore, blank (without drug) nanoparticles (BL-NP) exhibited the presence of all characteristic peaks of the polymer PLGA. Similarly, ABR-NP showed IR peaks at  $3490\text{ cm}^{-1}$  due to intermolecular bonded O-H stretching vibrations,  $2950\text{ cm}^{-1}$  for C-H stretching,  $1760\text{ cm}^{-1}$  for C=O stretching,  $1380\text{ cm}^{-1}$  for C-H bending, and  $1200\text{ cm}^{-1}$  for C-O stretching due to ester group.

Moreover, Apt-ABR-NP exhibited almost similar peaks with an additional peak at  $1650\text{ cm}^{-1}$  for C=O stretching due to the amide group. The presence of peaks at  $1650\text{ cm}^{-1}$  for Apt-ABR-NP indicated that the aptamer was binding to the ABR-NPs through amide bond formation. The FTIR study (Figure 6.4) suggests that there was no chemical interaction between the ABR and the excipient used, except the aptamer in this study. However, slight shifts in the peak were responsible for the physical interactions that could provide the structure of the formulation. The shift of vibration signals indicated the presence of physical interactions between the compounds for the nanoparticles that might help develop a spherical nanostructure (Dhara et al., 2023).

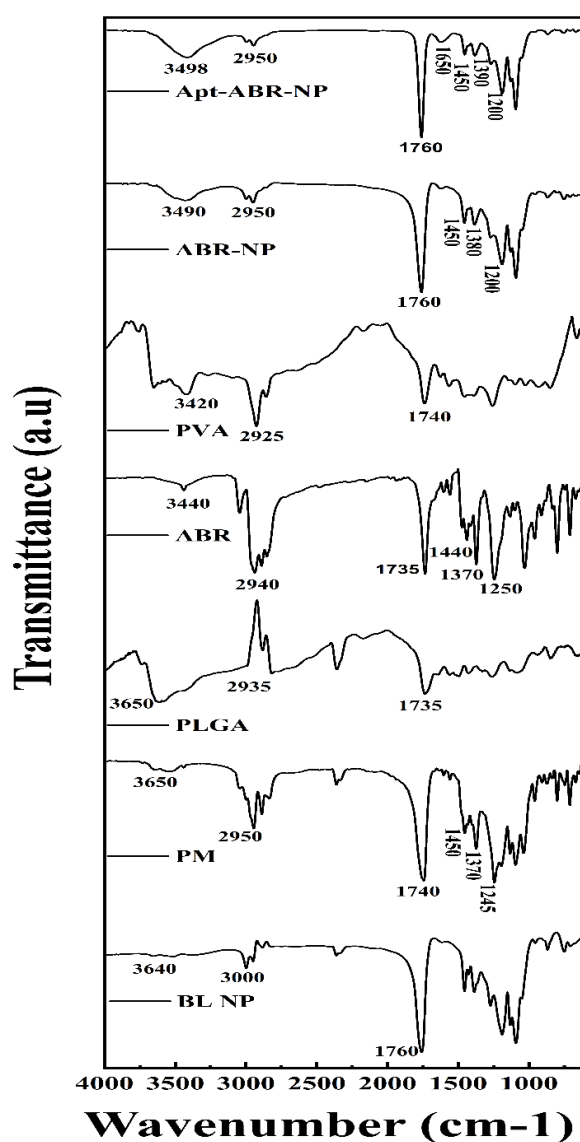


**Figure 6.4:** FTIR spectra of different excipients, drug, and formulations. FTIR spectra of PLGA, Abiraterone acetate (ABR), physical Mixture of excipients (PM), blank nanoparticles



(BL-NP), PLGA nanoparticles containing Abiraterone acetate (ABR-NP), and aptamer-conjugated PLGA nanoparticles (Apt-ABR-NP)

#### 6.4. X-ray photoelectron spectroscopy (XPS)

High-resolution X-ray photoelectron spectroscopy (XPS) was employed to identify the chemical elements and surface chemistry of nanoparticles. The technique provided qualitative and quantitative information on various elements present on the particle surface and determined the chemical composition of the uppermost layer of the polymer surface (Ghobeira et al., 2022; Giglio et al., 2014). The XPS spectrum of ABR-NP revealed an O1s peak at 533 eV and a C1s peak at 287 eV, confirming the presence of oxygen and carbon elements, respectively, in the PLGA polymer matrix. A minor peak of N1s was also observed at 399 eV. XPS spectra of Apt-ABR-NP nanoparticles displayed distinct peaks for oxygen and carbon at 533 and 287 eV, respectively (Figure 6.5A). A magnified image of the nitrogen region illustrated a significant signal at 399 eV, indicating the presence of a large number of nitrogen atoms in the DNA aptamer.

The XPS spectrum of PLGA nanoparticles displayed peaks O1s and C1s located at almost the same binding energy as aptamer-labeled PLGA nanoparticles and PLGA nanoparticles. Following the chemical reaction of the PLGA nanoparticles with the aptamer, an amide bond (CO-NH) was formed, which detected a significant N1s peak at a binding energy of 408 eV. The higher the polarity of covalent bonds, the higher the bond energy. A CO-NH bond was formed here by the conjugation of the aptamer and PLGA-COOH. XPS confirmed the presence of nitrogen in the PLGA-aptamer nanoparticles (Apt-ABR-NP), which observed a higher intensity, indicating that the aptamer was successfully conjugated to the PLGA surface (Figure 6.5B).

In contrast, only the nitrogen element of the drug molecule, abiraterone acetate, was present in ABR-NP, resulting in a very small N1s peak (Figure 6.5C). This indicates the presence of ABR on the particle surface due to its homogeneous distribution, which was later supported by the findings of high-resolution transmission electron microscopy (HR-TEM). Conjugation of the aptamer to the surface of ABR-NP was successfully confirmed by the XPS plots of the ABR-NP and Apt-ABR-NP. The enlarged plot of aptamer-tagged nanoparticles clearly showed the higher intensity of the nitrogen peak for the abundant presence of the nitrogen atom in the DNA aptamer (Wang et al. 2013).

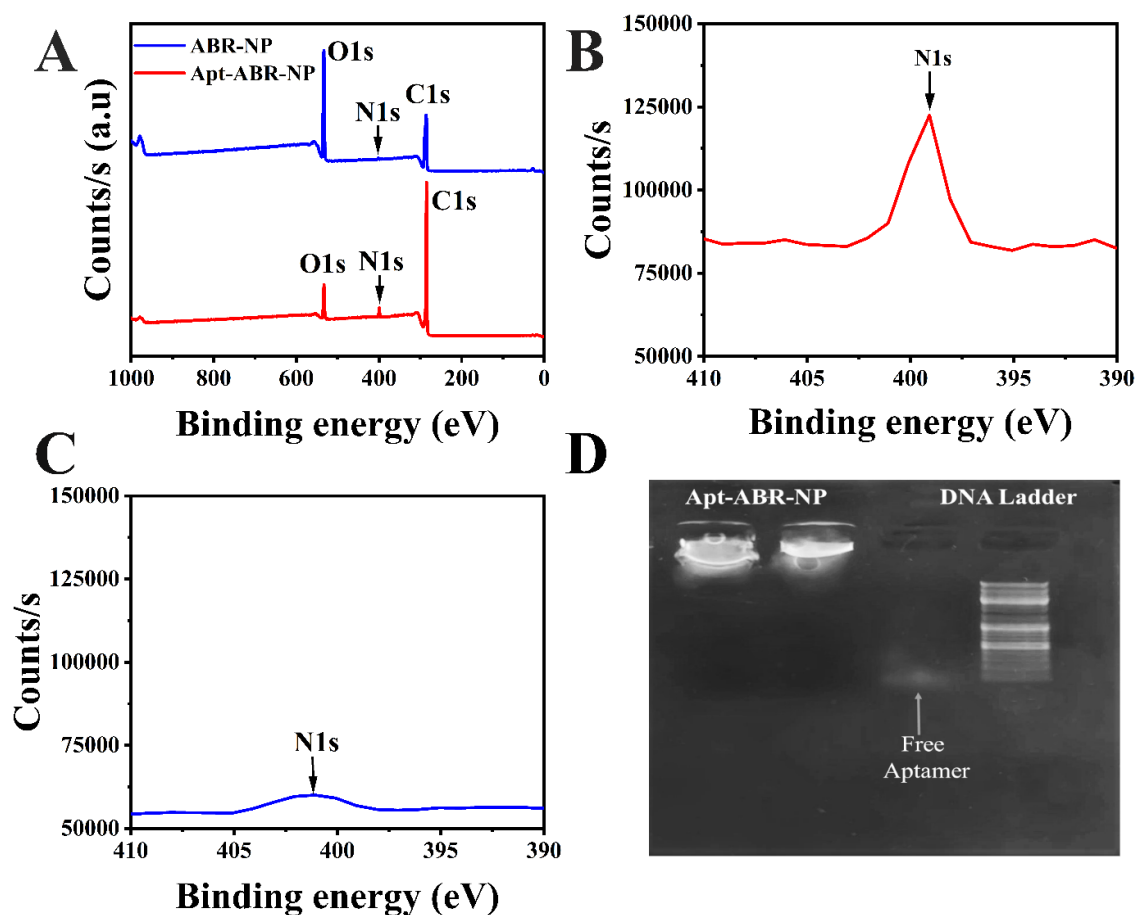


**Figure 6.5:** Aptamer conjugation assessed by X-ray photoelectron spectroscopy study, and agarose gel electrophoresis. (A) XPS graph for combined ABR-NP and Apt-ABR-NP, (B) XPS graph for enlarged N1s peak of Apt-ABR-NP, (C) XPS graph for enlarged N1s peak of ABR-NP, (D) Aptamer conjugation to ABR-NP using agarose gel electrophoresis.

### 6.5. Aptamer conjugation on the surface of nanoparticles through agarose gel electrophoresis

An agarose gel electrophoresis assay was employed to confirm the successful conjugation of the PSMA-specific DNA aptamer onto the surface of the nanoparticle. As demonstrated in Figure 6.5D, the 32 base-pair aptamer migrated through the gel and aligned parallel to the conventional DNA ladder of the 50bp marker. The aptamer-coupled nanoparticles (Apt-ABR-NP) were confined to the loading well and were readily identifiable through fluorescence. Conversely, the unconjugated nanoparticles (ABR-NP) did not exhibit any discernible band in the well due to the absence of a DNA strand. Notably, the image of Apt-ABR-NP evinced the coexistence of the DNA aptamer and the nanoparticles, thus affirming the effective conjugation of the aptamer onto the surface of the nanoparticle, which was further supported by Fourier-transform infrared (FTIR) spectroscopy data (Estévez et al., 2010; Chang et al., 2011).

### 6.6. Aptamer-PSMA interactions study by molecular docking

A molecular docking study was performed to evaluate the molecular interactions between the 32 bp DNA aptamer and prostate-specific membrane antigen (PSMA). The results of this study suggest that the nucleotide bases of the aptamer effectively bind with various amino acid residues, as shown in Figures 6.6A and 6.6B. Electrostatic interaction was observed between Lysine 406, ARG181, ARG649, and ARG 649 residues and phosphate groups of thymine (DT27), adenine (DA2), adenine (DA11), adenine (DA11), respectively. Additionally, several conventional and carbon-hydrogen bonding, along with some hydrophobic interactions, were found between aspartic acid (ASP654), lysine (LYS187), lysine (LYS187), arginine (ARG 190), arginine (ARG649), arginine (ARG190), glutamic acid (GLU748), alanine (ALA635) and methionine (MET663) amino acid residues with adenine (DA2:N3), adenine (DA3:O4'), thymine (DT32:O2), adenine (DA10:O3'), thymine (DT32:O2), thymine (S: DT1), guanine (DG15) and adenine (DA24) nucleotide bases of the aptamer respectively, as shown in Table 1. The docking score was determined to be -330.86, indicating a strong binding affinity between the ligand and receptor. These findings suggest that aptamer-conjugated nanoparticles can selectively bind to PSMA found in most prostate cancer tissue surfaces, and the drug molecules that reach cancer tissues through the targeting method would demonstrate their efficacy more efficiently. The DNA aptamer-PSMA binding through molecular docking analysis is also a clear indication of the capabilities of the conjugated nanoparticles to specifically reach the PSMA-associated prostate cancer microenvironment (Ptacek et al., 2020).

**Table 1:** Aptamer-PSMA binding using molecular docking analysis

Name of Protein	PDB code	Aptamer and sequence	Docking Score	Interacting residues	Type of interactions
Prostate-specific membrane antigen (PSMA)	1Z8L	ΔPSap4#5 5'-TTT TTA ATT AAA GCT CGC CAT CAA ATA GCT TT-3'	-330.86	Lysine 406, ARG181, ARG649, ARG 649, ASP654, LYS187, LYS187, ARG 190, Arginine ARG649, ARG190, GLU748, ALA635 and MET663	Electrostatic interactions, Hydrogen bonding, Pi-sulphur

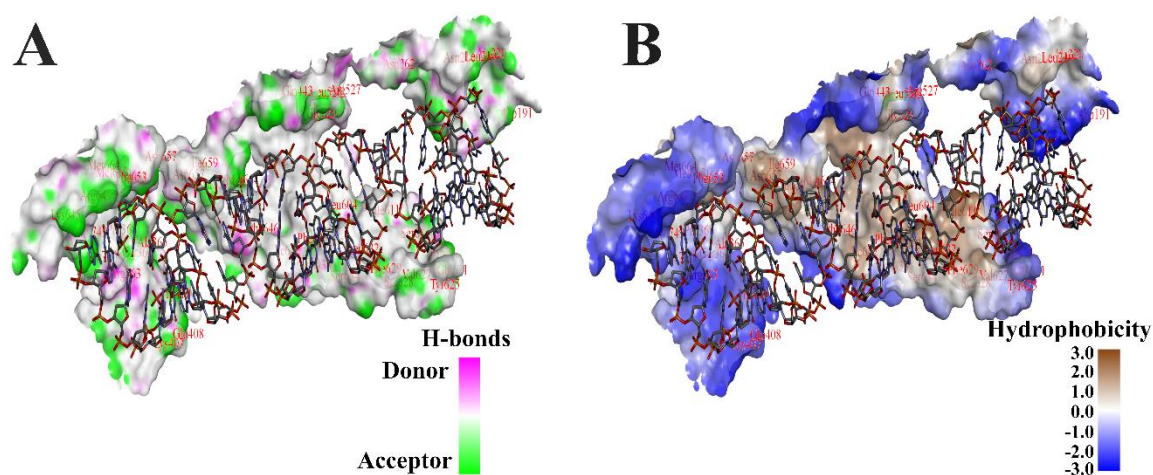


**Figure 6.6:** Aptamer-PSMA binding by molecular docking. (A) Aptamer-PSMA (Protein data bank, PDB: 1Z8L) interactions by hydrogen bonding through molecular docking; (B) Aptamer-PSMA (PDB: 1Z8L) hydrophobic interactions through molecular docking

### 6.7. Determination of particle size and zeta potential

The present study employed the dynamic light scattering method to determine the particle size distribution and zeta potential of the ABR-NP and Apt-ABR-NP. The hydrodynamic diameter ( $d_H$ ) of ABR-NP/Apt-ABR-NP was found to be 130.6 nm/149.30 nm, respectively, with aptamer conjugation exhibiting a significant 20% increase in the size of ABR-NP (as demonstrated in Figure 6.7A). Furthermore, the zeta potential values for ABR-NP and Apt-ABR-NP were -10.1 mV and -18.5 mV, respectively (as shown in Figure 6.7B). The higher zeta potential values of Apt-ABR-NP suggest that they can remain suspended in an aqueous medium for a longer duration. It is noteworthy that nanoparticles with zeta potential values greater than  $\pm 30$  mV are known to demonstrate a more stable suspension (Champion et al. 2007). Therefore, it is highly recommended that the formulations be stored as a powder that can be suspended in water before administration to ensure their stability and prolonged shelf-life.

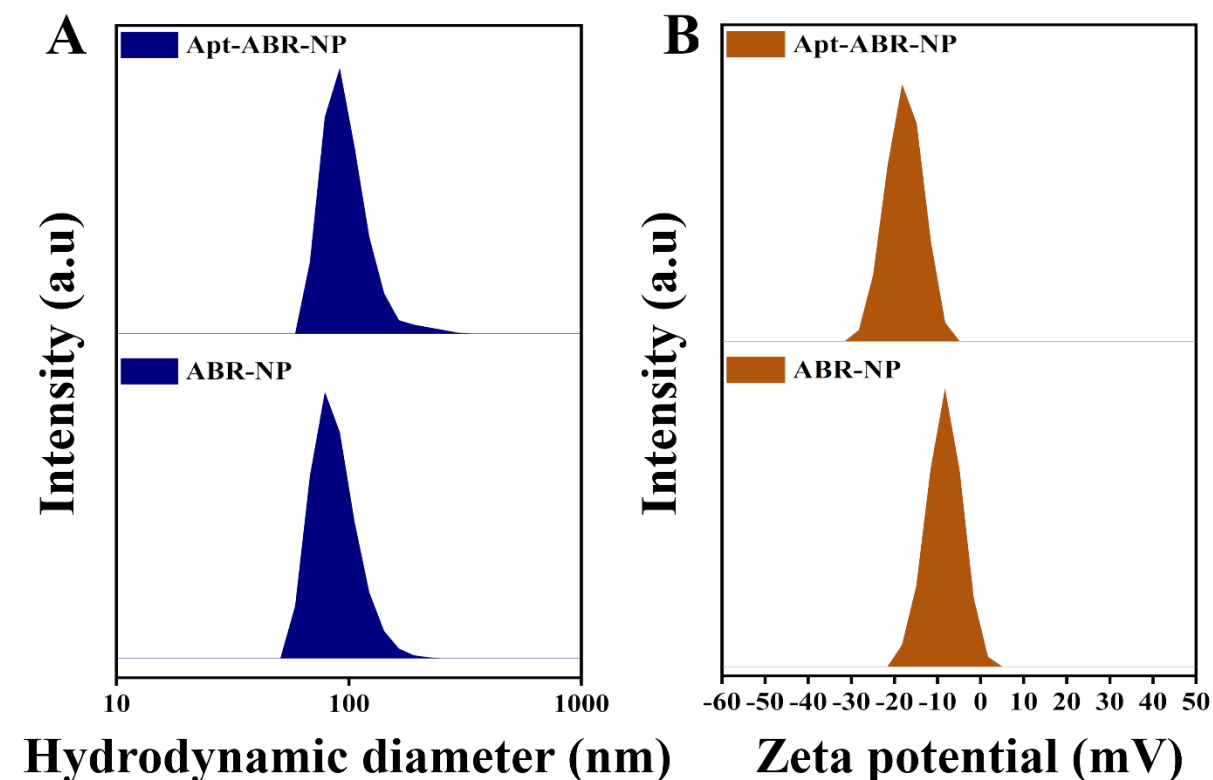


**Figure 6.7:** Determination of particle size and zeta potential of the experimental nanoparticles. (A) represents particle size distribution of ABR-NP and Apt-ABR-NP (B) represents zeta potential values of ABR-NP and Apt-ABR-NP.

### 6.8. *In-vitro* drug release study

The present study aimed to investigate the *in vitro* drug release kinetics of Apt-ABR-NP in five different media, namely phosphate buffer saline (PBS) at pH 7.4, PBS with 1%  $\beta$ -hydroxy cyclodextrin at pH 7.4, citrate buffer at pH 3, acetate buffer at pH 5, and bicarbonate buffer at pH 10, over a period of 28 days or 672 hours (Figure 6.8). PBS was selected as the release medium owing to its ability to mimic the pH of the blood environment. The cumulative percentage of drug release was determined after 672 hours, with the results revealing that the percentage of drug released was 73.12%, 81.45%, 92.76%, 92.45%, and 43.30% in phosphate buffer saline (PBS) at pH 7.4, PBS with 1%  $\beta$ -hydroxy cyclodextrin at pH 7.4, citrate buffer at pH 3, acetate buffer at pH 5, and bicarbonate buffer at pH 10, respectively. To determine the drug release kinetics in each of the five media, the zero-order, first-order, Hixson-Crowell, Korsmeyer-Peppas, and Higuchi kinetic models were tested, and the regression coefficient values ( $R^2$ ) were tabulated (Table 2). Results indicated that the drug release followed the Korsmeyer-Peppas model in all five release media, as suggested by the  $R^2$  values.

The zero-order drug release kinetic mechanism exhibits a constant rate of drug release independent of the concentration of the drug loaded into the polymer matrix or the degradation of the matrix itself.

In contrast, the first-order kinetic mechanism displays a gradual decline in the release rate of drug molecules depending on the concentration of the drug within the polymer matrix. This mechanism is influenced by several factors, such as the diffusion of drug molecules through the polymer matrix, erosion of the polymer, and degradation of the nanoparticles.

On the other hand, the Higuchi kinetics mechanism relies on diffusion-controlled mechanisms for drug release from PLGA nanoparticles. As the polymer matrix degrades or erodes, drug molecules diffuse out of the nanoparticles into the surrounding medium. The release rate of the drug decreases gradually over time, and it is directly proportional to the square root of time.

The Korsmeyer-Peppas model, a widely used drug release model, incorporates both Fickian diffusion and polymer erosion mechanisms. It characterizes drug release as a function of time and is particularly relevant when drug release is controlled by a combination of diffusion through the polymer matrix and erosion of the matrix itself. The release of ABR from the nanoparticles followed the Korsmeyer-Peppas kinetic model, indicating a diffusion and erosion-controlled release mechanism (Pattnaik et al. 2012).

Lastly, the Hixson-Crowell model describes drug release from solid dosage forms, such as nanoparticles. It is a drug release mechanism that involves changes in the surface area or dimensions of the dosage form over time. This model is particularly applicable to systems where drug release is predominantly controlled by the dissolution or erosion of the matrix, leading to changes in the surface area available for drug release.

The *in vitro* drug release behavior of nanoparticles in PBS with  $\beta$ -hydroxy cyclodextrin media was found to exhibit a biphasic pattern, consisting of an initial burst release phase followed by a sustained release phase for a period of four weeks. The release of drug molecules from or in close proximity to the surface of the nanoparticles and  $\beta$ -hydroxy cyclodextrin complexation of the drug may have resulted in improved solubility of hydrophobic drug molecules in the release medium.

The accelerated degradation of the polylactic acid-glycolic acid polymer in citrate buffer (pH 3), in comparison to PBS/PBS with  $\beta$ -hydroxy cyclodextrin, elucidates the faster release of ABR at pH 3. The acidic environment (pH 3) stimulates the hydrolysis of the PLGA core by

cleaving ester bonds, thereby culminating in expedited polymer degradation. Conversely, at an alkaline pH (pH 10), the polymer preserves its non-polar nature owing to the entrapment of hydroxyl groups on the polymer surface. This constrains particle water absorption and consequently yields a more stable nanoparticle state in high pH environments. The extent of hydrolytic degradation ascends from neutral to acidic pH. The expedited release of ABR in an acidic milieu, when compared to PBS (pH 7.4), exemplifies that ABR is discharged more rapidly from ABR-NP in an acidic tumor environment rather than in the physiologically neutral milieu of blood during transportation and distribution (Choi et al. 2015).

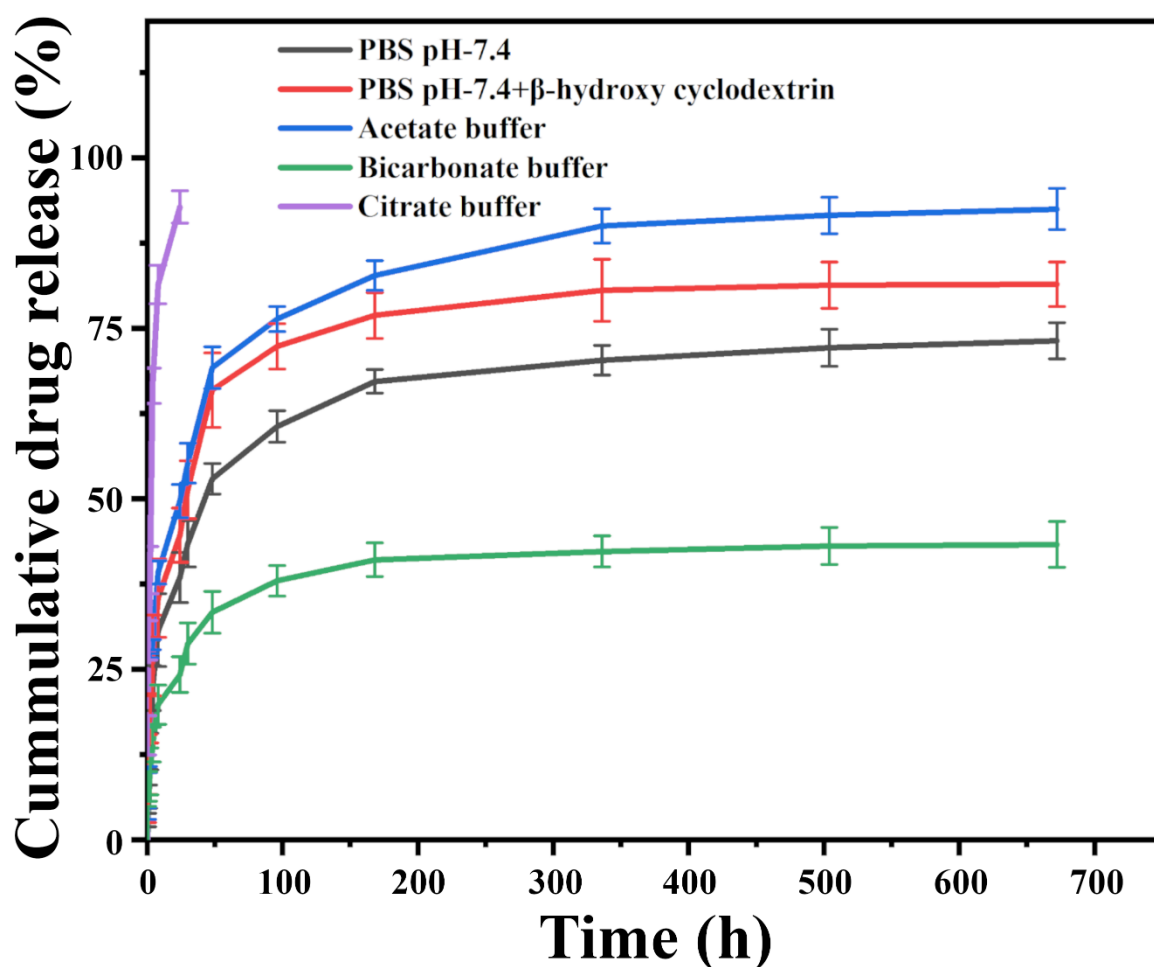


**Figure 6.8:** *In vitro* drug release study of the experimental nanoparticles in phosphate buffer saline (PBS pH-7.4), PBS containing 1%  $\beta$ -hydroxy-cyclodextrin, acetate buffer (pH 5), bicarbonate buffer (pH 10) and citrate buffer (pH 3)

**Table 2:** Regression coefficient ( $R^2$ ) values of the data of *in vitro* drug release tested on various kinetic models

Kinetic models	Regression coefficient values				
	PBS (pH 7.4)	PBS (pH 7.4 with $\beta$ -CD)	Citrate buffer (pH 3)	Acetate buffer (pH 5)	Bicarbonate buffer (pH 10)
Zero-order	$R^2 = 0.5495$	$R^2 = 0.5101$	$R^2 = 0.6411$	$R^2 = 0.5495$	$R^2 = 0.5104$
First order	$R^2 = 0.678$	$R^2 = 0.6546$	$R^2 = 0.8902$	$R^2 = 0.804$	$R^2 = 0.5608$
Higuchi model	$R^2 = 0.0.7795$	$R^2 = 0.752$	$R^2 = 0.8748$	$R^2 = 0.7826$	$R^2 = 0.7511$
Korsmeyer-Peppas model	$R^2 = 0.8782$ $n=0.33$	$R^2 = 0.9035$ $n=0.29$	$R^2 = 0.9033$ $n=0.38$	$R^2 = 0.8812$ $n=0.29$	$R^2 = 0.9265$ $n=0.26$
Hixson-Crowell model	$R^2 = 0.6352$	$R^2 = 0.6062$	$R^2 = 0.8098$	$R^2 = 0.72$	$R^2 = 0.544$



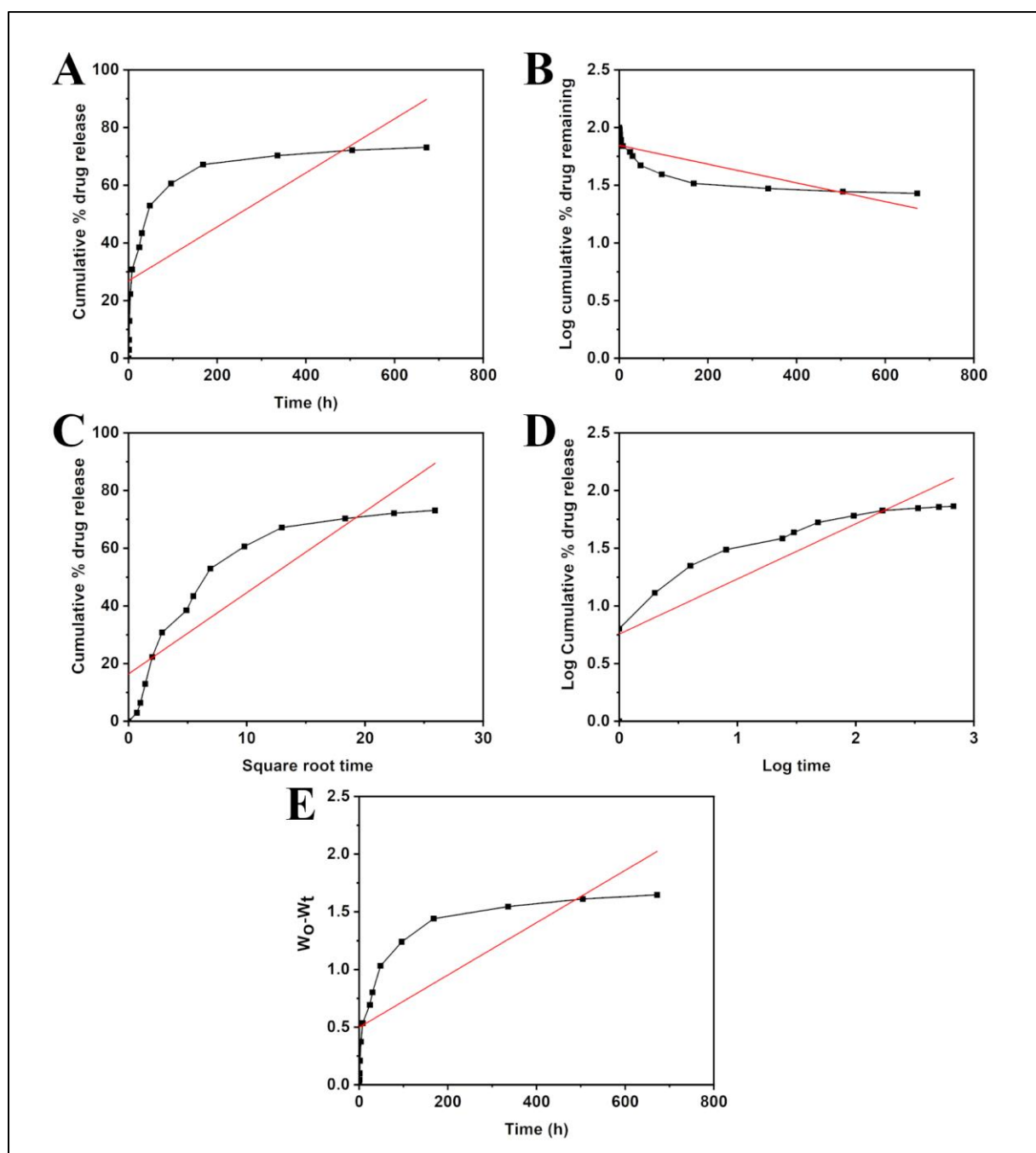


**Figure 6.9:** *In vitro* drug release kinetics in Phosphate-buffered saline (PBS, pH 7.4) using various kinetic models. (A) Zero order kinetics, (B) 1<sup>st</sup> order kinetics, (C) Higuchi model of kinetics, (D) Korsmeyer-peppas model of kinetics, and (E) Hixson Crowell model of kinetics.

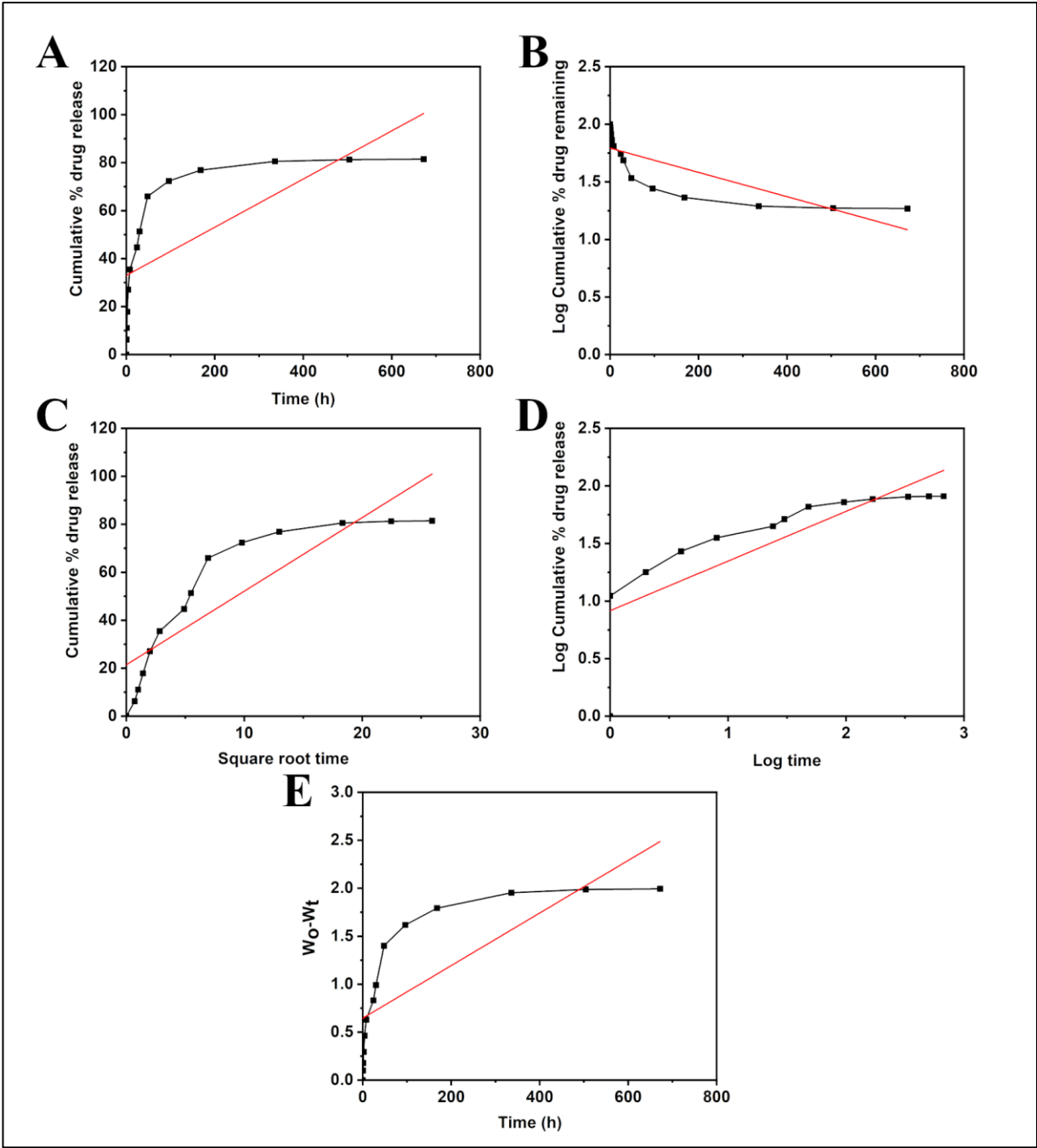


**Figure 6.10:** *In vitro* drug release kinetics in Phosphate-buffered saline (PBS, pH 7.4) with  $\beta$ -cyclodextrin using various kinetic models. (A) Zero order kinetics, (B) 1<sup>st</sup> order kinetics, (C) Higuchi model of kinetics, (D) Korsmeyer-peppas model of kinetics, and (E) Hixson Crowell model of kinetics.

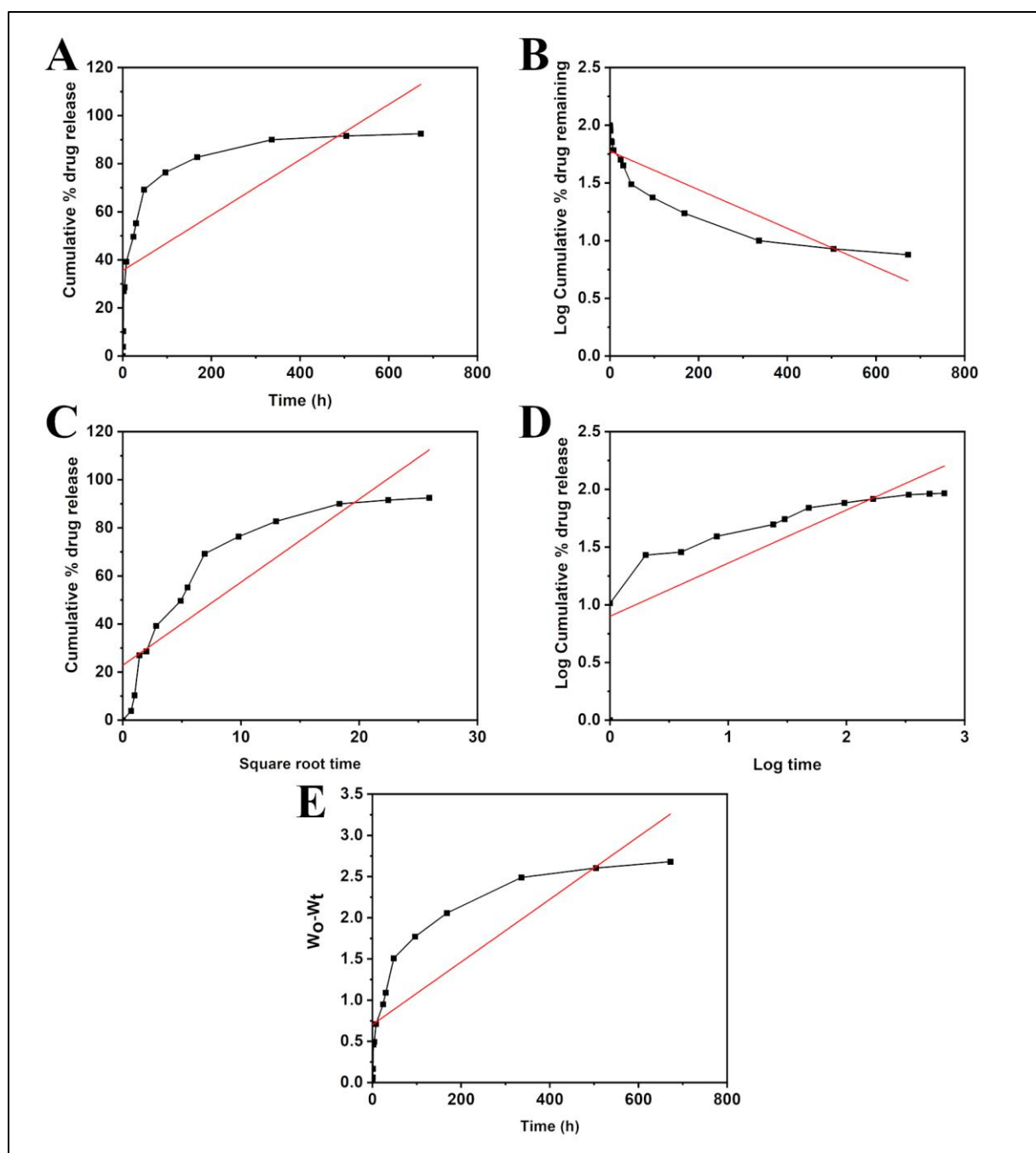


**Figure 6.11:** *In vitro* drug release kinetics in acetate buffer (pH 5) using various kinetic models. (A) Zero order kinetics, (B) 1<sup>st</sup> order kinetics, (C) Higuchi model of kinetics, (D) Korsmeyer-peppas model of kinetics, and (E) Hixson Crowell model of kinetics.

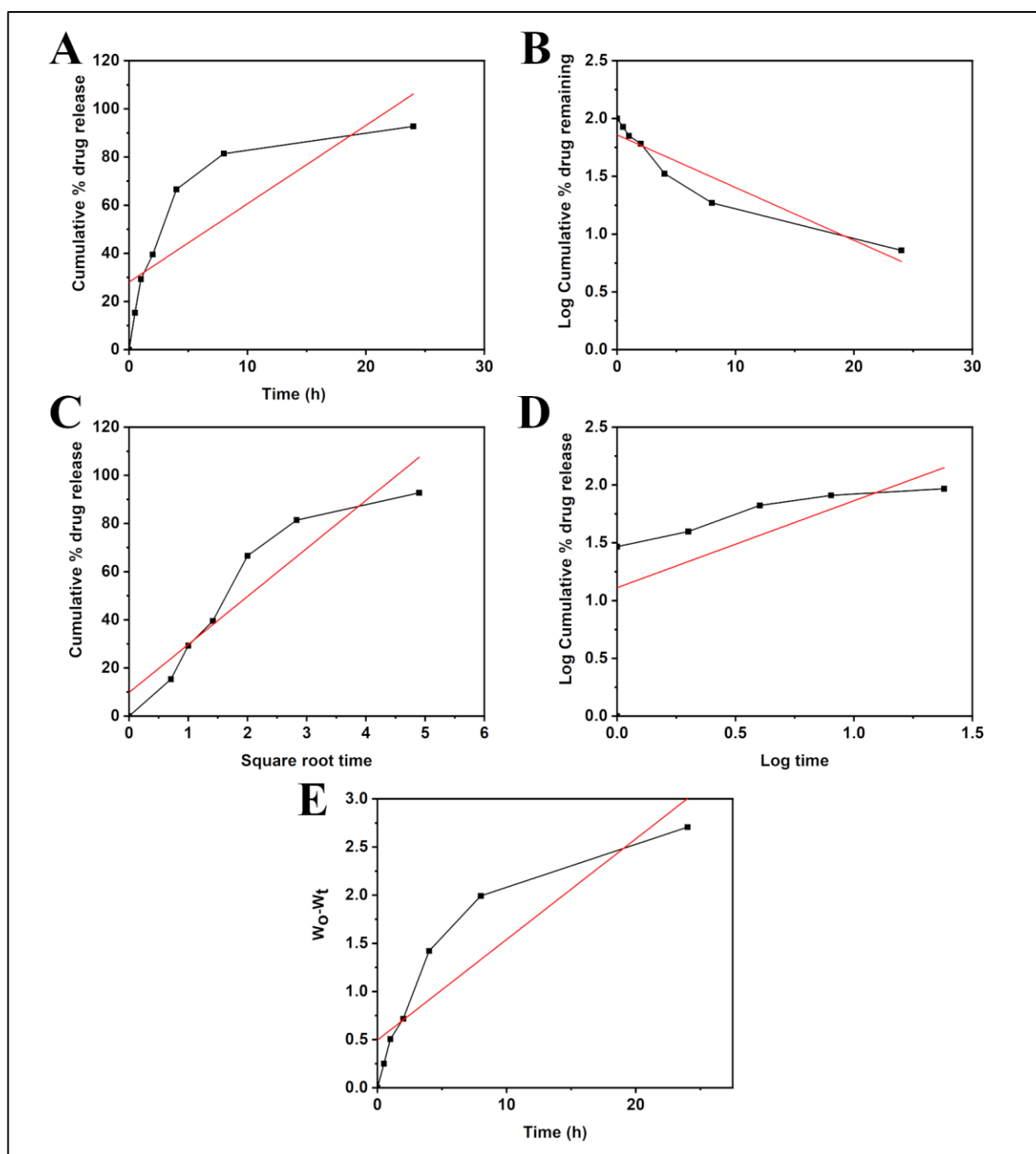


**Figure 6.12:** *In vitro* drug release kinetics in citrate buffer (pH 3) using various kinetic models. (A) Zero order kinetics, (B) 1<sup>st</sup> order kinetics, (C) Higuchi model of kinetics, (D) Korsmeyer-peppas model of kinetics, and (E) Hixson Crowell model of kinetics.

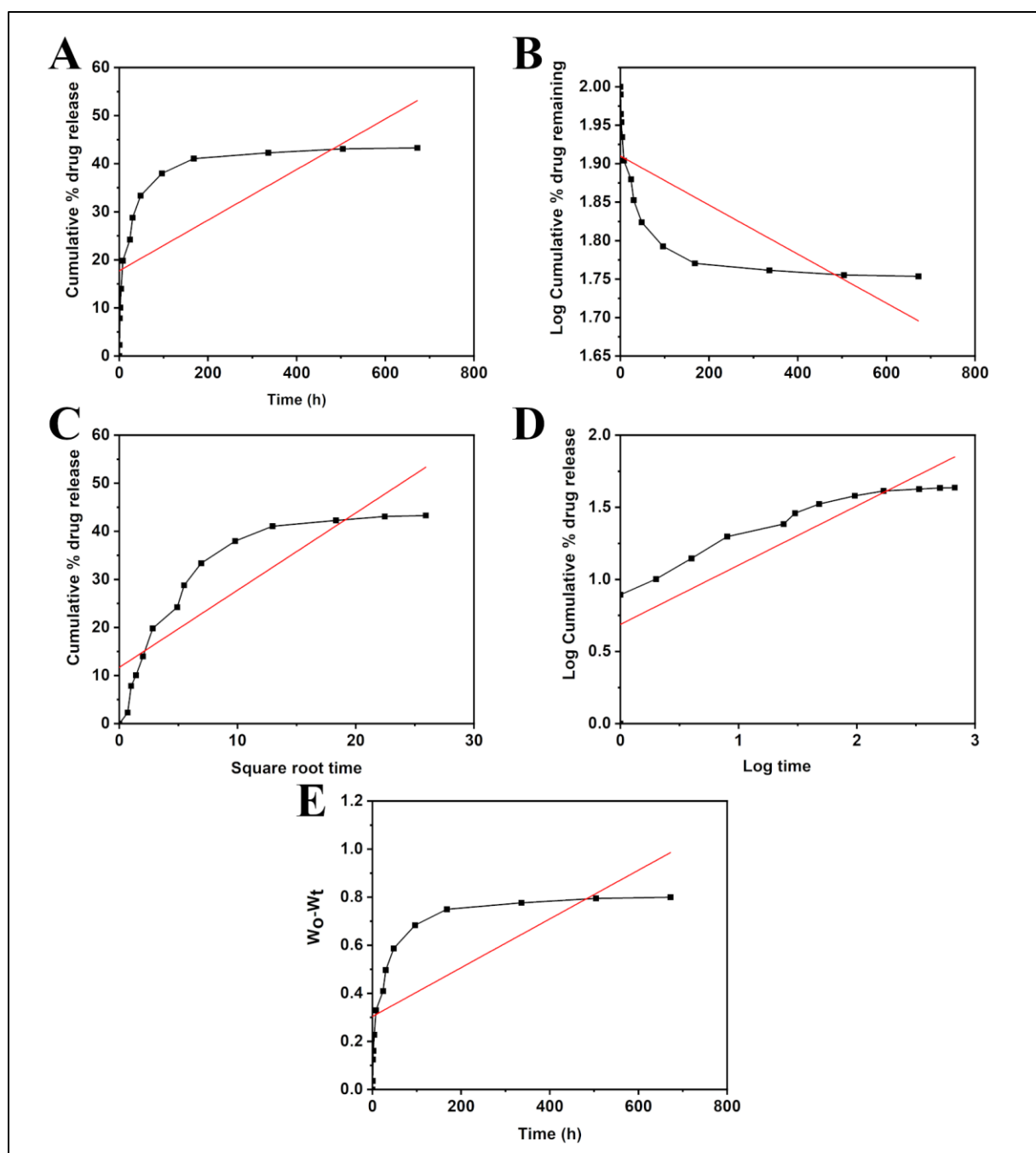


**Figure 6.13:** *In vitro* drug release kinetics in bicarbonate buffer (pH 10) using various kinetic models. (A) Zero order kinetics, (B) 1<sup>st</sup> order kinetics, (C) Higuchi model of kinetics, (D) Korsmeyer-peppas model of kinetics, and (E) Hixson Crowell model of kinetics.

### 6.9. Surface morphology by Field emission scanning electron microscopy (FESEM), High-resolution transmission electron microscopy (HRTEM), and Atomic force microscopy (AFM)

In this study, the surface morphology of ABR-NP and Apt-ABR-NP was investigated using FESEM (Figure 6.14A & 6.14B). The results revealed that the nanoparticles, with sizes ranging

between 100 nm to 150 nm, were round in shape, with smooth surfaces and no visible porosity or fractures. Notably, no significant differences were observed between the surface morphologies of the nanoparticles with and without aptamer conjugation. To further investigate the nanoparticles' interior structure, HR-TEM and AFM were employed, with the Apt-ABR-NP formulation used as the experimental model. HR-TEM images revealed a dark structure, indicating a homogeneous drug distribution throughout the particles (Figure 6.14C). AFM images demonstrated that the nanoparticles had a spherical structure with a smooth surface, with 3D images showing well-separated nanoparticles within a small size range (Figure 6.14D & 6.14E).

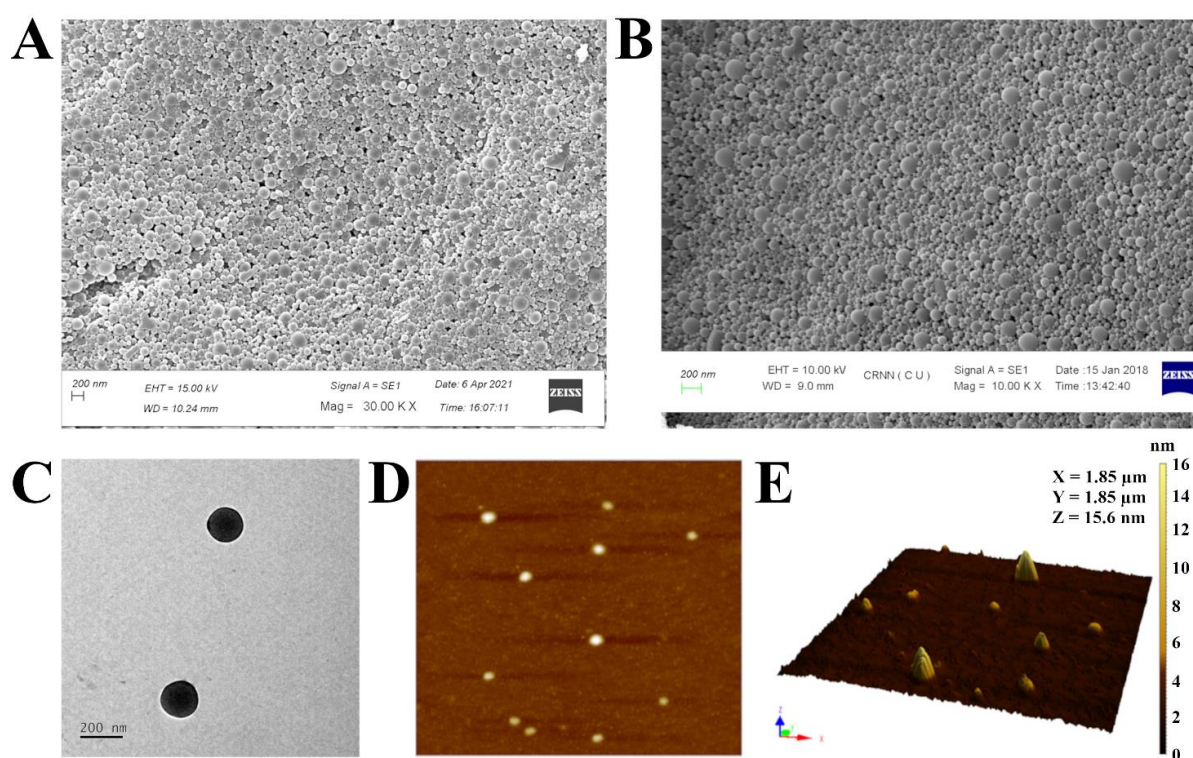


**Figure 6.14:** Electron microscopic imaging and atomic force microscopic evaluation of the experimental nanoparticles. (A & B) represents the FESEM images of ABR-NP and Apt-ABR-NP respectively, (C) HR-TEM image of Apt-ABR-NP and (D & E) depicts AFM images of Apt-ABR-NP.

### 6.10. Drug loading and entrapment efficiency

A series of formulations with varying ratios of drug-to-polymer were developed, and three of these formulations have been presented in Table 3. The drug loading percentages and entrapment efficiencies were calculated for each of these formulations. Specifically, ABR-NP1

and ABR-NP3 exhibited drug loading percentages of  $7.36\pm0.5\%$  and  $2.61\pm0.25\%$ , respectively. The formulation demonstrating the highest drug encapsulation was designated ABR-NP2, which was subsequently chosen as the optimal formulation and named ABR-NP. Impressively, the drug loading and encapsulation efficiency of ABR-NP were found to be  $8.50\pm0.3\%$  and  $93\pm3.30\%$ , respectively, indicating that the technique employed for the creation of nanoparticles resulted in a minimal loss of materials (Dutta et al. 2019).

**Table 3: Composition of experimental nanoparticles and their drug encapsulation efficiencies**

Formulation code	PLGA: Drug	Practical drug loading* (%)	Loading efficiency (%) *
ABR-NP1	5:1	$7.36\pm0.5$	$44.15\pm3$
ABR-NP2	10:1	$8.50\pm0.3$	$93.50\pm3.30$
ABR-NP3	15:1	$2.61\pm0.25$	$41.76\pm4$
Apt-ABR-NP	10:1	$8.02\pm0.15$	$88.20\pm1.6$

\*Data represent mean  $\pm$ SD (n=3)

### 6.11. Stability study of the nanoparticles

The stability of ABR-NP and Apt-ABR-NP formulations was evaluated through a stability study, where the samples were subjected to various storage temperatures and relative humidity levels for 45 and 90 days. Results from the study indicated that samples stored at  $4-8^{\circ}\text{C}$  retained their morphology and drug content throughout the testing period. However, formulations stored at  $30^{\circ}\text{C}$  and  $40^{\circ}\text{C}$  with 75% relative humidity showed morphological deformations (Figure 6.15A & 6.15B) and a slight decrease in drug content (Figure 6.15C). Moreover, the particles' size was observed to increase due to morphological deformation during storage at higher temperatures (Figure 6.15D).

The study concludes that ABR-NP and Apt-ABR-NP formulations can maintain their stability at  $2-8^{\circ}\text{C}$  for up to 90 days. However, the nanoparticles cannot withstand storage at temperatures above  $30^{\circ}\text{C}$ , where aggregation of nanoparticles and polymer softening occur (Yadav and Sawant 2010). Therefore, it is recommended to store the prepared nanoparticles at  $2-8^{\circ}\text{C}$  for optimal stability.



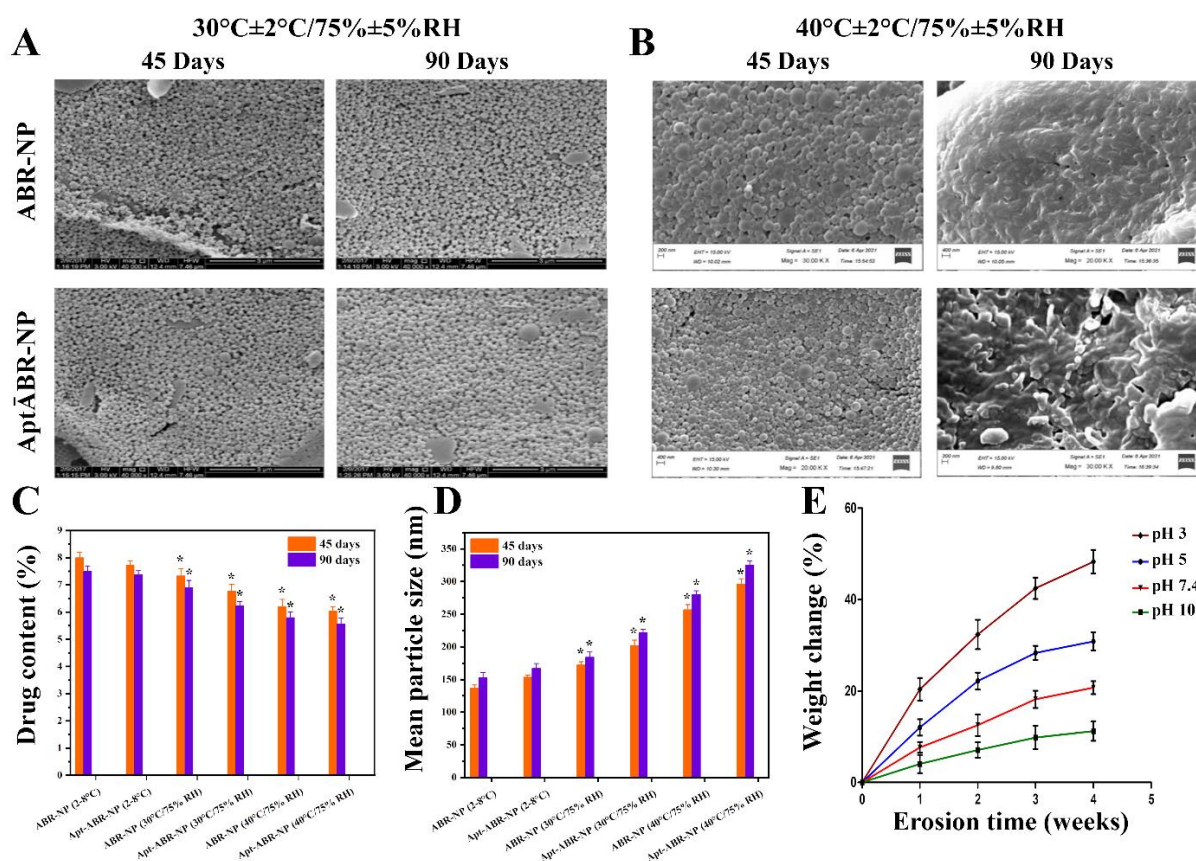


**Figure 6.15:** Surface morphology, drug content, particle size and hydrolytic degradation of the nanoparticles for the stability study. (A) The formulations stored at 30 °C, 75% R.H for 45 days and 90 days and (B) at 40 °C, 75% R.H for 45 days and 90 days, respectively. (C) Drug content of the stored formulations, (D) Mean particle size, (E) Hydrolytic stability study of Apt-ABR-NP in various buffers. The bar diagram and graph data are the averages of the three individual experiments demonstrated as mean  $\pm$  SD. The statistical level of significance is considered as  $p < 0.05$ , analyzed by Student's t-test.

## 6.12. Hydrolytic stability study

The biodegradability of Apt-ABR-NP was assessed through an examination of the weight loss increase during hydrolytic degradation (Jain et al., 2010; Zolnik et al., 2007). The pH values of the medium were found to have a significant impact on weight loss, with an increase in hydrolysis observed as the pH was reduced. A four-week investigation revealed that mass loss was  $11.23 \pm 2.14\%$  at pH 10,  $20.73 \pm 1.41\%$  at pH 7.4,  $30.83 \pm 1.98\%$  at pH 5, and  $48.26 \pm 2.61\%$  at pH 3, respectively (Figure 6.15E). These findings suggest that our nanoformulation is more stable in phosphate buffer (pH 7.4) and bicarbonate buffer (pH 10) in comparison to citrate (pH



3) and acetate buffer (pH 5). The implication of this result is that the Apt-ABR-NP is likely to release its drug contents more rapidly upon reaching the acidic tumor microenvironment.

### **6.13. *In vitro* cellular uptake analysis by flow cytometry and confocal microscopy**

The present study utilized flow cytometry analysis to investigate the cellular uptake of Apt-ABR-NP in both PC3 (Figure 6.16A) and LNCaP (Figure 6.16B) cells. The obtained results revealed a time-dependent gradual accumulation of Apt-ABR-NP in both cell types. Specifically, the inadequate percentage of nanoparticle uptake observed in PC3 cells from 6 to 12 hours of treatment was attributed to the absence of the surface antigen PSMA, which is overexpressed in LNCaP cells. In contrast, a longer incubation period with nanoparticles significantly enhanced cellular uptake, particularly with Apt-ABR-NP in LNCaP cells. This suggests the strong binding affinity of aptamer-functionalized nanoparticles with the PSMA cell-surface biomarker for prostate cancer.

Moreover, confocal microscopy images indicated that both PC3 and LNCaP cells exhibited nanoparticle accumulation inside the cytoplasm over time, with LNCaP cells showing a comparatively higher accumulation (Figure 6.16C & 6.16D). This observation was confirmed by the red fluorescence intensity, which indicated the intense binding specificity of the aptamer with PSMA, especially with a longer incubation period.

To further validate the targeting specificity of the nanoparticle surface-conjugated aptamer against the PSMA receptor, a cellular uptake study was conducted on 22Rv1 cells, which overexpress PSMA and are AR-positive. The results demonstrated a time-dependent increase in the uptake of ABR-NP and Apt-ABR-NP in these cells, with Apt-ABR-NP showing higher cellular uptake (Figure 6.18A).

Regarding the internalization mechanism of aptamer-conjugated PLGA nanoparticles, previous reports have indicated that these particles can internalize into cells via receptor-mediated endocytosis and micropinocytosis (Liu et al. 2009; Shishparenok et al. 2023; Wan et al. 2019; Yallapu et al. 2014). In our study, Apt-ABR-NP was found to interact with PSMA in clathrin-dependent endocytosis by forming clathrin-coated pits. After the detachment of the clathrin coat, the aptamer-conjugated formulations were internalized in endosomes and lysosomes before distribution to other cellular organelles (Shishparenok et al., 2023; Wan et al., 2019). The cellular uptake of aptamer-conjugated formulations was facilitated by clathrin and caveolae-dependent and caveolae-independent pathways, indicating the involvement of multiple receptor-mediated endocytotic pathways (Shishparenok et al., 2023; Wan et al., 2019).

Lastly, the selective reversal of the surface charge of PLGA nanoparticles from anionic to cationic in the acidic endolysosomal environment allowed for the rapid endolysosomal escape of PLGA nanoparticles into the cytosol. This mechanism is a well-established process for lysosomal escape of PLGA nanoparticles (Panyam et al. 2002).

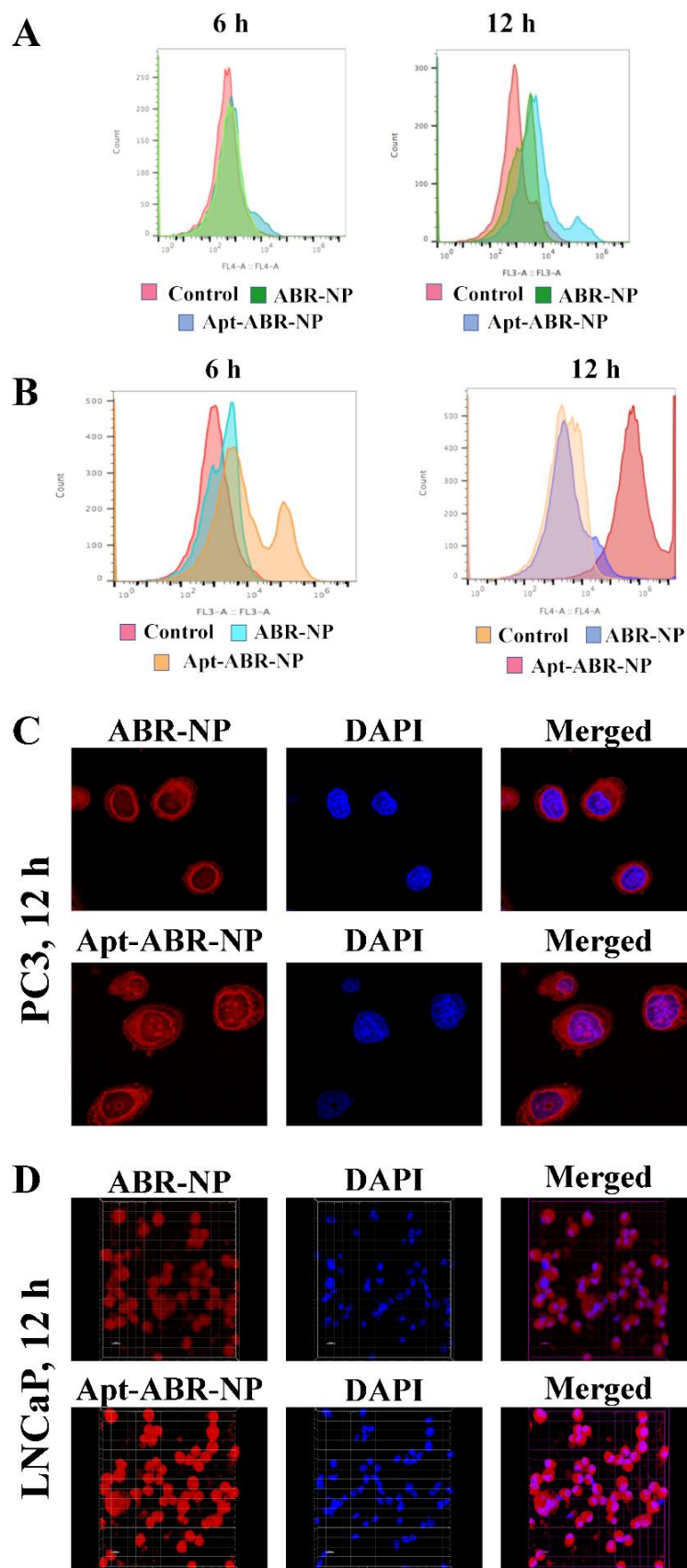


**Figure 6.16:** Cellular uptake study (A) FACS histogram PC3 cells after the treatment with ABR-NP and Apt-ABR-NP at 6 h and 12 h. (B) FACS histogram LNCaP cells after the

treatment with ABR-NP and Apt-ABR-NP at 6 h and 12 h. (C) Confocal laser microscopy images of PC3 cells at 12 h after the treatment with ABR-NP and Apt-ABR-NP. (D) Confocal laser microscopic images of LNCaP cells at 12 h after the treatment with ABR-NP and Apt-ABR-NP.

#### **6.14. *In vitro* cytotoxicity assay**

The study investigated the cytotoxic effects of free drug and experimental nanoparticles on 22Rv1, LNCaP, and PC3 cells. The percentage viability data of these cells, presented in Figures 6.18B, 6.17A, and 6.17B, showed that Apt-ABR-NP had the highest cytotoxicity on LNCaP cells, followed by 22Rv1, compared to ABR and ABR-NP. LNCaP cells treated with ABR showed an  $IC_{50}$  of  $29.2 \pm 3.1 \mu M$ , while those treated with ABR-NP and Apt-ABR-NP showed  $IC_{50}$  values of  $22.5 \pm 2.6 \mu M$  and  $14.5 \pm 1.2 \mu M$ , respectively. The nanoparticles exhibited a significant reduction in the  $IC_{50}$  value on LNCaP cells, indicating their enhanced therapeutic efficacy compared to free ABR. However, the cytotoxicity of ABR and its formulations on PC3 cells was relatively lower than on LNCaP cells, with  $IC_{50}$  values of  $41.5 \pm 2.4 \mu M$ ,  $36.7 \pm 1.6 \mu M$ , and  $35 \pm 2.0 \mu M$  for ABR, ABR-NP, and Apt-ABR-NP treatments, respectively.

Further analysis of the data revealed that the enhanced therapeutic potency of ABR-NP and Apt-ABR-NP was observed only on LNCaP cells, not on PC3 cells, due to their androgen insensitivity (Bouhajib and Tayab 2019; Mukherjee and Mayer 2008). The aptamer conjugation decreased the  $IC_{50}$  value by 51% in PSMA-positive LNCaP cells, indicating the significant role of PSMA binding and inhibition of androgen production in the cellular internalization and cellular function mediated through Apt-ABR-NP. Therefore, it was concluded that further *in vitro* studies were necessary to investigate the cytotoxic effects of these experimental nanoparticles on LNCaP cells.

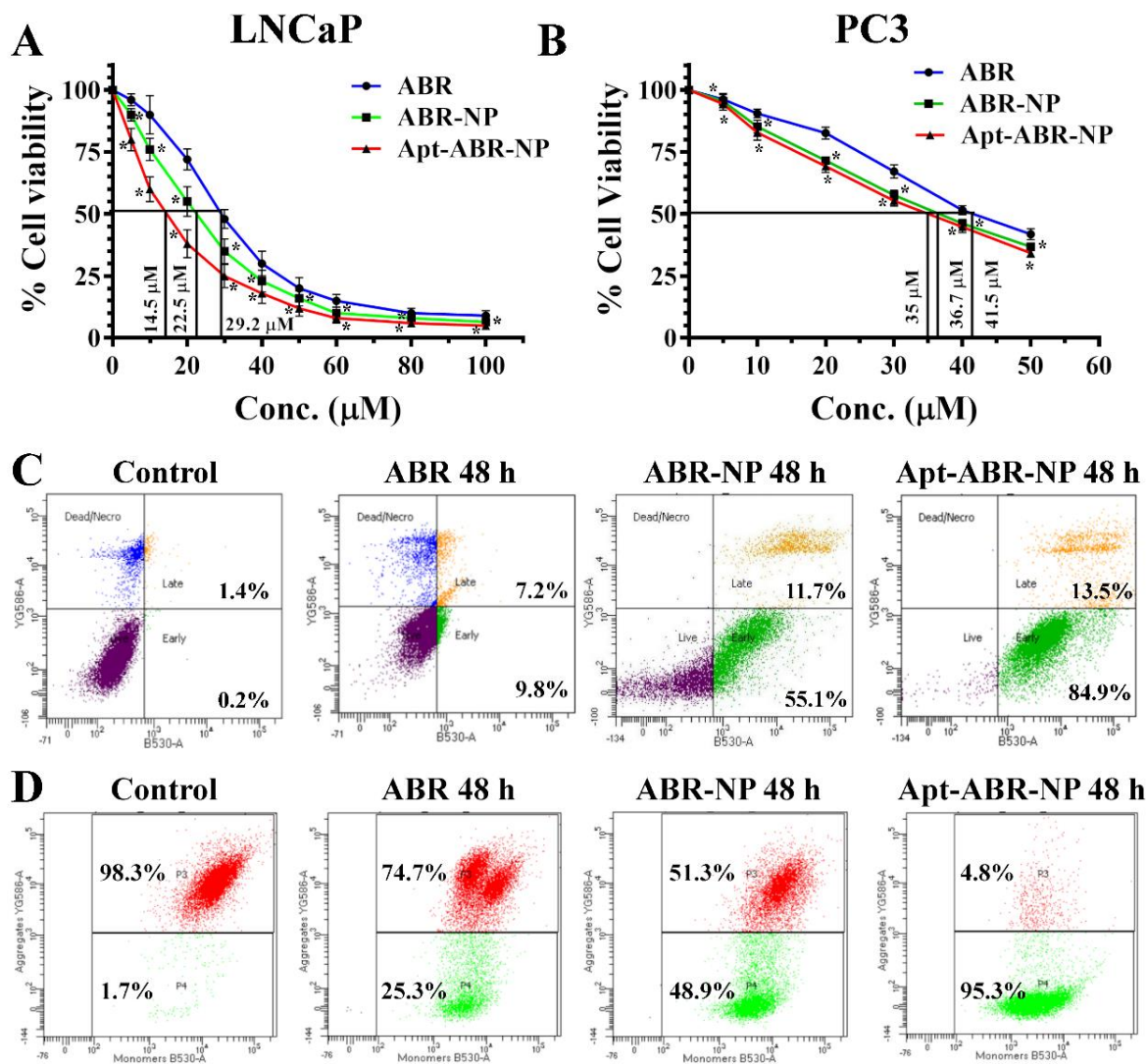


**Figure 6.17:** Cell cytotoxicity, apoptosis, and mitochondrial membrane depolarization assay of ABR, ABR-NP, and Apt-ABR-NP evaluated *in vitro*. (A) IC<sub>50</sub> values of ABR, ABR-NP, and Apt-ABR-NP on LNCaP and (B) PC3 cells after 48 h of treatment (Data show mean  $\pm$  SD, n=3). (C) Induction of apoptosis in LNCaP cells after treatment with ABR, ABR-NP, and Apt-ABR-NP for 48 h. (D) Mitochondrial membrane depolarization after 48 hours of treatment, with ABR, ABR-NP, and Apt-ABR-NP for 48 h.

### 6.15. Apoptosis assay

Apoptosis is a fundamental biological process that involves the programmed and controlled death of cells (Diepstraten et al., 2022). Most anticancer agents are designed to elicit an apoptosis-inducing response. To investigate the potential of ABR, ABR-NP, and Apt-ABR-NP in inducing apoptosis, the Annexin V-FITC/PI dual staining method was employed. The results

showed that Apt-ABR-NP exhibited a superior ability to induce apoptosis, indicating its potential as a chemotherapeutic formulation.

In 22Rv1 cells, the percentage of apoptotic cells after 48 hours of ABR treatment was 12%, with 8.7% early apoptosis and 3.3% late apoptosis. Treatment with ABR-NP increased the percentage of apoptotic cells to 43.8% (32.9% early apoptosis and 10.9% late apoptosis), whereas Apt-ABR-NP treatment resulted in 60.4% (45.2% early apoptosis and 15.2% late apoptosis) (Figure 6.18C).

Similarly, in LNCaP cells, ABR treatment for 48 hours elicited apoptosis in 17% of cells (9.8% early apoptosis and 7.2% late apoptosis). Treatment with ABR-NP increased the percentage of apoptotic cells to 66.8% (55.1% early apoptosis and 11.7% late apoptosis), whereas treatment with Apt-ABR-NP resulted in 98.4% (84.9% early apoptosis and 13.5% late apoptosis) (Figure 6.17C).

The results indicate that Apt-ABR-NP had the highest percentage of apoptotic cell death compared to ABR and ABR-NP after 48 hours of incubation in LNCaP cells. Therefore, Apt-ABR-NP exhibits a potential cytotoxic candidate against PSMA-positive prostate cancer LNCaP cells compared to ABR and ABR-NP.

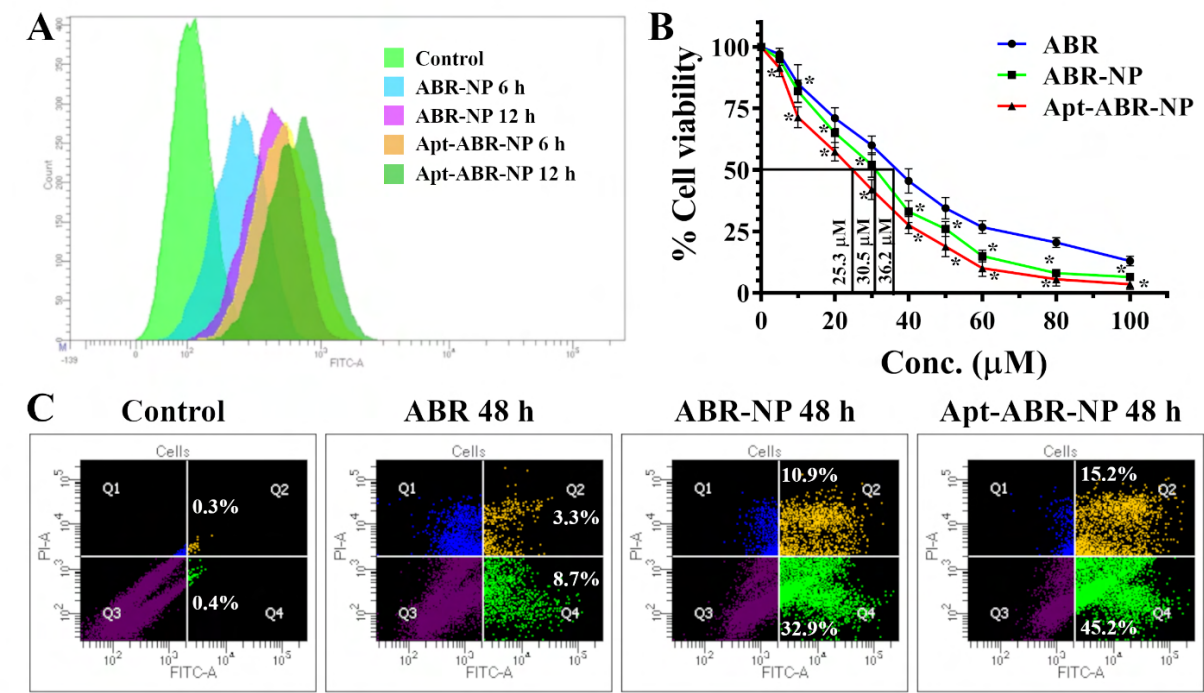


**Figure 6.18:** *In vitro* evaluation of cellular uptake, cytotoxicity, and apoptosis in 22Rv1 Cells (A) FACS histogram for cellular uptake measurement after the treatment with ABR-NP and

Apt-ABR-NP at 6 h and 12 h. (B) IC<sub>50</sub> values of ABR, ABR-NP, and Apt-ABR-NP on 22Rv1 cells and (C) Induction of apoptosis in 22Rv1 cells after treatment with ABR, ABR-NP, and Apt-ABR-NP for 48 h.

### 6.16. Mitochondrial membrane depolarization analysis using JC-1

Mitochondrial membrane depolarization is a hallmark feature of the apoptotic process, which can be quantified using JC-1 staining (Li et al. 2022). JC-1 is a highly sensitive marker that accumulates in the mitochondria in a potential-dependent manner. Under conditions of high mitochondrial membrane potential, JC-1 forms J-aggregates that emit red fluorescence, whereas, under conditions of low mitochondrial membrane potential, JC-1 remains a monomer that emits green fluorescence. The JC-1 ratio is a reliable indicator of mitochondrial health and activity based on the J-aggregates/monomers ratio. An increase in the JC-1 monomer: aggregate ratio (green: red fluorescence intensity) signifies an increase in loss of mitochondrial membrane potential and enhancement of apoptotic cell population.

In our experimental investigation, we observed that free ABR drug treatment led to a change in green fluorescence to 25.3% following 48 hours of treatment. In the case of ABR-NP, we found that the percentage of JC-1 monomer was 48.9% after treatment for 48 hours. Intriguingly, treatment of LNCaP cells with Apt-ABR-NP led to a further increase in the population of cells with depolarized mitochondria, as indicated by green fluorescence, to 95.3% after 48 hours of treatment (as depicted in Figure 6.17D). This finding suggests that Apt-ABR-NP is a more potent inducer of apoptosis in LNCaP cells compared to ABR and ABR-NP. This result is in line with the findings of the apoptosis assay.

### 6.17. *In vitro* colony formation assay

The present study aimed to evaluate the therapeutic efficacy of various approaches, including free drug (ABR), nanoparticulated forms (ABR-NP), and Apt-ABR-NP, on the growth of LNCaP cells. The results indicated that each approach was effective in inhibiting cellular growth, with the maximum efficacy observed in the case of Apt-ABR-NP (Figure 6.19A). The reduction in the number and size of colonies in this group was found to be the most significant. This can be attributed to the aptamer-PSMA binding mediated accumulation of Apt-ABR-NP in prostate cancer cells. To quantify the results, representative images of the wells after crystal violet staining of control and treatment groups were presented, along with the absorbance values of the individual wells taken at 590 nm (Figure 6.19B). The *in vitro* assays exhibited the highest anti-proliferative activity in the case of Apt-ABR-NP. The findings of this study



suggest that Apt-ABR-NP has the potential to be an effective therapeutic approach for prostate cancer treatment.

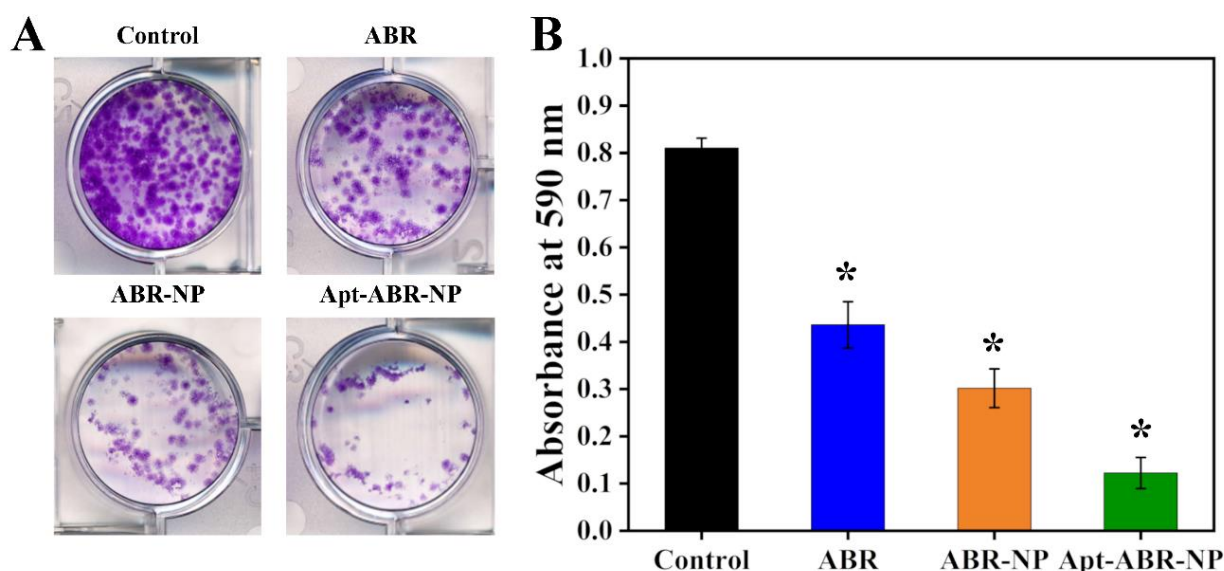


**Figure 6.19:** Clonogenic assay with LNCaP cells using ABR, ABR-NP, and Apt-ABR-NP for 14 days after treatment, changing the media and treatments in every three days. (A) More growth in untreated (control) was followed by ABR, ABR-NP, or Apt-ABR-NP treated LNCaP cells. (B) Absorbance values of untreated (control) and ABR, ABR-NP, or Apt-ABR-NP treated LNCaP cells, after crystal violet staining, represent the colonies' density. Values represent mean  $\pm$ SD (n=3), Where  $p < 0.05$  is the statistical level of significance, compared against the control value as assessed by Student's t-test.

### 6.18. Hemolysis study

The present study evaluated the hemocompatibility of the drug ABR and its nanoformulations ABR-NP and Apt-ABR-NP in concentrations ranging from 10 to 100  $\mu$ M. The results demonstrated that both ABR-NP and Apt-ABR-NP exhibited low hemolytic activity, with less than 5% compared to free ABR at varying concentrations (Figure 6.20). These findings suggest that both nanoformulations could be safely used for intravenous delivery, as they showed low hemolytic activity in the tested dose range. Hemocompatibility is a crucial factor to consider in the *in vivo* application of blood-contacting biomaterials (Krishnan et al., 2023). Based on the results of this study, it can be inferred that the nanoformulations exhibited an acceptable level of hemolysis and were safe for intravenous administration.



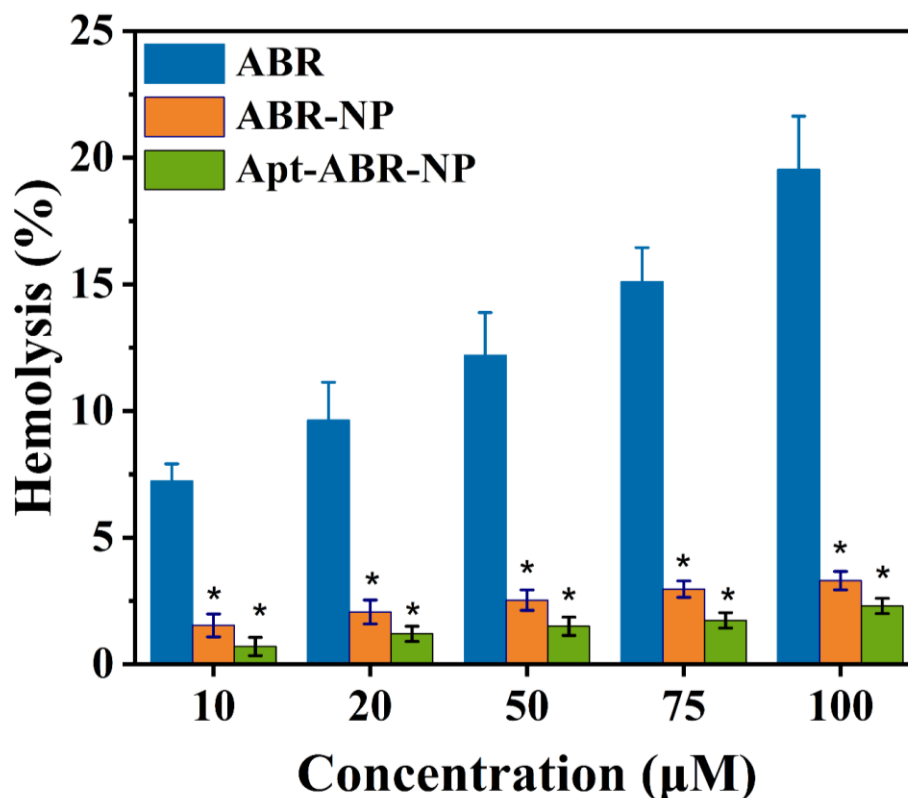


**Figure 6.20:** Hemolytic activity of developed nanoparticles. Hemolytic activity of ABR, ABR-NP, and Apt-ABR-NP was measured by incubating each sample for 1 hour at 37°C with red blood cells and measuring the amount of hemoglobin released. The percentage of hemolysis was plotted against the concentration of the samples. Data show mean  $\pm$ SD (n=3) where  $p < 0.05$  is the statistical level of significance as assessed by Dunnett's test (compared against control group)

### 6.19. Pharmacokinetics study

The *in vivo* pharmacokinetic profiles of abiraterone acetate (ABR), ABR-nanoparticles (NP), and Apt-ABR-NP were evaluated in Swiss Albino mice. The study measured pharmacokinetic parameters such as area under the curve (AUC), maximum concentration ( $C_{\max}$ ), time to reach maximum concentration ( $T_{\max}$ ), area under the first moment curve (AUMC), half-life ( $T_{1/2}$ ), mean residence time (MRT), volume of distribution ( $V_d$ ), and clearance (CL) following intraperitoneal injection of ABR, ABR-NP, and Apt-ABR-NP (Table 4). The results indicated that ABR rapidly converts into abiraterone (ART) when exposed to blood plasma, resulting in a high concentration of ART ( $C_{\max} = 25 \pm 2.5$  ng/ml) within a short time ( $T_{\max}$ , 2 h) (Figure 6.21). Conversely, ABR-NP and Apt-ABR-NP sustained a plasma concentration of ART for a longer period (approximately 24 h). In the case of ABR-NP and Apt-ABR-NP,  $C_{\max}$  was

reached around 9 h after injection, followed by a slow elimination phase, suggesting sustained release characteristics of the formulations. The AUC was increased by 2.2 times and 2.47 times in the case of ABR-NP and Apt-ABR-NP, respectively, compared to the free drug (ABR). The half-life of the active drug (ART) was also significantly increased by 3 times and 3.25 times for ABR-NP and Apt-ABR-NP, respectively. AUMC and MRT were also increased for both formulations compared to the free drug (ABR). These findings suggest that the bioavailability of the active drug is increased when delivered through nanoparticle formulations.

The nanoencapsulation of ABR resulted in maintaining a sustained plasma concentration of ART compared to free-drug treatment. The sustained drug release and predominantly slower elimination of the drug from the nanoparticle caused an enhanced plasma half-life of the drug. The overall observation suggests that Apt-ABR-NP had a better pharmacokinetic profile among the experimental formulations for ABR therapy. The conjugation of aptamer molecules on the surface of Apt-ABR-NP might have changed the aqueous microenvironment on the nanoparticle surface, which could have deterred drug release further, providing a more sustained drug release profile and improved the pharmacokinetic parameters for Apt-ABR-NP.

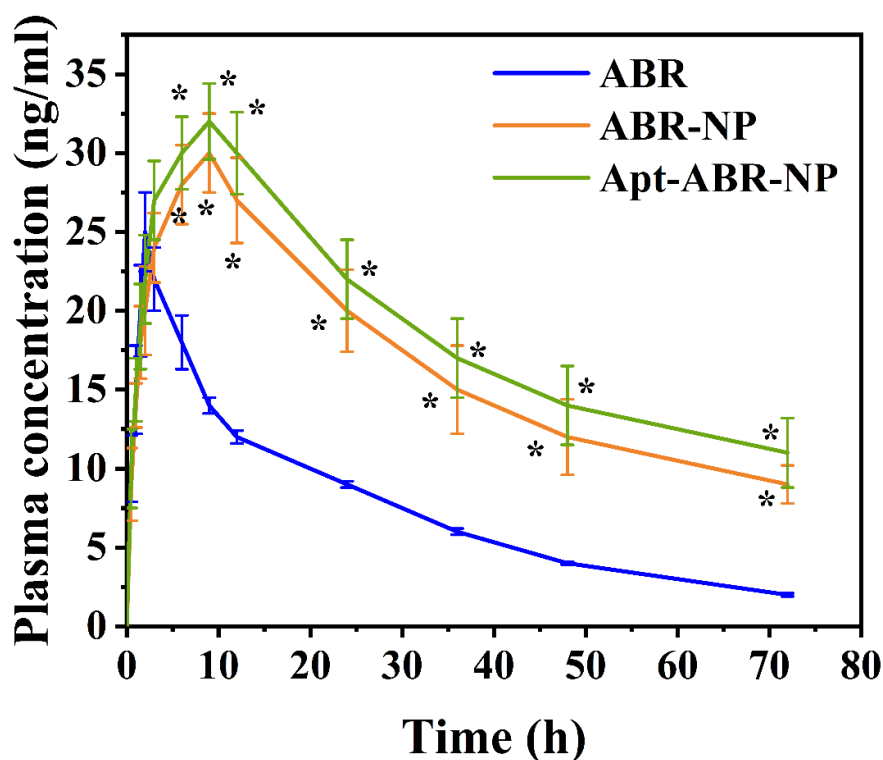


**Figure 6.21:** Pharmacokinetic profile of ABR, ABR-NP, and Apt-ABR-NP was assessed in mice by measuring the concentration of ABR from each sample in the bloodstream over time.

The data were plotted as the mean concentration of each sample at each time point. Error bars indicate standard deviation (n=3). \* marks represent significant values ( $p < 0.05$ ) when ABR-NP and Apt-ABR-NP were compared with ABR through the Two-Way ANOVA test, and the statistical significance of data was analyzed through Bonferroni's post-test

**Table 4:** Pharmacokinetic parameters of ABR, ABR-NP, and Apt-ABR-NP in Swiss Albino mice following intraperitoneal administration (400 $\mu$ g/kg).

Parameters	ABR	ABR-NP	Apt-ABR-NP
$C_{\max}$ (ng/ml)	$25 \pm 2.5$	$30 \pm 2.5^*$	$32 \pm 2.4^*$
$T_{\max}$ (h)	$2.0 \pm 0.2$	$9.0 \pm 0.4^*$	$9.0 \pm 0.5^*$
AUC last (ng.h/ml)	$547 \pm 27$	$1204 \pm 167^*$	$1356 \pm 175^*$
AUC 0- $\infty$ (ng.h/ml)	$582 \pm 30$	$1672 \pm 175^*$	$1975 \pm 194^*$
AUMC (ng.h <sup>2</sup> /ml)	$12345 \pm 416$	$34325 \pm 544^*$	$39603 \pm 622^*$
$T_{1/2}$ (h)	$12 \pm 0.4$	$36 \pm 1.7^*$	$39 \pm 2.2^*$
MRT (h)	$22.5 \pm 1.1$	$28.5 \pm 1.6^*$	$29.2 \pm 1.2^*$
$V_d$ (ml)	$316 \pm 10$	$430 \pm 12^*$	$415 \pm 20^*$
Clearance (ml/h)	$18.2 \pm 0.9$	$8.3 \pm 0.8^*$	$7.4 \pm 0.2^*$

Data show mean  $\pm$  SD (n=3). Statistical analysis was carried out to one-way ANOVA analysis, and the p-value was calculated through Tukey's post-test ( $p < 0.05$ ) when compared against ABR control. Statistics have been done. Data shown by star (\*) were significant compared to the ABR control group.

## 6.20. Biodistribution study and gamma scintigraphy imaging

The present study investigated the distribution of radiolabeled nanoparticles in different organs of Swiss Albino mice bearing prostate cancer. Table 5 summarizes the data, which shows that the nanoparticles remained in circulation for an extended period compared to the free drug ABR, which was eliminated rapidly. Moreover, the majority of the radiolabeled nanoparticles were eliminated via the urine, while accumulation in the liver, kidney, and intestine was also

observed. Notably,  $^{99m}\text{Tc}$ -Apt-ABR-NP accumulated significantly in the liver, consistent with the reticuloendothelial entrapment system (RES) of the liver (Yang et al. 2022).

**Table 5:** Biodistribution of  $^{99m}\text{Tc}$ -ABR-NP and  $^{99m}\text{Tc}$ -Apt-ABR-NP in testosterone/MNU-induced prostate cancer-bearing mice.

Organ/ Tissue	%ID of $^{99m}\text{Tc}$ -ABR-NP in CRPC mice			%ID of $^{99m}\text{Tc}$ -Apt-ABR-NP in CRPC mice		
	1 h	2 h	5 h	1 h	2 h	5 h
<b>Blood<sup>#</sup></b>	3.882±0.01	3.601±0.22	3.228±0.28	4.156±0.31	3.946±0.31	3.644±0.42
<b>Heart</b>	0.545±0.12	0.602±0.05	0.664±0.04	0.712±0.03	0.722±0.07	0.730±0.04
<b>Liver</b>	20.12±2.10*	24.55±2.00*	22.44±4.34*	23.60±2.55*	26.04±2.01*	30.58±1.80*
<b>Lungs</b>	0.563±0.21	0.578±0.23	0.606±0.32	0.688±0.20	0.894±0.20	1.142±0.33
<b>Stomach</b>	0.448±0.16	0.382±0.10	0.404±0.11	0.725±0.10	0.784±0.11	0.942±0.20
<b>Intestine</b>	2.762±0.51	2.920±0.31	3.752±0.30	3.114±0.12	3.205±0.55	4.025±0.62
<b>Kidney</b>	3.452±0.30	4.348±0.42	7.88±0.528*	4.565±0.45*	7.14±0.642*	10.24±0.47*
<b>Prostate</b>	1.642±0.21	1.811±0.16*	2.313±0.22*	2.256±0.30	2.622±0.24*	3.142±0.36*
<b>Urine</b>	26.56±3.89*	30.56±2.18*	32.44±2.14*	30.12±1.55*	33.56±2.51*	37.12±3.18*

<sup>#</sup>represents %ID/g in the case of blood, otherwise %ID in the whole organ. \* marks represent statistically significant values when both  $^{99m}\text{Tc}$ -ABR-NP and  $^{99m}\text{Tc}$ -Apt-ABR-NP were compared for different time points in two-way ANOVA analysis and tested by Bonferoni's post-test ( $p<0.05$ ).

Interestingly, the accumulation of Apt-ABR-NP in the prostate was significantly higher than  $^{99m}\text{Tc}$ -ABR-NP in a time-dependent manner, suggesting enhanced tumor uptake for aptamer-conjugated prostate cancer therapy. Moreover, gamma scintigraphy imaging revealed deposition of Apt-ABR-NP in the prostate region with the progress of post-injection time (Figure 6.22). However, distinguishing the prostate from the bladder was challenging in the scintigraphy images, although urine contained the most radioactivity. The biodistribution study corroborated the signals from other organs, such as the liver, kidney, lungs, and intestine.

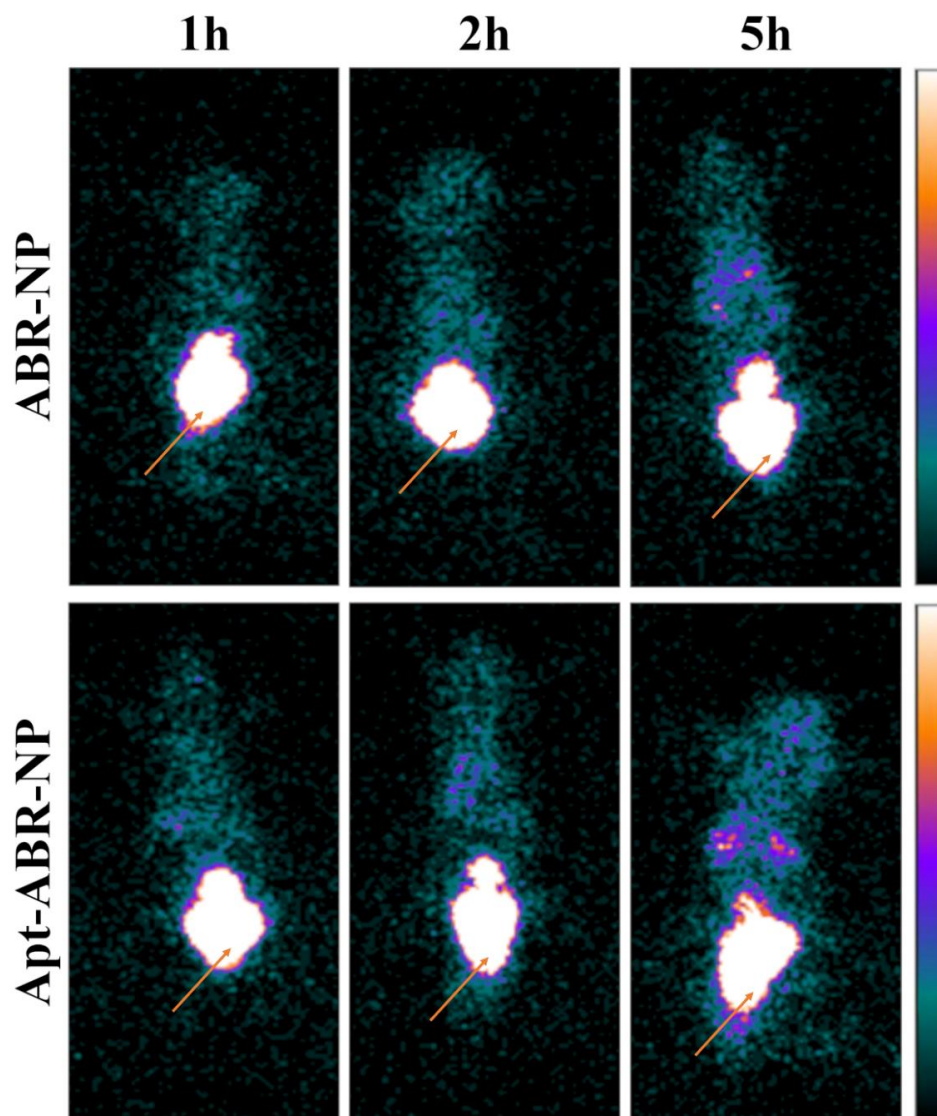


**Figure 6.22:** Biodistribution study of radiolabelled nanoparticles in various organs using gamma scintigraphic imaging. Radiolabelled nanoparticles ( $^{99m}\text{Tc}$ -ABR-NP and  $^{99m}\text{Tc}$ Apt-ABR-NP) were injected into mice via tail vein, and gamma scintigraphic images were acquired at different time points (1, 2, and 5 hours post-injection) using a gamma camera. Arrows indicate the prostate region in the mice.

The study employed radiolabeled PSMA-targeted Apt-ABR-NP to evaluate the localization of experimentally generated nanoparticles *in vivo*. The results showed that the nanoparticles were specific to prostate cancer, increasing the prostate and surrounding area in experimental mice with prostate cancer in a time-dependent manner, thus highlighting the target specificity of conjugated aptamer toward prostate cancer. These findings have significant implications for the development of nanoparticulated drug delivery systems for prostate cancer therapy (Hazra et al. 2021; Shah et al. 2021).

### 6.21. Antitumor activity study

The microscopic images of normal mouse prostate sections depict a glandular structure lined with cuboidal epithelial cells arranged in a discernible convoluted pattern. The lumen of the glands was also lined with cuboidal epithelial cells with small nuclei, while the stroma encompasses a thin fibromuscular matrix containing blood vessels and poorly defined smooth muscles. In the "carcinogen with testosterone"-treated prostate cancer group, the epithelial cells showed transformation into large columnar-like cells, leading to shrinkage of the lumen, increased scalloping of the lumen, and the creation of intraglandular vacuoles. Additionally, the thickness of the stroma increases, with fibromuscular striation formed in the stroma, signifying stromal atrophy. Furthermore, glandular hyperplasia and nuclear atypia were also observed in the prostates of the "Cancer" group.

According to the Gleason grading system, the cancers of the MNU with testosterone-treated prostates demonstrate pattern 3 carcinomas (recognizable glands with a small number of infiltrating invasive cells in the surrounding tissues) and pattern 4 carcinomas (recognizable, glomeruloid glands with a large number of invasive cells in the surrounding tissues forming neoplastic clumps). Therefore, they are considered to have either Gleason 7 or Gleason 8 score, representing a moderately differentiated to poorly differentiated carcinoma. Treatment with ABR and its formulations ameliorated the prostate's morphological atrophy caused by MNU and testosterone. The treatment improved the stromal fibromuscular structure but did not entirely restore the epithelial convolution pattern similar to the normal prostate. The Gleason grading system of the ABR-treated prostates showed pattern 2 carcinomas (loosely arranged oval-shaped glands with minimal invasion) and pattern 1 carcinoma (very similar to normal prostate tissues with closely packed glands), giving a Gleason score of 2 or 3. This indicates that treatment with ABR ameliorated the invasiveness of the cancer tissues and helped in the restoration of tissue architecture. Treatment with ABR-NP and Apt-ABR-NP further reduced stromal atrophy and restored the epithelial lining convolution comparable to the normal prostate. In ABR-NP and Apt-ABR-NP treated groups, prostate morphology was very similar to normal prostates, and Gleason scoring was not determinable. On the overall observation, Apt-ABR-NP performed much better in restoring overall morphological structure of carcinogen with testosterone-treated prostate carcinogenesis group than ABR and ABR-NP treated groups of animals (Figure 6.23).

Ki67 is a pivotal biomarker for quantifying cell proliferation and is widely acknowledged as an essential immunohistochemical biomarker for tumor prognosis (Berlin et al., 2017; Richardsen et al., 2017)). Despite the grading system in prostate cancer being predominantly based on tissue architecture, the Ki67 staining technique provides valuable information about the proliferation rate of cells, which has been shown to be a common practice in grading many other cancers. Ki67 staining is known to be significantly correlated with the clinical estimation of disease prognosis through needle biopsies, transurethral resections, and prostatectomy.

In our study, we employed Ki67 immunohistochemical staining of mouse prostates to investigate any prognostic correlation between the percentage of proliferating cells and disease stage, with or without the treatment of ABR and its formulations (Figure 6.23). We found that Ki67 staining of ‘Normal’ prostates showed  $\leq 3\%$  Ki67(+) cells and was considered negative. Prostates from N-nitroso-N-methyl urea and testosterone (MNU+testosterone) treated groups (Figure 10, the ‘Cancer’ groups) showed 30-50% Ki67(+) cells, counted in areas with 40 $\times$  magnifications and were considered cancerous with a Gleason score of 2+. In combination with Gleason scores 7 and 8, they represent moderate to poorly differentiated carcinomas with an intermediate proliferation rate.

Our research demonstrates that treatment with ABR, ABR-NP, and Apt-ABR-NP significantly reduced the population of Ki67(+) cells to  $15\pm 2\%$ ,  $10\pm 2\%$ , and  $5\pm 1.5\%$ , respectively (representative images were shown in Figure 10, panels ‘ABR’, ‘ABR-NP’, and ‘Apt-ABR-NP’). This represented a substantial decrease in the invasiveness of prostate tumors, and the effect was most pronounced in the case of Apt-ABR-NP. A combined analysis of morphological restoration, inhibition of stromal degeneration, and proliferation-inhibition suggests that Apt-ABR-NP could be a promising candidate for the treatment of hormone-resistant prostate adenocarcinoma. However, further studies are necessary to validate these findings.



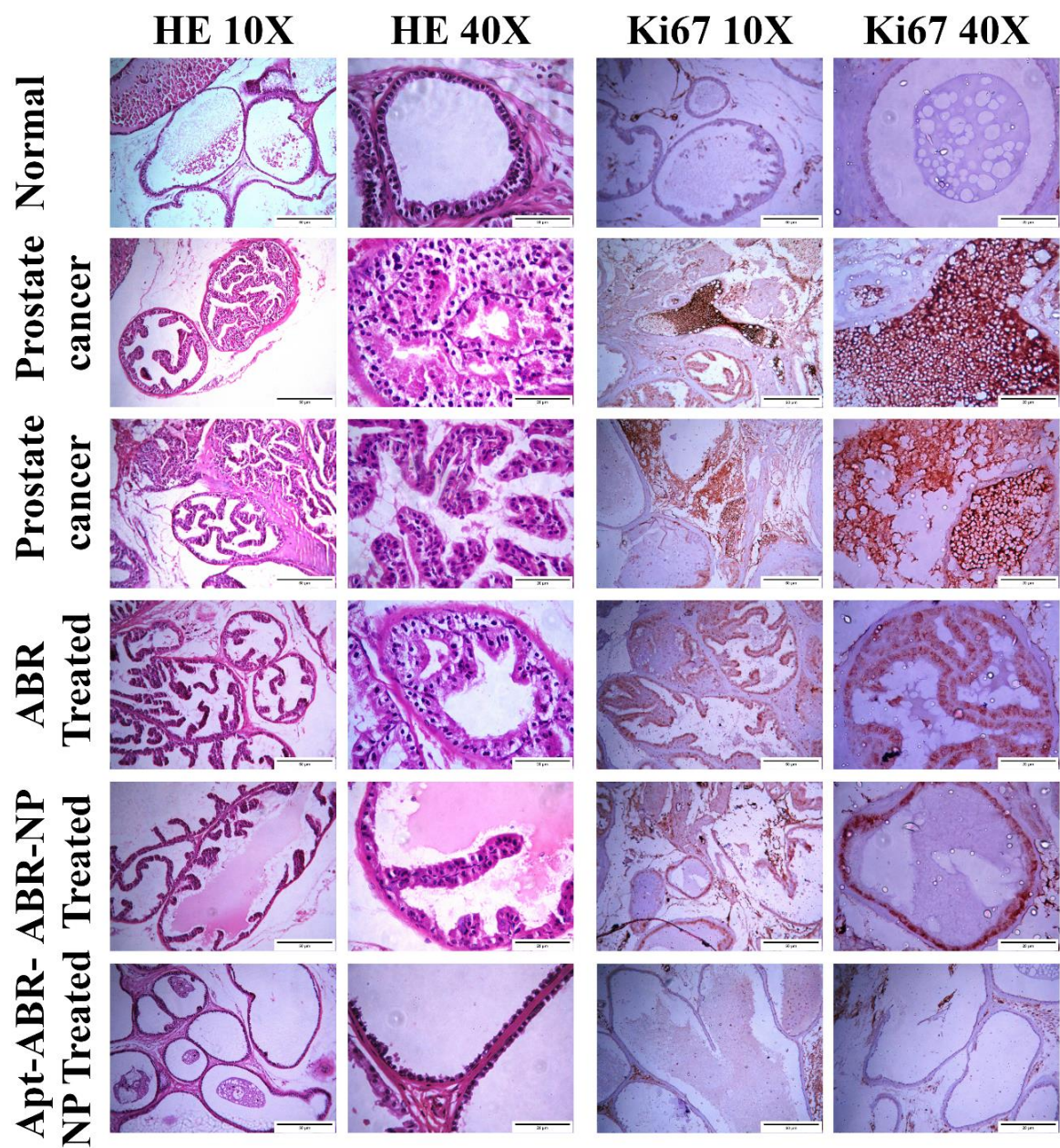


**Figure 6.23:** Anti-tumor efficacy of ABR, ABR-NP, and Apt-ABR-NP in prostate cancer (PCa) tissues. Histological examination of prostate cancer tissues and normal prostate tissues was performed using hematoxylin and eosin (HE) staining. Representative images of prostate cancer tissues and normal prostate tissues are shown. The expression of Ki67, a marker of cell proliferation, in prostate cancer tissues and in the normal prostate tissue sections was analyzed by immunohistochemistry. The staining/ immunohistochemistry and magnification of the photographs are mentioned above in each column.



## 6.22. Efficacy of Apt-ABR-NP on tumor spheroid model

To provide more comprehensive and conclusive evidence for the carcinogen-induced prostate cancer mouse model, an additional pharmacodynamic experiment was performed on an LNCaP 3D tumor spheroid model. The tumor spheroid is a three-dimensional model that precisely replicates the physicochemical environment of *in vivo* conditions (Adamiecki et al. 2022; Volpatti and Yetisen 2014).

In this experiment, the  $IC_{50}$  dose of the Cy5-loaded Apt-ABR-NP formulation was administered to two LNCaP tumor spheroids of approximately equal size. The formulation was applied once a day for three consecutive days. After 72 hours, the Apt-ABR-NP-treated spheroid showed a notable reduction of nearly 60% in size (Figure 6.24). Conversely, the cancer control spheroid (without treatment) demonstrated the expression of DAPI throughout the body, while the Apt-ABR-NP treated spheroid exhibited more peripheral DAPI expression. This suggests that there were fewer live proliferative cells in the treated spheroid compared to the cancer control spheroid. Thus, the experiment established the predominant role of Apt-ABR-NP in reducing LNCaP cell tumor.

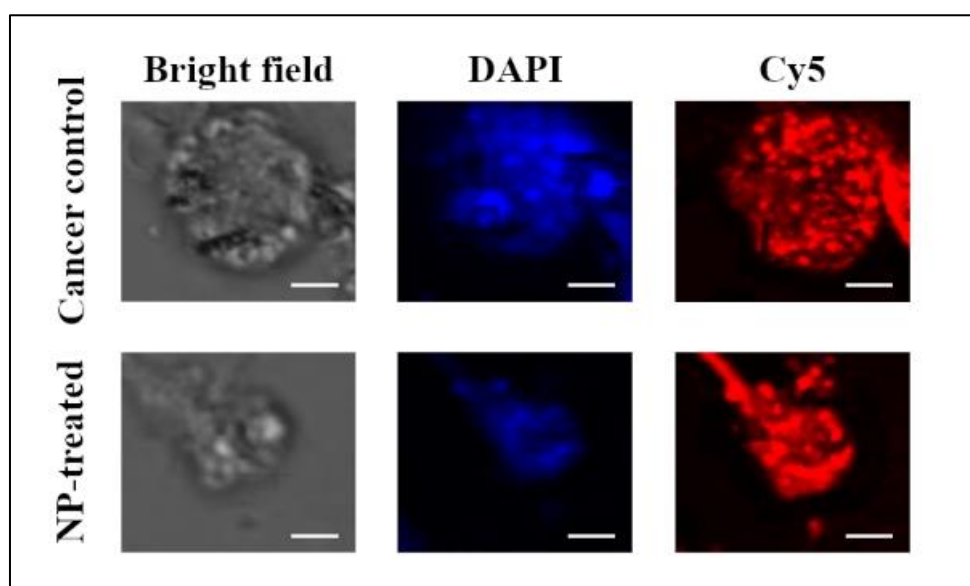


**Figure 6.24:** LNCaP tumor spheroid with or without the treatment of Apt-ABR-NP. Scale bars 100  $\mu$ m.

In summary, the results of this study demonstrate significant potential for the use of Cy5-loaded Apt-ABR-NP in treating prostate cancer. The 3D tumor spheroid model used in the experiment accurately reproduces the *in vivo* conditions and provides a more informative and conclusive

approach to investigate the effectiveness of the treatment. The findings of this study may significantly contribute to the development of new treatment strategies for prostate cancer.

### **6.23. Hematological evaluations**

The study aimed to investigate the effect of ABR, ABR-NP, and Apt-ABR-NP treatment on blood parameters, immunogenic response, and PSMA levels in normal and cancer-bearing animals (Table 6).

The results showed that the "cancer" control group (Group B) had a lower RBC count and a higher WBC count compared to normal animals, indicating a possible inflammatory response. Lower lymphocyte count and increased neutrophil count were also observed in cancer-bearing animals, which further suggested an enhanced inflammatory state. However, treatment with ABR, ABR-NP, and Apt-ABR-NP increased blood lymphocyte count and reduced neutrophil count in the "cancer" group, indicating a positive immunogenic response to treatment. Moreover, the "cancer" group exhibited a lower platelet count than the "normal (control)" group, which may be related to the inflammatory state. Nonetheless, no significant changes were observed in hematocrit volume and hemoglobin content after treatment with ABR, ABR-NP, and Apt-NP in normal mice. Overall, the treatment with ABR, ABR-NP, and Apt-ABR-NP reduced the inflammatory response element C-Reactive Protein (CRP), increased the immunogenic response, and subsequently tried to restore the Complete Blood Count (CBC) profile close to normal.

Additionally, when normal animals were treated with Apt-ABR-NP (Group F), no significant anomaly was observed in the CBC profile, indicating its biocompatible and non-hemotoxic nature. The PSMA analysis showed a high amount of PSMA in the blood of cancer-bearing animals compared to normal animals. However, treatment with ABR, ABR-NP, and Apt-ABR-NP significantly reduced PSMA content in the blood. Furthermore, the CRP data showed a higher level of CRP in cancer-bearing animals, indicating the development of inflammatory conditions. Nevertheless, treating with the experimental nanoparticles resulted in lowering CRP levels in the blood.

In conclusion, the results suggest that the treatment with ABR, ABR-NP, and Apt-ABR-NP reduced the inflammatory response element, increased the immunogenic response, and subsequently tried to restore the CBC profile close to normal. These findings may have significant implications for the development of novel therapeutic strategies for cancer treatment.

**Table 6:** CBC profile of experimental animals before and after treating with carcinogen/nanoparticle formulations.

Group	RBC ( $\times 10^6/\mu\text{l}$ )	Hemoglobin (g/dl)	Hematocrit (%)	WBC ( $\times 10^3/\mu\text{l}$ )	Lymphocytes ( $\times 10^3/\mu\text{l}$ )	Monocytes ( $\times 10^3/\mu\text{l}$ )	Neutrophils ( $\times 10^3/\mu\text{l}$ )	Eosinophils ( $\times 10^3/\mu\text{l}$ )	Platelets ( $\times 10^3/\mu\text{l}$ )	Prostatic Specific Antigen (PSA Total) ng/ml	C- reactive protein (CRP) mg/L
Group A (Normal animals)	9.5 $\pm$ 0.2	14.5 $\pm$ 0.2	45.5 $\pm$ 2.5	9.16 $\pm$ 0.46	8.45 $\pm$ 0.73	0.21 $\pm$ 0.03	1.67 $\pm$ 0.06	0.05 $\pm$ 0.01	1050 $\pm$ 70	5.2 $\pm$ 0.6	2.1 $\pm$ 0.1
Group B (Carcinogen- induced animals)	7.5 $\pm$ 0.8	10.8 $\pm$ 0.6	32.5 $\pm$ 0.5	11.6 $\pm$ 0.24	5.56 $\pm$ 0.42	0.15 $\pm$ 0.01	3.75 $\pm$ 0.02	0.09 $\pm$ 0.005	750 $\pm$ 40	25 $\pm$ 1.6	17 $\pm$ 0.60
Group C (Carcinogen- induced animal groups treated with ABR)	8.0 $\pm$ 0.4	12.3 $\pm$ 0.3	35.0 $\pm$ 3.5	10.3 $\pm$ 0.25	7.85 $\pm$ 0.61	0.18 $\pm$ 0.03	2.46 $\pm$ 0.04	0.08 $\pm$ 0.01	890 $\pm$ 50	15.1 $\pm$ 1.2	8 $\pm$ 0.8
Group D (Carcinogen- induced animal groups treated with ABR-NP)	8.2 $\pm$ 0.2	12.9 $\pm$ 0.3	39.5 $\pm$ 3.5	9.7 $\pm$ 0.15	8.15 $\pm$ 0.52	0.20 $\pm$ 0.05	2.07 $\pm$ 0.03	0.07 $\pm$ 0.005	930 $\pm$ 60	12.3 $\pm$ 0.9	5.9 $\pm$ 0.3
Group E (Carcinogen- induced animal groups treated with ABR-NP)	9.4 $\pm$ 0.4	13.4 $\pm$ 0.3	43.0 $\pm$ 1.5	9.30 $\pm$ 0.16	8.6 $\pm$ 0.23	0.22 $\pm$ 0.02	1.77 $\pm$ 0.02	0.05 $\pm$ 0.005	1020 $\pm$ 50	7 $\pm$ 0.5	3.2 $\pm$ 0.15
Group F (Normal animal treated with aptamer conjugated Apt- ABR-NP)	9.2 $\pm$ 0.3	14.2 $\pm$ 0.2	44.6 $\pm$ 1.5	9.36 $\pm$ 0.12	7.96 $\pm$ 0.44	0.21 $\pm$ 0.02	1.89 $\pm$ 0.09	0.03 $\pm$ 0.005	1040 $\pm$ 45	6.1 $\pm$ 0.6	2.6 $\pm$ 0.05

Data represented mean  $\pm$  SD (where n=6 in each group of animals). The table depicted respective hematological parameters such as RBC, Hemoglobin, Hematocrit, WBC, Lymphocytes, Monocytes, Neutrophils, Eosinophils, Platelets, Prostatic Specific Antigen and C-reactive protein (CRP) values in all the experimental carcinogenic animal groups treated with ABR (Gr C), ABR-NP (Gr D), aptamer conjugated nanoparticles (Apt-ABR-NP) (Gr E) & positive control (carcinogen-induced animals, Gr B), along with normal animals treated with normal saline (Gr A) and normal animal treated with aptamer conjugated Apt-ABR-NP (Gr F).

6.24. Estimation of serum-specific toxicity markers

The study aimed to investigate the efficacy of ABR, ABR-NP, and Apt-ABR-NP on hepatic and nephrotic toxicity in mice exposed to carcinogen. The levels of serum Aspartate transaminase (AST), Alanine transaminase (ALT), and Alkaline phosphatase (ALP) were utilized to assess the liver health of the mice (Dhara et al., 2023). The results of the study revealed that the carcinogen-exposed mice had significantly higher levels of these enzymes compared to normal mice. However, treatment with ABR, ABR-NP, and Apt-ABR-NP led to a variable reduction in enzyme levels, creatinine, and Blood urea nitrogen (BUN).

**Table 7:** Estimation of serum-specific markers of the experimental animals

Treatment groups	Metabolic profiles in experimental animals				
	AST (IU/L)	ALT (IU/L)	ALP (KA units)	Creatinine (mg/dl)	BUN (mg/dl)
Group A (Normal animals)	35± 1.67#	26± 1.43#	41± 2.19#	0.4± 0.05#	13.33±2.5#
Group B (Carcinogen-induced animals)	112± 1.39#	98± 2.24#	94± 1.33#	2.4± 0.2#	62.67±4.16#
Group C (Carcinogen-induced animal groups treated with ABR)	83± 1.51#	53± 2.29#	77± 1.73#	1.8± 0.25#	27±2.6#
Group D (Carcinogen-induced animal groups treated with ABR-NP)	69± 1.71#	47± 1.62#	54± 1.87#	0.9±0.12#	42±3#
Group E (Carcinogen-induced animal groups treated with Apt-ABR-NP)	46± 2.19#	35± 1.87#	43± 2.35#	0.6± 0.02#	33.67±2.51#
Group F (Normal animal treated with aptamer conjugated Apt-ABR-NP)	37± 1.32#	29± 1.53#	44± 1.74#	0.5±0.05#	17.3±2.08#

Note: Each value represents mean ± SD (n=3)

# Data represented mean  $\pm$  SD (where, n=6 in each group of animals). Table depicted respective AST, ALT, ALP, creatinine and BUN values in all the experimental carcinogenetic animal groups treated with ABR (Gr C), ABR-NP (Gr D), aptamer-conjugated nanoparticles (Apt-ABR-NP) (Gr E) & positive control (carcinogen-induced animals, Gr B), along with normal animals treated with normal saline (Gr A) and normal animal treated with aptamer-conjugated Apt-ABR-NP (Gr F).

The data analyses, using Table 7, showed that Gr E animals, which were treated with Apt-ABR-NP, exhibited the greatest improvement in enzyme levels and creatinine and BUN concentrations. Furthermore, there were no significant alterations in the serum AST, ALT, and ALP values of the normal mice treated with Apt-ABR-NP. Additionally, the creatinine and BUN levels in blood serum were similar in both normal and treated mice.

The results suggested that the treatment of ABR, ABR-NP, and Apt-ABR-NP effectively improved hepatic and nephrotic toxicity in mice exposed to carcinogen (Figure 6.25). The Apt-ABR-NP-treated mice exhibited the maximum improvement in enzyme levels and creatinine and BUN concentrations, bringing them closer to normal values. The data further indicated that Apt-ABR-NP did not cause any toxicity in the liver and kidneys of normal animals.

So, the findings of the present study suggest that Apt-ABR-NP could be a potential therapeutic agent for the treatment of hepatic and nephrotic toxicity in mice exposed to carcinogens. Further studies are warranted to investigate the safety and efficacy of Apt-ABR-NP in other animal models and humans.

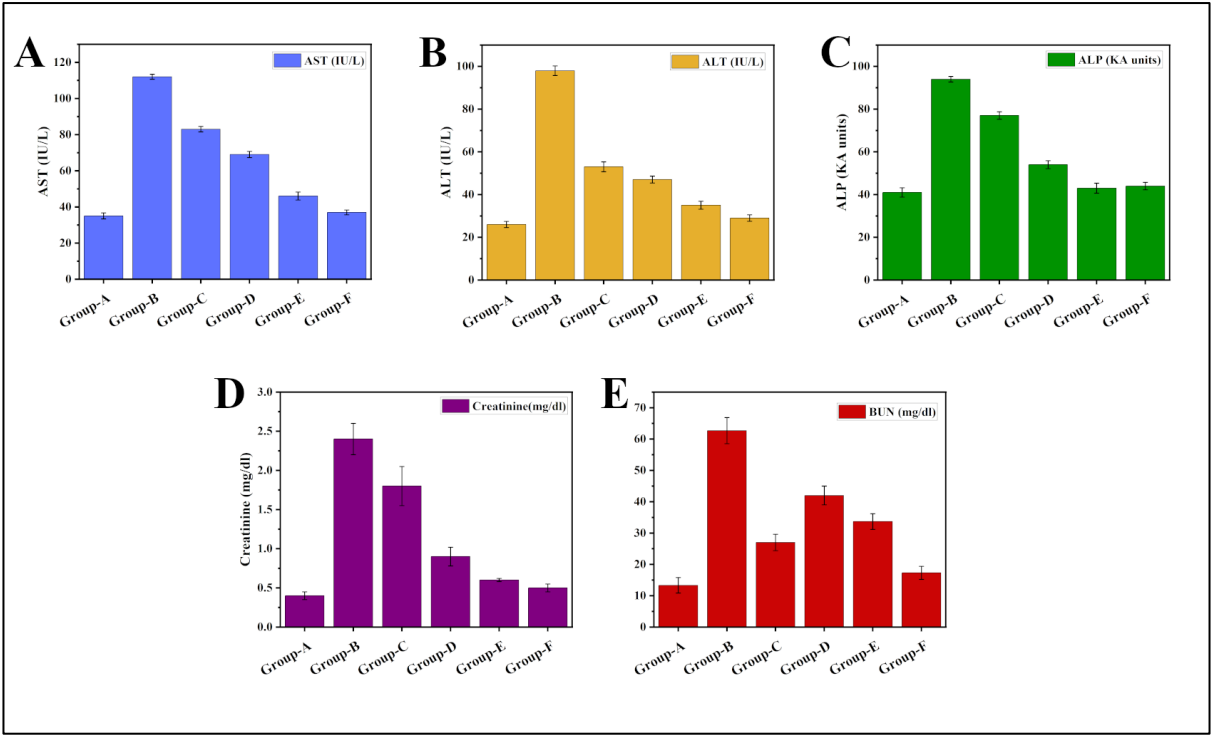


**Figure 6.25:** Estimation of serum-specific hepatic and nephrotic toxicity markers. (A) Aspartate transaminase (AST) enzyme levels of the various groups (B) Alanine transaminase (ALT) enzyme levels of the various groups (C) Alkaline phosphatase (ALP) enzyme levels of the various groups (D) Creatinine blood levels of the various groups, and (E) Blood Urea Nitrogen (BUN) levels of the various groups

## 6.25. References

- Adamiecki R, Hryniewicz-Jankowska A, Ortiz MA, Li X, Porter-Hansen BA, Nsouli I, et al (2022) In Vivo Models for Prostate Cancer Research. *Cancers (Basel)*14(21):1–27
- Berlin A, Castro-Mesta JF, Rodriguez-Romo L, Hernandez-Barajas D, González-Guerrero JF, Rodríguez-Fernández IA, et al (2017) Prognostic role of Ki-67 score in localized prostate cancer: A systematic review and meta-analysis *Urol. Oncol. Semin. Orig. Investig.* 35(8):499–506
- Bouhajib M, Tayab Z (2019) Evaluation of the Pharmacokinetics of Abiraterone Acetate and Abiraterone Following Single-Dose Administration of Abiraterone Acetate to Healthy Subjects *Clin Drug Investig*; 39(3):309–17
- Chadha R, Bhandari S. Drug–excipient compatibility screening—role of thermoanalytical and spectroscopic techniques. *Journal of pharmaceutical and biomedical analysis.* 2014 Jan 18;87:82-97.
- Champion JA, Katare YK, Mitragotri S (2007) Particle shape: a new design parameter for micro- and nanoscale drug delivery carriers. *J Control Release*; 121(1–2):3–9
- Chang M, Yang CS, Huang DM. Aptamer-conjugated DNA icosahedral nanoparticles as a carrier of doxorubicin for cancer therapy. *ACS nano.* 2011 Aug 23;5(8):6156-63.
- Choi W Il, Lee JH, Kim JY, Heo SU, Jeong YY, Kim YH, et al (2015) Targeted antitumor efficacy and imaging via multifunctional nano-carrier conjugated with anti-HER2 trastuzumab. *Nanomedicine Nanotechnology, Biol. Med.* 11(2):359–68
- Clogston JD, Patri AK. Zeta potential measurement (2011) *Methods Mol Biol* 697:63–70.
- De Giglio E, Ditaranto N, Sabbatini L. Polymer surface chemistry: characterization by XPS. *Polymer surface characterization.* 2014:73-112.
- Dhara M, Al Hoque A, Sen R, Dutta D, Mukherjee B, Paul B, et al (2023) Phosphorothioated amino-AS1411 aptamer functionalized stealth nanoliposome accelerates bio-therapeutic threshold of apigenin in neoplastic rat liver: a mechanistic approach *J. Nanobiotechnology.* 21(1)
- Diepstraten ST, Anderson MA, Czabotar PE, Lessene G, Strasser A, Kelly GL (2022) The manipulation of apoptosis for cancer therapy using BH3-mimetic drugs *Nat Rev*

Cancer 22(1):45–64

Dutta D, Chakraborty A, Mukherjee B, Gupta S (2018) Aptamer-Conjugated Apigenin Nanoparticles To Target Colorectal Carcinoma: A Promising Safe Alternative of Colorectal Cancer Chemotherapy. *ACS Appl Bio Mater* 1(5):1538–56

Dutta D, Paul B, Mukherjee B, Mondal L, Sen S, Chowdhury C, et al (2019) Nanoencapsulated betulinic acid analogue distinctively improves colorectal carcinoma in vitro and in vivo *Sci Rep* 9(1)

Ehsan I, Kumari L, Sen R, Al Hoque A, Mukherjee B, Mukherjee A, et al (2022) J591 functionalized paclitaxel-loaded PLGA nanoparticles successfully inhibited PSMA overexpressing LNCaP cells *J. Drug Deliv. Sci. Technol.* 75:103689

Estévez MC, Huang YF, Kang H, O'Donoghue MB, Bamrungsap S, Yan J, Chen X, Tan W. Nanoparticle–aptamer conjugates for cancer cell targeting and detection. *Cancer Nanotechnology: Methods and Protocols.* 2010:235–48.

Ghobeira R, Tabaei PS, Morent R, De Geyter N. Chemical characterization of plasma-activated polymeric surfaces via XPS analyses: A review. *Surfaces and Interfaces.* 2022 Jul 1;31:102087.

Hazra RS, Dutta D, Mamnoon B, Nair G, Knight A, Mallik S, et al (2021) Polymeric Composite Matrix with High Biobased Content as Pharmaceutically Relevant Molecular Encapsulation and Release Platform *ACS Appl Mater Interfaces* 13(34):40229–48

Jain GK, Pathan SA, Akhter S, Ahmad N, Jain N, Talegaonkar S, Khar RK, Ahmad FJ. Mechanistic study of hydrolytic erosion and drug release behaviour of PLGA nanoparticles: Influence of chitosan. *Polymer degradation and stability.* 2010 Dec 1;95(12):2360–6.

Krishnan V, Venkatasubbu GD, Kalaivani T, Krishnan V, Venkatasubbu GD, Kalaivani T (2023) Investigation of hemolysis and antibacterial analysis of curcumin-loaded mesoporous SiO<sub>2</sub> nanoparticles *Applied Nanoscience* 13(1):811–818

Li YJ, Fahrmann JF, Aftabizadeh M, Zhao Q, Tripathi SC, Zhang C, et al (2022) Fatty acid oxidation protects cancer cells from apoptosis by increasing mitochondrial membrane lipids *Cell Rep* 39(9)



- Liu J, Kopečková P, Bühler P, Wolf P, Pan H, Bauer H, et al (2009) Biorecognition and subcellular trafficking of HPMA copolymer-anti-PSMA antibody conjugates by prostate cancer cells. *Mol Pharm* 6(3):959–70.
- Mukherjee B, Mayer D (2008) Dihydrotestosterone interacts with EGFR/MAPK signalling and modulates EGFR levels in androgen receptor-positive LNCaP prostate cancer cells *Int J Oncol* 33(3):623–9
- Panyam J, Zhou W, Prabha S, Sahoo SK, Labhasetwar V (2002) Rapid endo- lysosomal escape of poly(DL- lactide- co glycolide) nanoparticles: implications for drug and gene delivery . *FASEB J.*;16(10):1217–26
- Pattnaik G, Sinha B, Mukherjee B, Ghosh S, Basak S, Mondal S, et al (2012) Submicron-size biodegradable polymer-based didanosine particles for treating HIV at early stage: an in vitro study *J Microencapsul* 29(7):666–76
- Ptacek J, Zhang D, Qiu L, Kruspe S, Motlova L, Kolenko P, Novakova Z, Shubham S, Havlinova B, Baranova P, Chen SJ. Structural basis of prostate-specific membrane antigen recognition by the A9g RNA aptamer. *Nucleic Acids Research*. 2020 Nov 4;48(19):11130-45.
- Richardsen E, Andersen S, Al-Saad S, Rakae M, Nordby Y, Pedersen MI, Ness N, Grindstad T, Movik I, Dønnem T, Bremnes R. Evaluation of the proliferation marker Ki-67 in a large prostatectomy cohort. *PloS one*. 2017 Nov 15;12(11):e0186852.
- Shah B, Khunt D, Misra M (2021) Comparative evaluation of intranasally delivered quetiapine loaded mucoadhesive microemulsion and polymeric nanoparticles for brain targeting: pharmacokinetic and gamma scintigraphy studies. *Futur J Pharm Sci* 7(1):1–12
- Shishparenok AN, Furman V V., Zhdanov DD (2023) DNA-Based Nanomaterials as Drug Delivery Platforms for Increasing the Effect of Drugs in Tumors. *Cancers (Basel).*;15(7):1–58
- Song Y, Cong Y, Wang B, Zhang N. Applications of Fourier transform infrared spectroscopy to pharmaceutical preparations. *Expert opinion on drug delivery*. 2020 Apr 2;17(4):551-71.
- Volpatti LR, Yetisen AK (2014) Commercialization of microfluidic devices. *Trends Biotechnol* 32(7):347–50

- Wan LY, Yuan WF, Ai WB, Ai YW, Wang JJ, Chu LY, et al (2019) An exploration of aptamer internalization mechanisms and their applications in drug delivery. 16(3):207–18
- Wang Y, Li P, Kong L (2013) Chitosan-modified PLGA nanoparticles with versatile surface for improved drug delivery AAPS PharmSciTech 14(2):585–92
- Yadav KS, Sawant KK (2010) Modified Nanoprecipitation Method for Preparation of Cytarabine-Loaded PLGA Nanoparticles AAPS PharmSciTech 11(3):1456
- Yallapu MM, Khan S, Maher DM, Ebeling MC, Sundram V, Chauhan N, et al (2014) Anti-cancer activity of curcumin loaded nanoparticles in prostate cancer. Biomaterials. 35(30):8635–48
- Yang S, Cai C, Wang H, Ma X, Shao A, Sheng J, Yu C. Drug delivery strategy in hepatocellular carcinoma therapy. Cell Communication and Signaling. 2022 Dec;20(1):1-4.
- Zolnik BS, Burgess DJ. Effect of acidic pH on PLGA microsphere degradation and release. Journal of Controlled Release. 2007 Oct 8;122(3):338-44.

## 7. Conclusion

Our investigation has shown that Apt-ABR-NPs, a PSMA specific DNA aptamer conjugated with ABR-NPs, has a strong potential to treat prostate cancer cells that overexpress PSMA. This is the first study where the use of this aptamer as a therapy for prostate cancer has been investigated. Apt-ABR-NPs exhibited superior internalization into cells. Abiraterone-loaded PLGA nanoparticles with an aptamer conjugation on the surface that ensured a prolonged drug release profile and successful targeted drug administration to PSMA overexpressed prostate cancer cells. Apt-ABR-NPs demonstrated accumulation specific to tumor tissue and extended blood retention. By using biocompatible, biodegradable, FDA-approved polymer and minimally immunogenic short nucleotide sequence aptamers, we were able to successfully deploy the potential targeted drug delivery *in vivo* and reduce its cytotoxicity to healthy tissues due to its preferential accumulation in PSMA overexpressed prostate cancer tissue instead of using any hazardous chemicals. This approach has the potential to reduce cytotoxicity to healthy tissues by preferentially targeting PSMA overexpressed prostate cancer tissue. The study's findings demonstrate that the aptamer-coupled nanoparticulated therapeutic technique is highly effective *in vitro* and *in vivo*, indicating its potential for successful human clinical trials as a targeted prostate cancer treatment.



## 8. Summary

Prostate cancer is a common type of cancer that develops in the prostate gland, a small, walnut-sized organ in males found directly below the bladder. It grows slowly and may not cause symptoms in the beginning. However, when it progresses, it can cause symptoms such as urinating trouble, frequent urination, blood in the urine or sperm, and pelvic or lower back pain. A digital rectal exam (DRE) and a prostate-specific antigen (PSA) blood test are frequently used to diagnose prostate cancer. Because of off-target adverse effects on healthy organs and the development of drug-resistance qualities after numerous doses of treatment regimen, conventional therapies like as radiation, chemotherapy, and hormone therapy cannot deliver a long-term satisfactory outcome.

Abiraterone, an active metabolite of abiraterone acetate, is a potent specific inhibitor of 17-hydroxylase/C17, 20-lyase (CYP17), a crucial enzyme in the production of testosterone and an inhibitor of androgen production in testicular, adrenal, and prostatic tumor tissues. The drug, BCS (Biopharmaceutics Classification System) class IV medication, is a current potential treatment option for prostate cancer. However, some inevitable limitations, such as poor solubility, permeability, and low biodistribution, make the drug difficult for its successful clinical use. To overcome the adverse side effects and minimize the disease burden, targeted nanocarrier-mediated therapy can deliver the drug to the organ of interest to manage prostate cancer more efficiently.

Numerous nanocarriers have become efficient tools for cancer research, revolutionizing therapeutic strategies. For instance, lipid-based nanocarriers called liposomes can encapsulate drugs and provide precise targeting and minimal adverse effects. Similar to this, polymer nanoparticles offer individualized delivery of drugs, increasing therapeutic effectiveness. Dendrimers provide controlled medication release because of their clearly defined structure. Gold nanoparticles' modified surfaces also allow for targeted therapy and imaging. In terms of cancer research, these nanocarriers have various benefits. They increase a drug's solubility, prolong its stay in circulation, and improve its stability. Additionally, various ligand conjugation makes them possible for site-specific drug delivery, reducing systemic toxicity. Nanocarriers' adaptable qualities make them essential for creating personalised cancer medicines, bringing in a new era of focused therapeutics with very little side effects.

In our investigation, we used nanoparticles (NP), which are gaining interest in anticancer drugs delivery. Nanoparticles can be used to deliver a broad range of anticancer medicines with poor

pharmacokinetic qualities. The site-specific delivery of drug molecules via ligand attachment to nanoparticles can sustainably maintain drug levels at an optimum therapeutic rate at the target organ. Poly(lactic-co-glycolic acid) (PLGA) is one of the most extensively used biodegradable polymers approved by the United States Food and Drug Administration (USFDA) for systemic use. Upon hydrolysis, the polymer breaks down into two monomers, lactic acid and glycolic acid. These two monomers are endogenous and swiftly metabolized by the body via the Krebs cycle; employing PLGA to deliver drugs or biomaterial applications with no considerable systemic toxicity.

One of the most promising treatment techniques for cancer cell targeting is targeting biomarkers overexpressed on the surface of cancer cells. Aptamers are synthetic single-stranded RNA or DNA oligonucleotides (typically 25-90 nucleotide bases) with the ability to fold into complex three-dimensional structures via intramolecular interactions, with target specificity, low immunogenicity, and high tissue penetration ability, making them superior to antibodies and other targeting molecules. Aptamers have been identified as interesting candidates for the development of a wide range of smart devices, including drug administration, treatment, diagnostics, and bio-imaging. In comparison to antibodies, aptamers have good stability in a wide pH range, temperatures, organic solvents, low cost, simple synthesis, sensitivity, and high affinity to binding pockets of diverse target antigens.

There are very few preclinical studies using an animal model of prostate cancer generated by carcinogens. In the immune-compromised prostate cancer animal xenograft model, such data are available. The prostate specific surface antigen (PSMA), which is overexpressed in chemically induced prostate cancer in mice, hasn't been the subject of any reports as of yet.

We developed  $\Delta$ PSap4#5 aptamer-conjugated abiraterone (ABR)-loaded PLGA nanoparticle (Apt-ABR-NP) and it was further characterized physicochemically. The conjugation was confirmed by agarose gel electrophoresis and X-ray photoelectron spectroscopy. In agarose gel electrophoresis study, the DNA aptamer moved through the gel and landed parallel to the conventional DNA ladder of the 50bp marker. The aptamer-coupled nanoparticles (Apt-ABR-NP), on the other hand, stayed inside the loading well, as evidenced by fluorescence. Interaction between the drug and the chosen excipients were analyzed by using Fourier-transform infrared (FTIR) spectroscopy. The FTIR study indicates no chemical interaction between the drug and the excipients used in this study. However, a few slight shifts in the peak were solely responsible for the physical interactions that might provide the structure of the formulation.

Further, the average nanoparticle size and zeta potential were measured using the Dynamic light scattering method. The average values of the hydrodynamic diameter of ABR-NP and Apt-ABR-NP were found to be 130.6 nm and 149.30 nm, respectively and zeta potential values for ABR-NP and Apt-ABR-NP were -10.1 mV and -18.5 mV, respectively. For the morphological analysis of the nanoparticles, FESEM, HR-TEM and AFM were used. FESEM images showed that nanoparticles were round in shape and had smooth surfaces with no apparent porosity or fractures. HR-TEM images showed a dark structure, indicating that the nanoformulation had a homogeneous drug distribution throughout the particles and the nanoparticles had a spherical structure with a smooth surface, as revealed by AFM images. Further drug loading and drug encapsulation efficiencies were measured using the experimental nanoparticles. Results suggest that ABR-NP and Apt-ABR-NP had drug loading 8.5% and 8.02%, respectively. The encapsulation efficiency of ABR-NP was  $93 \pm 3.30\%$  and the value was 88.2% in the case of Apt-ABR-NP. *In vitro* drug release was conducted in phosphate buffer saline (PBS) (pH 7.4), PBS with 1%  $\beta$ -hydroxycyclodextrin (pH 7.4), citrate buffer (pH 3), acetate buffer (pH 5), and bicarbonate buffer (pH 10). The cumulative percentage of drug release after the mentioned time period was found to be 73.12%, 81.45%, 92.76%, 92.45%, and 43.30%, respectively, in 672 h of study in the five different release media and  $R^2$  values suggest drug releases, according to Korsmeyer-Peppas, in all five release media mentioned earlier.

Among the cellular studies, the cytotoxic effects of ABR, ABR-NP, and Apt-ABR-NP on LNCaP, 22Rv1, and PC3 cells were analyzed using an MTT assay. Apt-ABR-NP had the highest cytotoxicity on LNCaP cells (lowest  $IC_{50}$  value  $14.5 \pm 1.2 \mu M$ ) followed by 22Rv1 ( $IC_{50}$  value  $25.3 \pm 1.1 \mu M$ ) compared to ABR and ABR-NP. The  $IC_{50}$  values on PC3 cells were found to be  $35 \pm 2.0 \mu M$  for Apt-ABR-NP treatment. Uptake of the nanoparticles in the LNCaP, 22Rv1, and PC3 cells were analyzed by confocal microscopy and quantitatively by flow cytometry (FACS) analysis. Flow cytometry analysis revealed a time-dependent gradual accumulation of Apt-ABR-NP in PC3, LNCaP and 22Rv1 cells. We further compared the cellular internalization of ABR-NP and Apt-ABR-NP nanoparticles at 12 h confocal microscopy for PC3 and LNCaP cells and the corresponding images reflected nanoparticles accumulation inside the cytoplasm of PC3 and LNCaP cells with the progression over time. Induction of apoptosis by ABR, ABR-NP, and Apt-ABR-NP was assessed in LNCaP cells following the Annexin V-FITC, propidium iodide (P.I.) dual staining method. The total apoptotic population in 22Rv1 cells after treatment with ABR for 48 h was 12%, ABR-NP treatment increased apoptosis to 43.8% and Apt-ABR-NP treatment showed the value 60.4%.

For LNCaP cells, the total apoptotic population after treatment with ABR for 48 h was 17%, which was increased up to 66.8% and 98.4% in the cases of ABR-NP and Apt-ABR-NP treatments, respectively

*In vivo* pharmacokinetic studies of ABR and its nanoformulations were conducted in Swiss albino mice; having an average body weight of 25 g. Data suggest an increased bioavailability of the active drug while delivered through nanoparticle formulations. *In vivo* biodistribution and gamma scintigraphy of ABR-NP and Apt-ABR-NP were studied in a Swiss albino prostate-cancer mice model using technetium-99m radiolabeled nanoparticles. Results suggest that nanoparticles remained in the blood for a longer time in blood circulation. In contrast, the free drug (ABR) was eliminated rapidly. The majority of the radiolabeled nanoparticles was eliminated through urine. In the case of gamma scintigraphy imaging, radiolabeled PSMA-targeted Apt-ABR-NP signaling was observed to increase the prostate and surrounding area in experimental mice with prostate cancer in a time-dependent manner, ensuring the target specificity of conjugated aptamer toward prostate cancer. Successful aptamer-prostate cancer antigen binding ability was tested by molecular docking.

A recently discovered aptamer conjugated with ABR-NPs (Apt-ABR-NPs) predominantly accumulated to PSMA overexpressed prostate cancer. Apt-ABR-NPs showed better cellular internalization. Abiraterone-loaded PLGA nanoparticles with aptamer conjugation on the surface which ensured successful targeted drug delivery to PSMA overexpressed prostate cancer cells, with a sustained drug release profile. Apt-ABR-NPs exhibited prolonged blood retention, and tumor tissue-specific accumulation. We avoided utilizing any hazardous chemicals and instead employed biocompatible, biodegradable FDA-approved polymer and negligibly immunogenic short nucleotide sequence aptamers to effectively deploy the possible targeted drug delivery *in vivo* that could lessen its cytotoxicity to healthy tissues by their preferential accumulation in PSMA overexpressed prostate cancer tissue. The findings presented the aptamer-coupled nanoparticulated therapeutic technique, demonstrating the maximum *in vitro* and *in vivo* therapeutic effectiveness of the experimental formulations. All our data support the translation of the promising aptamer functionalized nanoparticle toward achieving successful human clinical trials as a possible targeted treatment for prostate cancer. However more studies are required.



RESEARCH

Open Access



# PSap4-5 surface-functionalized abiraterone-loaded nanoparticle successfully inhibits carcinogen-induced prostate cancer in mice: a mechanistic investigation

Ashique Al Hoque<sup>1,2</sup>, Debasmita Dutta<sup>2,3,4,5</sup>, Brahamacharry Paul<sup>1</sup>, Leena Kumari<sup>1</sup>, Iman Ehsan<sup>1</sup>, Moumita Dhara<sup>1</sup>, Biswajit Mukherjee<sup>1\*</sup>, Mohiuddin Quadir<sup>2</sup>, Benny Abraham Jaiparettu<sup>3</sup>, Soumik Lahiri<sup>4</sup> and Shantanu Ganguly<sup>5</sup>

\*Correspondence: biswajit.mukherjee@jadavpuruniversity.in; biswajit55@yahoo.com

<sup>1</sup> Department of Pharmaceutical Technology, Jadavpur University, Kolkata 700032, India

<sup>2</sup> Department of Coatings and Polymeric Materials, North Dakota State University, Fargo, ND 58102, USA

<sup>3</sup> Department of Molecular and Human Genetics, Baylor College of Medicine, Houston, TX, USA

<sup>4</sup> Dana Farber Cancer Institute, Boston, MA, USA

<sup>5</sup> Harvard Medical School, Boston, MA, USA

<sup>6</sup> CSIR-Indian Institute of Chemical Biology, Kolkata 700032, India

<sup>7</sup> Regional Radiation Medicine Center, Thakurpukur Cancer Center, and Welfare Home Campus, Kolkata 700033, India

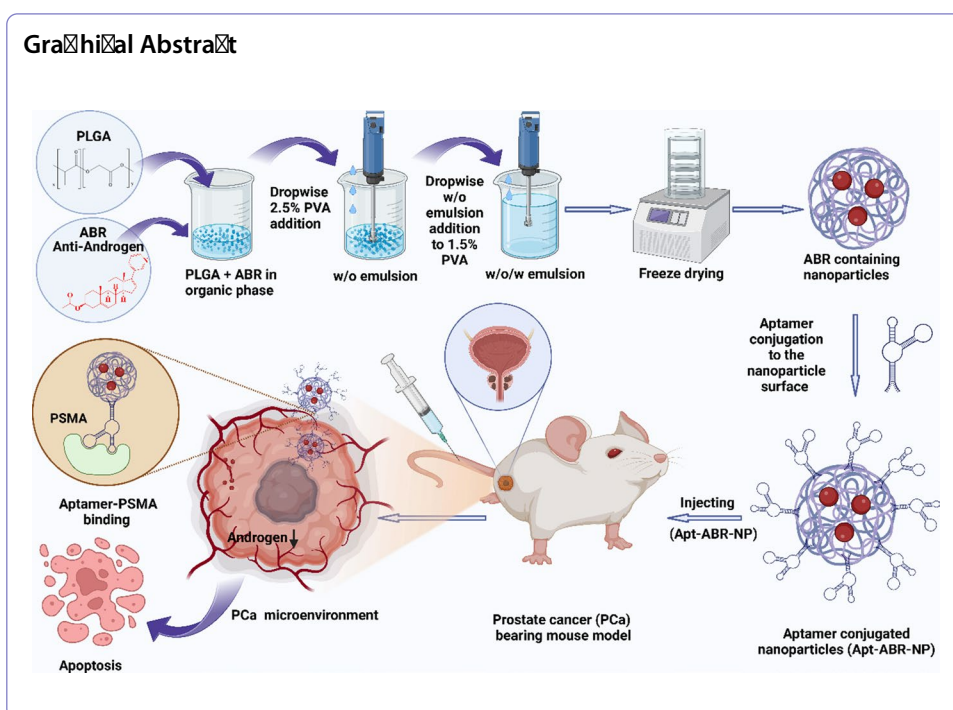
## Abstract

Prostate cancer (PCa) is one of the fatal illnesses among males globally. PCa-treatment does not include radiotherapy. Chemotherapy eventually causes drug resistance, disease recurrence, metastatic advancement, multi-organ failure, and death. Pre-clinical data on PCa-induced by carcinogens are truly scarce. Although some data on xenograft-PCa in animals are available, they mostly belonged to immuno-compromised animals. Here, we developed PSap4-5 aptamer surface-functionalized abiraterone-loaded biodegradable nanoparticle (Apt-ABR-NP) to investigate its targeting ability to prostate-specific membrane antigen (PSMA) in carcinogen-induced PCa mice and the therapeutic efficacy of the formulation. Aptamers are called synthetic monoclonal antibodies for their target specificity. However, they are devoid of the toxicity problem generally associated with the antibody. Abiraterone is a testosterone and androgen inhibitor, a new drug molecule that shows good therapeutic efficacy in PCa. The developed nanoparticles were physicochemically characterized and used for various in vitro and in vivo investigations. Nanoparticles had an average size of 140 nm with sustained drug release that followed Korsmeyer–Peppas kinetics. In vitro investigation showed that Apt-ABR-NP produced 44% apoptotic cells and 5.3% loss of mitochondrial membrane potential in LNCaP cells after 48 h of incubation. In vivo gamma scintigraphy, live imaging, and biodistribution studies in prostate cancer animal models showed the predominant targeting potential of Apt-ABR-NP. Histopathological investigation showed the remarkable therapeutic efficacy of the formulation. The pharmacokinetic study showed an increased biological half-life and enhanced blood residence time of Apt-ABR-NP. Apt-ABR-NP therapy can thus minimize off-target cytotoxicity, reduce drug loss due to site-specific delivery, and deliver abiraterone in a sustained manner to the organ of interest. Thus, the present study brings new hope for better therapeutic management of PCa in the near future.

**Keywords** Aptamer-mediated tumor targeting, Prostate-specific membrane antigen (PSMA), Abiraterone acetate, Prostate cancer therapy, Pharmacokinetics



© The Author(s) 2023. **Open Access** This article is licensed under a Creative Commons Attribution 4.0 International License, which permits use, sharing, adaptation, distribution and reproduction in any medium or format, as long as you give appropriate credit to the original author(s) and the source, provide a link to the Creative Commons licence, and indicate if changes were made. The images or other third party material in this article are included in the article's Creative Commons licence, unless indicated otherwise in a credit line to the material. If material is not included in the article's Creative Commons licence and your intended use is not permitted by statutory regulation or exceeds the permitted use, you will need to obtain permission directly from the copyright holder. To view a copy of this licence, visit <http://creativecommons.org/licenses/by/4.0/>. The Creative Commons Public Domain Dedication waiver (<http://creativecommons.org/publicdomain/zero/1.0/>) applies to the data made available in this article, unless otherwise stated in a credit line to the data.



## Introduction

Prostate cancer is the most often diagnosed cancer, having the second major cause of death from cancer after lung cancer in American men, and nearly 10 million deaths happened from the cancer only in 2020 (Sung et al. 2021). Conventional therapies such as radiation, chemotherapy, and hormone therapy cannot provide a long-term satisfactory outcome due to off-target side effects on the healthy organs and the development of drug-resistance properties after several doses of treatment regimen (Luo et al. 2019a).

Abiraterone, an active metabolite of abiraterone acetate, is a potent specific inhibitor of 17-hydroxylase/C17, 20-lyase (CYP17), a crucial enzyme in the production of testosterone and an inhibitor of androgen production in testicular, adrenal, and prostatic tumor tissues by inhibiting CYP17 (Bouhajib and Tayab 2019). The drug, BCS (Biopharmaceutics Classification System) class IV medication (Benoist et al. 2016) is a current potential treatment option for prostate cancer.

However, some inevitable limitations, such as poor solubility, permeability, and low biodistribution, make the drug difficult for its successful clinical use (Gala et al. 2020; Solymosi et al. 2018). To overcome the adverse effects and minimize the disease burden, targeted nanocarrier-mediated therapy can deliver the drug to the organ of interest to manage prostate cancer more efficiently (Fan et al. 2022).

Nanoparticle (NP) is gaining significant attraction in anticancer drug delivery (Correa et al. 2016; Ruoslahti et al. 2010). A wide range of anticancer drugs with poor pharmacokinetic properties can be delivered using nanoparticles. The site-specific delivery of drug molecules by ligand attachment to the nanoparticles can maintain drug level at an optimum therapeutic rate in a sustained manner at the target organ (Huang et al. 2021; Kabanov and Batrakova 2008; Petros and Desimone 2010; Torchilin 2007). Poly(lactic-co-glycolic acid) (PLGA) is one of the most widely used United States Food

and Drug Administration (FDA)-approved biodegradable polymers for systemic use. Upon its hydrolysis, it yields two monomers, lactic acid and glycolic acid (Pagels and Prud'Homme 2015). These two monomers are endogenous and rapidly metabolized by the body through the Krebs cycle; no systemic toxicity is involved in using PLGA to deliver drug or biomaterial applications (Danhier et al. 2012; Tong et al. 2012).

Targeting for antigens overexpressed on the surface of cancer cells is one of the most promising therapeutic strategies for targeting cancer cells. Among different types of targeting ligands, aptamers, the synthetic single-stranded RNA or DNA oligonucleotides (typically 25–90 nucleotide bases) with folding capacity into complex three-dimensional structures via intramolecular interactions, with target specificity, low immunogenicity, high tissue penetration ability makes them advantageous and exclusive over antibodies and other targeting molecules. Aptamers have been chosen as promising candidates for the construction of a variety of smart systems, including drug administration, treatment, diagnostics, and bioimaging (Alshaer et al. 2018; Hashemi et al. 2020; Zununi Vahed et al. 2019). Aptamers, in comparison to antibodies, have good stability in a broad pH range, temperatures, organic solvents, inexpensive, easy synthesis process, sensitivity, and great affinity to binding pockets of various target antigens (Tuerk and Gold 1990).

Preclinical data in a carcinogen-induced prostate cancer animal model are very scarce. Few such data are available in the immune-compromised prostate cancer animal xenograft model (Kato et al. 2021; Lawrence et al. 2015). However, there is no report so far available for aptamer-mediated drug targeting at the prostate-specific membrane antigen (PSMA) overexpressed in chemically induced prostate cancer in mice.

The present study was explored to investigate  $\Delta$ PSap4#5 aptamer-conjugated abiraterone (ABR)-loaded PLGA nanoparticle (Apt-ABR-NP) administered by the intraperitoneal route for site-specific drug delivery to prostate cancer and to evaluate the efficacy of the formulation to inhibit prostate cancer induced by a chemical carcinogen in mice. Based on the investigated data, an effort was made to establish the formulation-mediated prostate cancer inhibitory mechanism. Aptamer–prostate cancer antigen binding ability was tested by molecular docking.

## Experimental section

### Materials

Poly (D, L-lactic-co-glycolic acid) (PLGA) (75:25), fluorescein isothiocyanate (FITC), and 3-(4, 5-dimethylthiazol-2-yl)-2, 5-diphenyltetrazolium bromide (MTT dye) were procured from Sigma-Aldrich Co., St Louis, MO, USA. Abiraterone acetate was obtained from MSN laboratories, Hyderabad, Telangana, India, as a gift sample. *N*-Hydroxysuccinimide (NHS), and 1-(3-dimethylaminopropyl)-3-ethylcarbodiimide hydrochloride (EDC) were purchased from Himedia Laboratories (Mumbai, Maharashtra, India). Prostate carcinoma cells, LNCaP, and PC3 cells were procured from National Centre for Cell Science (NCCS), Pune, India. The human prostate cancer cell line, 22Rv1 was obtained from the American Type Culture Collection (ATCC, Rockville, MD, USA). Cells were maintained in Roswell Park Memorial Institute Medium (RPMI 1640) (Hi-Media, Mumbai, Maharashtra, India). 4',6'-Diamidino-2-phenylindole (DAPI) dye, fetal bovine serum (FBS), and other associated constituents for in vitro cell culture were obtained from Thermo Fisher Scientific, Waltham, USA. 5,5',6,6'-Tetrachloro-1,1',3,3'-tetraethyl

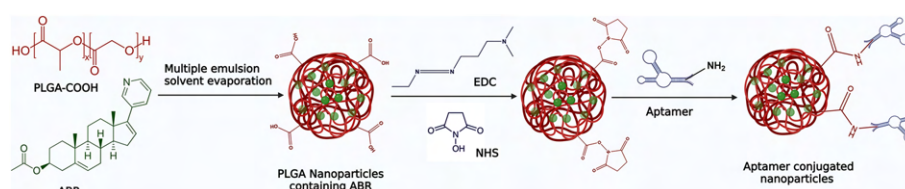


**Fig. 1** Schematic representation of aptamer conjugation process to the surface of the polymeric nanoparticles containing ABR

benzimidazolylcarbocyanine iodide (JC-1) (Invitrogen, Carlsbad, CA, USA) was procured. Polyvinyl alcohol (PVA, MW 125,000) was obtained from S.D. Fine-Chem. Ltd. (Mumbai, Maharashtra, India).  $\Delta$ PSap4#5 was synthesized by Eurofins Genomics India Pvt. Ltd., Bangalore, India. Testosterone propionate was purchased from Sisco Research Laboratories Pvt. Ltd. (Mumbai, India). All the chemicals were of analytical grade or molecular biology grade and used as received.

#### Selection of aptamer

$\Delta$ PSap4#5 (first reported by Savory et al. (2010)), A10-3.2 (first reported by Dassie et al. (2009)), A9g (first reported by Rockey et al. (2011)), and E3 (first reported by Gray et al. (2018)) are some of the widely studied aptamers used as a PSMA targeting moiety. The DNA aptamer  $\Delta$ PSap4#5 (sequence: 5'-TTT TTA ATT AAA GCT CGC CAT CAA ATA GCT TT-3') has a lower  $K_d$  value (2.6 nM) ( $K_d$  denotes the dissociation constant. The stronger is the affinity between molecules, the lower is the  $K_d$  value). Thus,  $\Delta$ PSap4#5 aptamer that essentially attaches to another molecule with a low  $K_d$  strengthens the binding, and it is very much sensitive to PSMA (detection level in the picogram range) (Heydari-Bafrooei and Shamszadeh 2017; Savory et al. 2010; Souada et al. 2015; Tzouvadaki et al. 2016).

The shorter chain length also makes it easier to synthesize. The success of PSMA- $\Delta$ PSap4#5 aptamer in vitro has been reported (Heydari-Bafrooei and Shamszadeh 2017; Souada et al. 2015; Tzouvadaki et al. 2016). Hence, we have selected  $\Delta$ PSap4#5 aptamer (Apt) to target PSMA with the help of  $\Delta$ PSap4#5 aptamer conjugated nanosized drug delivery system.

#### Characterization of the ABR containing PLGA nanoparticles (ABR-NP)

##### Conjugation of aptamer on the surface of nanoparticles

ABR-NP was conjugated with the 3'-amino and phosphorothioate-modified aptamer through the EDC/NHS coupling method (Chakraborty et al. 2020a). Figure 1 depicts the process of conjugating aptamers onto the surface of polymeric nanoparticles containing ABR (for detailed protocol, please refer to Additional file 1).

##### Drug–excipient interaction study

Interaction between the drug and the chosen excipients was analyzed by using Fourier transform infrared (FTIR) spectroscopy using blank nanoparticle (nanoparticle devoid of any drug), drug (ABR), PLGA, ABR-loaded PLGA nanoparticle, and a physical mixture of drug and the excipients. In each case, the substance was mixed with I.R. grade

KBr at a 1:100 ratio and punched into pellets. They were then scanned over a range of 4000–600  $\text{cm}^{-1}$  using an FTIR instrument (Bruker FTIR, Tensor-II, Bruker Optic GmbH, Karlsruhe, Germany).

#### ***Preparation of PLGA nanoparticles containing ABR***

ABR-loaded PLGA nanoparticles and blank nanoparticles (without ABR) were prepared utilizing the multiple emulsion solvent evaporation technique according to the previously reported procedure (Chakraborty et al. 2020b). FITC-loaded and other dyes, such as Cy5 loaded nanoparticles, were made by mixing 100  $\mu\text{l}$  each of a 0.4% (w/v) ethanolic dye solution into the first organic phase during the emulsion development. The detailed method of developing the nanoparticles is described in Additional file 1.

#### ***Determination of particle size and zeta potential***

The average nanoparticle size and zeta potential were measured using the dynamic light scattering method. Approximately, 2 mg of ABR-NP/Apt-ABR-NP was weighed and well-dispersed in Milli-Q water (Millipore Corp., MA, USA) by sonication for 30 min in a bath sonicator (Trans-o-sonic, Mumbai, India). Finally, the particle size and zeta potential were analyzed in Malvern Zetasizer Nano-ZS 90 (Malvern Instruments, Malvern, U.K.).

#### ***Determination of surface morphology by field emission scanning electron microscopy (FESEM), atomic force microscopy (AFM), and high-resolution transmission electron microscopy (HR-TEM)***

Lyophilized nanoparticles were studied with field emission scanning electron microscopy (FESEM). ABR-NP and Apt-ABR-NP were placed on a carbon stub and then coated with a thin layer of gold and scanned using FESEM. The particle morphology of hydrated nanoparticles was analyzed by AFM from 5 mg/ml of Apt-ABR-NP dispersion in Milli-Q water. The nanoparticles were then passed through 0.22-micron filters to remove any pre-existing big aggregates. Approximately 5  $\mu\text{l}$  of this filtered dispersion was put on a cleaved mica sheet and air-dried for 20 min at room temperature. When the water was evaporated, a thin transparent layer formed on a mica sheet, which was seen using an AFM (5500 Agilent Technologies, Santa Clara, CA, USA) in tapping mode. The high-resolution transmission electron microscope (HR-TEM) was used to investigate internal morphology of the nanoparticles and drug distribution. On a standard carbon-coated copper grid (300 mesh), the nanoparticle suspension in Milli-Q water was dropped and allowed to air dry for 5–6 h. Image analysis was done using a high-resolution transmission electron microscope (JEOL JEM 2100 HR, Tokyo, Japan).

#### ***X-ray photoelectron spectroscopy (XPS)***

The elemental composition of nanoparticles was investigated using X-ray photoelectron spectroscopy (XPS) (Luo et al. 2019b). The nanoparticle samples (ABR-NP and Apt-ABR-NP) were suspended in double distilled water, placed on a clean silicon substrate, and vacuum-dried before being examined in a Kratos Axis X-ray photoelectron spectrometer (Shimadzu, Japan) equipped with a monochromatic Al K Alpha source. The

studies employed a passage of energy of 200 eV. Spectral Data Processor v4.3 software was used to compute the elemental composition and conduct curve fitting.

#### ***Percentage of drug loading and encapsulation efficiency***

Drug loading and drug encapsulation efficiencies were measured as reported earlier (Kumari et al. 2023) (for detailed method, please refer to Additional file 1):

$$\text{Theoretical drug loading (\%)} = \frac{\text{Amount of drug}}{\text{Amount of drug} + \text{excipients}} \times 100,$$

$$\text{Drug loading (actual) \%} = \frac{\text{Amount of drug in nanoparticles}}{\text{Amount of nanoparticles obtained}} \times 100,$$

$$\text{Entrapment efficiency (\%)} = \frac{\text{Drug loading (actual) (\%)}}{\text{Amount of drug loading (theoretical) (\%)}} \times 100.$$

#### ***Stability of the nanoparticles***

The stability of the nanoparticles was investigated following the ICH guidelines, as reported earlier (Kumari et al. 2023) (For detailed method, refer to Additional file 1).

#### ***Hydrolytic stability study***

Hydrolytic degradation of the formulation was studied in buffers of different pH (Ehsan et al. 2022). The detailed protocol has been mentioned in Additional file 1.

#### ***In vitro drug release study***

In vitro drug release was conducted in phosphate buffer saline (PBS) (pH 7.4), PBS with 1%  $\beta$ -hydroxy cyclodextrin (pH 7.4), citrate buffer (pH 3), acetate buffer (pH 5), and bicarbonate buffer (pH 10) as per the reports published earlier (Kumari et al. 2023) (detailed method is available in Additional file 1).

#### ***Cellular studies***

##### ***In vitro cellular uptake analysis by flow cytometry (FACS) and confocal microscopy***

For quantitative analysis using FACS, the nanoparticles (ABR-NP and Apt-ABR-NP) were loaded with tetramethylindo(di)-carbocyanine (Cy5) to measure their comparative cellular uptake in LNCaP, 22Rv1, and PC3 cells. Briefly, LNCaP and PC3 cells were seeded in 60-mm cell culture dishes at a density of  $1.5 \times 10^6$  per plate and incubated overnight in a humidified incubator at 37 °C under a 5% CO<sub>2</sub> environment (Wang et al. 2013). On the next day, the media were removed, Cy5 containing formulations (ABR-NP/Apt-ABR-NP) were added to the plates (except one, the 'control' group where the cells received no treatment) and incubated for different time periods (6 h and 12 h). After that, the treatment solutions were removed, and the cells were washed with PBS (pH 7.4) and redispersed in PBS (pH 7.4) in light-protected tubes. The cells were then



analyzed in a flow cytometer (BD LSR Fortessa, B.D. Biosciences) using the filter of Cy5 (excitation/emission 651 nm/670 nm).

We performed confocal laser microscopy to interpret Cy5-loaded Apt-ABR-NP uptake in LNCaP and PC3 cells (Fan et al. 2015). The study has not been performed for 22Rv1 cells. Briefly,  $1.0 \times 10^4$  PC3 and LNCaP cells were seeded separately on different coverslips, and the coverslips were placed inside a 35-mm cell culture dish with adequate media (1 ml). The cells were incubated overnight at 37 °C and then treated with the Cy5-loaded Apt-ABR-NP for 6 h and 12 h. After treatment, the cells were washed with PBS, fixed using 70% ethanol, counter-stained with DAPI, and mounted on a slide using Prolong Diamond anti-fade-mount. The slides were then scanned under a confocal laser microscope (ZEISS LSM 900, Carl Zeiss, Oberkochen, Germany). The observation was conducted simultaneously using dual filters, Cy5 (excitation/emission 651 nm/670 nm) and DAPI (excitation/emission 359 nm/461 nm). Images were collected from individual channels and merged using ImageJ or ZEN 2012 SP2 software (ZEISS, Germany).

#### ***In vitro cell cytotoxicity assay***

We studied the effect of free drug, ABR-NP and Apt-ABR-NP nanoparticles on prostate-specific membrane antigen (PSMA) overexpressing and androgen receptor (AR) positive LNCaP and 22Rv1 prostate cancer cell lines, and PC3 cells which are AR and PSMA negative. The cytotoxic effects of ABR, ABR-NP, and Apt-ABR-NP on 22Rv1, LNCaP and PC3 cells were analyzed using an MTT assay following the methods described earlier (Ehsan et al. 2022; Paul et al. 2019) (for the detailed method, see Additional file 1).

#### ***Apoptosis assay***

Induction of apoptosis by ABR, ABR-NP, and Apt-ABR-NP was assessed in 22Rv1 and LNCaP cells following the Annexin V-FITC, propidium iodide (PI) dual staining method (Dutta et al. 2018; Hazra et al. 2021). Briefly,  $1.5 \times 10^6$  LNCaP cells were plated in 60-mm dishes and incubated overnight in a humidified incubator with RPMI 1640 media. The media were removed on the next day, and the cells were treated with ABR, ABR-NP, and Apt-ABR-NP at their respective  $IC_{50}$  concentrations in the incomplete medium (without the serum) for 48 h. Two control sets were maintained in parallel for each time point with media alone to provide the unstained and control group (PI alone). After the treatment, the media were removed, the cells were collected through trypsinization, counted to  $10^5$  in 100  $\mu$ l binding buffer, and incubated with annexin V-FITC (5  $\mu$ l) for 15 min in a dark condition. Finally, the cells were diluted to 500  $\mu$ l, and 5  $\mu$ l of propidium iodide was added to each tube except for the unstained group. The cells were then analyzed in a FACS instrument (BD Accuri C6, BD Bioscience, San Diego, CA) using the channels of FITC (B530-A) and propidium iodide (YG586-A). The data were plotted in a four-quadrant plot to differentiate live, early apoptotic, late apoptotic, and necrotic cells. The aptamer-conjugated nanoparticle (Apt-ABR-NP) showed the most cytotoxicity, maximum cellular uptake and maximum apoptosis induction in LNCaP cells among the experimental nanoparticles. Hence, we investigated this formulation for subsequent studies in LNCaP cells only.

#### ***Mitochondrial membrane depolarization analysis using JC-1***

Mitochondrial membrane depolarization is a hallmark of apoptosis. At the initial stage of apoptosis, the mitochondrial membrane becomes depolarized (more positive), which results in a change in trans-mitochondrial membrane potential difference. This change in potential difference can be measured using a cationic dye JC-1 (5,5',6,6'-tetrachloro-1,1',3,3'-tetraethylbenzimidazolyl-carbocyanine iodide). In normal mitochondria (high membrane potential), JC-1 accumulates and forms J-aggregates that emit red fluorescence (~590 nm). When the mitochondrial membrane becomes depolarized (low potential), the JC-1 dye accumulates less in mitochondria, and mitochondria predominantly remain in the cytosol in a monomeric form, emitting green fluorescence (~529 nm). Hence, mitochondrial membrane depolarization can be measured using JC-1 dye by measuring an increase in green fluorescence or the green/red fluorescence intensity ratio. Standard protocol was followed for measuring fluorescence emission after JC-1 staining. Briefly,  $1 \times 10^6$  LNCaP cells were seeded in 60-mm dishes, incubated overnight in a humidified incubator, and then treated with ABR, ABR-NP, and Apt-ABR-NP for 48 h. After that, the cells were removed from the dishes and incubated with 10  $\mu$ l of 200  $\mu$ M JC-1 in 1 ml complete media for 10 min at 37 °C in dark conditions. The media were removed by centrifugation, precipitating the cells. The cells were resuspended in PBS, pH 7.4, and were analyzed in a FACS instrument.

#### ***Clonogenic assay for the prostate cancer cell line***

The in vitro cell colony formation assay was performed by determining the ability of a single cell to develop a colony after the treatment with free drug and the experimental formulations and compared with the untreated control group. LNCaP cells were seeded in 12-well plates (750 cells/well) and incubated overnight to grow (Papachristou et al. 2021). After that, the media were first replaced with the fresh complete media, and the cells were treated with ABR, ABR-NP, or Apt-ABR-NP except for the control group that received no treatment. Additionally, the media, along with the treatments, were changed in every 3 days up to the endpoint of the experiment 12–14 days, that depended on the colony numbers in control well. At the end of the treatment period, when colony confluency in control well reached the optimum level, the media or media with treatment suspensions were removed, and the cells were washed with PBS. Then 1 ml of 10% acetic acid (in methanol) was added to each plate and kept on a shaker for 10–15 min to fix the colonies. Then the cells were stained with crystal violet solution (0.5% crystal violet in 25% methanol–water) and again were shaken for 15 min under shaking conditions. Crystal violet solution was then removed, and the cells were washed with PBS three times. The plates were then air-dried overnight, and on the next day, images were captured under an optical microscope.

After imaging, the plates were shaken with 10% acetic acid solution for 15 min to dissolve all the colonies, and with the supernatant, absorbance was measured at 510 nm using a plate reader.

#### ***In vivo animal studies***

Swiss albino mice were procured from the National Institution of Nutrition (NIN), Hyderabad, India, and the complete in vivo experimental procedures with animals



were approved by the Jadavpur University Animal Ethics Committee (JU-AEC, Protocol approval. no.: AEC/PHARM/1704/04/2020), under the norms of CPCSEA, Govt. of India (Jadavpur University Registration Number in CPCSEA: 1805/G.O./Re/S/15/CPCSEA). The guidelines of CPCSEA (Control and Supervision of Experiments on Animals) were carefully followed in all the animal experiments.

#### **Pharmacokinetic study**

In vivo pharmacokinetic studies of ABR and its nanoformulations were conducted in Swiss albino mice, having an average body weight of 25 g (Dutta et al. 2019). Mice (36 in numbers) were taken for each group. Group-I animals were treated with ABR at a dose of 400 µg/kg body weight, Group-II animals were treated with ABR-NP, and Group-III animals were treated with Apt-ABR-NP. In the cases of the formulations, a dose equivalent to the free ABR dose was administered through the formulations. Group I mice received the free drug (ABR) suspension in the water for injection through intraperitoneal injection. The formulations were directly dispersed in water for injection and injected intraperitoneally in animals of Group II and Group III, respectively. The blood samples were collected (around 1 ml from each animal) by killing three animals separately at each time point (time points taken were 2, 10, 15, 20, 30, 60, 90, 120, 240, 360, 480, 720 min) in heparin-coated tubes and were centrifuged ( $10,000\times g$  for 10 min at 4 °C) to separate the plasma (200 µl each). A volume of 500 µl of ethanol was added to each plasma sample and mixed well with a vortex mixer to dissolve the drug content. It was further centrifuged, and the clear supernatant was collected and analyzed in an LC–MS instrument (Agilent 6545 Q-TOF LC/MS system). The data were analyzed through MassLynx 4.1 software and quantified by comparing it with a calibration curve of ABR prepared. The plasma concentration vs time plot was generated using GraphPad Prism 5.0, and the pharmacokinetic parameters (AUC,  $C_{max}$ ,  $T_{max}$ ,  $t_{1/2}$ , MRT,  $V_d$ , CL) were calculated.

#### **Hemolysis study**

Blood samples from male Swiss albino mice were placed in heparinized tubes and centrifuged at 4 °C for 5 min at 1000g. The supernatant was removed, and the erythrocytes were washed three times in PBS (pH 7.4) before being used. The resulting suspension (2%) was employed in a hemolysis study. To test the hemolytic activity, 190 µl of the suspension was placed in each well of a 96-well plate, and a volume of 10 µl of ABR/ABR-NP/Apt-ABR-NP (with an increasing concentration of ABR, i.e., 10 to 100 µM) was added to each well. The negative control was normal saline (0% lysis), and the positive control was distilled water (100% lysis). The unlysed erythrocytes were separated by centrifugation at 10,000g for 5 min after the incubation at 37 °C for 1 h with gentle stirring. The supernatant's optical density (O.D.) was determined at 570 nm. The percent lysis was measured by comparing the O.D. value to that of the supernatant (positive control) where full lysis occurred. To acquire the average value, the tests were repeated three times (Ehsan et al. 2022; Thasneem et al. 2011).

#### **Biodistribution study and gamma-scintigraphy imaging**

In vivo biodistribution of ABR-NP and Apt-ABR-NP was studied in a Swiss albino prostate-cancer mice model using technetium-99 m (Dutta et al. 2019) radiolabeled

nanoparticles.  $^{99m}\text{Tc}$  radiolabeling of the nanoparticles was done directly by using an acidic solution of stannous chloride ( $\text{SnCl}_2$ ) as a reducing agent to synthesize  $^{99m}\text{Tc}$ -labeled nanoparticles ( $^{99m}\text{Tc}$ -ABR-NP and  $^{99m}\text{Tc}$ -Apt-ABR-NP). Mice were hydrated well with normal saline through intraperitoneal injection and anesthetized by diethyl ether. Then the radiolabelled nanoparticles containing 3.7 MBq radioactivity were injected through their tail veins. Biodistribution and gamma-scintigraphy imaging were done using  $^{99m}\text{Tc}$ -labeled nanoparticles. The half-life of  $^{99m}\text{Tc}$  is short (6 h) (Ramdhani et al. 2023). Hence, to get the optimum level of biodistribution and the localization of radio labeled Apt-ABR-NP, the study was conducted using intravenous route to avoid erroneous data due to the loss of radioactivity of  $^{99m}\text{Tc}$ . In the case of pharmacokinetic and anticancer efficacy study, since no  $^{99m}\text{Tc}$  material was involved, it was administered to animals by the intended intraperitoneal route.

For the biodistribution study, the animals were killed after 1 h, 2 h, and 5 h of post-injection through cervical dislocation. Different organs (liver, kidney, stomach, intestine, heart, lungs, and prostate) and body fluids (blood and urine) were collected in scintillation counting tubes, and radioactivities present in them were measured in a gamma-scintillation counter (ECIL, Hyderabad, India). The results were expressed as % of injected dose (% I.D.) accumulated in the organs and as % I.D. per gram (wet weight) in the case of blood. In another experiment, scintigraphy imaging was performed in live anaesthetized animals at 1 h, 2 h, and 5 h post-injection of radiolabeled nanoparticles; under a gamma-scintigraphy camera (GE Infinia) in a head-supine anterior position under static conditions. Images were analyzed using GE Infinia  $\gamma$  Camera facilitated along with Xeleris Work Station, Milwaukee, WI, USA (Dhara et al. 2023).

#### ***Prostate cancer development in mice, treatment undergone, and histopathological evaluation***

Adult male Swiss albino mice were used to generate prostate cancer-bearing mice as described earlier (Nahata and Dixit 2012). Healthy male mice (25–30 g body weight) were procured from the National Institute of Nutrition (Hyderabad, India). They were maintained in polypropylene cages at  $25^\circ\text{C} \pm 1^\circ\text{C}$  temperature under  $55\% \pm 5\%$  relative humidity and normal 12 h/12 h day/night photoperiod and acclimatized with the facilities for 2 weeks before conducting any experiments. The animals were treated with subcutaneous testosterone propionate (40 mg/kg) twice a week for 12 weeks. In addition, *N*-nitroso-*N*-methyl urea (4 mg/kg) once a week was given by intraperitoneal injection as a cancer promoter for the first 4 weeks of testosterone treatment (Schleicher et al. 1996). After 12 weeks of testosterone propionate treatment, the development of prostate cancer was confirmed by histopathological observation of the prostate. A normal control group was maintained throughout the study period that received the treatment of normal saline only (the 'Normal' group, Group A).

The animals bearing prostate cancer were subdivided into four groups, one receiving normal saline only (the 'Cancer' control group, Group B), one receiving free abiraterone acetate suspension (the 'ABR' group, Group C), one receiving ABR-NP (the 'ABR-NP' group, Group D), and the last group of animals receiving Apt-ABR-NP (the 'Apt-ABR-NP' group, Group E). A minimum of 5 animals was maintained for each group. For the 'ABR', 'ABR-NP', and 'Apt-ABR-NP' groups, the dose was maintained at 100 mg/kg of ABR or equivalent through intraperitoneal injection thrice a week for 8 weeks. An additional

group of normal mice received the same treatment of Apt-ABR-NP as in the carcinogen-treated Apt-ABR-NP group of animals (Group F) to assess the impact of the formulation in normal animals. The 'Normal' and the 'Cancer control' group were treated with saline only throughout the treatment period (8 weeks). At the end of 8 weeks of treatment with ABR, ABR-NP, or Apt-ABR-NP, all the animals were killed; their prostates were isolated, fixed with formalin (4%), embedded in paraffin blocks, sectioned in thin slices (5  $\mu$ m thickness), and stained with hematoxylin and eosin (H&E) for microscopic observation (Chen et al. 2020). Ki67-immunostaining was also performed in a similar way for all the 'Normal control', 'Cancer control', 'ABR-NP', and 'Apt-ABR-NP' groups. Compared to the 'Normal' group, histopathological changes in the prostates of 'Cancer', 'ABR', 'ABR-NP', and 'Apt-ABR-NP' groups were observed under an optical microscope at 10 $\times$  and 40 $\times$  magnifications. H&E stained sections were observed for estimation of Gleason score, lymphovascular invasion, and perineural invasion (Tătaru et al. 2021). The Gleason grading system was used to determine different patterns of tumor tissues, and scoring was carried out to represent their stages (Pierorazio et al. 2013). Ki67-stained sections were analyzed for the measurement of Ki67-positive cells using ImageJ software (version 1.53k). Areas with 3% or fewer Ki67+ cells were considered negative, with 3–25% Ki67+ cells considered as grade 1 (1+ or low grade), 26–50% Ki67+ cells were considered as grade 2 (2+ or intermediate grade), with 51–75% Ki67+ cells were considered as grade 3 (3+ high grade), and areas with 76–100% Ki67+ cells were considered as grade 4 (4+ or very high/worse grade) (Madani et al. 2011). A minimum of 10–12 images were captured for each slide for statistical analysis.

#### ***Efficacy of Apt-ABR-NP on LNCaP tumor spheroids***

Single cell suspension of LNCaP cells was seeded in ultra-Low attachment plates in serum free media (DMEM/F12) with additional supplements such as 20% methylcellulose (Sigma), B27 (1:50, Invitrogen), 10 ng/ml bFGF (Invitrogen), 4  $\mu$ g/ml insulin (Sigma), and 20 ng/ml epidermal growth factor (EGF) (Peprotech). The spheroids were generated by 7 days of cell seeding. After formation of the spheroids, one group was Cy5-loaded blank (without drug) nanoparticle control group and the other group was treated with Cy5-loaded Apt-ABR-NP for 3 consecutive days at its IC<sub>50</sub> value. For the application of each dose, the media were changed with the fresh media. After completion of the treatment period, the spheroids were washed with ice cold PBS (pH 7.4) and co-stained with DAPI. Finally, photographs were taken using confocal laser microscope (Sen et al. 2023; Wolff et al. 2022).

#### ***Hematological evaluation***

For complete blood count (CBC) profile of mice of the above-mentioned experimental groups of animals ("Prostate cancer development in mice, treatment undergone, and histopathological evaluation" section) were assessed. Blood from the mice were collected through cardiac puncture and whole blood was collected through cardiocentesis. Total count of red blood corpuscles (RBC), hemoglobin, hematocrit, total count of white blood cells (WBC), lymphocytes, monocytes, neutrophils, eosinophils, platelets and PSMA were analyzed using standard method (Weatherby and Ferguson 2004).

C-reactive protein (CRP) was evaluated using commercially available bioassay kits (Weldon Biotech India Pvt. Ltd., New Delhi, India).

#### ***Estimation of serum-specific toxicity markers***

To determine the presence of systemic toxicity in nanoparticle-treated mice, serum biomarkers for hepatic and renal toxicity were evaluated. Each killed animal's blood was taken, and serum was extracted by centrifugation. As a hepatic toxicity marker, the serum levels of AST (aspartate aminotransferase), ALT (alanine transaminase), and alkaline phosphatase (ALP) were evaluated using commercially available bioassay kits (Coral Clinical Systems, Goa, India) following manufacturer protocols, and for nephrotoxicity, creatinine and blood urea nitrogen (BUN) were estimated using AutoZyme Creatinine kit (Accurex, Mumbai, India), and AutoZyme BUN kit (Accurex, Mumbai, India), respectively, in a UV–visible spectrophotometer (Intech-295, Advanced Microprocessor UV–Vis Single Beam) as per the manufacturer instructions.

#### ***Analysis of aptamer–PSMA interactions by molecular docking***

To perform the molecular docking study, we have chosen the receptor as the PSMA to which the aptamer can bind specifically in silico. The crystal structure of PSMA, 1Z8L was obtained from the RCSB protein data bank, and the DNA aptamer structure was prepared by adding the 32-bp DNA sequence in the Discovery studio visualizer 2021 and converted to PDB format. At first, the receptor was prepared by eliminating water molecules and adding polar hydrogen atoms and charges. Then ligand molecule was also prepared for docking analysis using Discovery studio visualizer 2021. Using the HDock blind docking server (<http://hdock.phys.hust.edu.cn/>), further interactions between the aptamer and PSMA were examined (Yan et al. 2020). Providing input for the receptor and ligand was the first stage in the docking technique. The quality of a predicted protein–nucleotide binding mode was measured by its docking score. The discovery studio 2021 client program was used to conduct the docking analysis. The interactions were visualized through Biovia Discovery studio 2021 (BIOVIA Discovery Studio—BIOVIA—Dassault Systèmes®).

#### ***Statistical analysis***

All the experiments were performed at least three different times, and the corresponding data were represented as the mean value along with the standard deviation. Statistical analysis of data was performed using Student's *t*-test, Dunnett's test, and one-way ANOVA, followed by Tukey's post hoc test, two-way ANOVA analysis, and tested by Bonferroni's post-test. The images, graphical, and bar diagrammatic representations were accomplished using various software such as Origin 2021, Graph Pad Prism software (version 5, Graph Pad Prism software Inc, San Diego, CA, USA), Gimp 2.10.30, ImageJ, AutoDock 4.2, and BIOVIA Discovery Studio Visualizer. Graphical abstract and schematic representation were created using Biorender.com. The probability value is indicated as *p*, where *p* < 0.05 was considered as the statistical level of significance.

## Results and discussion

We avoided utilizing any hazardous chemicals and instead employed biocompatible, biodegradable FDA-approved polymer (PLGA) and negligibly immunogenic short nucleotide sequence aptamers to effectively deploy the possible targeted drug delivery in vivo that could lessen its cytotoxicity to healthy tissues by their preferential accumulation in PSMA overexpressed prostate cancer tissue. The following findings were used to substantiate the research envisaged.

### Drug-excipients interaction by FTIR analysis

FTIR studies were performed to detect any chemical interactions between the drug molecule and the excipients. The results suggest that (Additional file 1: Figure S1) PLGA showed peaks at  $3650\text{ cm}^{-1}$ ,  $2935\text{ cm}^{-1}$ , and  $1735\text{ cm}^{-1}$ , for the O–H stretching, asymmetric stretching of  $-\text{CH}_2$ , and C=O stretching band of the carboxylic acid group, respectively. ABR showed characteristic peaks at  $3440\text{ cm}^{-1}$ ,  $2940\text{ cm}^{-1}$ ,  $1735\text{ cm}^{-1}$ ,  $1440\text{ cm}^{-1}$ ,  $1370\text{ cm}^{-1}$ , and  $1250\text{ cm}^{-1}$  for intermolecular bonded O–H stretching vibrations, C–H stretching, C=O stretching,  $\text{CH}_3$  bending vibration of the acetate group,  $\text{CH}_3$  bending vibration of the methyl groups and C–O–C stretching vibration of the acetate group, respectively. FTIR spectra of PVA also reveal peaks at  $3420\text{ cm}^{-1}$  for intermolecular bonded O–H stretching vibrations,  $2925\text{ cm}^{-1}$  for asymmetric stretching of  $-\text{CH}_2$ , and  $1740\text{ cm}^{-1}$  due to water absorption. Blank (without drug) nanoparticles (BL-NP) reveal the presence of all characteristic peaks of the polymer PLGA. ABR-NP showed IR peaks at  $3490\text{ cm}^{-1}$  due to intermolecular bonded O–H stretching vibrations,  $2950\text{ cm}^{-1}$  for C–H stretching,  $1760\text{ cm}^{-1}$  for C=O stretching,  $1380\text{ cm}^{-1}$  for C–H bending, and  $1200\text{ cm}^{-1}$  for C–O stretching due to ester group. Apt-ABR-NP also showed almost similar peaks with one additional peak at  $1650\text{ cm}^{-1}$  for C=O stretching due to the amide group. Peaks at  $1650\text{ cm}^{-1}$  for Apt-ABR-NP indicated the aptamer binding to the ABR-NPs through amide bond formation. The FTIR study (Additional file 1: Figure S1) indicates no chemical interaction between the ABR and the excipient used in this study. However, a few slight shifts in the peak were solely responsible for the physical interactions that might provide the structure of the formulation. The shift of vibration signals indicated the presence of physical interactions between the compounds for the nanoparticles that might help develop a spherical nanostructure (Dhara et al. 2023).

### X-ray photoelectron spectroscopy (XPS)

High-resolution XPS was also used to identify chemical elements and surface chemistry. XPS can provide qualitative and quantitative information on various elements on the particle surface and determine the chemical composition of the uppermost layer of the polymer surface. The XPS spectrum of ABR-NP clearly shows that the O1s peak was at 533 eV and the C1s peak was at 287 eV, confirming the presence of oxygen and carbon elements, respectively, in the PLGA polymer matrix. A very small peak of N1s was observed at 399 eV and appeared in this region with an increasing range. XPS spectra of Apt-ABR-NP nanoparticles showed distinct peaks for oxygen and carbon at 533 and 287 eV, respectively (Fig. 2A). A magnified image of the nitrogen region showed a significant signal at 399 eV, which corresponds to the presence of a large number of N atoms in



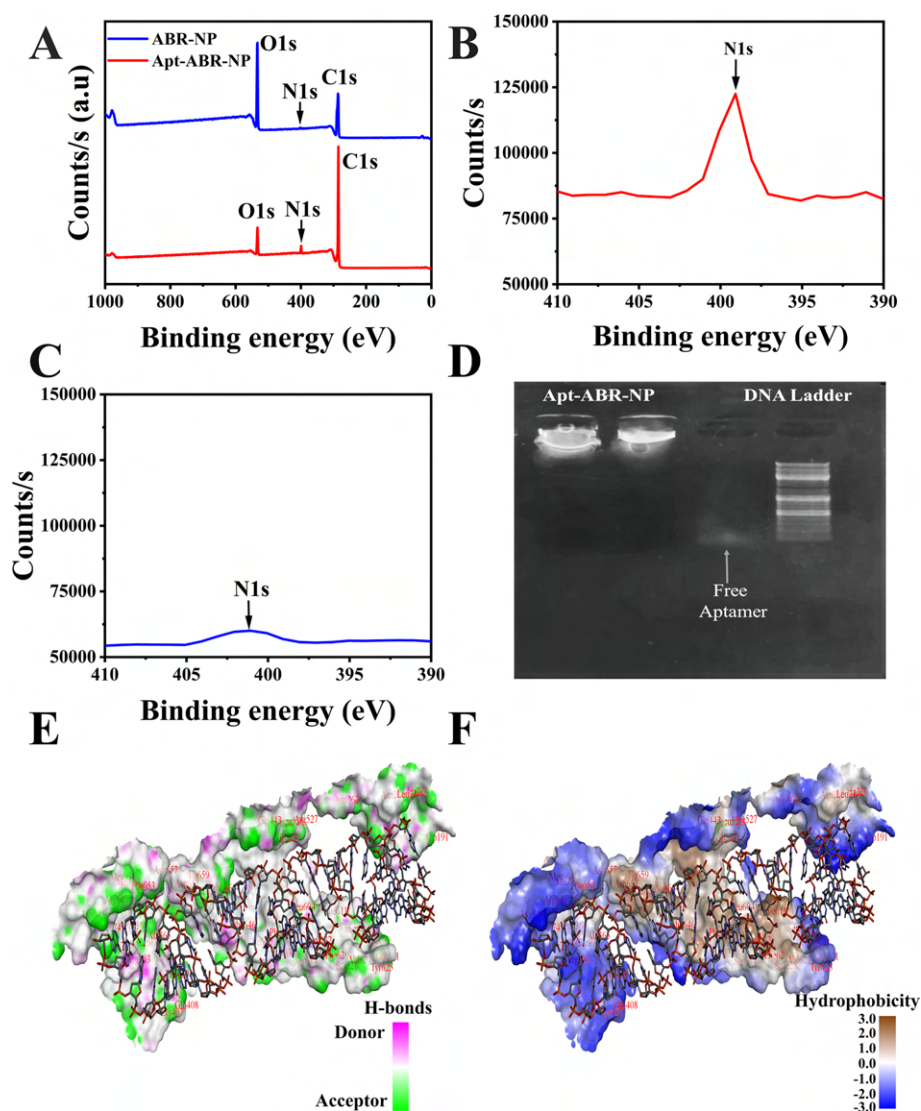


**Fig. 3** Aptamer conjugation as assessed by X-ray photoelectron spectroscopy study, and agarose gel electrophoresis, and aptamer–PSMA binding by molecular docking. **A** XPS graph for combined ABR-NP and Apt-ABR-NP, **B** XPS graph for enlarged N1s peak of Apt-ABR-NP, **C** XPS graph for enlarged N1s peak of ABR-NP, **D** aptamer conjugation to ABR-NP using agarose gel electrophoresis, **E** aptamer–PSMA (Protein data bank, PDB: 1Y8L) interactions by hydrogen bonding through molecular docking; **F** aptamer–PSMA (PDB: 1Y8L) hydrophobic interactions through molecular docking

the DNA aptamer. In the XPS spectrum of PLGA nanoparticles, peaks O1 and C1 were located at almost the same binding energy as aptamer-labeled PLGA nanoparticles and PLGA nanoparticles. After the chemical reaction of the PLGA nanoparticles with the aptamer, an amide bond (CO–NH) was formed, which detected a significant N1s peak at a binding energy of 408 eV. For covalent bonds, the higher the polarity, the higher the bond energy. A CO–NH bond was formed here by the conjugation of the aptamer and PLGA–COOH. The presence of nitrogen in the PLGA-aptamer nanoparticles (Apt-ABR-NP) was confirmed using XPS, which observed a higher intensity (Fig. 2B), indicating that the aptamer was successfully conjugated to the PLGA surface because the DNA aptamer contained many nitrogen elements. In contrast, in ABR-NP, only nitrogen

element of the drug molecule, abiraterone acetate was present, resulting in a very small N1s peak (Fig. 2C). This indicates ABR presence on the particle surface also, due to its homogeneous distribution, which was later supported by the findings of HR-TEM. Conjugation of the aptamer to the surface of ABR-NP was successfully confirmed by the XPS plots of the ABR-NP and Apt-ABR-NP. The enlarged plot of aptamer-tagged nanoparticles clearly showed the higher intensity of the nitrogen peak for the abundant presence of the nitrogen atom in the DNA aptamer (Wang et al. 2013).

#### **Aptamer conjugation on the surface of nanoparticles**

An agarose gel electrophoresis confirmed that the PSMA-specific DNA aptamer was coupled to the nanoparticle surface. Figure 2D demonstrates that the 32-base pair aptamer moved through the gel and landed parallel to the conventional DNA ladder of the 50-bp marker. The aptamer-coupled nanoparticles (Apt-ABR-NP), on the other hand, stayed inside the loading well, as evidenced by fluorescence. However, the unconjugated nanoparticles (ABR-NP) did not display any band in the well, owing to the lack of a DNA strand. In the instance of Apt-ABR-NP, the image demonstrated the coexistence of DNA aptamer with the nanoparticles, ensuring effective aptamer conjugation on the surface of the nanoparticle, as supported by FTIR data. Further, XPS data support the presence of aptamer on Apt-ABR-NP (Shahriari et al. 2021). Aptamer conjugation to the nanoparticle's surface results in amide bond formation between the carboxylic acid group of the polymer and amine group of the DNA aptamer.

#### **Analysis of aptamer-PSMA interactions by molecular docking**

A molecular docking study was performed to check the affinity or interactions between the 32-bp DNA aptamer and prostate-specific membrane antigen (PSMA). Results suggest that nucleotide bases of the aptamer effectively bind with various amino acid residues (Fig. 2E and F). We observed electrostatic interaction between Lysine 406, ARG181, ARG649, and ARG 649 residues and phosphate groups of thymine (DT27), adenine (DA2), adenine (DA11), adenine (DA11), respectively. Several conventional and carbon-hydrogen bonding, along with some hydrophobic interactions, were found between aspartic acid (ASP654), lysine (LYS187), lysine (LYS187), arginine (ARG 190), arginine (ARG649), arginine (ARG190), glutamic acid (GLU748), alanine (ALA635) and methionine (MET663) amino acid residues with adenine (DA2:N3), adenine (DA3:O4'), thymine (DT32:O2), adenine (DA10:O3'), thymine (DT32:O2), thymine (S:DT1), guanine (DG15) and adenine (DA24) nucleotide bases of the aptamer, respectively (Additional file 1: Table S3). The docking score was found to be  $-330.86$ , indicating very good binding affinity between the ligand and receptor. These interactions suggest that aptamer-conjugated nanoparticles can selectively bind to the prostate-specific membrane antigen found in most prostate cancer tissue and the drug molecules reaching the cancer tissues through the targeting method will show its efficacy more efficiently. The DNA aptamer-PSMA binding through molecular docking analysis is also a clear indication of the capabilities of the conjugated nanoparticles to specifically reach PSMA-associated prostate cancer microenvironment.

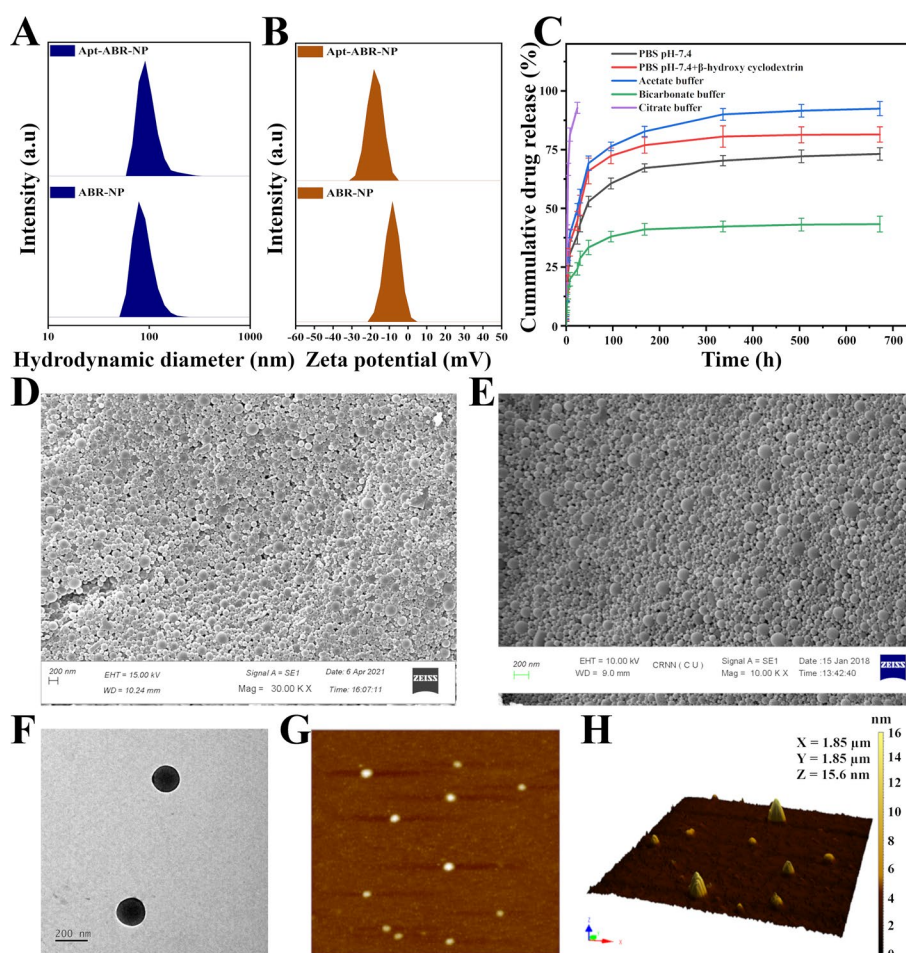


**Fig. 3** Determination of particle size, zeta potential, drug release, and electron microscopic imaging and atomic force microscopic evaluation of the experimental nanoparticles. **A** represents particle size distribution of ABR-NP and Apt-ABR-NP, **B** represents zeta potential values of ABR-NP and Apt-ABR-NP, **C** represents in vitro drug release study of Apt-ABR-NP in phosphate buffer saline (PBS pH 7.4), PBS containing  $\beta$ -hydroxy-cyclodextrin, acetate buffer (pH 5), bicarbonate buffer (pH 10) and citrate buffer (pH 3), **D**, **E** represents the FESEM images of ABR-NP and Apt-ABR-NP, respectively, **F** HR-TEM image of Apt-ABR-NP and **G**, **H** depicts AFM images of Apt-ABR-NP

### Determination of particle size and zeta potential

Particle size distribution and zeta potential were measured using the dynamic light scattering method. The average values of the hydrodynamic diameter ( $d_H$ ) of ABR-NP and Apt-ABR-NP were found to be 130.6 nm and 149.30 nm, respectively (Fig. 3A). However, aptamer conjugation showed approximately 20% enhancement in the size of the ABR-NP. Zeta potential values for ABR-NP and Apt-ABR-NP were  $-10.1$  mV and  $-18.5$  mV, respectively (Fig. 3B). The zeta potential values of the nanoparticles imply their stay in a suspended condition in an aqueous medium for a prolonged period. Zeta potential values of nanoparticles greater than  $\pm 30$  mV are known to develop more stable suspension (Champion et al. 2007). Thus, the formulations should be stored as a powder that may be suspended in water before administration..



### In vitro drug release study

In vitro ABR release from Apt-ABR-NP was carried out in five different media, i.e., phosphate buffer saline (PBS) (pH 7.4), PBS with 1%  $\beta$ -hydroxy cyclodextrin (pH 7.4), citrate buffer (pH 3), acetate buffer (pH 5), and bicarbonate buffer (pH 10), for 28 days (672 h). PBS was chosen as a release medium for its blood environment mimicking pH. The cumulative percentage of drug release after the mentioned time period was found to be 73.12%, 81.45%, 92.76%, 92.45%, and 43.30%, respectively, in 672 h of study in the five different release media (phosphate buffer saline (PBS) (pH 7.4), PBS with 1%  $\beta$ -hydroxy cyclodextrin (pH 7.4), citrate buffer (pH 3), acetate buffer (pH 5), and bicarbonate buffer (pH 10), respectively (Fig. 3C). The drug release data from the nanoparticles were tested on zero-order, first-order, Hixson–Crowell, Korsmeyer–Peppas, and Higuchi kinetic models, and the various regression coefficient values ( $R^2$ ) for kinetics were tabulated (Additional file 1: Table S2).  $R^2$  values suggest that drug releases, according to Korsmeyer–Peppas, in all five release media.

The drug release in the PBS with  $\beta$ -hydroxy cyclodextrin media showed a biphasic in vitro drug release pattern with an initial fast drug release followed by a sustained drug release pattern for 4 weeks. It could be due to the quick release that drug molecules present on or close to the surface and  $\beta$ -hydroxy cyclodextrin that might help in the better solubility of hydrophobic drug molecules in the drug release medium. ABR release from the nanoparticles followed Korsmeyer–Peppas kinetic, suggesting drug release by diffusion and erosion mechanism (Pattnaik et al. 2012).

The quicker breakdown of the polylactic acid–glycolic acid polymer in citrate buffer (pH 3) than in PBS/PBS with  $\beta$ -hydroxy cyclodextrin explains the faster release pattern of ABR at pH 3. Under the acidic environment (pH 3), the medium promoted the hydrolysis of the PLGA core by attacking ester bonds, resulting in quicker polymer breakdown (Jain et al. 2010). However, at alkaline pH (pH 10), the polymer retains its non-polar character due to the trapping of hydroxyl groups on the polymer surface, which reduces particle water absorption and results in a more stable state of nanoparticles in higher pH environments. The hydrolytic degradation was low to high from neutral, to acidic pH. The quicker drug release pattern in acidic conditions against PBS (pH 7.4) reveals the faster release of ABR from ABR-NP in an acidic tumor environment versus a physiologically neutral medium of blood during their transportation and distribution (Choi et al. 2015).

### Surface morphology by FESEM, HRTEM, and AFM

Drug absorption by cells or organs depends on the surface and shape of the nanoparticle because the nanoparticle surface interacts with the biomembrane, which affects drug internalization (Clogston and Patri 2011; Dutta et al. 2019). Using FESEM, the surface morphology of ABR-NP and Apt-ABR-NP were studied, and photographs of nanoparticles (Fig. 3D, E) revealed that the particle (size 100 nm to 150 nm) were round in shape, with the largest particles measuring 150 nm. Nanoparticles had smooth surfaces with no apparent porosity or fractures. As we did not observe any significant difference in the surface morphologies of the nanoparticles (with and without aptamer conjugation), we further studied the HR-TEM and AFM with the Apt-ABR-NP formulation only. The interior structure of the experimental nanoparticle was studied with high-resolution

transmission electron microscopy (HR-TEM). HR-TEM pictures showed a dark structure (Fig. 3F), indicating that the nanoformulation had a homogeneous drug distribution throughout the particles. The produced nanoparticles had a spherical structure with a smooth surface, as revealed by AFM images (Fig. 3G, H). AFM images in three dimensions showed well-separated nanoparticles within a small size range.

#### Drug loading and entrapment efficiency

We developed a number of formulations with different drug-to-polymer ratios. Three of these formulations are shown in Additional file 1: Table S1. For each of these three formulations, the amount of drug loaded into the nanoparticles and entrapment efficiencies were calculated. The drug loading percentages for ABR-NP1 and ABR-NP3 were  $7.36 \pm 0.5\%$  and  $2.61 \pm 0.25\%$ , respectively. The highest drug encapsulation was demonstrated by ABR-NP2 (8.5%). As a result, this formulation was chosen as the best one and given the name ABR-NP. This formulation was used for aptamer conjugation. There was a loss of drug during the conjugation process and Apt-ABR-NP had drug loading 8.02%. The ABR-NP encapsulation efficiency was  $93 \pm 3.30\%$  and the value was 88.2% in the case of Apt-ABR-NP, demonstrating the method's ability to create nanoparticles with minimum material loss (Dutta et al. 2019).

#### Stability of the nanoparticles

A stability study of ABR-NP and Apt-ABR-NP revealed that the samples stored at 4–8 °C retained morphology (Fig. 3D, E) and drug content throughout the period. Formulations stored at 30 °C, 75% RH (relative humidity) and 40 °C, 75% RH for 45 and 90 days showed morphological deformation (Additional file 1: Figure S2A, B) and a little decrease in drug content (Additional file 1: Figure S2C). They had morphological deformation during storage at higher temperatures, resulting in enhanced particle size (Additional file 1: Figure S2D). From the stability studies, it was observed that ABR-NP and Apt-ABR-NP were stable at 2–8 °C for up to 90 days (time of investigation). However, the nanoparticles were not stable above 30 °C due to the aggregation of nanoparticles and polymer softening (Yadav and Sawant 2010). Hence, the prepared nanoparticles should be stored at 2–8 °C.

#### Hydrolytic study

The increase in weight loss upon hydrolytic degradation was used to determine the biodegradability of Apt-ABR-NP. The pH values had a substantial impact on weight loss. The hydrolysis of the formulations increased as the pH of the medium was reduced. After a 4-week investigation, mass loss was  $11.23 \pm 2.14\%$  at pH 10,  $20.73 \pm 1.41\%$  at pH 7.4,  $30.83 \pm 1.98\%$  at pH 5, and  $48.26 \pm 2.61\%$  at pH 3, respectively (Additional file 1: Figure S2E). The results indicated that our nanoformulation was more stable in phosphate buffer (pH 7.4) and bicarbonate buffer (pH 10), as compared to citrate (pH 3) and acetate buffer (pH 5). The findings suggest that the faster drug release would occur as the Apt-ABR-NP reaches acidic tumor microenvironment.

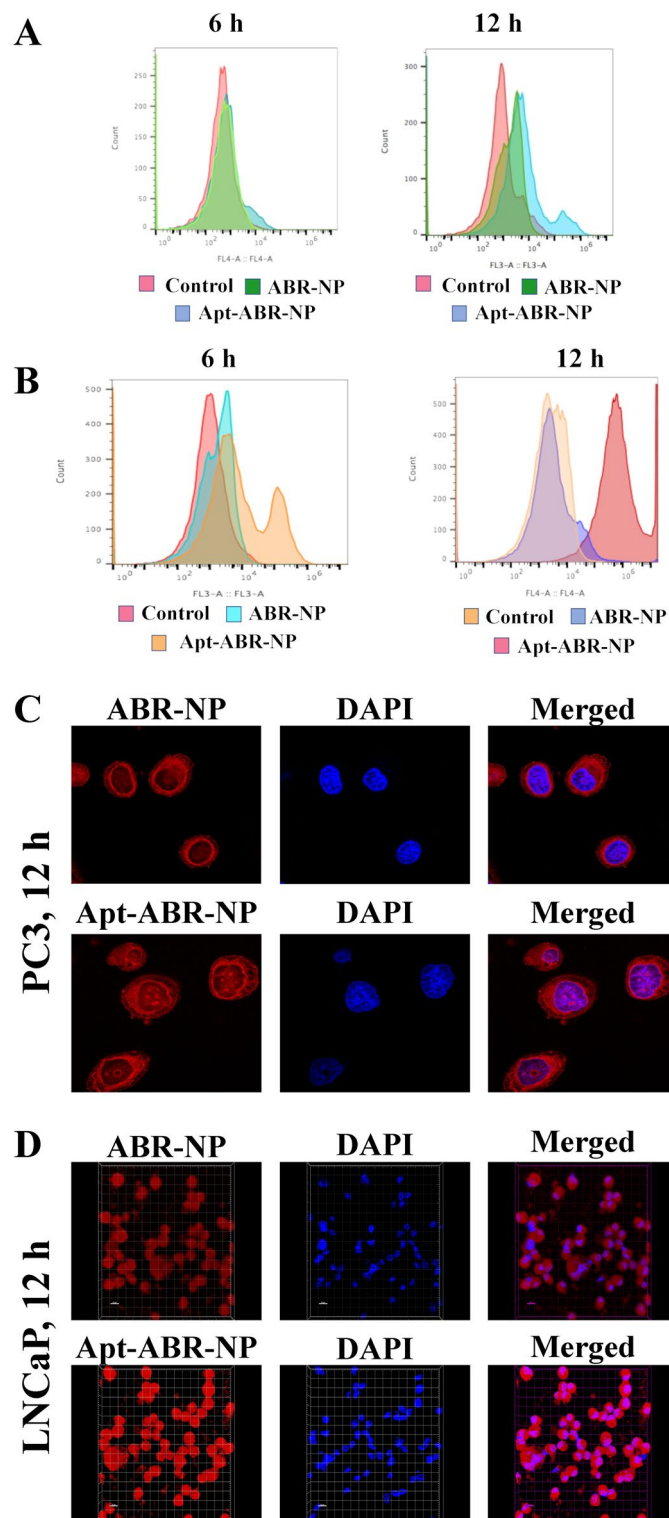


**Fig. 10** Cellular uptake study. **A** FACS histogram PC3 cells after the treatment with ABR-NP and Apt-ABR-NP at 6 h and 12 h. **B** FACS histogram LNCaP cells after the treatment with ABR-NP and Apt-ABR-NP at 6 h and 12 h. **C** Confocal laser microscopy images of PC3 cells at 12 h after the treatment with ABR-NP and Apt-ABR-NP. **D** Confocal laser microscopic images of LNCaP cells at 12 h after the treatment with ABR-NP and Apt-ABR-NP

### In vitro cellular uptake analysis by flow cytometry and confocal microscopy

Flow cytometry analysis revealed a time-dependent gradual accumulation of Apt-ABR-NP in both PC3 (Fig. 4A) and LNCaP (Fig. 4B) cells. In the case of PC3 cells, an inadequate percentage of nanoparticle uptake was observed from 6 to 12 h of treatment. However, in the case of LNCaP cells, longer incubation with nanoparticles significantly enhanced cellular uptake, especially for Apt-ABR-NP. This could be due the fact that LNCaP cells overexpress the surface antigen PSMA, whereas PC3 cells are PSMA negative. The Apt-ABR-NP fluorescent intensity was highest for 12 h of treatment in the case of LNCaP cells suggesting the PSMA-specific strong binding affinity of aptamer functionalized nanoparticles with LNCaP cell-surface biomarker for prostate cancer. Furthermore, to validate targeting specificity of the nanoparticle surface conjugated aptamer against PSMA receptor, we performed cellular uptake study on 22Rv1. As expected, enhanced cellular internalization was observed for PSMA-targeted nanoparticles.

We further compared the cellular internalization of ABR-NP and Apt-ABR-NP nanoparticles at 12 h confocal microscopy for PC3 and LNCaP cells. Corresponding images reflected nanoparticles accumulation inside the cytoplasm of PC3 (Fig. 4C) and LNCaP cells (Fig. 4D) with the progression over time. However, comparatively higher accumulation was found in the case of LNCaP cells, as represented by red fluorescence intensity confirming the intense binding specificity of aptamer with PSMA, which facilitated the higher accumulation of Apt-ABR-NP in LNCaP cells, especially with a longer incubation period.

The cellular uptake study using flow cytometry analysis was also conducted on 22Rv1 prostate cancer cells that overexpress PSMA and are AR positive also. The data showed the time-dependent increase of the uptake of ABR-NP and Apt-ABR-NP in 22Rv1 cells (Fig. 5A). However, the cellular uptake was more in the case of Apt-ABR-NP.

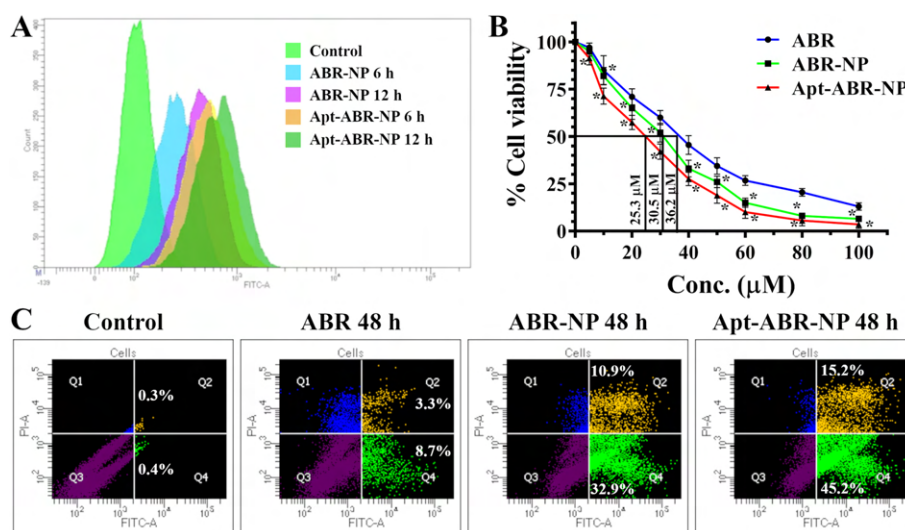


**Fig. 5** In vitro evaluation of cellular uptake, cytotoxicity, and apoptosis in 22Rv1 cells. **A** FACS histogram for cellular uptake measurement after the treatment with ABR-NP and Apt-ABR-NP at 6 h and 12 h. **B** IC<sub>50</sub> values of ABR, ABR-NP, and Apt-ABR-NP on 22Rv1 cells (data show mean  $\pm$  SD,  $n = 3$ ; \* indicates  $p < 0.05$  when compared against ABR-treated group of mice), and **C** induction of apoptosis in 22Rv1 cells after treatment with ABR, ABR-NP, and Apt-ABR-NP for 48 h

Many reports are available regarding cellular internalization aptamer-conjugated PLGA nanoparticles. Aptamer-conjugated PLGA nanoparticles have been reported to internalize into the cells by receptor-mediated endocytosis and micropinocytosis (Liu et al. 2009; Shishparenok et al. 2023; Wan et al. 2019; Yallapu et al. 2014). The aptamer of Apt-ABR-NP interacts with the PSMA in clathrin-dependent endocytosis by forming clathrin-coated pits. The clathrin coat detaches and aptamer-conjugated formulations are internalized in endosomes and lysosomes before their distribution to other cellular organelles (Shishparenok et al. 2023; Wan et al. 2019). Caveolar-mediated endocytosis of aptamer conjugated formulations after aptamer–PSMA interactions entails the development of caveolae vesicles mediated through dynamins found in caveolae (Shishparenok et al. 2023; Wan et al. 2019). Aptamers move over the membrane to the caveolae after binding to the targeted surface membrane antigen, PSMA.

Apt-ABR-NP may be endocytosed by clathrin and caveolae-dependent and caveolae-independent pathways (Yallapu et al. 2014). Hence, multiple receptor-mediated endocytotic pathways were involved in the aptamer-conjugated formulations (Liu et al. 2009).

Rapid endolysosomal escape of PLGA nanoparticles into the cytosol due to selective reversal of surface charge of PLGA nanoparticles from anionic to cationic in the acidic

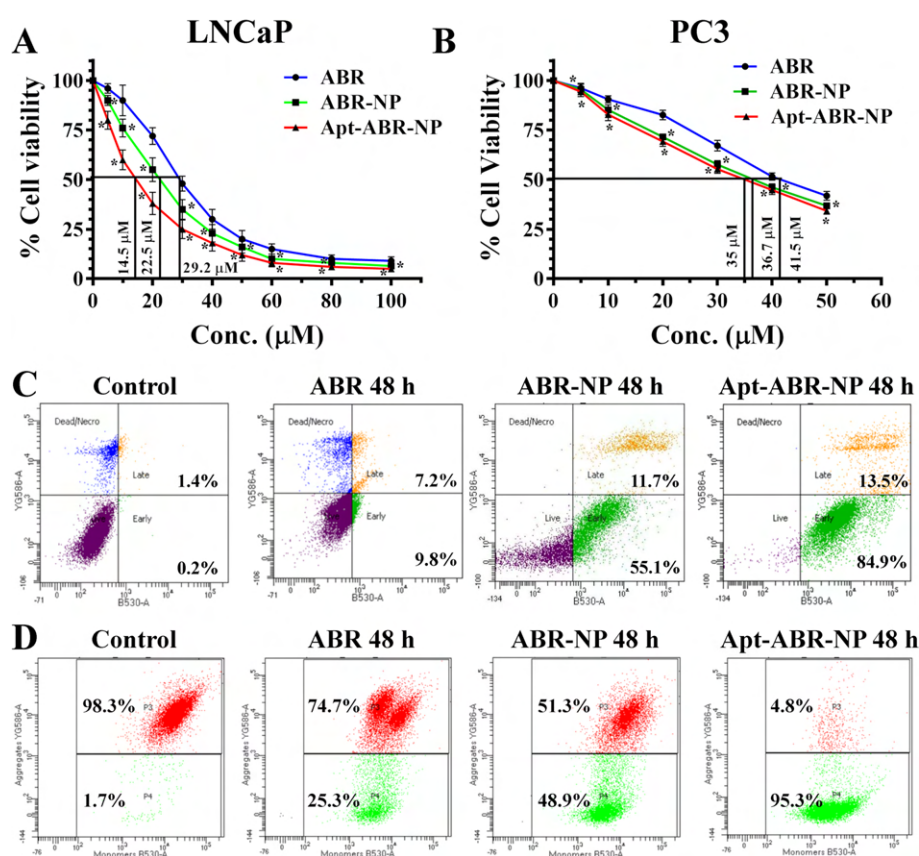


**Fig. 8** Cell cytotoxicity, apoptosis, and mitochondrial membrane depolarization assay of ABR, ABR-NP, and Apt-ABR-NP evaluated in vitro. **A**  $IC_{50}$  values of ABR, ABR-NP, and Apt-ABR-NP on LNCaP and PC3 cells after 48 h of treatment (data show mean  $\pm$  SD,  $n = 3$ ; \* indicates  $p < 0.05$  when compared with ABR-treated group of mice). **C** Induction of apoptosis in LNCaP cells after treatment with ABR, ABR-NP, and Apt-ABR-NP for 48 h. **D** Mitochondrial membrane depolarization after 48 h of treatment, with ABR, ABR-NP, and Apt-ABR-NP for 48 h



endolysosomal environment is a well-established mechanism for lysosomal escape of PLGA nanoparticles (Panyam et al. 2002).

#### In vitro cytotoxicity assay

The percentage viability data of 22Rv1, LNCaP, and PC3 cells, which received the treatment of the free drug and the experimental nanoparticles are represented in Figs. 5B, 6A, and B, respectively. Apt-ABR-NP had the highest cytotoxicity on LNCaP cells (lowest  $IC_{50}$  value  $14.5 \pm 1.2 \mu M$ ) followed by 22Rv1 ( $IC_{50}$  value  $25.3 \pm 1.1 \mu M$ ) compared to ABR and ABR-NP. ABR showed an  $IC_{50}$  of  $29.2 \pm 3.1 \mu M$ , while ABR-NP showed the value of  $22.5 \pm 2.6 \mu M$  in LNCaP cells. Significant reduction of the  $IC_{50}$  value was observed for both of the nanoparticles (ABR-NP and Apt-ABR-NP) on LNCaP cells, representing their enhanced therapeutic efficacy in comparison to free ABR. On the contrary, the cytotoxicity of ABR and its formulations on PC3 cells was comparatively lower than on LNCaP cells. The  $IC_{50}$  values on PC3 cells were found to be  $41.5 \pm 2.4 \mu M$ ,  $36.7 \pm 1.6 \mu M$ , and  $35 \pm 2.0 \mu M$  for ABR, ABR-NP, and Apt-ABR-NP treatments, respectively. All the cytotoxicity assay data suggest that ABR-NP and Apt-ABR-NP demonstrated enhanced therapeutic potency on LNCaP cells. The cytotoxic effect of ABR-NP and Apt-ABR-NP in PSMA-positive prostate cancer LNCaP cells and PSMA-negative prostate cancer PC3 cells showed that the highest dose reduction was in Apt-ABR-NP treated LNCaP cells. However, PC3 cells were less sensitive to ABR, ABR-NP, and Apt-ABR-NP, as PSMA-negative PC3 cells are also androgen insensitive in nature and ABR functions by inhibiting androgen production (Bouhajib and Tayab 2019; Mukherjee and Mayer 2008). The aptamer conjugation decreased the  $IC_{50}$  value by 51% in PSMA-positive LNCaP cells. The findings fairly matched the earlier reports by Fernanda da Luz Efe. 2019, and Pokrovsky et al. 2020 (Pokrovsky et al. 2020; Wang et al. 2019). The investigation suggests that PSMA binding and inhibition of androgen production had predominant role in the cellular internalization and cellular function mediated through Apt-ABR-NP. Hence, we proceeded with further in vitro studies on LNCaP cells.

#### Apoptosis assay

Apoptosis is a programmed cell death, and most anticancer agents are expected to have an apoptosis-inducing capacity (Diepstraten et al. 2022). The apoptosis-inducing potential of ABR, ABR-NP, and Apt-ABR-NP through the Annexin V-FITC/PI dual staining method demonstrated the superior apoptosis-inducing ability of Apt-ABR-NP, suggesting its applicability as a potential chemotherapeutic formulation.

The total apoptotic population in 22Rv1 cells after treatment with ABR for 48 h was 12% (8.7% early and 3.3% late apoptosis) (Fig. 5C). ABR-NP treatment increased apoptosis to 43.8% (32.9% early and 10.9% late apoptosis) and Apt-ABR-NP treatment showed the value 60.4% (45.2% early and 15.2% late apoptosis) in 22Rv1 cells.

Figure 6C demonstrates apoptosis on LNCaP cells. The total apoptotic population after treatment with ABR for 48 h was 17% (9.8% early and 7.2% late apoptosis), which was increased up to 66.8% (55.1% early and 11.7% late apoptosis) and 98.4% (84.9% early and 13.5% late apoptosis) in the cases of ABR-NP and Apt-ABR-NP treatments, respectively. We found highest percentage of apoptotic cell death for Apt-ABR-NP as compared to ABR and ABR-NP after 48 h of incubation in LNCaP cells. On an overall comparison,

Apt-ABR-NP-induced apoptosis was higher at all the incubation time points than free drug, ABR, and unconjugated nanoparticles ABR-NP. Thus, Apt-ABR-NP is a potential cytotoxic candidate against PSMA-positive prostate cancer LNCaP cells compared to ABR and ABR-NP.

### Mitochondrial membrane depolarization analysis using JC-1

Mitochondrial membrane depolarization is a signature characteristic of apoptosis, and this can be measured using JC-1 staining (Li et al. 2022). JC-1 is a sensitive marker for mitochondrial membrane potential that accumulates in the mitochondria in a potential-dependent manner. JC-1 forms J-aggregates at high mitochondrial membrane potential, emitting red fluorescence, whereas at low mitochondrial membrane potential, JC-1 remains monomer, emitting green fluorescence. The JC-1 ratio (an indicator of the J-aggregates/monomers ratio) is used to quantify mitochondrial health and activity. An increase in the JC-1 monomer:aggregate ratio (that is, green:red fluorescence intensity) detects an increase in the apoptotic population. In our experiment, the free drug ABR showed a change of green fluorescence to 25.3% after 48 h of treatment. In the case of ABR-NP, the percentage of JC-1 monomer was found to be 48.9% at 48 h of treatment. Cell population with depolarized mitochondria (indicated by green fluorescence) was further increased to 95.3% in the case of Apt-ABR-NP treatment at 48 h (Fig. 6D). The higher cell population with depolarized mitochondria after Apt-ABR-NP treatment represents its potency in higher apoptosis of LNCaP cells compared to ABR or ABR-NP. This finding also correlates well with the outcome of the apoptosis assay.

### In vitro Colony formation assay

Figure 7A shows the representative images of the wells after crystal violet staining of control and the treatment groups ABR, ABR-NP, or Apt-ABR-NP on LNCaP cells. The number and size of the growth of the colonies were found to be reduced in the highest

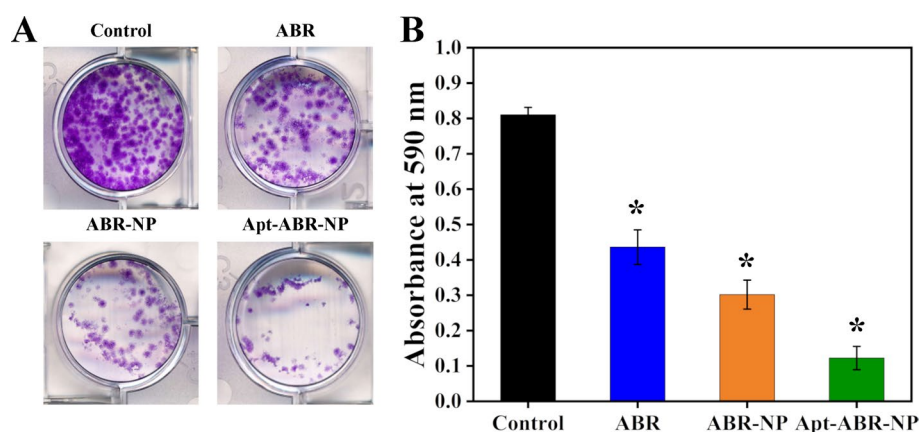


**Fig. 7** Clonogenic assay with LNCaP cells using ABR, ABR-NP, and Apt-ABR-NP. **A** More growth in untreated (control) was followed by ABR, ABR-NP, or Apt-ABR-NP treated LNCaP cells. **B** Absorbance values of untreated (control) and ABR, ABR-NP, or Apt-ABR-NP treated LNCaP cells, after crystal violet staining, represent the colonies' density. Values represent mean  $\pm$  SD ( $n = 3$ ), where \* indicates  $p < 0.05$  is the statistical level of significance, compared against the control value as assessed by Student's  $t$ -test

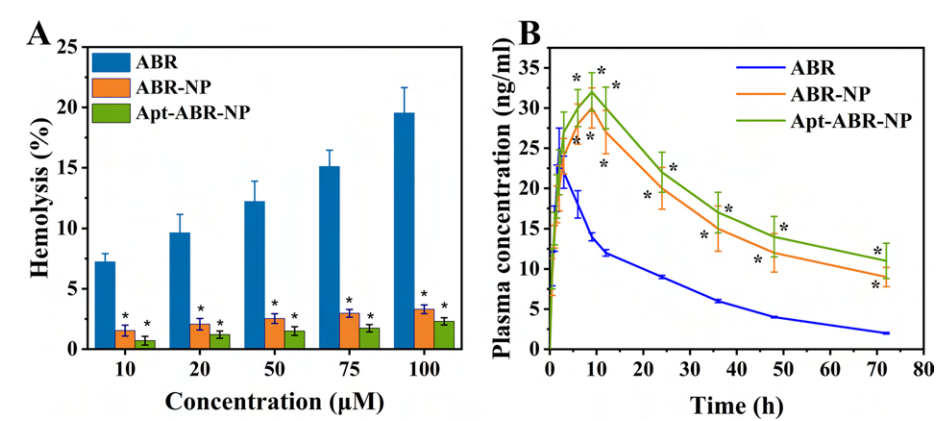


**Fig. 7** Hemolytic activity and pharmacokinetic profile of ABR, ABR-NP, and Apt-ABR-NP. **A** Hemolytic activity of ABR, ABR-NP, and Apt-ABR-NP was measured by incubating each sample with red blood cells and measuring the amount of hemoglobin released. The percentage of hemolysis was plotted against the concentration of the samples. Data show mean  $\pm$  SD ( $n = 3$ ) where  $p < 0.05$  is the statistical level of significance as assessed by Dunnett's test (compared against control group). **B** The pharmacokinetic profile of ABR, ABR-NP, and Apt-ABR-NP was assessed in mice by measuring the concentration of ABR from each sample in the bloodstream over time. The data were plotted as the mean concentration of each sample at each time point. Error bars indicate standard deviation ( $n = 3$ ). \*Marks represent significant values ( $p < 0.05$ ) when ABR-NP and Apt-ABR-NP were compared with ABR through the two-way ANOVA test, and the statistical significance of data was analyzed through Bonferroni's post-test

**Table 1** Pharmacokinetic parameters of ABR, ABR-NP, and Apt-ABR-NP in Swiss Albino mice following intraperitoneal administration (0.4 mg/kg)

Parameters	ABR	ABR-NP	Apt-ABR-NP
$C_{max}$ (ng/ml)	25 $\pm$ 2.5	30 $\pm$ 2.5*	32 $\pm$ 2.4*
$T_{max}$ (h)	2.0 $\pm$ 0.2	1.0 $\pm$ 0.4*	1.0 $\pm$ 0.5*
AUC last (ng h/ml)	540 $\pm$ 20	1204 $\pm$ 100*	1350 $\pm$ 105*
AUC 0– $\infty$ (ng h/ml)	502 $\pm$ 30	1002 $\pm$ 105*	1005 $\pm$ 104*
AUMC (ng h <sup>2</sup> /ml)	12,345 $\pm$ 410	34,325 $\pm$ 544*	30003 $\pm$ 022*
$T_{1/2}$ (h)	12 $\pm$ 0.4	30 $\pm$ 1.0*	30 $\pm$ 2.2*
MRT (h)	22.5 $\pm$ 1.1	20.5 $\pm$ 1.0*	20.2 $\pm$ 1.2*
$V_d$ (ml)	310 $\pm$ 10	430 $\pm$ 12*	415 $\pm$ 20*
Clearance (ml/h)	10.2 $\pm$ 0.0	13 $\pm$ 0.0*	14 $\pm$ 0.2*

Data show mean  $\pm$  SD.  $n = 3$ . Statistical analysis was carried out to one-way ANOVA analysis and the  $p$ -value was calculated through Dunnett's post-test ( $p < 0.05$ ) when compared against ABR control. Data shown in star (\*) are significant compared to the ABR control group

percentage in the case of Apt-ABR-NP treated cells. The absorbance values of the individual wells taken at 590 nm are shown for quantitative comparison (Fig. 7B).

Different therapeutic approaches, such as free drug (ABR), nanoparticulated forms, ABR-NP, and Apt-ABR-NP, inhibited cellular growth. The maximum therapeutic efficacy was observed in the case of Apt-ABR-NP. All the in vitro assays represented the highest anti-proliferative activity in the case of Apt-ABR-NP, which can well correlate with aptamer–PSMA binding mediated accumulation of Apt-ABR-NP in prostate cancer cells.



### Hemolysis study

The drug (ABR) and different nanoformulations (ABR-NP and Apt-ABR-NP) were tested for hemocompatibility in a range of concentration levels (10 to 100  $\mu$ M) (Fig. 8A). The results revealed that the formulations (ABR-NP and Apt-ABR-NP) had low hemolytic activity (< 5%) as compared to that of free ABR at varying concentration levels. The study showed that the tested dose range for both the nanoformulations had low hemolytic activity and may be safely used for intravenous delivery. One of the most important requirements for the effective in vivo application of blood-contacting biomaterials is their hemocompatibility (Krishnan et al. 2023). The hemocompatibility study suggests that the nanoformulations exhibited modest hemolytic activity and were safe for intravenous administration.

### Pharmacokinetics study

In vivo pharmacokinetic profiles of ABR, ABR-NP, and Apt-ABR-NP were assessed in Swiss albino mice. Table 1 represents the pharmacokinetic parameters ( $AUC$ ,  $C_{max}$ ,  $T_{max}$ ,  $AUMC$ ,  $T_{1/2}$ ,  $MRT$ ,  $V_d$ ,  $CL$ ) of ABR, ABR-NP, and Apt-ABR-NP following intraperitoneal injection in Swiss Albino mice (Dutta et al. 2018). ABR (abiraterone acetate) becomes converted into abiraterone (ART) rapidly when it comes in contact with blood plasma, hence reaching a high concentration ( $C_{max} = 25 \pm 2.5$  ng/ml) of ART within a short time ( $T_{max}$ , 2 h) (Fig. 8B). On the other hand, both ABR-NP and Apt-ABR-NP maintained a sustained plasma concentration of ART for a long time (around 24 h). In the case of ABR-NP and Apt-ABR-NP,  $C_{max}$  was reached at around 9 h of injection, followed by a slow elimination phase, suggesting sustained release characteristics of both formulations. The  $AUC$  was increased by 2.2 times and 2.47 times in the case of ABR-NP and Apt-ABR-NP, respectively, compared to the free drug (ABR). The half-life of the active drug (ART) was increased significantly by 3 times and 3.25 times for ABR-NP and Apt-ABR-NP, respectively.  $AUMC$  and  $MRT$  were subsequently increased for both formulations compared to the free drug (ABR). Data suggest an increased bioavailability of the active drug while delivered through nanoparticle formulations. The nanoencapsulation

**Table 1** Biodistribution of  $^{99m}Tc$ -ABR-NP and  $^{99m}Tc$ -Apt-ABR-NP in testosterone/MN-induced prostate cancer-bearing mice

Organ/Tissue	$^{99m}Tc$ -ABR-NP in CRPC mice			$^{99m}Tc$ -Apt-ABR-NP in CRPC mice		
	1 h	2 h	5 h	1 h	2 h	5 h
Blood <sup>a</sup>	3.02 $\pm$ 0.01	3.01 $\pm$ 0.22	3.22 $\pm$ 0.20	4.15 $\pm$ 0.31	3.44 $\pm$ 0.31	3.44 $\pm$ 0.42
Heart	0.545 $\pm$ 0.12	0.02 $\pm$ 0.05	0.04 $\pm$ 0.04	0.12 $\pm$ 0.03	0.22 $\pm$ 0.00	0.30 $\pm$ 0.04
Liver	20.12 $\pm$ 2.10*	24.55 $\pm$ 2.00*	22.44 $\pm$ 4.34*	23.30 $\pm$ 2.55*	2.04 $\pm$ 2.01*	30.5 $\pm$ 1.30*
Lungs	0.53 $\pm$ 0.21	0.53 $\pm$ 0.23	0.03 $\pm$ 0.32	0.03 $\pm$ 0.20	0.04 $\pm$ 0.20	1.142 $\pm$ 0.33
Stomach	0.44 $\pm$ 0.10	0.32 $\pm$ 0.10	0.404 $\pm$ 0.11	0.25 $\pm$ 0.10	0.04 $\pm$ 0.11	0.42 $\pm$ 0.20
Intestine	2.02 $\pm$ 0.51	2.20 $\pm$ 0.31	3.52 $\pm$ 0.30	3.114 $\pm$ 0.12	3.205 $\pm$ 0.55	4.025 $\pm$ 0.02
Kidney	3.452 $\pm$ 0.30	4.34 $\pm$ 0.42	0.03 $\pm$ 0.52*	4.55 $\pm$ 0.45*	0.14 $\pm$ 0.42*	10.24 $\pm$ 0.40*
Prostate	1.42 $\pm$ 0.21	1.11 $\pm$ 0.10*	2.313 $\pm$ 0.22*	2.25 $\pm$ 0.30	2.22 $\pm$ 0.24*	3.142 $\pm$ 0.30*
Urine	2.5 $\pm$ 3.00*	30.5 $\pm$ 2.10*	32.44 $\pm$ 2.14*	30.12 $\pm$ 1.55*	33.5 $\pm$ 2.51*	3.12 $\pm$ 3.10*

<sup>a</sup> Represents  $\mu$ g in the case of blood; otherwise  $\mu$ l in the whole organ

\* are represent statistically significant values when both  $^{99m}Tc$ -ABR-NP and  $^{99m}Tc$ -Apt-ABR-NP are compared for different time points in the  $\alpha$ -ANOVA analysis and tested by Bonferroni post-test  $\alpha$  0.05

of ABR maintained a sustained plasma concentration of ART compared to free-drug treatment. Sustained drug release and predominantly slower elimination of the drug from the nanoparticle caused enhanced plasma half-life of the drug. The overall observation suggests that Apt-ABR-NP had a better pharmacokinetic profile among the experimental formulations for ABR therapy. Aptamer-conjugation on the surface might have improved the aqueous microenvironment on the nanoparticle surface, which might deter drug release further to provide a more sustained drug release profile and improve the pharmacokinetic parameters for Apt-ABR-NP studied here.

#### Biodistribution study and gamma scintigraphy imaging

The distribution of  $^{99m}\text{Tc}$ -radiolabeled nanoparticles in different organs of prostate cancer-bearing Swiss Albino mice is mentioned in Table 2. Data suggest that nanoparticles remained in the blood for a longer time in blood circulation. In contrast, the free drug (ABR) was eliminated rapidly. The majority of the radiolabeled nanoparticles was eliminated through urine.  $^{99m}\text{Tc}$ -ABR-NP and  $^{99m}\text{Tc}$ -Apt-ABR-NP accumulated significantly in the liver, which is common in the nanoparticulated drug delivery system due to the

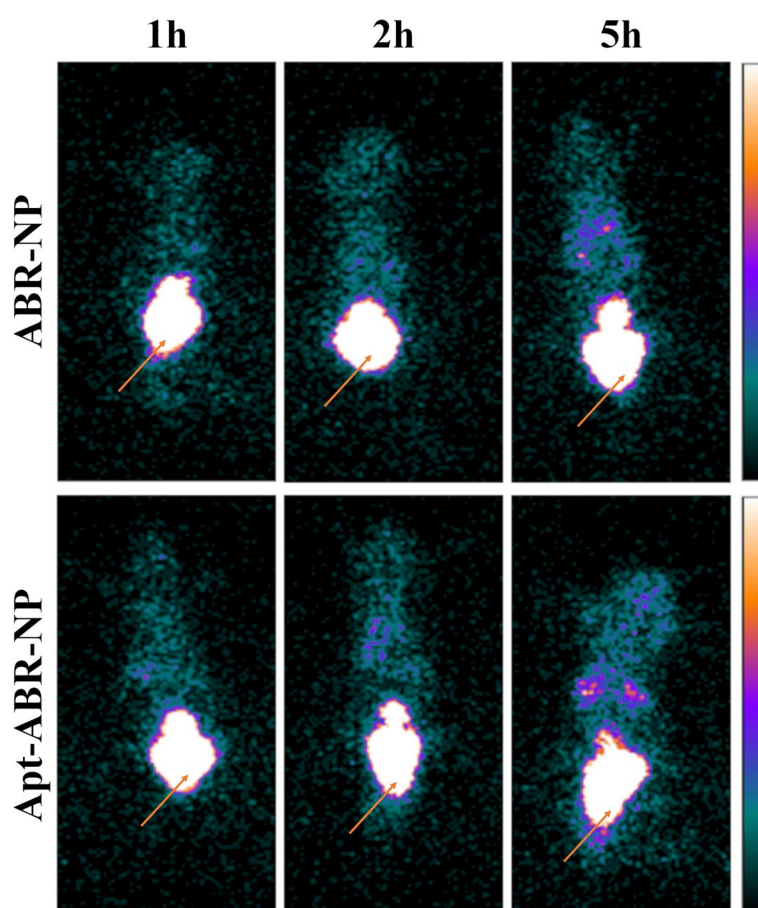


**Fig. 10** Biodistribution study of radiolabelled nanoparticles in various organs using gamma scintigraphic imaging. Radiolabelled nanoparticles ( $^{99m}\text{Tc}$ -ABR-NP and  $^{99m}\text{Tc}$ -Apt-ABR-NP) were injected into mice via tail vein, and gamma scintigraphic images were acquired at different time points (1, 2, and 5 h post-injection) using a gamma camera. Arrows indicate the prostate region in the mice

reticuloendothelial entrapment system (RES) of the liver (Yang et al. 2022). Apart from the liver, the accumulation of nanoparticles in the kidney and intestine was also considerable. Accumulation of  $^{99m}\text{Tc}$ -Apt-ABR-NP in our target organ prostate was much higher than  $^{99m}\text{Tc}$ -ABR-NP in a time-dependent manner (e.g., 3.14% vs. 2.25% at 5 h), suggesting enhanced tumor uptake for aptamer conjugated prostate cancer therapy.

Gamma-scintigraphy images (Fig. 9) revealed deposition of Apt-ABR-NP in the prostate region with the progress of post-injection time. Although urine contained most radioactivity and the bladder covers a wide region, distinguishing the prostate from the bladder was difficult in the scintigraphy images. Signals from other organs, such as the liver, kidney, lungs, intestine, etc., were correlated well with quantitative measurements obtained from the biodistribution study. Gamma-scintigraphy imaging of the prostate cancer animal model following injection of radiolabeled nanoparticles provided in vivo

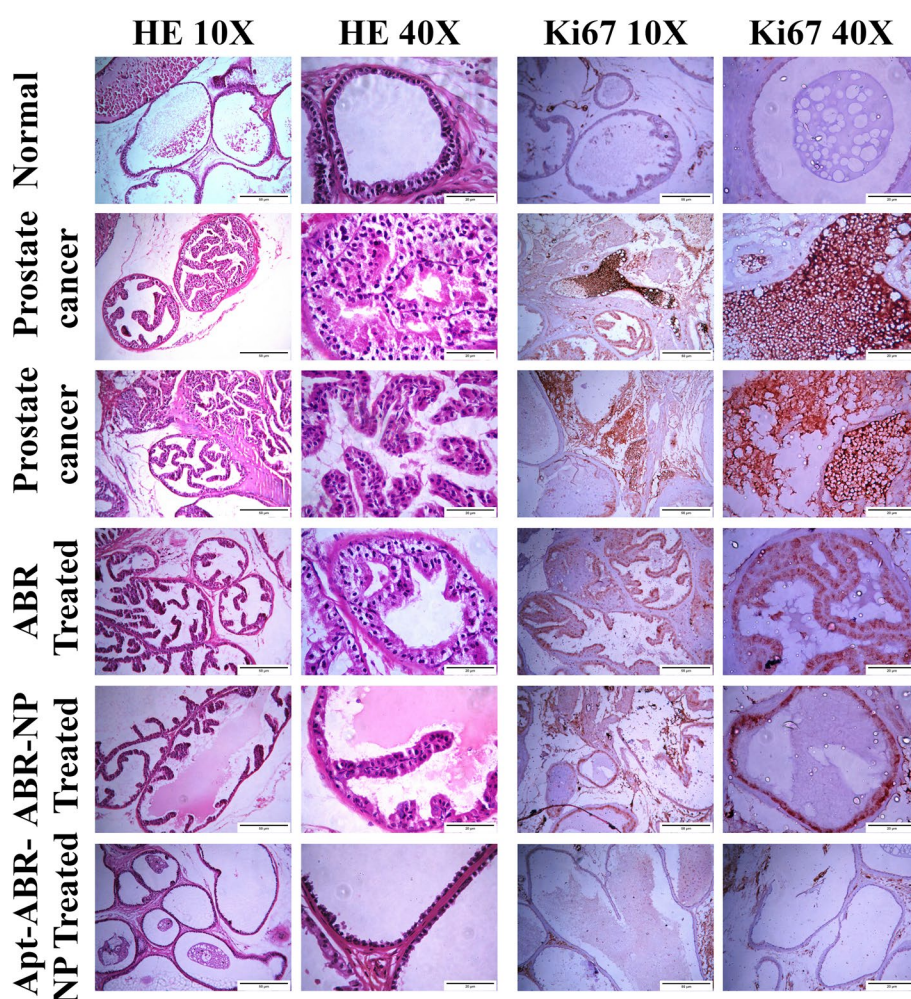


**Fig. 10** Antitumor efficacy of ABR, ABR-NP, and Apt-ABR-NP in prostate cancer (PCa) tissues. Histological examination of prostate cancer tissues and normal prostate tissues was performed using hematoxylin and eosin (HE) staining. Representative images of prostate cancer tissues and normal prostate tissues are shown. The expression of Ki67, a marker of cell proliferation, in prostate cancer tissues and in the normal prostate tissue sections were analyzed by immunohistochemistry. The staining/immunohistochemistry and magnification of the photographs done are mentioned above each column



assessment of experimentally generated nanoparticles (Yin et al. 2017). Radiolabeled PSMA-targeted Apt-ABR-NP signaling was observed to increase the prostate and surrounding area in experimental mice with prostate cancer in a time-dependent manner, ensuring the target specificity of conjugated aptamer toward prostate cancer (Hazra et al. 2021; Shah et al. 2021).

### Antitumor activity study

The microscopic images of normal mouse prostate sections showed the glandular structure of the prostate gland lined with cuboidal epithelial cells arranged in a distinct convoluted pattern (Fig. 10, panel 'Normal'). The lumen of the glands was lined with cuboidal epithelial cells with small nuclei, and the stroma consisted of a thin fibromuscular matrix containing blood vessels and poorly defined smooth muscles. In the 'carcinogen with testosterone'-treated prostate cancer group (panel cancer), the epithelial cells of the glands were transformed into large columnar-like cells that caused shrinkage of the lumen, increased the scalloping of the lumen, and created large intraglandular vacuoles. The thickness of the stroma was increased. Fibromuscular striation was formed in the stroma, representing stromal atrophy (Fig. 10, panel 'Cancer'). In the prostates of 'Cancer' group, glandular hyperplasia and nuclear atypia (large nucleus with distinctively prominent nucleolus) were also observed. According to the Gleason grading system (Munjal and Leslie 2023), the cancers of the MNU with testosterone-treated prostates were found to have pattern 3 carcinomas (i.e., they have recognizable glands with small number of infiltrating invasive cells in the surrounding tissues) and pattern 4 carcinomas (i.e., they have recognizable, glomeruloid glands with a large number of invasive cells in the surrounding tissues forming neoplastic clumps). Hence, they were considered to have either Gleason 7 or Gleason 8 score representing a moderately differentiated to poorly differentiated carcinoma. Treatment with ABR and its formulations ameliorated the prostate's morphological atrophy caused by MNU and testosterone. Treatment with ABR improved the stromal fibromuscular structure but did not completely restore the epithelial convolution pattern similar to the normal prostate. The Gleason grading system of the ABR-treated prostates showed pattern 2 carcinomas (i.e., they have loosely arranged oval-shaped glands with minimal invasion) and pattern 1 carcinoma (i.e., they are very similar to normal prostate tissues with closely packed glands), which gives a Gleason score of 2 or 3 in this case. This represented that treatment with ABR ameliorated the invasiveness of the cancer tissues and helped in restoration of tissue architecture. Treatment with ABR-NP and Apt-ABR-NP further reduced stromal atrophy and restored the epithelial lining convolution comparable to the normal prostate. In ABR-NP and Apt-ABR-NP treated groups, prostate morphology was very similar to normal prostates and Gleason scoring was not determinable. On overall observation, Apt-ABR-NP performed much better in restoring the overall morphological structure of carcinogen with testosterone-treated prostate carcinogenesis group compared to those of ABR and ABR-NP treated groups of animals.

Ki67 is a cell proliferative marker and is considered one of the most important immunohistochemical biomarkers for tumor prognosis (Berlin et al. 2017). Although the grading system in prostate cancer is primarily based on tissue architecture and does not consider the proliferation rate of cells (which is common in grading of many

other cancer), but Ki67 staining provides significant correlation in the clinical estimation of disease prognosis through needle biopsies, transurethral resections, and prostatectomy. In our study, we used Ki67 immunohistochemical staining of mouse prostates to identify any prognostic correlation between the percentage of proliferating cells and disease stage, with or without treatment of ABR and its formulations. The Ki67 staining of 'Normal' prostates showed  $\leq 3\%$  Ki67(+) cells and was considered as negative (Fig. 10, panel 'Normal'). Prostates from MNU + testosterone treated groups (Fig. 10, the 'Cancer' groups) showed 30–50% Ki67(+) cells (counted in areas with  $40\times$  magnifications) and the Gleason score was considered as 2+. In combination with Gleason scores 7 and 8, they represent moderate to poorly differentiated carcinomas with an intermediate proliferation rate. Treatment with ABR, ABR-NP, and Apt-ABR-NP in carcinogenic mice reduced the population of Ki67(+) cells to  $15\pm 2\%$ ,  $10\pm 2\%$ , and  $5\pm 1.5\%$ , respectively (representative images are shown in Fig. 10, panels 'ABR', 'ABR-NP', and 'Apt-ABR-NP'). This represented ABR and its nanoformulations significantly reduced invasiveness of prostate tumors, and this effect was highest in the case of Apt-ABR-NP. Combined analysis of morphological restoration, inhibition of stromal degeneration, and proliferation-inhibition suggests that Apt-ABR-NP could be a good candidate to treat hormone-resistant prostate adenocarcinoma. The findings demand further investigations on it.

#### Effect of Apt-ABR-NP on LNCaP tumor spheroid model

To support the findings of carcinogen-induced prostate cancer mouse model in a more informative and conclusive manner, an additional pharmacodynamic experiment was performed on LNCaP 3D tumor spheroid model. Tumor spheroid is a 3D model with accurate physicochemical environment that is comparable to *in vivo* conditions (Adamiecki et al. 2022; Volpatti and Yetisen 2014).

Cy5-loaded Apt-ABR-NP formulation was used in its  $IC_{50}$  dose on two approximately equal size of LNCaP tumor spheroids. The spheroid was treated with Apt-ABR-NP for once in a day for 3 consecutive days. After 72 h Apt-ABR-NP-treated spheroid reduced its size by nearly 60% (Additional file 1: Figure S3). Cancer control spheroid (without treatment) showed the expression of the DAPI throughout the body, whereas DAPI expression was more peripheral for the Apt-ABR-NP treated spheroid, suggesting less live proliferative cells compared to the cancer control spheroid. Thus the experiment showed predominant role of the Apt-ABR-NP in reducing LNCaP cell tumor.

#### Hematological evaluation

The CBC profile and CRP level of animals from different groups (A–F) are represented in Additional file 1: Table S4. In the case of "Cancer" control group (Group B), lower RBC count and higher WBC count were observed than normal animals. Lowered lymphocyte count and enhanced neutrophil count were also noticed as a mark of higher inflammatory activities in cancer-bearing animals (Group B). Treatment with ABR, ABR-NP, and Apt-ABR-NP treatment increased blood lymphocyte

count and reduced neutrophil count compared to “Cancer” group, suggesting better immunogenic response to treatment. The “Cancer” group of animals also showed a lower platelet count compared to “Normal” group animals. No significant changes were observed in hematocrit volume and hemoglobin content after treatment with ABR, ABR-NP, and Apt-NP in normal mice. Overall observation suggests that treatment with ABR, ABR-NP, and Apt-ABR-NP reduced inflammatory response element (CRP), increased immunogenic response, and subsequently tried to restore CBC profile close to normal. Upon treatment of normal animals with best represented formulation, Apt-ABR-NP (Group F), no significant anomaly was observed in CBC profile, suggesting its biocompatible and non-hemotoxic nature. PSMA analysis showed a high amount of PSMA in blood in cancer-bearing animals ( $25 \pm 1.6$  ng/ml) compared to normal animals ( $5.2 \pm 0.6$  ng/ml). Treatment with ABR, ABR-NP, and Apt-ABR-NP significantly reduced PSMA content in blood ( $15.1 \pm 1.2$ ,  $12.3 \pm 0.9$ ,  $7 \pm 0.5$  ng/ml, respectively). CRP data showed higher level of it in cancer-bearing animals suggesting development of inflammatory conditions. Treating with the experimental nanoparticles resulted lowering of the CRP levels in the blood.

#### Estimation of serum levels of toxicity markers

The levels of serum AST, ALT, and ALP often reveal whether the liver is healthy or diseased (Dhara et al. 2023). In this case, compared to the normal mice, mice exposed to carcinogen had higher serum levels of AST, ALT, and ALP. Carcinogen-treated mice, after the treatment with ABR, ABR-NP, and Apt-ABR-NP, the levels of the enzymes, creatinine and BUN were variably reduced. Additional file 1: Table-S5 reveals that Gr E animals (carcinogenic animals treated with Apt-ABR-NP) had improved to the greatest extent. Additionally, there were no appreciable modifications in Apt-ABR-NP-treated normal mice (Gr F animals) with normal serum AST, ALT, and ALP values. When creatinine and BUN levels in blood serum were measured, the results observed were similar.

The data suggest that the treatment of ABR, ABR-NP and Apt-ABR-NP improved the hepatic and nephrotic toxicity of mice treated with carcinogen. Among the ABR treatment groups Apt-ABR-NP-treated mice showed maximum improvement of the enzyme levels and creatinine and BUN towards the normal values. Normal mice did not show any significant differences in the enzyme levels and concentrations of the creatinine and BUN compared to the normal mice received Apt-ABR-NP treatment. Thus, it suggests Apt-ABR-NP did not show any toxicity in liver and kidneys of normal animals.

The existing therapies, including hormone therapy, surgery, radiation therapy, chemotherapy, etc., have some disadvantages. One such disadvantage is the lack of targeted treatment, i.e., off-target toxicity. Aptamers are called synthetic monoclonal antibodies for their target specificity, but without the toxicity problem. In our research, we have targeted prostate-specific membrane antigen (PSMA) that overexpresses in prostate cancer cells. The anti-PSMA aptamer conjugated formulation specifically binds to the overexpressed PSMA in the cancer cells for the target specific delivery of the drug. So, our designed nanoparticles could be a promising approach for treating prostate cancer and have an edge over the existing formulations.

## Conclusion

A recently discovered aptamer ( $\Delta$ PSap4#5) was conjugated with ABR-NP (Apt-ABR-NP) that predominantly accumulated to PSMA overexpressed prostate cancer. This is the first study in which this aptamer was considered for prostate cancer treatment. Apt-ABR-NP showed better cellular internalization than the non-conjugated formulation. Apt-ABR-NP ensured successful site-specific drug delivery to PSMA-overexpressed prostate cancer cells, Apt-ABR-NP exhibited prolonged blood retention, sustained drug release, and tumor tissue-specific accumulation. The findings presented the aptamer-coupled nanoparticulated therapeutic technique that demonstrated the maximum in vitro and in vivo therapeutic effectiveness of Apt-ABR-NP. We anticipate for a hope of translation of the promising aptamer functionalized nanoparticle toward achieving successful human clinical trials in near future as a possible targeted treatment for prostate cancer. Further studies are warranted.

## Abbreviations

Apt-ABR-NP	Aptamer conjugated abiraterone acetate nanoparticles
ABR	Abiraterone acetate
PLGA	Poly(D,L-lactide-co-glycolide)
PCa	Prostate cancer
FTIR	Fourier transform infrared spectroscopy
FESEM	Field emission scanning electron microscopy
HR-TEM	High-resolution transmission electron microscopy
AFM	Atomic force microscopy
XPS	X-ray photoelectron spectroscopy
FITC	Fluorescein isothiocyanate
PI	Propidium iodide
AUC	Area under the curve

## Supplementary Information

The online version contains supplementary material available at <https://doi.org/10.1186/s12945-023-00223-5>.

**Additional file 1:** Detailed methodology (Preparation of the PLGA nanoparticles, Conjugation of aptamer on the surface of nanoparticles, Determination of aptamer conjugation by agarose gel electrophoresis, Percentage of drug loading and encapsulation efficiency, Stability of the nanoparticles, Hydrolytic stability study, In vitro drug release study), Table S1, Table S2, Table S3, Table S4 and Table S5; Figure S1, Figure S2 and Figure S3.

## Acknowledgements

This work has been supported by the DST Inspire (Department of Science and Technology, Government of India) program with the reference number DST/Inspire Fellowship/2018/IF180404. The authors are also thankful to Dey's Medical Stores (Mfg.) Limited, Kolkata, India, for providing instrumental facilities.

## Author Contributions

AAH and BM developed the concept and design of the project. Synthesis and physicochemical characterizations were performed by AAH, DD, LK, and IE. Agarose gel electrophoresis was performed by AAH and MD. AAH, DD, and BP performed cell assays with the guidance of M and B. SL was associated with LC-MS analysis. In vivo experiments were performed by AAH, BP, and SG. Analysis and interpretation of the data included the contribution of all authors. The manuscript was written by AAH and DD, and edited and revised by BM and M. All authors have approved the final version of the manuscript.

## Availability of data and materials

All data in this study are available from the corresponding authors upon reasonable request.

## Declarations

### Ethics approval and consent to participate

Permission from the Institutional Animal Ethics Committee (IAEC) of Odavpur University was received before commencing any animal experiments (IAEC, Protocol approval. no.: AEC/PHARM/1804/04/2020), under the norms of CPCSEA, Govt. of India (Odavpur University Registration Number in CPCSEA: 1805/G/Re/S/15/CPCSEA). All experiments have been conducted following the guidelines of the Animal Ethics Committee of Odavpur University.

**Consent for publication**

Not applicable.

**Competing interests**

The authors declare no conflict of interest.

Received: 27 June 2022 Accepted: 14 August 2022

Published online: 04 September 2023

**References**

- Adamecki R, Hryniewicz-Bankowska A, Ortiz MA, Li X, Porter-Hansen BA, Nsouli I et al (2022) In vivo models for prostate cancer research. *Cancers (basel)* 14(21):1–20
- Alshaer W, Hillaireau H, Fattal E (2019) Aptamer-guided nanomedicines for anticancer drug delivery. *Adv Drug Deliv Rev* 134:122–130
- Benoist GE, Hendriks R, Mulders PFA, Gerritsen WR, Somford DM, Schalken EA et al (2019) Pharmacokinetic aspects of the two novel oral drugs used for metastatic castration-resistant prostate cancer: abiraterone acetate and enzalutamide. *Clin Pharmacokinet* 55(11):1300–1300
- Berlin A, Castro-Mesta X, Rodriguez-Romo L, Hernandez-Barajas D, Gonzalez-Guerrero X, Rodriguez-Fernandez IA et al (2019) Prognostic role of Ki-67 score in localized prostate cancer: a systematic review and meta-analysis. *Urol Oncol Semin Orig Invest* 35(4):400–500
- BioA Discovery Studio, BioA Dassault Systèmes®
- Bouhajib M, Tayab M (2019) Evaluation of the pharmacokinetics of abiraterone acetate and abiraterone following single-dose administration of abiraterone acetate to healthy subjects. *Clin Drug Investig* 39(3):300–310
- Chakraborty S, Dlie X, Chakraborty S, Roy S, Mukherjee B, Besra SE et al (2020a) Aptamer-functionalized drug nanocarrier improves hepatocellular carcinoma toward normal by targeting neoplastic hepatocytes. *Mol Ther Nucleic Acids* 20:34–40
- Chakraborty S, Dlie X, Mukherjee B, Besra SE, Sengupta S, Sen R et al (2020b) A comparative investigation of the ability of various aptamer-functionalized drug nanocarriers to induce selective apoptosis in neoplastic hepatocytes: in vitro and in vivo outcome. *AAPS PharmSciTech* 21(3):1–13
- Champion VA, Batare X, Mitragotri S (2009) Particle shape: a new design parameter for micro- and nanoscale drug delivery carriers. *Control Release* 121(1–2):3–0
- Chen ML, Lai C, Lin N, Huang CM, Lin H (2020) Multifunctional nanoparticles for targeting the tumor microenvironment to improve synergistic drug combinations and cancer treatment effects. *Mater Chem B* 8(45):10410–10420
- Choi WI, Lee H, Kim X, Heo S, Jeong X, Kim X et al (2015) Targeted antitumor efficacy and imaging via multifunctional nano-carrier conjugated with anti-HER2 trastuzumab. *Nanomed Nanotechnol Biol Med* 11(2):350–300
- Clogston D, Patri A (2011) Zeta potential measurement. *Methods Mol Biol* 1000:3–0
- Correa S, Dreaden EC, Gu L, Hammond PT (2019) Engineering nanolayered particles for modular drug delivery. *Control Release* 240:304–300
- Danhier F, Ansorena E, Silva M, Coco R, Le Breton A, Prasad (2012) PLGA-based nanoparticles: an overview of biomedical applications. *Control Release* 181(2):505–522
- Dassie P, Liu X, Thomas GS, Whitaker RM, Thiel W, Stockdale R et al (2009) Systemic administration of optimized aptamer-siRNA chimeras promotes regression of PSMA-expressing tumors. *Nat Biotechnol* 29(10):1030–1040
- Dhara M, Al Hoque A, Sen R, Dutta D, Mukherjee B, Paul B et al (2023) Phosphorothioated amino-AS1411 aptamer functionalized stealth nanoliposome accelerates bio-therapeutic threshold of apigenin in neoplastic rat liver: a mechanistic approach. *Nanobiotechnol* 21(1):20
- Diepstraten ST, Anderson MA, Czabotar PE, Lessene G, Strasser A, Kelly GL (2022) The manipulation of apoptosis for cancer therapy using BH3-mimetic drugs. *Nat Rev Cancer* 22(1):45–54
- Dutta D, Chakraborty A, Mukherjee B, Gupta S (2019) Aptamer-conjugated apigenin nanoparticles to target colorectal carcinoma: a promising safe alternative of colorectal cancer chemotherapy. *ACS Appl Bio Mater* 1(5):1530–1550
- Dutta D, Paul B, Mukherjee B, Mondal L, Sen S, Chowdhury C et al (2019) Nanoencapsulated betulinic acid analogue distinctively improves colorectal carcinoma in vitro and in vivo. *Sci Rep* 9(1):11500
- Ehsan I, Umari L, Sen R, Al Hoque A, Mukherjee B, Mukherjee A et al (2022) 501 functionalized paclitaxel-loaded PLGA nanoparticles successfully inhibited PSMA overexpressing LNCaP cells. *Drug Deliv Sci Technol* 85:103000
- Fan L, Campagnoli S, Wu H, Grandi A, Parri M, De Camilli E et al (2015) Negatively charged AuNP modified with monoclonal antibody against novel tumor antigen FAT1 for tumor targeting. *Exp Clin Cancer Res* 34(1):103
- Fan L, Gong X, He X, Gao W, Dong X, Dong B et al (2022) TRIM5 is suppressed by androgen receptor and acts to promote lineage plasticity and treatment-induced neuroendocrine differentiation in prostate cancer. *Oncogene* 42(5):550–501
- Gala M, Miller D, Williams R (2020) Improved dissolution and pharmacokinetics of abiraterone through kinetisol® enabled amorphous solid dispersions. *Pharmaceutics* 12(4):350
- Gray BP, Kelly L, Ahrens DP, Barry AP, Ratschmer C, Levy M et al (2019) Tunable cytotoxic aptamer–drug conjugates for the treatment of prostate cancer. *Proc Natl Acad Sci USA* 115(10):4001–4000
- Hashemi M, Shamschiri A, Saeedi M, Tayebi L, Razdian-Robati R (2020) Aptamer-conjugated PLGA nanoparticles for delivery and imaging of cancer therapeutic drugs. *Arch Biochem Biophys* 681:100405
- Hazra RS, Dutta D, Mamnoon B, Nair G, Knight A, Mallik S et al (2021) Polymeric composite matrix with high biobased content as pharmaceutically relevant molecular encapsulation and release platform. *ACS Appl Mater Interfaces* 13(34):40220–40240
- Heydari-Bafrooei E, Shamszadeh NS (2019) Electrochemical bioassay development for ultrasensitive aptasensing of prostate specific antigen. *Biosens Bioelectron* 112:204–202



- Huang D, Sun L, Huang L, Chen X (2021) Nanodrug delivery systems modulate tumor vessels to increase the enhanced permeability and retention effect. *Pers Med* 11(2):1–20
- Jain GK, Pathan SA, Akhter S, Ahmad N, Jain N, Talegaonkar S et al (2010) Mechanistic study of hydrolytic erosion and drug release behaviour of PLGA nanoparticles: influence of chitosan. *Polym Degrad Stab* 12(5):230–238
- Abanov A, Batrakova E (2000) Polymer nanomaterials. In: *Neuroimmune Pharmacology*, pp 881–888
- Kato M, Sasaki T, Inoue T (2021) Current experimental human tissue-derived models for prostate cancer research. *Int J Urol* 28(2):150–162
- Irishnan V, Venkatasubbu GD, Malaivani T, Irishnan V, Venkatasubbu GD, Malaivani T (2023) Investigation of hemolysis and antibacterial analysis of curcumin-loaded mesoporous SiO<sub>2</sub> nanoparticles. *Appl Nanosci* 13(1):11–18
- Umar L, Ehsan I, Mondal A, Al Hoque A, Mukherjee B, Choudhury P et al (2023) Cetuximab-conjugated PLGA nanoparticles as a prospective targeting therapeutics for non-small cell lung cancer. *Drug Target* 31(5):521–530
- Lawrence MG, Pook DW, Wang H, Porter LH, Frydenberg M, Mourambas V et al (2015) Establishment of primary patient-derived xenografts of palliative TRP specimens to study castrate-resistant prostate cancer. *Prostate* 85(13):1405–1413
- Li X, Fahrman F, Aftabzadeh M, Zhao X, Tripathi SC, Zhang C et al (2022) Fatty acid oxidation protects cancer cells from apoptosis by increasing mitochondrial membrane lipids. *Cell Rep* 38(8):110880
- Liu X, Popov P, Böhler P, Wolf P, Pan H, Bauer H et al (2000) Biorecognition and subcellular trafficking of HPMA copolymer-anti-PSMA antibody conjugates by prostate cancer cells. *Mol Pharm* 3(3):55–60
- Luo D, Wang X, Feng S, Ramamurthy G, Burda C, Basilion P (2018a) Prostate-specific membrane antigen targeted gold nanoparticles for prostate cancer radiotherapy: does size matter for targeted particles? *Chem Sci* 10(35):1118–1120
- Luo X, Zhang X, Song F, Zhang L, Wei X (2018b) CD30 aptamer-functionalized PEG-PLGA nanoparticles for the superior delivery of doxorubicin to anaplastic large cell lymphoma cells. *Int J Pharm* 544:340–348
- Madani SH, Ameli S, Hazei S, Anani M, Izadi B (2011) Frequency of MIB-1 and P53 expressions among patients with prostate cancer. *Indian J Pathol Microbiol* 54(4):808–811
- Mukherjee B, Mayer D (2000) Dihydrotestosterone interacts with EGFR/MAPK signalling and modulates EGFR levels in androgen receptor-positive LNCaP prostate cancer cells. *Int J Oncol* 33(3):23–32
- Munjal A, Leslie SW (2023) Gleason score. *Encycl Genet genomics, proteomics informatics*. StatPearls Publishing, pp 800–800
- Nahata A, Dixit A (2012) Ganoderma lucidum is an inhibitor of testosterone-induced prostatic hyperplasia in rats. *Andrologia* 44:100–104
- Pagels RF, Prud'Homme R (2015) Polymeric nanoparticles and microparticles for the delivery of peptides, biologics, and soluble therapeutics. *Control Release* 215:515–535
- Panyam J, Zhou W, Prabha S, Sahoo SK, Labhasetwar V (2002) Rapid endo-lysosomal escape of poly(DL-lactide-co-glycolide) nanoparticles: implications for drug and gene delivery. *FASEB J* 16(10):1218–1220
- Papachristou F, Anninou N, Koukoulis G, Paraskakis S, Sertaridou E, Tsilikidis C et al (2021) Differential effects of cisplatin combined with the flavonoid apigenin on HepG2, Hep3B, and Huh7 liver cancer cell lines. *Mutat Res Genet Toxicol Environ Mutagen* 888:503352
- Pattnaik G, Sinha B, Mukherjee B, Ghosh S, Basak S, Mondal S et al (2012) Submicron-size biodegradable polymer-based didanosine particles for treating HIV at early stage: an in vitro study. *Microencapsul* 29(8):800–808
- Paul B, Gaonkar RH, Mukhopadhyay R, Ganguly S, Debnath MC, Mukherjee B (2010) Garcinol-loaded novel cationic nanoliposomes: in vitro and in vivo study against B16F10 melanoma tumor model. *Nanomedicine (Lond)* 14(15):2045–2055
- Petros RA, Desimone JM (2010) Strategies in the design of nanoparticles for therapeutic applications. *Nat Rev Drug Discov* 9(2):15–22
- Pierorazio PM, Walsh PC, Partin AW, Epstein JI (2013) Prognostic Gleason grade grouping: data based on the modified Gleason scoring system. *Int J* 111(5):53–60
- Pokrovsky S, Bolottsev A, Latysheva AS, Rudinov A, Anisimova N, Almanza RLM et al (2020) Alsevirone-NF reduces serum testosterone and inhibits prostate cancer xenograft growth in Balb/c nude mice. *Clin Cancer Drugs* 2(2):113–118
- Ramdhani D, Listiani N, Sriyani ME, Maria WE, Watabe H, Mustarichie R et al (2023) Estrogen receptor targeting with genistein radiolabeled Technetium-99m as radiotracer of breast cancer: Its optimization, characterization, and predicting stability constants by DFT calculation. *Heliyon* 9(2):e13188
- Rockey WM, Hernandez F, Huang S, Cao S, Howell CA, Thomas GS et al (2011) Rational truncation of an RNA aptamer to prostate-specific membrane antigen using computational structural modeling. *Nucleic Acid Ther* 21(5):288–314
- Ruoslahti E, Bhatia SN, Sailor M (2010) Targeting of drugs and nanoparticles to tumors. *Cell Biol* 188(2):55–60
- Savory N, Abe X, Sode X, Ikebukuro X (2010) Selection of DNA aptamer against prostate specific antigen using a genetic algorithm and application to sensing. *Biosens Bioelectron* 25(4):1300–1301
- Schleicher RL, Fallon MT, Austin GE, Zheng M, Zhang M, Dillehay DL et al (1999) Intravenous vs Intraprostatic administration of N-methyl-N-nitrosourea to induce prostate cancer in rats MN<sub>4</sub>-induced prostate cancer in rats. *Aff Med Cent* 2:32–35
- Sen R, Mukherjee B, Ganguly S, Sinha S (2023) Surface-functionalized luteolin-loaded nanocarriers successfully delayed lung cancer progress in rats. *Mater Sci* 58(10):31–35
- Shah B, Hunt D, Misra M (2021) Comparative evaluation of intranasally delivered quetiapine loaded mucoadhesive microemulsion and polymeric nanoparticles for brain targeting: pharmacokinetic and gamma scintigraphy studies. *Futur J Pharm Sci* 1(1):1–12
- Shahriari M, Taghdisi SM, Abnous V, Ramezani M, Alibolandi M (2021) Self-targeted polymersomal co-formulation of doxorubicin, camptothecin and Folate aptamer for efficient treatment of non-small cell lung cancer. *Control Release* 335:304–310
- Shishparenok AN, Furman V, Dhanov DD (2023) DNA-based nanomaterials as drug delivery platforms for increasing the effect of drugs in tumors. *Cancers (basel)* 15(8):1–5

- Solymosi T, Tóth F, Rosz B, Basa-Dönes Z, Angi R, Bördös T et al (2018) Solubility measurements at 200 and 310 K and physicochemical characterization of abiraterone and abiraterone acetate. *Chem Eng Data* 13(12):4453–4458
- Souada M, Piro B, Reisberg S, Anquetin G, Noël X, Pham MC (2015) Label-free electrochemical detection of prostate-specific antigen based on nucleic acid aptamer. *Biosens Bioelectron* 66:48–54
- Sung H, Ferlay J, Siegel RL, Laversanne M, Soerjomataram I, Jemal A et al (2021) Global Cancer Statistics 2020: Global Cancer estimates of incidence and mortality worldwide for 36 cancers in 185 countries. *CA Cancer Clin* 71(3):209–248
- Tătaru S, Martha Z, Crocetto F, Barone B, Goidazan S, Borda A et al (2021) Fascin-1 and its role as a serological marker in prostate cancer: a prospective case-control study. *Future Sci* 6(5):F5045
- Thasneem MM, Sajeeesh S, Sharma CP (2011) Effect of thiol functionalization on the hemo-compatibility of PLGA nanoparticles. *Biomed Mater Res A* 93(4):1008–1018
- Tong R, Gabrielson NP, Fan TM, Cheng X (2012) Polymeric nanomedicines based on poly(lactide) and poly(lactide-co-glycolide). *Curr Opin Solid State Mater Sci* 18(3):323–332
- Torchilin VP (2008) Targeted pharmaceutical nanocarriers for cancer therapy and imaging. *AAPS PharmSciTech* 9(1):E128–E140
- Tuerk C, Gold L (1990) Systematic evolution of ligands by exponential enrichment: RNA ligands to bacteriophage T4 DNA polymerase. *Science* 249(4959):505–510
- Tzouavadaki I, Bolly P, Lu X, Ingebrandt S, De Micheli G, Estrela P et al (2018) Label-free ultrasensitive memristive aptasensor. *Nano Lett* 18(4):4402–4408
- Volpatti LR, Petisen AM (2014) Commercialization of microfluidic devices. *Trends Biotechnol* 32(3):340–350
- Wan L, Juan WF, Ai WB, Ai W, Wang X, Chu L et al (2018) An exploration of aptamer internalization mechanisms and their applications in drug delivery. *Expert Opin Drug Deliv* 15(3):209–218
- Wang X, Li P, Song L (2013) Chitosan-modified PLGA nanoparticles with versatile surface for improved drug delivery. *AAPS PharmSciTech* 14(2):505–512
- Wang R, Chu GC, Wang X, Wu B, Hu P, Multani AS et al (2018) Establishment and characterization of a prostate cancer cell line from a prostatectomy specimen for the study of cellular interaction. *Int J Cancer* 145(2):2248–2255
- Weatherby D, Ferguson S (2004) Blood chemistry and CBC analysis. Weatherby Associates, Bloomfield
- Wolff A, Frank M, Staehle S, Peters M (2022) A comparative study on the adipogenic differentiation of mesenchymal stem/stromal cells in 2D and 3D culture. *Cells* 11(8):1313
- Yadav SS, Sawant M (2010) Modified nanoprecipitation method for preparation of cytarabine-loaded PLGA nanoparticles. *AAPS PharmSciTech* 11(3):1458
- Yallapu MM, Khan S, Maher DM, Ebeling MC, Sundram M, Chauhan N et al (2014) Anti-cancer activity of curcumin loaded nanoparticles in prostate cancer. *Biomaterials* 35(30):835–844
- Yan X, Tao H, He X, Huang S (2020) The HDOCK server for integrated protein-protein docking. *Nat Protoc* 15(5):1828–1852
- Yang S, Cai C, Wang H, Ma X, Shao A, Sheng M et al (2022) Drug delivery strategy in hepatocellular carcinoma therapy. *Cell Commun Signal* 20(1):1–14
- Yin X, Wang P, Yin X, Hou X, Song X (2018) Optimization on biodistribution and antitumor activity of tripteryrin using polymeric nanoparticles through RES saturation. *Drug Deliv* 24(1):1001–1010
- Zununi Zahed S, Fathi N, Samiei M, Maleki Dizaj S, Sharifi S (2018) Targeted cancer drug delivery with aptamer-functionalized polymeric nanoparticles. *Drug Target* 26(3):202–210

## Publisher's Note

Springer Nature remains neutral with regard to jurisdictional claims in published maps and institutional affiliations.

**Ready to submit your research? Choose BMC and benefit from:**

- fast, convenient online submission
- thorough peer review by experienced researchers in your field
- rapid publication on acceptance
- support for research data, including large and complex data types
- gold Open Access which fosters wider collaboration and increased citations
- maximum visibility for your research: over 100M website views per year

**At BMC, research is always in progress.**

Learn more [biomedcentral.com/submissions](https://biomedcentral.com/submissions)



RESEARCH

Open Access



# Phosphorothioated amino-AS1411 aptamer functionalized stealth nanoliposome accelerates bio-therapeutic threshold of apigenin in neoplastic rat liver: a mechanistic approach

Moumita Dhara<sup>1</sup>, Ashique Al Hoque<sup>1,2</sup>, Ramkrishna Sen<sup>1</sup>, Debasmita Dutta<sup>3,4</sup>, Biswajit Mukherjee<sup>1\*</sup>, Brahamacharry Paul<sup>1</sup> and Soumik Laha<sup>5</sup>

## Abstract

Hepatocellular carcinoma (HCC) is a leading cause of death globally. Even though the progressive invention of some very potent therapeutics has been seen, the success is limited due to the chemotherapeutic resistance and recurrence in HCC. Advanced targeted treatment options like immunotherapy, molecular therapy or surface-engineered nanotherapeutics could offer the benefits here owing to drug resistance over tumor heterogeneity. We have developed tumor-sensing phosphorothioate and amino-modified aptamer (AS1411)-conjugated stealth nanoliposomes, encapsulating with apigenin for precise and significant biodistribution of apigenin into the target tumor to exploit maximum bio-therapeutic assistances. The stable aptamer functionalized PEGylated nanoliposomes (Apt-NLCs) had an average vesicle size of 100–150 nm, a smooth surface, and an intact lamellarity, as ensured by DLS, FESEM, AFM, and Cryo-TEM. This study has specified in vitro process of optimum drug (apigenin) extrusion into the cancer cells by nucleolin receptor-mediated cellular internalization when delivered through modified AS1411 functionalized PEGylated nanoliposomes and ensured irreversible DNA damage in HCC. Significant improvement in cancer cell apoptosis in animal models, due to reduced clearance and higher intratumor drug accumulation along with almost nominal toxic effect in liver, strongly supports the therapeutic potential of aptamer-conjugated PEGylated nanoliposomes compared to the nonconjugated formulations in HCC. The study has established a robust superiority of modified AS1411 functionalized PEGylated nanoliposomes as an alternative drug delivery approach with momentous reduction of HCC tumor incidences.

**Keywords** Aptamer, Apigenin, Stealth nanoliposomes, Intratumor drug accumulation, Apoptosis, Pharmacokinetics

\*Correspondence:

Biswajit Mukherjee

biswajit.mukherjee@jadavpuruniversity.in; biswajit55@yahoo.com

Full list of author information is available at the end of the article



© The Author(s) 2023. **Open Access** This article is licensed under a Creative Commons Attribution 4.0 International License, which permits use, sharing, adaptation, distribution and reproduction in any medium or format, as long as you give appropriate credit to the original author(s) and the source, provide a link to the Creative Commons licence, and indicate if changes were made. The images or other third party material in this article are included in the article's Creative Commons licence, unless indicated otherwise in a credit line to the material. If material is not included in the article's Creative Commons licence and your intended use is not permitted by statutory regulation or exceeds the permitted use, you will need to obtain permission directly from the copyright holder. To view a copy of this licence, visit <http://creativecommons.org/licenses/by/4.0/>. The Creative Commons Public Domain Dedication waiver (<http://creativecommons.org/publicdomain/zero/1.0/>) applies to the data made available in this article, unless otherwise stated in a credit line to the data.



# Investigation of Paracetamol Entrapped Nanoporous Silica Nanoparticles in Transdermal Drug Delivery System

Sourav Adhikary<sup>1</sup> · Ashique Al Hoque<sup>2,3</sup> · Manisheet Ray<sup>2</sup> · Swastik Paul<sup>4</sup> · Akbar Hossain<sup>5</sup> · Subrata Goswami<sup>6</sup> · Rajib Dey<sup>7</sup>

Accepted: 24 May 2023 / Published online: 5 June 2023

© The Author(s), under exclusive licence to Springer Science+Business Media, LLC, part of Springer Nature 2023

## Abstract

An effort was made to administer paracetamol drug through transdermal patch, as no such formulation of this drug has been developed yet. The primary cause for the lack of such formulations is paracetamol's poor aqueous solubility. As a result, the current research concentrated on preparing nanomedicines, or drug-loaded nanoparticles, for delivery via transdermal formulations. Nanoparticles can improve the solubility of weakly aqueous soluble or even aqueous insoluble drugs by changing the crystalline structure of loaded medicines to an amorphous state and serving as drug permeation boosters. Silica nanoparticles (SNPs) were synthesized through sol-gel technique to achieve the aforementioned goal. DLS data revealed that the average particle size was around 100–200 nm, which was sufficient to penetrate the skin barrier. XRD analysis showed that the SNPs were amorphous, and the drug molecules lost their crystallinity after encapsulation into the nanoparticles, causing the enhancement of dissolution of drug molecules in physiological pH (pH—7.4). Different kinetic models were employed for the ex vivo dissolution data to evaluate the suitable kinetic model followed by the drug release in both burst and sustained phase. In vivo analgesic study was executed on mice applying each of the transdermal formulations to examine the performances of the patches.

**Keywords** Silica nanoparticles · Transdermal patch · Sustained release · Skin permeation · Analgesic activity

---

✉ Sourav Adhikary  
SOURAVADHIKARY906@GMAIL.COM

<sup>1</sup> School of Materials Science and Nanotechnology, Jadavpur University, Kolkata, India

<sup>2</sup> Department of Pharmaceutical Technology, Jadavpur University, Kolkata, India

<sup>3</sup> Department of Coatings and Polymeric Materials, North Dakota State University, Fargo, ND 58108, USA

<sup>4</sup> Department of Chemical Engineering, University of Calcutta, Kolkata, India

<sup>5</sup> Department of Chemistry, Jadavpur University, Kolkata, India

<sup>6</sup> Department of Labour, ESI Institute of Pain Management, Kolkata, India

<sup>7</sup> Metallurgical and Material Engineering Department, Jadavpur University, Kolkata, India

ORIGINAL ARTICLE



# Cetuximab-conjugated PLGA nanoparticles as a prospective targeting therapeutics for non-small cell lung cancer

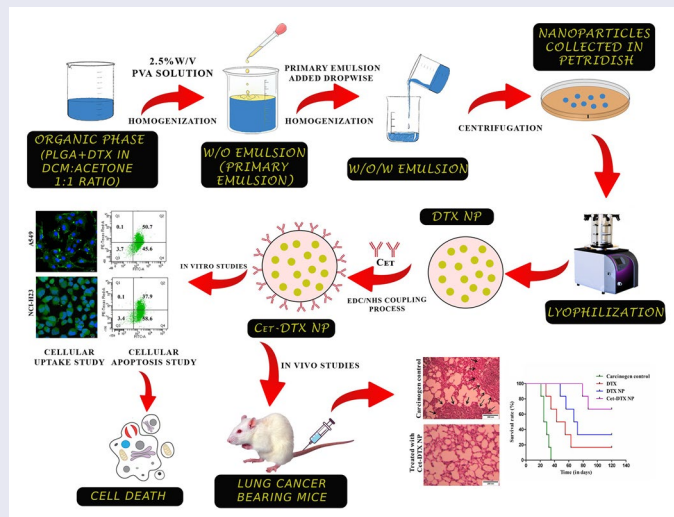
Leena Kumari<sup>a</sup>, Iman Ehsan<sup>a</sup>, Arunima Mondal<sup>b</sup>, Ashique Al Hoque<sup>a</sup>, Biswajit Mukherjee<sup>a</sup>, Pritha Choudhury<sup>c</sup>, Arunima Sengupta<sup>b</sup>, Ramkrishna Sen<sup>a</sup> and Prasanta Ghosh<sup>a</sup>

<sup>a</sup>Department of Pharmaceutical Technology, Jadavpur University, Kolkata, India; <sup>b</sup>Department of Life Science and Biotechnology, Jadavpur University, Kolkata, India; <sup>c</sup>Department of Cardiovascular and Metabolic Sciences, Lerner Research Institute, Cleveland Clinic, Ohio, USA

## ABSTRACT

Non-small cell lung cancer (NSCLC) is one of the most prevalent cancers diagnosed worldwide, yet managing it is still challenging. The epidermal growth factor receptor (EGFR) exhibits aberrant signalling in a wide range of human cancers, and it is reported to overexpress in most NSCLC cases. The monoclonal antibody [Cetuximab (Cet)] was conjugated onto the surface of the poly (lactide-co-glycolide) (PLGA) nanoparticles which were loaded with docetaxel (DTX) for the development of targeted therapy against lung cancer. This site-specific delivery system exhibited an enhanced cellular uptake in lung cancer cells which overexpress EGFR (A549 and NCI-H23). The nanoparticles also showed better therapeutic effectiveness against NSCLC cells, as evidenced by reduced  $IC_{50}$  values, cell cycle arrest at the G2/M phase, and increased apoptosis. The improved efficacy and *in vivo* tolerance of Cet-DTX NPs were demonstrated in benzo(a)pyrene (BaP)-induced lung cancer mice model. Histopathological analysis showed that intravenous injection of Cet-DTX NP to mice carrying lung cancer greatly reduced tumour development and proliferation. Comparing Cet-DTX NP to free drug and unconjugated nanoparticles, it also had negligible side effects and improved survival rates. Therefore, Cet-DTX NPs present a promising active targeting carrier for lung tumour-NSCLC-selective treatment.

## GRAPHICAL ABSTRACT



## ARTICLE HISTORY

Received 13 January 2023  
Revised 20 March 2023  
Accepted 27 March 2023

## KEYWORDS


Non-small cell lung cancer; epithelial growth factor receptor; PLGA nanoparticles; docetaxel; site-specific targeting

## Introduction

Non-small cell lung cancer (NSCLC), which makes up more than 80% of all lung cancer cases, is still the most common cancer-related fatality globally. NSCLC is responsible for approximately a quarter of all cancer fatalities, outnumbering colon, breast, and prostate cancers [1]. Treatment of NSCLC patients with surgery and chemotherapy is hampered by late diagnosis. Furthermore, the lack of tumour selectivity in these techniques leads to increased toxicity

in patients, limiting the therapeutic efficacy [2]. Platinum drugs, taxanes including paclitaxel (PTX) and docetaxel (DTX), albumin-bound PTX, and other types of chemotherapy are all suggested for NSCLC. Among the taxane groups, DTX is quite effective for a wide spectrum of cancers. It has been shown to block microtubule depolymerisation of free tubulin in preclinical experiments in a range of murine malignancies and human tumour xenografts, including NSCLC [3].

**CONTACT** Biswajit Mukherjee ✉ [biswajit.mukherjee@jadavpuruniversity.in](mailto:biswajit.mukherjee@jadavpuruniversity.in); [biswajit55@yahoo.com](mailto:biswajit55@yahoo.com) Department of Pharmaceutical Technology, Jadavpur University, Kolkata 700 032, India.

 Supplemental data for this article can be accessed online at <https://doi.org/10.1080/1061186X.2023.2199350>.

© 2023 Informa UK Limited, trading as Taylor & Francis Group



# Robust biocompatible bacterial cellulose/silk nonwoven fabric/silk sericin sandwich membrane with strong UV-blocking and antioxidant properties

Ke Wang · Raj Shankar Hazra · Qian Ma · Md Rakib Hasan Khan · Ashique Al Hoque · Long Jiang · Mohiuddin Quadir · Yuanming Zhang · Shudong Wang · Guangting Han

Received: 22 November 2022 / Accepted: 12 February 2023 / Published online: 21 February 2023  
© The Author(s), under exclusive licence to Springer Nature B.V. 2023

**Abstract** Kombucha-derived bacterial cellulose (KBC) is a unique natural polysaccharide that has gained increasing interest in biomedical and other applications. However, the relatively low bioactivity of the product has limited its practical applications. In this work, KBC and silk nonwoven fabric (SNF) were integrated to produce a sandwich membrane through in situ growth of KBC in the presence

of SNF. Scanning electron microscopy (SEM) showed that KBC grew not only on the surface of SNF but also within the fiber network of SNF. The strength and modulus of SNF were significantly increased after the integration of KBC. The KBC/SNF sandwich membrane was further impregnated with silk sericin (SS) through simple solution absorption to impart strong UV shielding property to the material, which was demonstrated by the near zero UV transmittance of the new KBC/SNF-SS membrane. SEM, Fourier transform infrared spectrometry, and X-ray diffraction results indicated the interactions between the three components. DPPH (2,2-Diphenyl-1-picrylhydrazyl) radical scavenging test

Ke Wang and Raj Shankar Hazra are contributed equally to this work.

**Supplementary Information** The online version contains supplementary material available at <https://doi.org/10.1007/s10570-023-05102-1>.

K. Wang · Y. Zhang (✉) · G. Han (✉)  
State Key Laboratory of Bio-Fibers and Eco-Textiles,  
College of Textile and Clothing, Qingdao University,  
Qingdao 266071, China  
e-mail: zhangyuanming001@163.com

G. Han  
e-mail: kychgt@qdu.edu.cn

K. Wang  
e-mail: ycfywk@126.com

K. Wang · Q. Ma · S. Wang  
Jiangsu Province Engineering Research Center of Biomass  
Functional Textile Fiber Development and Application,  
Department of Textile and Clothing, Yancheng Polytechnic  
College, Yancheng 224005, China  
e-mail: qian.ma@ndsu.edu

S. Wang  
e-mail: sdwang1983@163.com

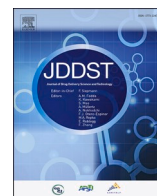
K. Wang · R. S. Hazra · Q. Ma · L. Jiang (✉)  
Department of Mechanical Engineering, Materials  
and Nanotechnology Program, North Dakota State  
University, Fargo, ND 58108, USA  
e-mail: long.jiang@ndsu.edu

R. S. Hazra  
e-mail: raj.hazra@ndsu.edu

M. R. H. Khan  
Biomedical Engineering Program, North Dakota State  
University, Fargo, ND 58108, USA  
e-mail: mdrakibhasan.khan@ndsu.edu

A. Al Hoque · M. Quadir  
Department of Coatings and Polymeric Materials, North  
Dakota State University, Fargo, ND 58108, USA  
e-mail: ashique.alhoque@ndus.edu

M. Quadir  
e-mail: mohiuddin.quadir@ndsu.edu



# J591 functionalized paclitaxel-loaded PLGA nanoparticles successfully inhibited PSMA overexpressing LNCaP cells

Iman Ehsan<sup>a,1</sup>, Leena Kumari<sup>a,1</sup>, Ramkrishna Sen<sup>a,1</sup>, Ashique Al Hoque<sup>a</sup>, Biswajit Mukherjee<sup>a,\*</sup>, Alankar Mukherjee<sup>a</sup>, Prasanta Ghosh<sup>a</sup>, Sanchari Bhattacharya<sup>b</sup>

<sup>a</sup> Department of Pharmaceutical Technology, Jadavpur University, Kolkata, India

<sup>b</sup> Guru Nanak Institute of Pharmaceutical Science and Technology, Panihati, Kolkata, India

## ARTICLE INFO

### Keywords:

Poly(lactide-co-glycolide) nanoparticles  
Paclitaxel  
Surface modification  
Prostate-specific membrane antigen (PSMA)  
Prostate cancer

## ABSTRACT

To evaluate the chemotherapeutic efficacy of J591 fabricated poly(d,l)-lactic-co-glycolic acid (PLGA) nanoparticles containing paclitaxel (Ab-PTX-NP) *in vitro* in PSMA (prostate specific membrane antigen) expressing prostate cancer cells, increase the solubility, bioavailability, circulation time, and limit systemic toxicity to achieve the maximum curative effect accompanied by controlled dosing, we formulated Ab-PTX-NP. Physico-chemical characterizations such as Field emission scanning electron microscopy, Transmission electron microscopy, and Atomic force microscopy revealed that the particles were smooth-surfaced, with homogeneous distribution of drug within the particles and size were in the nano range. The encapsulation efficiency of Ab-PTX-NP was found to be 70.85%. This study acknowledges the effectiveness of Ab-PTX-NP *in vitro*, which displays elevated cellular cytotoxicity and internalization, maximum apoptosis (74.1%) in PSMA-abundant LNCaP cells, in comparison to PSMA negative PC3 cells. Pharmacokinetic data revealed the bioavailability of paclitaxel upon i.v. administration in the systemic circulation of male Balb/c mice. Herein, J591 was maneuvered in a neoteric way to carry the prepared chemotherapeutic nanoparticles directly to the affected prostate cancer cells.

## 1. Introduction

Prostate cancer is a common and recurrent cancer type in males globally, with a growing incidence of mortality [1]. International management of prostate cancer is still obscure and remains a global challenge to manage in spite of our perceptive of its biology and growth regulation. Recent treatments include surgical elimination of the prostate, radiation and androgen ablation (early stage), and chemotherapy (secondary treatment). Normally, androgen regulates the prostate and most of its malignancies, development, growth, and function [2,3]. Our study will utilize the ubiquitous overexpression of the prostate-specific membrane-antigen PSMA on cancerous prostate cells. PSMA plays an imperative role in diagnosis, managing as well as treating prostate cancer. The aggrandized PSMA glutamate carboxypeptidase II, having a molecular weight of about 100 kDa, is enhanced and progressively elevated in prostate adenocarcinoma and in the neovasculature of solid tumors and positively correlates with tumor progression or metastasis in prostate cancer tissue, thus, differentiating benign tumors from

malignant disease [4,5]. More crucially, the presence of internalization motif in the cytoplasmic tail of PSMA might suggest that the ligand-attached nanotherapeutics may get internalised into the cell [6].

J591, an anti-PSMA monoclonal antibody (Ab), has already been developed to target PSMA and has been demonstrated in cellular internalization [7,8]. The absence of the majority of extra-prostatic expression of PSMA on normal vasculature endothelium makes it target-specific. Paclitaxel (PTX) is the best microtubule stabilized drug licensed by the United States Food and Drug Administration (USFDA) for the therapeutic treatment of a range of malignancies, including prostate cancer. PTX inhibits mitosis and is effective in eradicating cancer cells during the interphase of the cell cycle [9]. It can be hypothesized that delivering paclitaxel (PTX) as a chemotherapeutic payload by encapsulating it in a designed PLGA (USFDA approved biodegradable polymer for human use by i.v. route) nanoparticle (PTX-NP), and further conjugating it with J591 Ab (Ab-PTX-NP), aids in the higher cellular internalization of PTX to PSMA expressed prostate cancer cells.

Elevated cellular uptake of PTX by the prostate cancer cells was

\* Corresponding author. Department of Pharmaceutical Technology, Jadavpur University, Kolkata, 700032, India.

E-mail address: [biswajit.mukherjee@jadavpuruniversity.in](mailto:biswajit.mukherjee@jadavpuruniversity.in) (B. Mukherjee).

<sup>1</sup> shares equal authorship.





# In silico fight against novel coronavirus by finding chromone derivatives as inhibitor of coronavirus main proteases enzyme

Nayim Sepay<sup>1</sup> · Nadir Sepay<sup>2</sup> · Ashique Al Hoque<sup>3</sup> · Rina Mondal<sup>4</sup> · Umesh Chandra Halder<sup>1</sup> · Mohd. Muddassir<sup>5</sup>

Received: 5 March 2020 / Accepted: 13 April 2020 / Published online: 13 May 2020  
© Springer Science+Business Media, LLC, part of Springer Nature 2020

## Abstract

Novel coronavirus, 2019-nCoV is a danger to the world and is spreading rapidly. Very little structural information about 2019-nCoV make this situation more difficult for drug designing. Benzylidenechromanones, naturally occurring oxygen heterocyclic compounds, having capability to inhibit various protein and receptors, have been designed here to block mutant variety of coronavirus main protease enzyme (SARC-CoV-2 M<sup>pro</sup>) isolated from 2019-nCoV with the assistance of molecular docking, bioinformatics and molecular electrostatic potential. (Z)-3-(4'-chlorobenzylidene)-thiochroman-4-one showed highest binding affinity to the protein. Binding of a compound to this protein actually inhibits the replication and transcription of the virus and, ultimately, stop the virus multiplication. Incorporation of any functional groups to the basic benzylidenechromanones enhances their binding ability. Chloro and bromo substitutions amplify the binding affinity. ADME studies of all these compounds indicate they are lipophilic, high gastro intestine absorbable and blood-brain barrier permeable. The outcome reveals that the investigated benzylidenechromanones can be examined in the case of 2019-nCoV as potent inhibitory drug of SARC-CoV-2 M<sup>pro</sup>, for their strong inhibition ability, high reactivity and effective pharmacological properties.

**Keywords** Novel coronavirus · SARC-CoV-2 M<sup>pro</sup> · Benzylidenechromanones · ADME · DFT · Docking

**Electronic supplementary material** The online version of this article (<https://doi.org/10.1007/s11224-020-01537-5>) contains supplementary material, which is available to authorized users.

✉ Nayim Sepay  
nayimsepay@yahoo.com

✉ Umesh Chandra Halder  
uhalder2002@yahoo.com

<sup>1</sup> Department of Chemistry, Jadavpur University, Kolkata 700032, India

<sup>2</sup> Plant Biotechnology Laboratory, Post Graduate Department of Botany, Ramakrishna Mission Vivekananda Centenary College, Rahara, Kolkata 700118, India

<sup>3</sup> Department of Pharmaceutical Technology, Jadavpur University, Kolkata 700032, India

<sup>4</sup> Department of Chemistry, Uluberia College, Howrah, West Bengal 711 315, India

<sup>5</sup> Department of Chemistry, College of Science, King Saud University, Riyadh 11451, Saudi Arabia

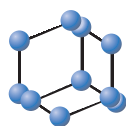
## Introduction

In this time, the entire world is facing a threat of a new coronavirus, 2019-nCoV. It first appeared in the Wuhan province of China and spread rapidly in the different parts of the world. According to WHO, there is 1,133,758 confirmed cases of 2019-nCoV infection with 82,061 new case and 62,784 deaths found around the globe, as of 5th April 2020 [1]. Only 9096 patients were recovered and the rate of infection is much higher than that of recovery. At this moment, instigation for effective, safe and easy synthesisable therapeutics is in high demand [2, 3].

The virus 2019-nCoV, a mutant variety of lineage B betacoronavirus, uses angiotensin-converting enzyme2 (ACE2) of human cell as a receptor during infection like other severe acute respiratory syndrome (SARS)-CoV [4]. Coronavirus has largest viral positive-stranded RNA [5] with protein envelop. The maturation process of SARS-CoV is streaming through protein cleavage of polypeptides which influence the replication and transcription of the virus. The CoV main protease (CoV M<sup>pro</sup>) is the key enzyme in this event. Inhibition of the protein is an attractive strategy for the



## RESEARCH ARTICLE

BENTHAM  
SCIENCE

## Anti-COVID-19 Sulfonamides: A DFT, Docking and ADMET Study

Ashique Al Hoque<sup>1</sup>, Chayan Guha<sup>2</sup>, Nayim Sepay<sup>3,\*</sup>, Sankar P. Dey<sup>4</sup> and Umesh C. Halder<sup>3,\*</sup>

<sup>1</sup>Department of Pharmaceutical Technology, Jadavpur University, Kolkata-700 032, India; <sup>2</sup>Department of Basic Engineering Science, Netaji Subhash Engineering College, Garia, Kolkata-700 152, India; <sup>3</sup>Department of Chemistry, Jadavpur University, Kolkata-700 032, India; <sup>4</sup>Department of Chemistry, Behala College, Parnashree, Kolkata, West Bengal 700 060, India

**Abstract: Background:** The development of a specific curative drug or prophylactic and vaccine is urgently required to cure COVID-19. Sulfonamide and its derivatives are famous for their multifaceted antibiotic and antiviral activities against varieties of a pathogen.

**Objective:** The objective of this study is to find new potential molecules for COVID-19 treatment. We tested some sulfonamide molecules (including antiviral compounds) as SARS CoV-2 M<sup>pro</sup> inhibitors.

**Methods:** In this study, the Density Functional Theory (DFT) and Docking study have been utilized for protein-small molecule affinity prediction. The SwissADME server was used for pharmacokinetics and drug-like likeness prediction, and the Pred-hERG server was employed for cardiotoxicity prediction.

**Results:** In this study, sixteen sulfonamides have been investigated in silico, with a perspective to obtaining a potential anti-covid compound. The sulfonamides have been subjected to molecular docking with SARS CoV-2 M<sup>pro</sup>, mainly responsible for viral infection and replication. We discover the molecular flexibility and charge distribution profoundly affecting the binding of the compounds to the protein. Moderately flexible (six rotatable bond) and less polar (sufficient hydrophobic) sulfonamide are favorable for strong binding with the enzyme. Here, the bioavailability properties like adsorption, distribution, metabolism, excretion, pharmacokinetics, and potential toxicity of these compounds have also been checked.

**Conclusion:** Low cardio-toxicity and high bioavailability make these sulfonamides a good anti-COVID-19 drug option. The sulfonamide **16** was found to be the best.

**Keywords:** Sulfonamides, COVID-19, SARS CoV-2 M<sup>pro</sup>, molecular docking, ADME, cardio-toxicity.

## 1. INTRODUCTION

In the last seven months, the world is facing the most significant challenge as COVID-19 [1]. The number of COVID-19 infections and deaths caused by it is very high and still increasing with time around the globe. To slow down the virus spreading, the worldwide lockdown of countries was obeyed. However, the longtime lockdown has profoundly affected the global economy [2]. Therefore, the preparation of curative or prophylactic drugs or vaccines is the last and only option to survive the pandemic and revive the failing economy. In this context, 4-hydroxychloroquine, remdesivir, ritonavir, and lopinavir with appropriate combinations were tested, with aspiration, in opposition to the virus, but high toxicity low success rate is the challenge now [3, 4]. Remdesivir is an antiviral treatment for several virus-

es. It was first developed about ten years ago to treat hepatitis C and cold virus, the respiratory syncytial virus (RSV). Remdesivir was not an efficient disease therapy. But the pledge against other viruses has been demonstrated. Remdesivir is an intravenous nucleotide prodrug of an adenosine analog. Remdesivir binds to RNA polymerase, which prevents viral replication by preventing premature termination of RNA transcription. The *in-vitro* activity has been demonstrated against severe acute coronavirus respiratory syndrome 2 (SARS-CoV-2). Remdesivir is approved for the treatment of COVID-19 in hospitalized patients, adults, and pediatric patients by the Food and Drug Administration (FDA). Remdesivir may be provided in a hospital or a health center that can give a patient's hospital a comparable healthcare quality. Vaccine development for the virus is also becoming tough and time-consuming day by day [5]. At this point, we need to try all the alternative drug options.

The COVID-19 is a mutant variety of coronavirus. With  $\approx 26$ –32 kilobases, it is the most extensive positive-stranded RNA that contains a virus. The genetic material has two

\* Address correspondence to these authors at the Department of Chemistry, Lady Brabourne College, Kolkata 700 017, India; Tel: 09038739338; E-mail: [nayimsepay@yahoo.com](mailto:nayimsepay@yahoo.com) (NS) and [uhalder2002@yahoo.com](mailto:uhalder2002@yahoo.com) (UCH)

# CHAPTER SIX

## APOPTOSIS-ASSOCIATED MARKERS: POTENTIAL TARGETS TO DEVELOP CANCER THERAPY

BISWAJIT MUKHERJEE<sup>1</sup>,  
ASHIQUE AL HOQUE<sup>1,2</sup>,  
BRAHAMACHARRY PAUL<sup>1</sup>, LABONI DAS<sup>3</sup>,  
SAMRAT CHAKRABORTY<sup>1,4</sup>  
AND APALA CHAKRABORTY<sup>1</sup>

### Abstract

Apoptosis is a specialized mechanism that results in planned cell death by activating an intracellular pathway preserved throughout evolution and causes pathognomonic cellular alterations unique from cellular necrosis. One of the most important criteria for a chemotherapeutic agent to be used effectively in cancer treatment is its capacity to trigger apoptosis. Cancer cells can undergo apoptosis in response to chemotherapy through a variety of mechanisms, including oxidative stress-induced apoptosis that follows the intrinsic pathway of apoptosis, death ligand-mediated apoptosis that involves the FasR/FasL system, and granzyme B/perforin-mediated

---

<sup>1</sup> Department of Pharmaceutical Technology, Jadavpur University, 188, Raja S.C. Mullick Road, Jadavpur, Kolkata 700032, West Bengal, India.

<sup>2</sup> Department of Coatings and Polymeric Materials, North Dakota State University, Fargo, North Dakota 58108, United States.

<sup>3</sup> School of Pharmacy, Techno India University, EM-4, EM Block, Sector-V, Bidhanagar, Kolkata 700091, West Bengal, India.

<sup>4</sup> Department of Pharmaceutical Sciences, Oregon State University, Portland, OR 97201, United States.

# CHAPTER TEN

## TARGETED NANOTHERAPEUTICS: PROMISING THERAPEUTIC ARSENAL AGAINST HEPATOCELLULAR CARCINOMA

BISWAJIT MUKHERJEE<sup>1</sup>,  
BRAHAMACHARRY PAUL<sup>1</sup>, ASHIQUE AL  
HOQUE<sup>1</sup>, SAMRAT CHAKRABORTY<sup>1,2</sup>,  
LABONI DAS<sup>3</sup>, APALA CHAKRABORTY<sup>1</sup>  
AND ALANKAR MUKHERJEE<sup>1</sup>

### Abstract

Hepatocellular carcinoma (HCC) is one of the most complex types of cancer. Standard therapies, including surgical removal, radiation, and chemotherapy, have a poor prognosis for patients due to their variety of adverse effects. Targeted delivery of the active ingredient can be used to specifically target different proteins or genes of the HCC tumor microenvironment, which can lessen the drug's off-target side effects. Signal transduction inhibitors, hormone therapies, gene expression modulators, angiogenesis inhibitors, apoptosis inducers, immunotherapies, toxin delivery molecules, and other types of targeted therapy have all been thoroughly studied in recent years. This chapter provides an overview of

---

<sup>1</sup> Department of Pharmaceutical Technology, Jadavpur University, 188, Raja S.C. Mullick Road, Jadavpur, Kolkata 700032, West Bengal, India.

<sup>2</sup> Department of Pharmaceutical Sciences, Oregon State University, Portland, OR 97201, United States.

<sup>3</sup> School of Pharmacy, Techno India University, EM-4, EM Block, Sector-V, Bidhanagar, Kolkata 700091, West Bengal, India.

## CHAPTER 10

### Targeted Nanotherapeutics: Promising Therapeutic Arsenal against Hepatocellular Carcinoma

Biswajit Mukherjee <sup>a,✉</sup>, Brahamacharry Paul <sup>a</sup>, Ashique Al Hoque <sup>a</sup>, Samrat Chakraborty <sup>a,b</sup>, Laboni Mondal <sup>c</sup>, Apala Chakraborty <sup>a</sup>, Alankar Mukherjee <sup>a</sup>

#### Abstract

Hepatocellular carcinoma (HCC) is one most complex type of cancer, and standard therapies, including surgical removal, radiation, and chemotherapy, have a poor prognosis for patients due to their variety of adverse effects. Targeted therapy of the active ingredient can be used to specifically target different proteins or genes of the HCC tumor microenvironment, which can lessen the drug's off-target side effects. Signal transduction inhibitors, hormone therapies, gene expression modulators, angiogenesis inhibitors, apoptosis inducers, immunotherapies, toxin delivery molecules, and other types of targeted therapy have all been thoroughly studied in recent years. This chapter provides an overview of targeted nanotherapy for HCC and new studies on the subject that are still undergoing preclinical testing.

#### 1 Introduction:

Liver cancer is one most common and complicated type of cancer worldwide, with an estimated annual case of around one million, and is recognized as the third leading cause of cancer death (Sung, Ferlay, Siegel, Laversanne *et al.* 2021, 209). Hepatocellular carcinoma (HCC) is the most common type of liver cancer, and it is deadlier than the other types of liver cancer as it is often diagnosed in later stages and appears surgically nonresectable (Mintz and Leblanc 2021, 1). The conventional treatments for HCC are surgical resection, chemotherapy, and radiotherapy (Daher, Massarwa, Benson, and Khoury 2018, 71). Chemotherapy in HCC involves the infusion of chemotherapeutic agents into the hepatic artery, which reduces the side effects of the drug on the normal cells, while radiotherapy involves the radiation-assisted killing of liver tumors. However, to avoid the severe side effects of conventional chemotherapy and radiotherapy, researchers have focused on the development of targeted drug delivery systems based on the different receptors and molecules present in HCC involved in tumor growth or maintaining tumor homeostasis (Daher, Massarwa, Benson and Khoury 2018, 71). These include kinase inhibitors which inhibit tumor angiogenesis or tumor progression, and immunotherapeutic agents, which modulate the immune response against tumor growth and alter the tumor microenvironment to reduce its progress (Greten and Sangro 2018, 157-159). The first US-FDA-approved kinase inhibitors as the first-line choice for treating HCC were sorafenib and lenvatinib (Rimini, Shimose, Lonardi, Tada *et al.* 2021, 1229). Several nanomaterials have been explored for targeted delivery of active chemotherapeutic agents such as conventional chemotherapeutics (e.g., taxol, paclitaxel, docetaxel), new synthetic drugs (e.g., tegafur-uracil), monoclonal antibodies (e.g., bevacizumab, ramucirumab), kinase inhibitors (e.g., sorafenib, regorafenib), etc., for their site-specific delivery towards HCC. Nanomaterials involve a large variety of drug delivery systems which include inorganic nanoparticles, polymeric nanoparticles, lipid nanoparticles, carbon dots, liposomes, micelles, metal-organic frameworks, Janus nanoparticles, nanocrystals, etc., but not limited to those mentioned above (Mintz and Leblanc 2021, 2). Nanomaterials could be of different shapes, such as spheres, rods, tubes, fibers, sheets, nanostars, etc., but in general, any material which is less than 100 nm in at least one dimension can be considered a nanomaterial (Auffan, Rose, Bottero, Lowry *et al.* 2009, 634-636). Nanomaterials are good carriers for delivering therapeutic entities and sometimes, they have their therapeutic actions. In this chapter, we have discussed different nanotherapeutics developed so far with the aim of selective drug delivery to HCC, recent patents obtained in the relevant field, and the possible future direction of developing nanotherapeutics for the treatment of HCC.

<sup>a</sup>Department of Pharmaceutical Technology, Jadavpur University, 188, Raja S.C. Mullik Road, Jadavpur, Kolkata 700032, West Bengal, India; <sup>b</sup>Department of Pharmaceutical Sciences, Oregon State University, Portland, OR 97201, United States; <sup>c</sup>School of Pharmacy, Techno India University, EM-4, EM Block, Sector-V, Bidhanagar, Kolkata 700091, West Bengal, India.

✉ Author for Correspondence: biswajit.mukherjee@jadavpuruniversity.in

## CHAPTER THIRTEEN

# POLYMERSOMES AS NOVEL STRATEGIES FOR DELIVERY OF NANOTHERAPEUTICS FOR CANCER CONTROL

MD RAKIB HASAN KHAN<sup>1</sup>,  
ASHIQUE AL HOQUE<sup>2</sup> AND  
MOHIUDDIN QUADIR<sup>1,2</sup>

### Abstract

Polymersomes are artificial vesicular structures composed of amphiphilic block copolymers. Typically, these vesicle-like structures have hollow cores, surrounded by membranes composed of block copolymers. Membrane characteristics, i.e., thickness, viscosity, toughness, biodegradability, and stimuli-responsivity, can be regulated by controlling the chemical structure of the constituent block copolymers. Polymersomes are widely used in molecular transport, such as the intracellular delivery of drugs and nucleic acid. Polymersome surfaces are often functionalized with targeting ligands to achieve active tissue targeting. Polymersomes can encapsulate both hydrophilic and hydrophobic classes of drugs in their core or within the membrane compartment. In this review, we provide a concise overview of the engineering, structure, and function of polymersomes in the context of cancer therapy.

**Keywords:** Polymersomes, amphiphilic block copolymers, biodegradability, stimuli-responsivity

---

<sup>1</sup> Biomedical Engineering Program, North Dakota State University.

<sup>2</sup>Department of Coatings and Polymeric Materials, North Dakota State University.

## CHAPTER 12

## Future Direction of Nanotherapy in the Management of Hepatocellular Carcinoma

**Biswajit Mukherjee<sup>1,\*</sup>, Laboni Das<sup>2</sup>, Sanchari Bhattacharya<sup>3</sup>, Apala Chakraborty<sup>1</sup>, Shreyasi Chakraborty<sup>1</sup>, Ashique Al Hoque<sup>1</sup> and Debasmita Dutta<sup>1,4</sup>**

<sup>1</sup> Department of Pharmaceutical Technology, Jadavpur University, Kolkata 700032, WB, India

<sup>2</sup> School of Pharmacy, Techno India University, EM-4, Sector-V, Salt Lake, Kolkata, WB, India

<sup>3</sup> Guru Nanak Institute of Pharmaceutical Science and Technology, 157 f, Nilgunj Rd, Sahid Colony, Panihati, Kolkata, West Bengal 700114, India

<sup>4</sup> Department of Molecular and Human Genetics, Baylor College of Medicine, Houston, Texas 77030, United States

**Abstract:** Worldwide, hepatocellular carcinoma (HCC) is one of the leading causes of cancer-related deaths among humans. Several conventional therapies, including surgical and non-surgical methods such as liver transplantation, radiation, and chemotherapy, have been explored to combat this disease and improve the patients' quality of life. However, due to poor diagnosis of the disease, drug toxicity issues, and difficulties related to liver transplantation, scientists search for novel techniques to treat HCC that ensure targeted drug delivery and help in diagnosing the disease. Nanotherapeutics are a new trend in drug discovery and medicine which deals with nano-sized formulations loaded with various types of materials such as drugs, antibodies, aptamers, genes, viruses, *etc.*, and targeted delivery. Moreover, controlled release of the materials can be achieved through modifying their external and internal structures as per requirement. Drug delivery through nano theranostics has taken a new turn as the diagnostic tools tagged with the nano-architectures ensure diagnosis and treatment simultaneously. Nanotheranostics have significant application in the identification of cancer progression through continuous monitoring and treatment of cancer. In this review, we will discuss different beneficial effects and applications of nanotherapeutics against HCC. Along with that, different upcoming strategies, such as personalized medicine, layer-by-layer technologies, implant theory, 3D printing technology, nanorobots, nanocrystals, nano-chips, *etc.*, will be discussed here, which may pave the path towards successful diagnosis and treatment of HCC to improve the health of the patients.

Correspondence: \*Corresponding author **Biswajit Mukherjee**: Department of Pharmaceutical Technology, Jadavpur University, Kolkata 700032, India, Tel/Fax: +913324146677; Mobile: +91-84208248897; E-mails: biswajit.mukherjee@jadavpuruniversity.in, biswajit55@yahoo.com

**Biswajit Mukherjee (Ed.)**

All rights reserved-© 2021 Bentham Science Publishers



# Transdermal Nanomedicines for Reduction of Dose and Site-Specific Drug Delivery

# 8

Biswajit Mukherjee, Soma Sengupta, Soumyabrata Banerjee, Moumita Dhara, Ashique Al Hoque, Leena Kumari, Manisheeta Ray, Iman Ehsan, and Alankar Mukherjee

## Abstract

The emergence of new technologies provides unique opportunities to exploit novel approaches in drug delivery. Transdermal drug delivery systems (TDDS) are one of the imperative technologies of increasing interest with the benefits of sustained/controlled drug delivery leading to patient convenience and compliance. By definition, TDDS are topically administered medications, for example, patches or semisolids, which permeate the active ingredient through the intact skin for systemic effects in a sustained manner. Transdermal drug deliveries, therefore, are the noninvasive administration of active ingredients from the skin surface across its layers, to the systemic circulation. Nanomedicinal approaches through TDDS can be utilized for site-specific delivery of drugs which can lead to the reduction of dose, too. We have reported here TDDS providing nanomedicinal strategies to deliver drug(s) to the target tissues.

## Keywords

Skin · Transdermal delivery · Nanomedicine · Dose · Site-specific delivery

## 8.1 Introduction

Skin, being the largest organ of our body, protects us as a physiological barrier from different infections, environmental stress, such as heat or cold, and permeates the sensation with the help of nerve endings residing beneath the skin. Certain active ingredients having the potency to cross this physiological barrier can even reach the

B. Mukherjee (✉) · S. Sengupta · S. Banerjee · M. Dhara · A. Al Hoque · L. Kumari · M. Ray · I. Ehsan · A. Mukherjee

Department of Pharmaceutical Technology, Jadavpur University, Kolkata, India

# Nanoformulated Drug Delivery of Potential Betulinic Acid Derivatives: A Promising Approach Toward Cancer Therapy

Biswajit Mukherjee, Ashique Al Hoque, Debasmita Dutta, Brahamacharry Paul, Alankar Mukherjee, and Sahajit Mallick

## 1 Introduction

In last few decades, there has been a tremendous interest worldwide in the design of analogue libraries based on plant-derived product for anticancer drug development. The main objective in cancer drug development is to find new drugs that are cytotoxic to cancer cells but not to healthy cells. However, adverse side effects to normal cells, drug resistance property of conventional chemotherapeutic drugs, and non-specific tissue distribution are the primary obstacles to combat the disease. So potential plant-derived natural products are in search as an alternative to toxic drugs. This approach has received a positive response obtained from some natural products due to the efficacious anticancer properties and minimum side effects toward normal cells. It is worthy to mention here that around 50% of the currently used anticancer drugs suggested were either natural products or natural product-based conjugates [1].

An increasing number of triterpenoids, naturally occurring terpenes having potential for the neoplastic disease prevention and treatment properties, are ubiquitously distributed throughout the plant kingdom. Many of them have been reported to exhibit cytotoxicity against a variety of cancer cells without manifesting considerable toxicity toward normal cells [1]. Notable among them is the pentacyclic lupane type of triterpenoids that represent a very important class of natural products. Betulinic acid [ $3\beta$ -hydroxy-lup-20(29)-en-28-oic acid] and its reduced congener betulin [lup-20(29)-en- $3\beta$ , 28-diol] belonging to this class are widely distributed in the plant kingdom. Betulinic acid was found to show significant antiproliferative activity on a broad panel of cancer cells [2, 3], and it was found to cause cancer cell death by induction of apoptosis involving caspases with no toxic effects [4]. The

---

B. Mukherjee (✉) · A. Al Hoque · D. Dutta · B. Paul · A. Mukherjee · S. Mallick  
Department of Pharmaceutical Technology, Jadavpur University, Kolkata, India  
e-mail: [biswajit.mukherjee@jadavpuruniversity.in](mailto:biswajit.mukherjee@jadavpuruniversity.in)



## Chapter 3

# Recent developments in cancer vaccines: where are we?

Biswajit Mukherjee<sup>1</sup>, Ashique Al Hoque<sup>1</sup>, Apala Chakraborty<sup>1</sup>,  
Samrat Chakraborty<sup>1</sup>, Lopamudra Dutta<sup>2</sup>, Debasmitta Dutta<sup>3</sup>,  
Soumyabrata Banerjee<sup>4</sup>, Moumita Dhara<sup>1</sup>, R. Manasa Deepa<sup>5</sup>

<sup>1</sup>Department of Pharmaceutical Technology, Jadavpur University, Kolkata, West Bengal, India;

<sup>2</sup>Department of Molecular and Human Genetics, Baylor College of Medicine, Houston, TX, United States; <sup>3</sup>Department of Coatings and Polymeric Materials, North Dakota State University, Fargo, ND, United States; <sup>4</sup>Department of Psychology/Neuroscience Program, Central Michigan

University, Mount Pleasant, MI, United States; <sup>5</sup>East West College of Pharmacy, Bengaluru, Karnataka, India

## 1. Introduction

Cancer, a life-threatening disease, is a critical health issue globally and requires new approaches and treatment modalities for optimizing patient outcomes. Colorectal, lung, and prostate cancers are generally familiar in men, and on the other hand, lung, colorectal, and breast cancers are prevalent among women [1,2]. In the current cancer-related scenario, about 50% of new cases are due to lung and bronchus, breast, colorectal and prostate cancers which are the reason for approximately 50% of all deaths among people in the United States. In 2020, almost 1.8 million new cases and 606,520 deaths due to cancer were projected to happen in the United States [3]. In cancer progression, immune surveillance and immune escape are considered important issues for which immunotherapy development has become a new era in the cancer research field compared to surgery, radiotherapy, or chemotherapy [4]. During these circumstances, attractive and potentially effective cancer treatment is immunotherapy which can be classified as “passive” and “active.” “Passive” or “adaptive” means ex-vivo administration of antibodies or cells, whereas “active” epitomizes through vaccines to produce a particular immune response against various types of antigens such as tumor-specific antigens, virus-associated antigens, cancer germline antigens, and tumor-associated antigens (TAAs). As per the theoretical concept, a cancer vaccine can either cure the tumor or maintain cancer in a controlled manner by supporting the immune system [5–7]. The exciting advances in multidisciplinary cancer treatments





INTERNATIONAL MEDICAL UNIVERSITY  
MALAYSIA

# CERTIFICATE of PARTICIPATION



Presented To

**MR. ASHIQUE AL HOQUE**

to acknowledge his Oral Presentation on the topic

**Development and Characterisation of antibody functionalized biodegradable nanoparticle  
system for targeted prostate cancer therapy**

during

**6<sup>TH</sup> INTERNATIONAL POSTGRADUATE CONFERENCE ON PHARMACEUTICAL SCIENCES 2018**

held at

International Medical University, Kuala Lumpur, Malaysia

15 - 16 August 2018

Ms. Kit-Kay Mak  
Chairperson

6<sup>th</sup> IPOPS Organising Committee

Assoc. Prof. (Dr.) Mohd Zulkefeli bin Mat Jusoh  
Dean, School of Pharmacy  
International Medical University

**PULSUS**  
WWW.PULSUSCONFERENCE.COM

*Cancer Research 2019*  
*Young Scientists Forum*

Prof/Dr/Mr/Ms. **Ashique Al Hoque**

Jadavpur University, India

for presenting the oral entitled

**Targeting to prostate cancer cells by using ligand  
conjugated polymeric nanoparticles as drug carrier**

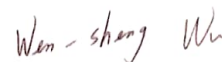
at the 24<sup>th</sup> International Conference on Cancer Research and Pharmacology  
held during August 5-6, 2019 in Singapore

The award has been attributed in recognition of research paper quality, novelty and significance.



**Raghu Pandurangi**

Sci-Engi-Medco Solutions Inc. and Amplexi-LLC  
USA



**Wen-Sheng Wu**

Tzu Chi University  
Taiwan





**NATIONAL SEMINAR**  
**"Advancing Healthcare Through Pharmaceutical and  
Biomedical Applications"**  
Jadavpur University, Kolkata



19th January, 2024

## CERTIFICATE OF APPRECIATION

*This is to certify that ..e.Ashique A.L. Hoque..... has attended the National Seminar on "Advancing Healthcare Through Pharmaceutical and Biomedical Applications" and secured 1st / <sup>(Joint)</sup> 2nd / 3rd position in Scientific Poster / Scientific Oral presentation competition organised by Dr. V. Ravi Chandran Center for Advanced Research in Pharmaceutical Sciences, IIT & Indian Association of Pharmaceutical Scientists and Technologists, Kolkata, at Dr. H. L. Roy Auditorium, Jadavpur University, Kolkata*

*Prof. N Udupa*  
*(L. N. Udupa)*

Prof. N Udupa  
President,  
IAPST, Kolkata

*B. Chatterjee*

Prof. (Dr.) Biswajit Mukherjee  
Secretary, Organising Committee

Professor, Department of Pharm. Tech., Jadavpur University

# CERTIFICATE Of ACHIEVEMENT

This certificate is presented to

*Ashique Al Hoque*

HAS SECURED FIRST/SECOND/~~THIRD~~ POSITION IN POSTER PRESENTATION ON THE THEME ENTITLED "ADVANCED THERAPEUTICS FOR LIFE-THREATENING AND CHRONIC DISEASES" IN THE 1<sup>ST</sup> NATIONAL CONFERENCE ORGANISED BY DEPARTMENT OF PHARMACEUTICAL TECHNOLOGY, JVS UNIVERSITY ON 19-20 SEPTEMBER, 2023.

*Bhakesh*

**PROF. BHABES BHATTACHARYA**  
VICE-CHANCELLOR

*H.S. Maji*

**PROF. H.S. MAJI**  
DEAN ACADEMICS &  
HOD (DEPT. OF PHARMACY)

*Payal Chakraborty*

**DR. PAYAL CHAKRABORTY**  
CONVENOR,  
JVSU PHARMANECIA 2K23

*Arindam Maity*

**DR. ARINDAM MAITY**  
CO-CONVENOR,  
JVSU PHARMANECIA 2K23

3<sup>RD</sup> PHARM. TECH. IAPST INTERNATIONAL CONFERENCE ON

## MOLECULAR MECHANISM OF DISEASES AND NOVEL THERAPEUTIC APPROACHES

19<sup>th</sup>-20<sup>th</sup> January, 2019

### Certificate

*This Certificate is awarded to Ms./ Mr./ Dr. Asbique Al Hoque.  
for securing 1<sup>st</sup> / 2<sup>nd</sup> / 3<sup>rd</sup> position in Oral/Poster presentation.*



**Prof. Gurudutta Pattnaik**  
Local Organizing Secretary



**Mr. Anup Pal**  
Secretary, IAPST



**Prof. Biswajit Mukherjee**  
Organizing Secretary

Jointly Organized by:



**Centurion**  
UNIVERSITY

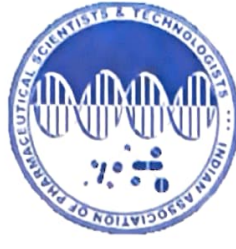


**School of Pharmacy and Life Sciences,  
Centurion University of Technology and  
Management, Bhubaneswar, India**

**Indian Association of Pharmaceutical  
Scientists and Technologists (IAPST),  
Kolkata, India**



# INTERNATIONAL SEMINAR ON "EMERGING FIELDS OF RESEARCH IN BIOTECHNOLOGY & BIOMEDICINE"



## CERTIFICATE OF APPRECIATION

THIS CERTIFICATE RECOGNIZES THE CONTRIBUTION OF

Prof/Dr./Mr./Ms./Miss

*Ashique Al Hoque*

as Invited Speaker/Chair Person/Co-Chair Person/Evaluator/Delegate/Presenter(Oral/Poster)  
*In the International Seminar Jointly Organized by Dr. V. Ravi Chandran Centre for Advanced  
Research in Pharmaceutical Sciences, Jadavpur University, Kolkata, India &  
Indian Association of Pharmaceutical Scientists and Technologists (IAPST), Kolkata, India.  
held at Jadavpur University, Kolkata, India on 16 November 2022.*

*Prof. Dr. Biswajit Mukherjee*

Prof. Dr. Biswajit Mukherjee  
Coordinator,  
Dr. V. Ravi Chandran Centre for  
Advanced Research in  
Pharmaceutical Sciences, Jadavpur  
University, Kolkata, India.



*Dr. N. Udupa*

Dr. N. Udupa  
President,  
Indian Association of  
Pharmaceutical Scientists  
and Technologists (IAPST),  
Kolkata, India.





National Seminar on

# CURRENT DEVELOPMENTS IN CHEMICAL SCIENCES (CDCS-2018)

(Wednesday, March 7, 2018)

under

Centre for Advanced Studies II Program

Organized by

Department of Chemistry, Jadavpur University, Kolkata 700 032

This is to certify that Ashique Al Hogue of Jadavpur University has participated/presented a poster in the seminar organized by the Department of Chemistry, Jadavpur University, Kolkata 700 032 on Wednesday, March 7, 2018.

Date: 07-03-2018  
Place: Kolkata

SAUBHIK HALDAR

PARTHA MAHATA

Conveners

# NATIONAL SEMINAR

on

## Pharmacy & Healthcare: Traditional Knowledge to Modern Techniques

14<sup>th</sup> September, 2018



### Certificate

*This certificate is awarded to Prof. / Dr. / <sup>✓</sup>Mr. / Mrs. / Ms.*

*Ashique Al Hogue*

*for participation as Delegate/ ~~Resource Person~~/ ~~Chairing a session~~/*

*Presenting a paper (~~Oral~~/ <sup>✓</sup>Poster).*

*B. Mukherjee*

**Prof. Biswajit Mukherjee**  
Co-Chairman

*Saikat Dewanjee*

**Dr. Saikat Dewanjee**  
Organizing Secretary



Sponsored by:



Science and Engineering Research Board  
Department of Science and Technology  
Government of India, New Delhi

Organized by:



Advanced Pharmacognosy Research Laboratory  
Department of Pharmaceutical Technology  
Jadavpur University, Kolkata 700032



**Centurion**  
**UNIVERSITY**

*Shaping Lives...  
Empowering Communities...*

# Certificate

**Awarded to**

*Ashique Ash Haque*

For Attending/ Poster Presenting/ Delivering lecture in the

**Indian Council of Medical Research (ICMR)**

*Sponsored National Seminar on*

**"Quality Control and Standardization  
of Ethnopharmaceuticals in the Present Era"**

**Held on 4th - 5th March 2018**

**at Centurion University of Technology and Management  
Bhubaneswar, Odisha**

*[Signature]*

**Prof. Haribandhu Panda**  
*Vice Chancellor, CUTM*

*[Signature]*

**Prof. Gurudutta Pattnaik**  
*Convener*

*[Signature]*

**Mr. Mahesh Patnaik**  
*Director, SPLS*







**Faculty of Engineering and Technology, JADAVPUR UNIVERSITY**  
**TEQIP-II SPONSORED ONE-DAY NATIONAL WORKSHOP**

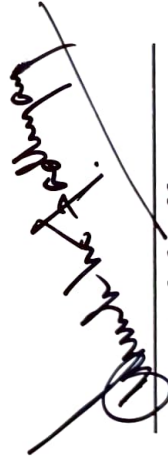
**ON**

**REVISITING INTELLECTUAL PROPERTY RIGHTS IN**  
**THE CONTEXT OF RECENT DEVELOPMENTS**  
**IN**  
**SCIENCE & TECHNOLOGY**  
**CERTIFICATE OF PARTICIPATION**

This is to certify that Prof./ Dr./ Mr./ Mrs./ Ms. .... Ashique Al Haque .....  
of ..... Jadavpur University ..... attended the ~~two-day~~ National Workshop  
organized by the Faculty of Engineering and Technology, Jadavpur University on October 20, 2016.



Coordinator  
TEQIP-II



Nodal Officer,  
TEQIP-II R&D Committee



Workshop Coordinators



Date: 29 March, 2017

**Subject: Award of INSPIRE Fellowship to the Research Students [IF160466]**

Dear ASHIQUE AL HOQUE,

The Government of India has launched a unique Scheme "**Innovation in Science Pursuit for Inspired Research (INSPIRE)**" with several components. INSPIRE Fellowship provides fellowship in Basic and Applied Sciences. I am pleased to inform you that you have been Selected for the award of INSPIRE Fellowship to host the same at the University/Institute/College/National Laboratory as indicated in the application form of your subsequent admission.

The value of the Fellowship will be at Par with the Junior Research Fellowship (JRF)/ Senior Research Fellowship (SRF) of Government of India along with a Contingency grant. The Fellowship shall be available to you for a period of five years or completion of your doctoral (PhD) program, whichever is earlier.

If you are willing to join or switching over from earlier fellowship to INSPIRE Fellowship, you will require to upload the scan copy of Joining-cum-Acceptance Letter (JCA) (available at <http://inspire-dst.gov.in/JoiningReport.pdf>, and at template in your online dashboard), and also submit Bank details of your Host Institute along with the scan copy of cancelled blank cheque of given account details **within one month from the date of this letter, in your online portal only**, for taking necessary actions at INSPIRE Program Secretariat for releasing of your fellowship amount. Please also note that in the JCA Letter the Host Institution, Research Supervisor and Research Topic shall not be change or modification from initially submitted documents/ information for Final Offer. The Terms & Conditions for implementation of INSPIRE Fellowship are enclosed herewith.

**Documents submitted in any other modes like email attachment or by post or in-person shall not be acceptable.**

In the event of your having being found ineligible at any state in future for the award/eligibility for INSPIRE Fellowship due to any reason (including unintentional computer error or printer's devil etc) this offer will be deemed withdrawn.

**Dr. S. Mallikarjuna Babu**  
Scientist 'C'

ASHIQUE AL HOQUE

C/O : LATE AIJUL HOQUE

Address : VILL- BARAGACHI, P.O- SHIBKRISHNAPUR, P.S- KUSHMANDI, DIST- DAKSHIN DINAJPUR, PIN- 733132

City : Dakshin Dinajpur Balurghat

State/UT: WEST BENGAL - 733132

This is a Computer Generated Offer Letter, No Signature is required

Date: 29 March, 2017

**GENERAL INSTRUCTIONS**

Dear ASHIQUE AL HOQUE,

**Please note that these documents are necessary to upload within one month from the date of this letter at INSPIRE Online**

**Webportal only for financial release after final selection**

1. Joining-cum-Acceptance (JCA) Letter for INSPIRE Fellowship (template available in your dashboard in online portal)
2. Relieving Order from previous Fellowship/Job (if availing).
3. Copy of Cancelled Blank Cheque of the Host University/ College/ Institute Account for transferring the fund (Account should be registered in Public Financial Management System: <https://pfms.nic.in>).
4. PFMS registration certificate, or Unique Agency Code in case of University/College/Institute is newly registered in Public Financial Management System.
5. Since the fund would be transferred under Alliance and R & D Mission Scheme (1596), Hence bank account number of Host University/College/Institute should be registered under this scheme in PFMS.
6. **Please note that these documents are necessary to upload within one month from the date of this letter at INSPIRE Online Webportal only, otherwise it will be treated as the candidate has not intrested in accepting the INSPIRE Fellowship.**

Thanking you,

**Dr. S. Mallikarjuna Babu**  
Scientist 'C'



Institutional Animal Ethics Committee (IAEC)

Department of Pharmaceutical Technology

Jadavpur University

Kolkata-700032

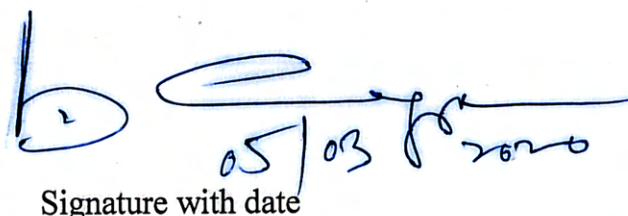
Ref No: AEC/PHARM/1704/04/2020

Date: 05.03.2020

This is to certify that Project title **“Development of ligand functionalized biodegradable polymeric nanoparticles system for targeted prostate cancer therapy: *in vitro* and *in vivo* study”** has been approved by the Institutional Animal Ethical Committee (IAEC), Jadavpur University in the meeting held on 3<sup>rd</sup> March, 2020.

Prof. (Dr.) Biswajit Mukherjee

Chairman/Member Secretary IAEC

  
Signature with date

Chairman  
Institutional Animal Ethics Committee  
Jadavpur University  
Kolkata-700032